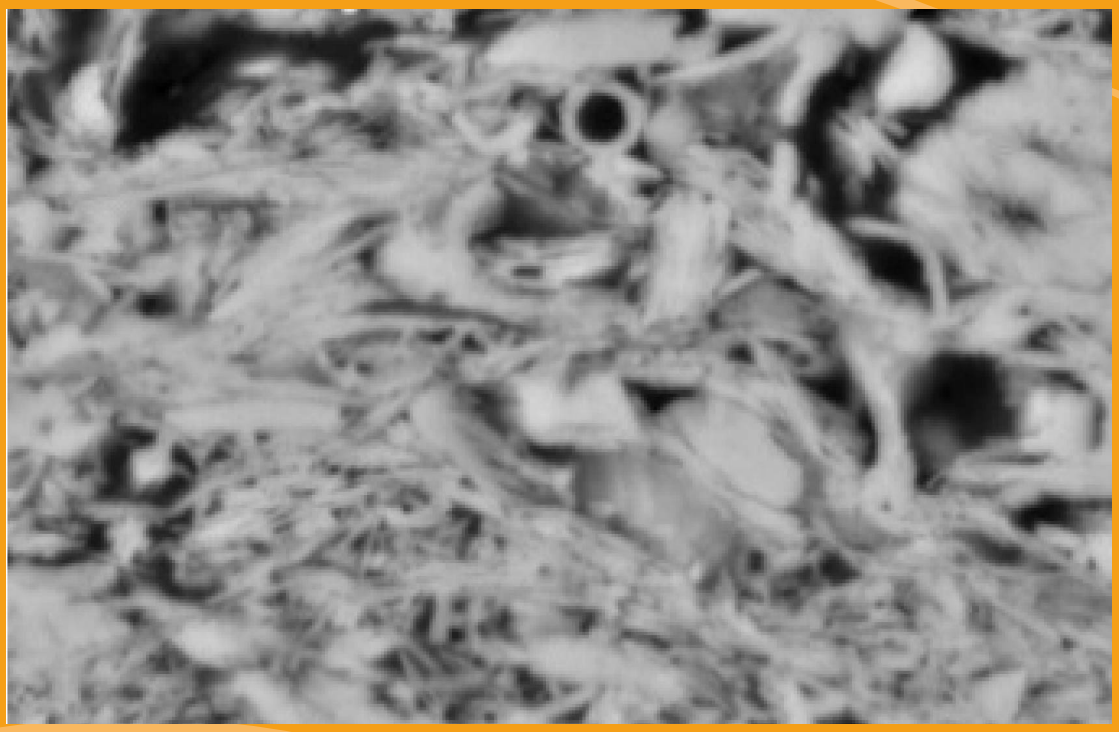
Bulletin of the Geological Society of Denmark



VOLUME 71 | 2022-2025 | COPENHAGEN

DGF

Bulletin of the Geological Society of Denmark

is published by the Geological Society of Denmark (DGF, Dansk Geologisk Forening), founded in 1893

Chief editor
Ole Bennike, Geological Survey of Denmark and Greenland (GEUS), Øster Voldgade 10, DK-1350 Copenhagen K. Tel: 91333527; obe@geus.dk

Co-editors: Lotte Melchior Larsen [lml@geus.dk] and *Gunver Krarup Pedersen* [gkp@geus.dk], both Geological Survey of Denmark and Greenland (GEUS), Øster Voldgade 10, DK-1350 Copenhagen K.

Scientific editors
Lars B. Clemmensen, Department of Geosciences and Natural Resource Management, University of Copenhagen, Øster Voldgade 10, DK-1350 Copenhagen K. Tel: 35322449; E-mail: larsc@ign.ku.dk (clastic sedimentology, sedimentary basins and palaeoclimatology).

Nicolaj Krog Larsen, Globe Institute, University of Copenhagen, Øster Voldgade 5–7, DK-1350 Copenhagen K, Denmark. Tel: 20693350; E-mail: nicl@sund.ku.dk (Quaternary geology).

Bodil Wesenberg Lauridsen, Geological Survey of Denmark and Greenland (GEUS), Øster Voldgade 10, 1350 Copenhagen K, Denmark. Tel: +45 91333708; E-mail: bwl@geus.dk (palaeontology, sedimentology).

Jesper Milàn, Kalk/Østsjællands Museer, Østervej 2, 4640 Faxe, Denmark. Tel: +45 23319488; E-mail: jesperm@oesm.dk (palaeontology).

Lars Nielsen, Geological Survey of Denmark and Greenland (GEUS), Øster Voldgade 10, DK-1350 Copenhagen K. Tel: 91333870; E-mail: larni@geus.dk (geophysics).

Stig Schack Pedersen, GEOTECTO. Tel: 24483098; E-mail: Geotecto.sasp@gmail.com (structural geology and tectonics).

Jan Audun Rasmussen, Museum Mors, Fossil- og Molermuseet, Skarrehagevej 8, DK-7900 Nykøbing Mors. Tel: 42149792; E-mail: jan.rasmussen@museummors.dk (palaeontology).

Mette Elstrup Steeman, Museum Sønderjylland, Naturhistorie og Palæontologi, Lergravsvej 2, DK-6510 Gram. Tel: 73820909; E-mail: mese@museum-sonderjylland.dk (palaeontology)

Erik Thomsen, Department of Geoscience, University of Aarhus, Høegh-Guldbergs Gade 2, DK-8000 Aarhus C. Tel: 87156443; E-mail: erik.thomsen@geo.au.dk (palaeontology and stratigraphy).

Henrik Tirsgaard, Total Upstream Danmark A/S, Amerika Plads 29, DK-2100 Copenhagen Ø. Tel: 61209140; E-mail: Henrik.tirsgaard@total.com (carbonate sedimentology, petroleum geology and sedimentary basins).

Tod Waight, Department of Geosciences and Natural Resource Management, University of Copenhagen, Øster Voldgade 10, DK-1350 Copenhagen K. Tel: 35 32 24 82; E-mail: todw@ign.ku.dk (igneous petrology and geochemistry).

The *Bulletin* publishes contributions of international interest in all fields of geological sciences on results of new work on material from Denmark, the Faroes and Greenland. Contributions based on foreign material may also be submitted to the Bulletin if the subject is relevant for the geology of the area of primary interest. The rate of publishing is one volume per year. All articles are published as pdf-files immediately after acceptance and technical production.

Scientific editing and reviewing are done on an unpaid collegial basis; technical production expenses are covered by the membership fees.

The bulletin is freely accessible on the web page of the Geological Society of Denmark:
www.2dgf.dk/publikationer/bulletin/index.html

Cover photo: SEM images of the brachiopod *Rugia stenius.* See this volume pp. 49–118: Surlyk, F.: Maastrichtian brachiopods from the chalk of Denmark.

LOwer CRETAceous project, summary of results

IDA LYKKE FABRICIUS & BODIL WESENBERG LAURIDSEN

Geological Society of Denmark
https://2dgf.dk

Received 10 January 2025
Accepted in revised form 29 March 2025
Published online 7 August 2025

© 2025 the authors. Re-use of material is permitted, provided this work is cited. Creative Commons License CC BY: https://creativecommons.org/licenses/by/4.0/

Fabricius, I.L. & Lauridsen, B.W. 2025. LOwer CRETAceous project, summary of results. Bulletin of the Geological Society of Denmark, Vol. 71, pp. 1–6. ISSN 2245-7070. https://doi.org/10.37570/bgsd-2025-71-01

We present summary of results from the LOCRETA project, grouped according to scientific approach: 1) Sedimentology and stratigraphy, 2) Structural geology, 3) Petrography and Petrophysics, and 4) Rock mechanics.

Keywords: Chalk, North Sea Basin, sedimentology, rock mechanics, geophysics.

Ida L. Fabricius [ilfa@dtu.dk], Department of Environmental and Resource Engineering, Technical University of Denmark, Denmark. Bodil W. Lauridsen [bwl@geus.dk]. Geological Survey of Denmark and Greenland, Denmark.

This thematic volume presents results from the LOCRETA project (2017–2021) which addressed some aspects of the Lower Cretaceous Cromer Knoll Group of the North Sea Basin. The group includes two chalk formations that host hydrocarbons in the North Sea and are subject to petroleum production: The Tuxen Formation of Hauterivian (BC 8) to Barremian (BC15) age and the Sola Formation of Barremian (BC15) to Albian (BC23–BC24) age. In the area around the Valdemar Field (central part of the Danish Central Graben, DCG), each formation is up to 100 m thick and buried to a depth of more than 2 km. The chalk is clay bearing and relatively soft, and the mechanical stability is a concern during hydrocarbon production. The interpretation of geophysical surface- and borehole data has also proven challenging, partly due to complex mineralogy and sparse information on pore water composition.

The LOCRETA project was initiated to address these rock mechanical and geophysical issues based on a revised architectural framework involving sedimentology, stratigraphy, paleontology and geochemistry. To increase our understanding of the Lower Cretaceous, a study of the nearby and equivalent Vedsted (Valanginian–Aptian/Albian) and Rødby (Aptian/Albian) formations in the Danish Basin was also included.

Sedimentology and stratigraphy

Investigations into the sedimentology and stratigraphy of the upper part of the Cromer Knoll Group, the Tuxen and Sola formations, are highly relevant for understanding the controlling factors of reservoir properties and heterogeneities (Fig. 1A). One of the aims during the LoCRETA project was to refine and better constrain the architectural framework of the Lower Cretaceous in the DCG and to understand equivalent strata of the Danish Basin. Data and interpretations presenting this part of the study have been published in the following articles: Blok *et al*. (2022, 2023), Ineson *et al*. (2022a, b), Jelby *et al*. (2022, 2024), Lauridsen *et al*. (2022) and Rudra *et al*. (2021).

The Tuxen and Sola formations comprise a heterogeneous succession of white to marly grey pelagic chalk interbedded with hemipelagic dark-grey marlstone and black marlstone (Ineson 1993, Jelby *et al*. 2022). The presence of chalk in the Hauterivian to Aptian part of the Vedsted Formation of the Danish Basin demonstrates that carbonate-rich pelagic sediments accumulated locally in the siliciclastic-dominated Danish Basin and indicates that benthic carbonate production was insignificant in this setting (Lauridsen *et al*. 2022; Fig. 1B).

A comprehensive facies analysis of the pelagic and hemipelagic carbonates has been conducted based on the cored sections of seven wells from the Lower Cretaceous Tuxen and Sola formations in the DCG (Jelby *et al*. 2022). The study identifies 50 facies based on a continuous series of six lithologies, eight sedimentary structures and two colours related to redox level (Jelby *et al*. 2022). A detailed SEM study of 22 facies identified in the Boje 2C well found that the microscopic character corresponds to the identified macroscopic sedimentary facies, and only bioturbation and shear deformation were not consistently identified (Fabricius *et al*. 2025). Diagenesis was reflected in the occurrence of calcite-cementation, silicification, pyrite, calcite-rimmed dolomite and more euhedral calcite mud particles with depth (Fabricius *et al*. 2025).

The black marlstones of early Barremian age (BC14, Munk Marl Bed), and of early Aptian age (BC18, Fischschiefer Member), are widely recognized in the North Sea subsurface and used as marker horizons (e.g. Ineson *et al*. 2022a, b); the latter is commonly correlated with the globally recognized OAE1a (Blok *et al*. 2023). In the deep Adda-1 well, the base of the Munk Marl Bed is a fractured, highly bioturbated and cemented hardground indicative of relative sea-level fall followed by laminated, organic-rich marlstone reflecting poorly oxygenated bottom waters (Ineson *et al*. 2022a). The lamination is also reflecting colour banding as shifts in the relative dominance of carbonate (nannofossils and micarb), framboidal pyrite, organic material, and clay (Ineson *et al*. 2022a). The Fischschiefer Member consists of black, finely laminated organic-rich marlstones and is typically 2 to 5 m thick (Ineson *et al*. 2022b). High-resolution clay-mineral assemblage analyses were conducted on the Lower Cretaceous marlstone and chalk of several cores from the Danish Central Graben to evaluate potential source areas of the detrital material, to understand the palaeogeographic evolution and to obtain more information on the climatic evolution during Early Cretaceous in the Boreal Realm (Blok *et al*. 2022, 2023).

In clay-rich marl samples, kaolinite is the dominant clay mineral and calcite particles are separated and embedded in clay (Blok *et al*. 2023). In more calcite-rich samples, the particles are in full contact (Fabricius *et al*. 2025).

The formations represent an overall gradual change from siliciclastic- to carbonate-dominated sedimentation attributed to a regional sea-level rise culminating in the Late Cretaceous eustatic highstand (Michelsen *et al*. 1987; van Buchem *et al*. 2018). An updated depositional model was published identifying four major depositional sequences, recording 20 Myr of transgressive-regressive cycles from 1) late Hauterivian to earliest Barremian highstand (Fig. 1B), 2) early Barremian inversion and lowstand controlled basin-isolation with reduced water circulation (Munk Marl Bed) (Fig. 1C), followed by late Barremian highstand and deposition of clean chalk, 3) latest Barremian lowstand and finally early Aptian transgression (transgression-controlled anoxia during Fischschiefer Member), 4) late Aptian highstand and latest Aptian to earliest Albian lowstand (Jelby *et al*. 2024). The depositional model correlates to the four depositional units identified in the Hauterivian to Aptian Vedsted and Rødby formations in the Danish Basin (Lauridsen *et al*. 2022).

The distribution of kaolinite in the different wells

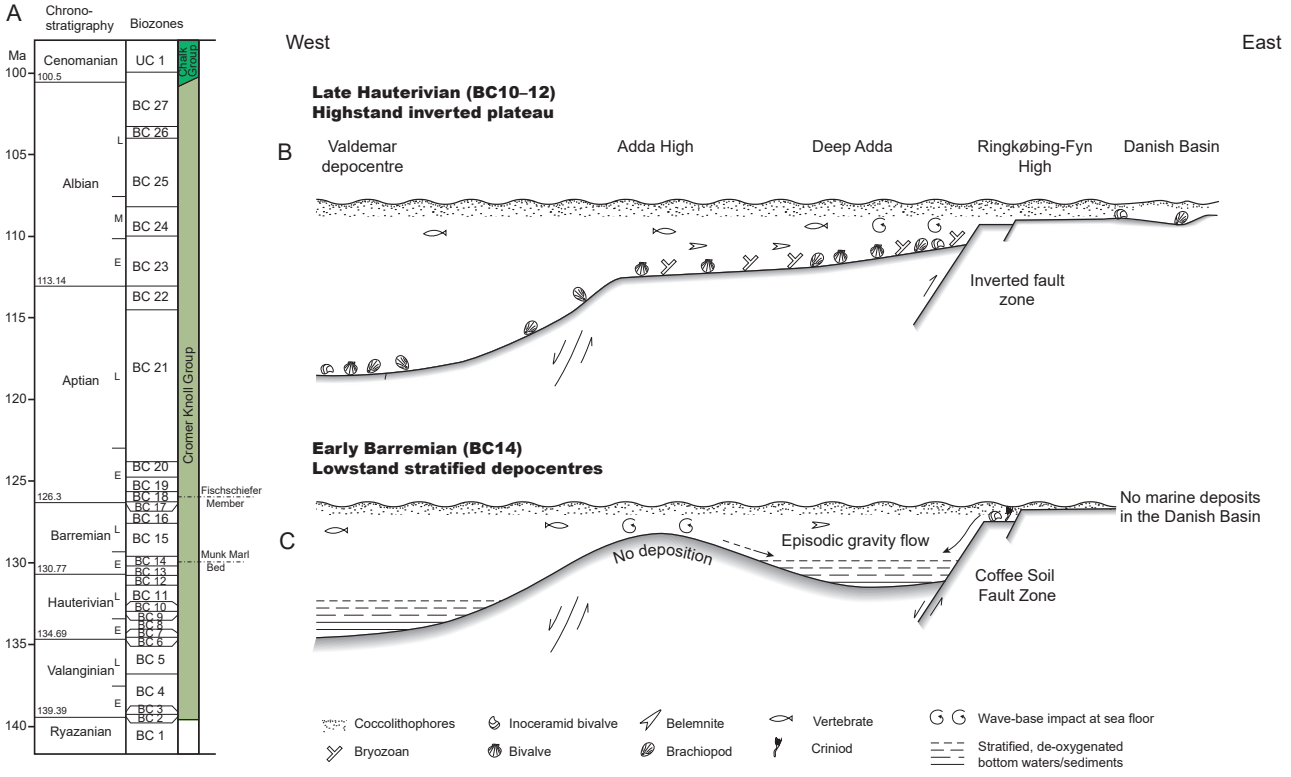


Fig. 1. A. Stratigraphic chart of the Lower Cretaceous Cromer Knoll Group from Jelby *et al*. (2022). The biozones are based on nannofossils. **B-C.** Schematic palaeo-environmental reconstructions of the DCG and Danish Basin contrasting the Late Hauterivian highstand with the earliest Barremian lowstand (modified from Ineson *et al*. 2022a and Lauridsen *et al*. 2022). Note that the different wells studied in the LoCRETA project occur within the Valdemar depocentre (e.g. North Jens-1), the Adda High (Adda-cores), the Deep Adda area (Deep Adda-1) and the Danish Basin (e.g. Vinding-1 and Haldager-1).

suggests a clay source located in the southwestern part of the DCG (Blok *et al*. 2023). The overall decrease in kaolinite in the DCG from the late Hauterivian to the late Barremian indicates a climatic change towards drier conditions with some minor, slightly more humid periods (Blok *et al*. 2023).

Structural geology

Using seismic data for unravelling the pattern of faults and fractures in the Valdemar Field area is relevant, not least for the detection of open fractures that are possible fluid conduits, or conversely sealed clay-bearing fractures that can potentially enclose pressure departments in the petroleum bearing intervals. Results from the PRIORITY research programme (1997–2002) found this task too complex (Madsen & Britze 1999, as cited in Lorentzen *et al*. 2022a), in part due to the limited seismic resolution aggravated by interfering signals from the overlying Upper Cretaceous chalk (Bredesen *et al*. 2021). In order to enhance the information gained from seismic sections and horizons, Lorentzen *et al.* (2022a) used a convolution neural network (CNN) method to map out possible fractures, and concluded that the method could help but not replace manual interpretation.

Another approach to assist seismic interpretation is to calibrate rock physical methods to borehole data. Lorentzen *et al*. (2022b) focused on modelling shear velocity, V_s from P-wave, V_P velocity data. This is relevant because if bulk density, V_P and V_S are known, the elastic moduli can be calculated, and elasticity and composition of pore fluids can be modelled. Lorentzen *et al*. (2022b) used a supervised learning approach and found the results to be possibly more precise than the results from the more conventional rock physical isoframe model. Rock physical interpretation is facilitated when the elastic moduli of the constituting minerals are known. This is of little concern in rocks with simple mineralogy, but for the clay-bearing chalks of Tuxen and Sola formations, the concern is high, and consequently Meireles & Fabricius (2023) developed an isoframe based method for modelling mineral moduli logs from well data, where both V_P and V_S have been measured.

The presence of fractures can be directly observed in borehole image logs or borehole cores. Glad *et al*. (2022) performed a detailed fracture study on cores from the Valdemar Field. They found that the most prevalent fractures are open fractures with plumose structure and hackle marks followed by small-offset shear fractures, shear fractures and rubble zones. Cemented fractures and deformation bands were found to be less dominant. Flow-enhancing fractures were found with the following densities: 7.2/m in chalk, 5.0/m in slightly marly chalk, 3.1/m in marly chalk and 4.8/m in chalky marlstone. No fractures were observed in the marlstones. A substantial number of the fractures seen to be open in cores seem not to be coated with cementing crystals and could thus possibly be closed or absent under reservoir conditions.

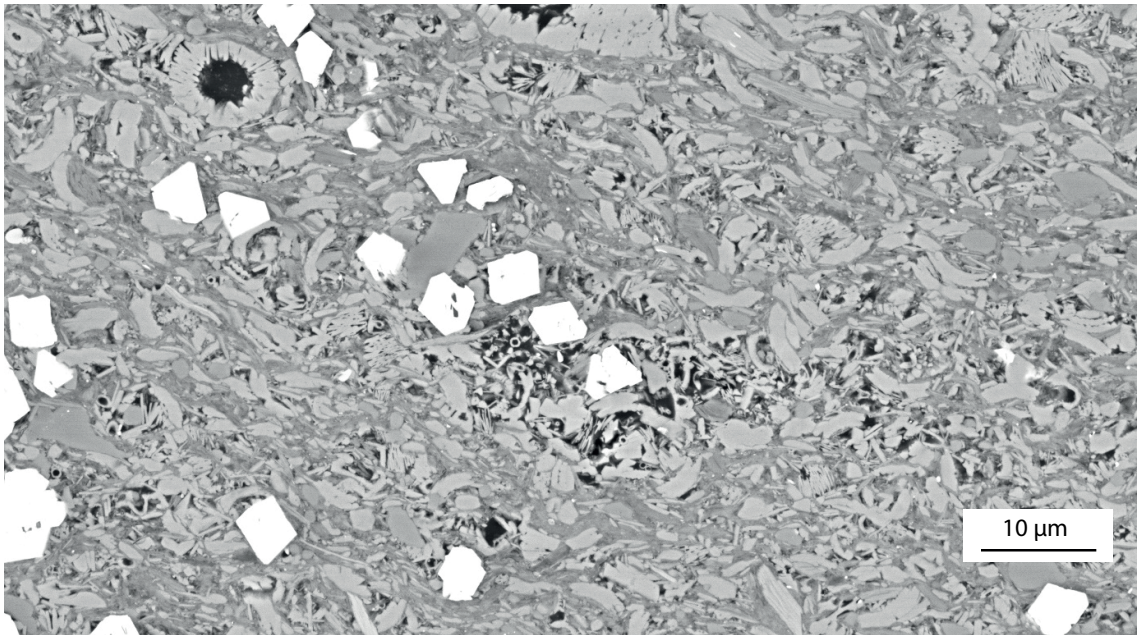


Fig. 2. Backscatter electron micrograph of polished vertical sample from well Boje-2C, 8388'4", Lower Sola Formation. The sample has carbonate content of 79%, porosity of 27% and Klinkenberg permeability of 0.02 mD (Storebø *et al*. 2022a). White crystals are diagenetic pyrite; light grey particles are mainly (?) biogenic calcite, some are recognizable nannoconids. Medium grey distinct particles are quartz silt; darker grey silt-size and clay size particles are mainly detrital kaolinite. Black is porosity, mainly interparticlar, but also intrafossil in nannoconids. The clay is heterogeneously distributed among calcitic particles (Photo: Morten Leth Hjuler).

Petrography and petrophysics

Blok *et al*. (2023) undertook a comprehensive mineralogical study of the Tuxen and Sola formations in the North Jens-1 core. They found a dominating but varying content of calcite and that the non-carbonates primarily constitute covarying quartz and kaolinite. They also identified minor contingents of other clay minerals as well as sporadic occurrence of pyrite and dolomite. Petrographic description of backscatter electron micrographs indicate that the calcite probably primarily forms biogenic micritic particles, some recognisable nannoconids, and rare planktonic microfossils. The quartz and kaolinite represent detrital silt and clay. Porosity is almost exclusively interparticular, although nannoconids contain intrafossil porosity (Fabricius *et al*. 2025; Fig. 2). Probably due to over-pressure, the porosity is high (20–45%) (e.g. Jakobsen *et al*. 2004). These authors noticed that when cross-plotting porosity and insoluble residue, data representing the Sola Formation fall on a 10 p.u. higher trend than data representing the Tuxen Formation. Fabricius *et al*. (2025) noticed a depth-trend in diagenetic recrystallization of calcite, causing the deeper samples into closer packing. This smoothing of particles could cause samples from Tuxen Formation to have lower porosity for a given insoluble residue and higher permeability for a given porosity.

Estimating the content of hydrocarbons from porosity, ϕ, and water saturation, S_w, is a key part of petrophysics. When porosity has been assessed from radioactive logs, water saturation can be derived from electrical resistivity, R_t, by using Archie's equation directly or in modified versions. Archie's equation states $S_w^n = (R_w/(R_t\ \phi^m))$, where R_w is electrical resistivity of the pore water. The parameters m and n can be measured by core analysis. Consistent interpretation of logging data for the Tuxen and Sola

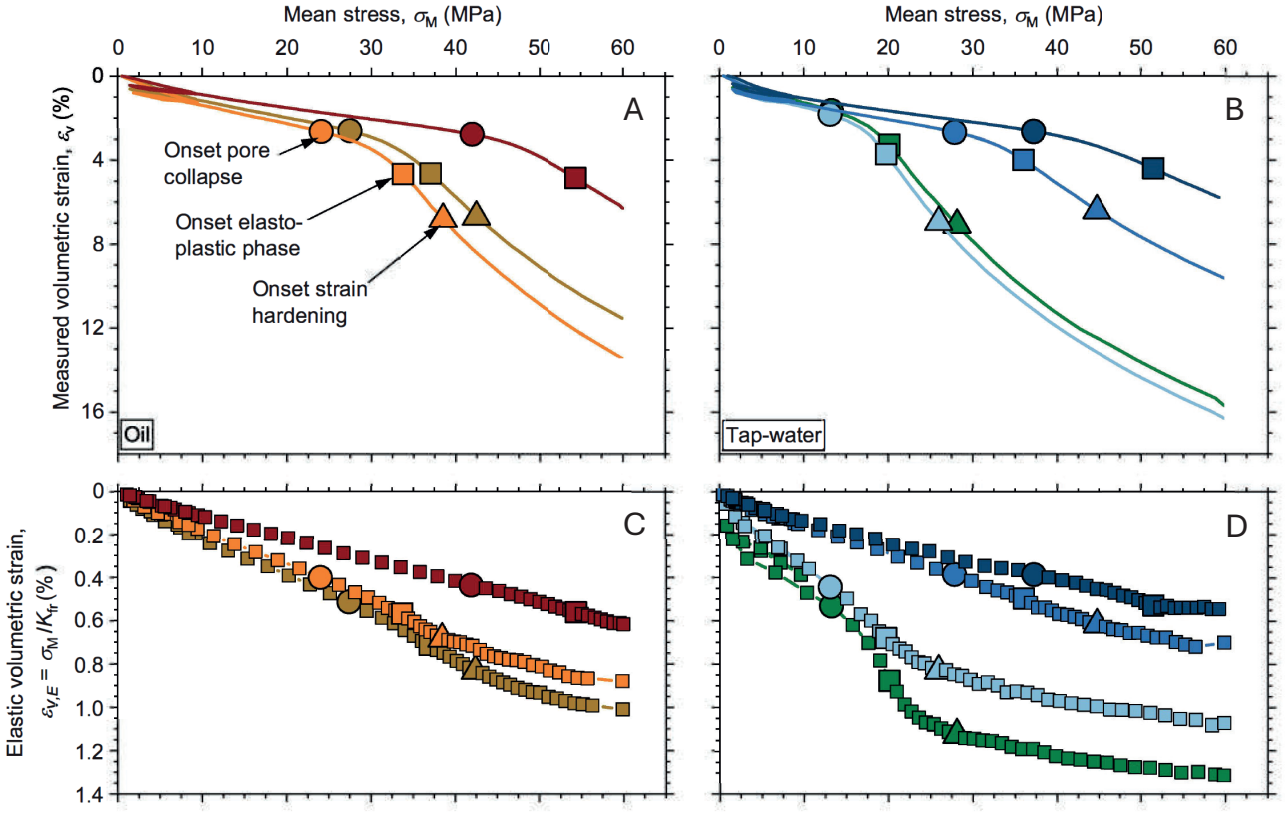


Fig. 3. Results from rock mechanical testing under hydrostatic stress conditions. Pore fluid was drained out of samples during testing. The samples were cut from three horizontal drill cores: 1) dark blue symbols, non-carbonate content 37% and porosity 31%, 2) red and medium blue symbols, non-carbonate content 21% and porosity 37%, 3) olive, orange, green and light blue symbols, non-carbonate content 12% and porosity 44%. **A**. During increasing hydrostatic/mean stress (σ_M) the oil saturated samples deform close to linearly by a volumetric strain, ε_v, until the frame of the rock starts breaking down (Onset pore collapse) at a mechanical strain of 2.5%. When the frame of the samples has practically disintegrated into particles at a strain of *c*. 5% (Onset elastoplastic phase) the increasing stress causes particles into a denser packing. At a mechanical strain of 7% (Onset strain hardening) stress must increase at an increasing rate to cause denser packing. **B**. For water saturated samples we find similar transitions among deformation phases as for the oil saturated samples and at similar strain, but the transitions take place at significantly lower stress for the water saturated samples than the oil saturated samples. **C**, **D**. Strain calculated from elastic wave velocities and mean stress, $\varepsilon_{v,E}$ is markedly lower than mechanically measured strain. (Modified after Orlander & Christensen 2024).

formations has proven difficult; Fabricius *et al*. (2005) accepted water saturations above 100%, whereas Storebø *et al*. (2022b) obtained consistent results by assuming a possibly unrealistically low R_w, and a significant contribution from pyrite to the electrical conductivity. A new approach based on specific surface measured on cuttings or cores was advocated by Proestakis *et al*. (2025) and Proestakis & Fabricius (2025). At the probably relatively high pore water salinity in the studied formations, the specific surface is covered by an adsorbed layer in which the concentration of hydrated ions is so high that it does not conduct the electrical current. When the volume of this adsorbed water is subtracted from the porosity, the water saturation can be calculated by using the theoretical value of m = 1.5.

Rock mechanics

Rock mechanical testing on chalk samples from the Tuxen Formation of the Valdemar Field was done in order to assess possible compaction development during hydrocarbon production. Laboratory tests included hydrostatic stress loading (Orlander & Christensen 2024) as well as loading involving uniaxial strain where axial stress is increased, but lateral strain is prevented by lateral stress-increase (Orlander & Christensen 2025). The tests were done on water saturated samples and on samples saturated with laboratory oil. Testing results led to the new insight that mechanical pore collapse happens at a specific and critical elastic strain of the rock irrespective of porosity or pore fluid (Fig. 3). This finding makes mineralogical sense because calcite supports the rock frame in all samples, so that it is the calcite crystal contacts that break at a critical strain of the calcite crystals.

Strain measured mechanically during testing includes both elastic strain and plastic strain, and before the onset of pore collapse, the plastic strain arises due to closure of microcracks. They are unloading cracks present in rocks that have been exhumed (*e.g*. Glad *et al*. 2024). After pore collapse, plastic strain reflects the particles becoming more densely packed. The stress causing the deformation is transmitted via the elastic strain of the particles, so in order to calculate the elastic strain, elastic wave velocities were measured throughout the testing. When mineralogy and pore fluid composition are known, we can calculate the bulk modulus of the rock frame, K_{fr}, and then elastic strain (Figs 3C, 3D; Orlander & Christensen 2024). Under hydrostatic conditions, pore collapse happens at an elastic strain of 0.4% (Figs 3C, 3D), and under uniaxial strain conditions, pore collapse happens at an elastic strain of 0.2–0.25% (Orlander & Christensen 2025). This focus on elastic strain is relevant for assessing the risk of pore collapse from logging data. A simple methodology for this assessment is given in Fabricius & Meireles (2025).

Although the onset of pore collapse is controlled by a given elastic strain irrespective of pore fluid, the collapse happens at significantly lower stress when the chalk is water saturated, than when it is oil saturated (Fig. 3). This so called "water weakening" has been noticed by numerous workers, but the present study shows that in terms of strain, the chalk is not weaker when water saturated.

Acknowledgements

We gratefully acknowledge the Danish Underground Consortium (TotalEnergies E&P Denmark, Noreco and Nordsøfonden) for granting permission to publish this work. The study was funded by the Danish Offshore Technology Centre (DTU Offshore). Tobias Orlander, Geo, is thanked for rock mechanical information (Fig. 3). Tobias Orlander, Ermis Proestakis and Michael Welch are thanked for constructive comments on parts of the manuscript.

References

Blok, C., Ineson, J., Anderskouv, K., Fantasia, A., Sheldon, E., Thibault, N., Jelby, M.E., Adatte, T. & Bodin, S. 2022: Latitude-dependant climate changes across the Aptian Oceanic Anoxic Event 1a. Palaeogeography, Palaeoclimatology, Palaeoecology 601, 111085. https://doi.org/10.1016/j.palaeo.2022.111085

Blok, C.N., Adatte, T., Ineson, J.R., Sheldon, E., Jelby, M.E., Smit, F.W.H., Lauridsen, B.W., Anderskouv, K. & Bodin, S. 2023.: Clay mineral assemblages as a tool in source-to-sink studies: an example from the Lower Cretaceous of the North Sea Basin. Bulletin of the Geological Society of Denmark 71, 99–113. https://doi.org/10.37570/bgsd-2023-71-06

Bredesen, K., Lorentzen, M., Nielsen, L. & Mosegaard. K. 2021: Quantitative seismic interpretation of the Lower Cretaceous reservoirs in the Valdemar Field, Danish North Sea. Petroleum Geoscience 27, 2021-016, 17 pp. https://doi.org/10.1144

Fabricius, I.L. & Meireles, L.P.T. 2025: Assessment of pore collapse in North Sea Lower Cretaceous carbonates using downhole elastic strain. Bulletin of the Geological Society of Denmark 71, 115–125. https://doi.org/10.37570/bgsd-2025-71-07.

Fabricius, I.L., Olsen, C. & Prasad, M. 2005: Log interpretation of marly chalk, the Lower Cretaceous Valdemar Field, Danish North Sea: application of iso-frame and pseudo water film concepts. The Leading Edge 24, 496–505.

Fabricius, I.L, Hjuler, M.L., Jelby, M.E. & Anderskouv, M. 2025: Microscopic character of the Lower Cretaceous Tuxen and Sola Formations in the Boje-2C well, central North Sea. Bulletin of the Geological Society of Denmark 71, 127-159. https://doi.org/10.37570/bgsd-2025-71-08

Glad, A.C., Amour, F., Welch, M.J., Clausen, O.R., Anderskouv, K., Ineson, J.R., Sheldon, E. & Nick, H.M. 2022: Natural fractures and discontinuities in a Lower Cretaceous chalk-marlstone reservoir, Valdemar Field, Danish North Sea. Marine and Petroleum Geology 136 105445. https://doi.org/10.1016/j.marpetgeo.2021.105445

Glad, A.C., Afrough, A., Amour, F., Ferreira, C.A.S., Price, N., Clausen, O.R. & Nick, H.M. 2023: Anatomy of fractures: Quantifying fracture geometry utilizing X-ray computed tomography in a chalk-marl reservoir; the Lower Cretaceous Valdemar Field (Danish Central Graben). Journal of Structural Geology 174, 104936. https://doi.org/10.1016/j.jsg.2023.104936

Glad, A.C., Orlander, T., Fabricius, I.L., Clausen, O.R. & Clemmensen, L.B. 2024: Characteristics and formation of natural fractures in a silica-rich chalk, Coniacian Arnager Limestone Formation, Bornholm, Denmark. Bulletin of the Geological Society of Denmark 73, 157–173. https://doi.10.37570/bgsd-2024-73-09

Ineson, J.R. 1993: The Lower Cretaceous chalk play in the Danish Central Trough. In: Parker, J.R. (Ed.), Petroleum Geology of Northwest Europe: Proceedings of the 4th Conference. Petroleum Geology Conference Series. Vol. 4. Geological Society, London, pp. 175–183. https://doi.org/10.1144/0040175.

Ineson, J.R., Lauridsen, B.W. Lode, S., Sheldon, E., Sørensen, H.O., Wisshak, M. & Anderskouv, M. 2022a: A condensed chalk-marl succession on an Early Cretaceous intrabasinal structural high, Danish Central Graben: implications for the sequence stratigraphic interpretation of the Munk Marl Bed. Sedimentary Geology 440, 106–234. https://doi.org/10.1016/j.sedgeo.2022.106234

Ineson, J.R., Petersen H.I., Andersen, C., Bjerager, M., Jakobsen, G.C., Kristensen, L., Mørk, F. & Sheldon, E. 2022b: Early Cretaceous stratigraphic and basinal evolution of the Danish Central Graben: a review. Bulletin of the Geological Society of Denmark 71, 75–98. https://doi.org/10.37570/bgsd-2022-71-05

Jakobsen, F., Ineson, J.R., Kristensen, L. & Stemmerik, L. 2004: Characterization and zonation of a marly chalk reservoir: the Lower Cretaceous Valdemar Field of the Danish Central Graben. Petroleum Geoscience 10, 21–33.

Jelby, M.E., Ineson, J.R., Thibault, N., Bodin, S., Blok, C.N., Edvardsen, N., Clemmensen, T.S., Buls, T. & Anderskouv, K. 2022: Facies and depositional processes of Lower Cretaceous carbonates, Danish Central Graben. Bulletin of the Geological Society of Denmark 71, 51–74. ISSN 2245-7070. https://doi.org/10.37570/bgsd-2022-71-04

Jelby, M.E., Ineson, J.R., Sheldon, E. & Anderskouv, M. 2024: Old chalk, new tricks: revisiting the Lower Cretaceous carbonates of the Danish Central Graben. In Hart et al. (Eds). Cretaceous Project 200 Volume 2: Regional Studies. Geological Society, London, Special Publications, 545, 1–25. https://doi.org/10.1144/SP545-2023-134

Lauridsen, B.W., Lode, S., Sheldon, E., Frykman, P., Anderskouv, K. & Ineson, J. 2022: Lower Cretaceous (Hauterivian–Aptian) pelagic carbonates in the Danish Basin: new data from the Vinding-1 well, central Jylland, Denmark. Bulletin of the Geological Society of Denmark 71, 7–29. https://doi.org/10.37570/bgsd-2022-71-02

Lorentzen, M.C.L., Bredesen, K., Smit, F.W.H., Hansen, T.H., Nielsen, L. & Mosegaard, K. 2022a: Mapping Cretaceous faults using a convolutional neural network – A field example from the Danish North Sea. Bulletin of the Geological Society of Denmark, 71, 31–50. ISSN 2245-7070. https://doi.org/10.37570/bgsd-2022-71-03

Lorentzen, M., Bredesen, K., Mosegaard, K. & Nielsen, L. 2022b: Estimation of shear sonic logs in the heterogeneous and fractured Lower Cretaceous of the Danish North Sea using supervised learning. Geophysical Prospecting 70, 1410–1431. https://doi.org/10.1111/1365-2478.13252

Madsen, L. & Britze, P. 1999: PRIORITY - Improved oil recovery and productivity from Lower Cretaceous Carbonates – EFP- 97. Sub-project 1.4.a: Seismic interpretation of the Cretaceous in the Valdemar Area. The Geological Survey of Denmark and Greenland.

Meireles, L.T.P. &. Fabricius, I.L. 2023: Deriving mineral moduli of the noncarbonate fraction in a marly chalk reservoir using petrophysical logging data and an isoframe model. Geophysics 88, D411-D425. https://doi.org/10.1007/s00603-025-04691-6

Michelsen, O., Frandsen, N., Holm, L., Jensen, T.F., Møller, J.J. & Vejbæk, O.V. 1987: Jurassic - Lower Cretaceous of the Danish Central Trough; – depositional environments, tectonism, and reservoirs. Danmarks Geologiske Undersøgelse, Serie A, 16, 44 pp. https://doi.org/10.34194/seriea.v16.7035

Orlander, T. & Christensen, H.F. 2024: Compaction phases and pore collapse in Lower Cretaceous chalk – insight from Biot's coefficient. Rock Mechanics and Rock Engineering. https://doi.org/10.1007/s00603-024-03963-x

Orlander, T. & Christensen, H.F. 2025: Elastic and plastic deformation of Lower Cretaceous North Sea Chalk during stress and time-dependent uniaxial strain compaction. Rock Mechanics and Rock Engineering. https://doi.org/10.1007/s00603-025-04691-6

Proestakis, E., Meireles, L.T.P. & Fabricius, I.L. 2025: Complex conductivity of diatomites and chalks. Geophysics 90, M181-M202. https://doi.org/10.1190/geo2024-0372.1

Proestakis, E. & Fabricius, I.L. 2025: Log interpretation for petrophysical and elastic properties of fine-grained sedimentary rocks. Petrophysics.

Rudra, A., Sanei, H., Nytoft, H.P., Petersen, H.I., Blok, C., Bodin, S. & Bojesen-Koefoed, J.A. 2021: Organic matter characterization of the Lower Cretaceous tight reservoirs in the Danish North Sea. International Journal of Coal Geology 238, 103714. https://doi.org/10.1016/j.coal.2021.103714

Storebø, E., Hjuler, M.L. & Fabricius, I.L. 2022a: Permeability modeling in clay rich carbonate reservoir. Petrophysics 63, 141 – 170. https://doi.org/10.30632/PJV63N2-2022a2

Storebø, E.M., Hjuler, M.L., Meireles, L.T.P. & Fabricius, I.L. 2022b: Effect of pyrite in water saturation evaluation of clay-rich carbonate. Petrophysics 63, 172–198. https://doi.10.30632/PJV63N2-2022a3

van Buchem, F.S.P., Smit, F.W.H., Buijs, G.J.A., Trudgill, B. & Larsen, P.H. 2018: Tectonostratigraphic framework and depositional history of the Cretaceous-Danian succession of the Danish Central Graben (North Sea) – new light on a mature area. In: Bowman, M., Levell, B. (Eds.), Petroleum Geology of NW Europe: 50 Years of Learning – Proceedings of the 8th Petroleum Geology Conference. https://doi.10.1144/PGC8.24

Lower Cretaceous (Hauterivian–Aptian) pelagic carbonates in the Danish Basin: new data from the Vinding-1 well, central Jylland, Denmark

BODIL W. LAURIDSEN, STEFANIE LODE, EMMA SHELDON, PETER FRYKMAN, KRESTEN ANDERSKOUV & JON INESON



Geological Society of Denmark
https://2dgf.dk

Received 12 November 2020
Accepted in revised form
5 July 2021
Published online
17 May 2022

© 2022 the authors. Re-use of material is permitted, provided this work is cited. Creative Commons License CC BY: https://creativecommons.org/licenses/by/4.0/

Lauridsen, B.W., Lode, S., Sheldon, E., Frykman, P., Anderskouv, K. & Ineson, J. 2022: Lower Cretaceous (Hauterivian–Aptian) pelagic carbonates in the Danish Basin: new data from the Vinding-1 well, central Jylland, Denmark. Bulletin of the Geological Society of Denmark, Vol. 71, pp. 7–29. ISSN 2245-7070. https://doi.org/10.37570/bgsd-2022-71-02

Understanding of the shallow shelf system in the Danish Basin during the Early Cretaceous has benefitted significantly from studying the previously overlooked Hauterivian–Aptian section of the Vedsted Formation of the Vinding-1 drill core. The presence of chalks in this section demonstrates that carbonate-rich pelagic sediment accumulated locally in the siliciclastic-dominated Danish Basin and that benthic carbonate production was insignificant. The area was not a carbonate platform in the Early Cretaceous and does not indicate any reworked carbonate supply from platform environments in the vicinity. The scarcity of benthic macrofossils in the cored section is due to the lack of a specialised boreal chalk fauna at that time, and the adjacent nearshore environment apparently did not support any substantial benthic carbonate production. A revised biostratigraphy of the cored section is presented based primarily on calcareous nannofossils, supported by foraminifera, ostracods, and belemnites. Four lithofacies describe the spectrum from marlstone to slightly marly chalk, and the facies succession characterises four depositional units recording two discrete transgressive–regressive cycles. The study provides a depositional record that permits sequence stratigraphic correlation to the Valdemar and Adda Fields in the Central Graben.

Keywords: Danish Basin, Lower Cretaceous, chalk and marl, old wells, biostratigraphy.

Bodil W. Lauridsen [bwl@geus.dk], Geological Survey of Denmark and Greenland (GEUS), Øster Voldgade 10, DK-1350 Copenhagen K, Denmark. Stefanie Lode [stefanie.lode@ntnu.no], Department of Geoscience and Petroleum, Norwegian University of Science and Technology, Postbox 8900, NO-7491 Trondheim, Torgarden, Norway. Emma Sheldon, [es@geus.dk], GEUS. Peter Frykman [pfr@geus.dk], GEUS. Kresten Anderskouv [ka@ign.ku.dk], Department of Geosciences and Natural Resource Management, Øster Voldgade 10, DK-1350 Copenhagen K, Denmark and Jon Ineson [ji@geus.dk], GEUS.

Hauterivian–Aptian chalks of the Tuxen and Sola Formations in the Danish Central Graben, North Sea, are important both due to their hydrocarbon reservoir potential (Copestake *et al.* 2003; Jakobsen *et al.* 2004, 2005; van Buchem *et al.* 2017), and from a palaeoecological and palaeoceanographic point of view as a unique Early Cretaceous precursor to the Late Cretaceous chalk sea of northern Europe (Ineson 1993; Ineson *et al.* 1997; Mutterlose 1998; Bischoff & Mutterlose 1998; Löb & Mutterlose 2012; Mutterlose & Bottini 2013).

Renewed focus on these Lower Cretaceous carbonate reservoirs has underlined the requirement for detailed predictive models of this complex layered heterogeneous chalk–marl reservoir (e.g., van Buchem *et al.* 2017) and this demands a refined depositional and palaeogeographical understanding of the successions. Central to the understanding of the carbonate component of the dual carbonate–siliciclastic system are the relative roles of pelagic and benthic carbonate production in the accumulation of reservoir-quality

chalks in the Central Graben. In addition to a detailed study of the carbonates of the Tuxen and Sola Formations, a better understanding of the regional palaeogeography is required to assess the potential role of benthic carbonate production in the shelf regions bordering the Central Graben. In particular, the eastern parts of the Danish Basin may potentially have exported significant carbonate sediment to the Danish Central Graben (Fig. 1). In this context, vintage exploration wells in the Danish Basin were screened and investigated, focussing particularly on wells with significant cored sections in the Lower Cretaceous Vedsted Formation.

The aim of this paper is to present a previously overlooked cored Hauterivian–Aptian carbonate-rich section of the Vedsted Formation from the Vinding-1 well and to correlate the sequences to the Central Graben.

Geological and stratigraphic setting

Danish Basin

The intracratonic Danish Basin is separated from the stable Precambrian Baltic shield by the Fennoscandian Border Zone to the north-east and bounded by the Ringkøbing –Fyn High towards the south (Fig. 1). The basin comprises a Permian to Cenozoic sedimentary succession formed due to Late Carboniferous to Early Permian crustal extension followed by subsidence controlled by thermal cooling and local faulting (Sorgenfrei & Buch 1964; Nielsen 2003). Subsidence accelerated during the Late Jurassic and the depositional area gradually increased in size and depth (Vejbæk 1989, 1997). Previous studies have suggested that continuous deposition is recorded in the north-western part of the Danish Basin from the Late Jurassic to the Early Cretaceous, with hiati recorded along the boundaries of the basin (Larsen 1966). A general shallowing of the basin towards the Ringkøbing –Fyn High characterised the same period (Nielsen 2003). Halokinetic related movements affected the Danish Basin from the middle to the Late Triassic. The Sorgenfrei –Tornquist Zone was repeatedly reactivated during the Triassic, Jurassic and Early Cretaceous, although movement was minor compared to the tectonic events of the Late Carboniferous to Early Permian and the Late Cretaceous (Mogensen & Korstgård 2003).

From the Valanginian to the early Barremian, the Central Graben and the Danish Basin experienced an overall sea-level rise and the climate generally became more arid, and consequently less siliciclastic material entered the area (Ruffell 1991; Ineson 1993; Hardenbol *et al.* 1998; Mutterlose 1998; Copestake *et al.* 2003; Haq 2014, van Buchem *et al.* 2017). By the late Hauterivian to early Barremian, pelagic carbonate production was dominant in areas remote from clastic input and in sediment starved zones. Some beds contained nannoconids (a group of calcareous nannofossils) and coincide with increased nutrient and clay input connected to short-term sea-level falls and greenhouse conditions (Mutterlose 1998; Copestake *et al.* 2003; Löb & Mutterlose 2012; Mutterlose & Bottini 2013).

The Barremian to Aptian boundary is marked by a major change in the palaeoceanographic setting caused by a widespread transgression that altered marine circulation patterns and was probably linked to an increase in sea-floor spreading rate that peaked in the early Aptian (Ruffel 1991; Mutterlose 1998; Copestake *et al.* 2003). During the Aptian, several transgressions and regressions characterised the Danish Basin and new seaways between the Tethys and the Boreal Realm opened via northern France and southern England (Mutterlose & Böckel 1998). These palaeoceanographic changes from restricted marginal seas to widespread homogenous pelagic-dominated seas resulted in the extinction of various floral and faunal elements in the Tethyan and Boreal realms followed by the evolution of new genera and species (Mutterlose 1998).

Lower Cretaceous stratigraphy

The Vedsted Formation of the Danish Basin spans the Valanginian to Albian and is named after the Vedsted-1 borehole in Jylland (Larsen 1966; Table, 1). The lower boundary of the Vedsted Formation coincides with the transition from marine silty clay to less silty clay (Larsen 1966). The Rødby Formation, which overlies or in some places was possibly deposited at the same time as the upper part of the Vedsted Formation, consists of marine red marlstones and marly chalks (Table, 1). Its base is suggested to be late Aptian or early Albian in age in the Danish Basin (Sorgenfrei & Buch 1964).

The lower part of the Vedsted Formation is equivalent to the Valhall Formation in the Danish Central Graben (Table 1). The upper Vedsted Formation is time-equivalent to the Tuxen Formation (Hauterivian to late Barremian; Heilmann-Clausen 1987; Thomsen 1987), the succeeding Sola Formation (late Barremian to early Albian; Jensen *et al.* 1986) and the Rødby Formation (from late Aptian, Sorgenfrei & Buch 1964 mainly in the Albian, Heilmann-Clausen 1987 to possibly early Cenomanian, Jensen *et al.* 1986).

To the east, Danish Lower Cretaceous deposits outcrop on Bornholm and include latest Ryazanian to

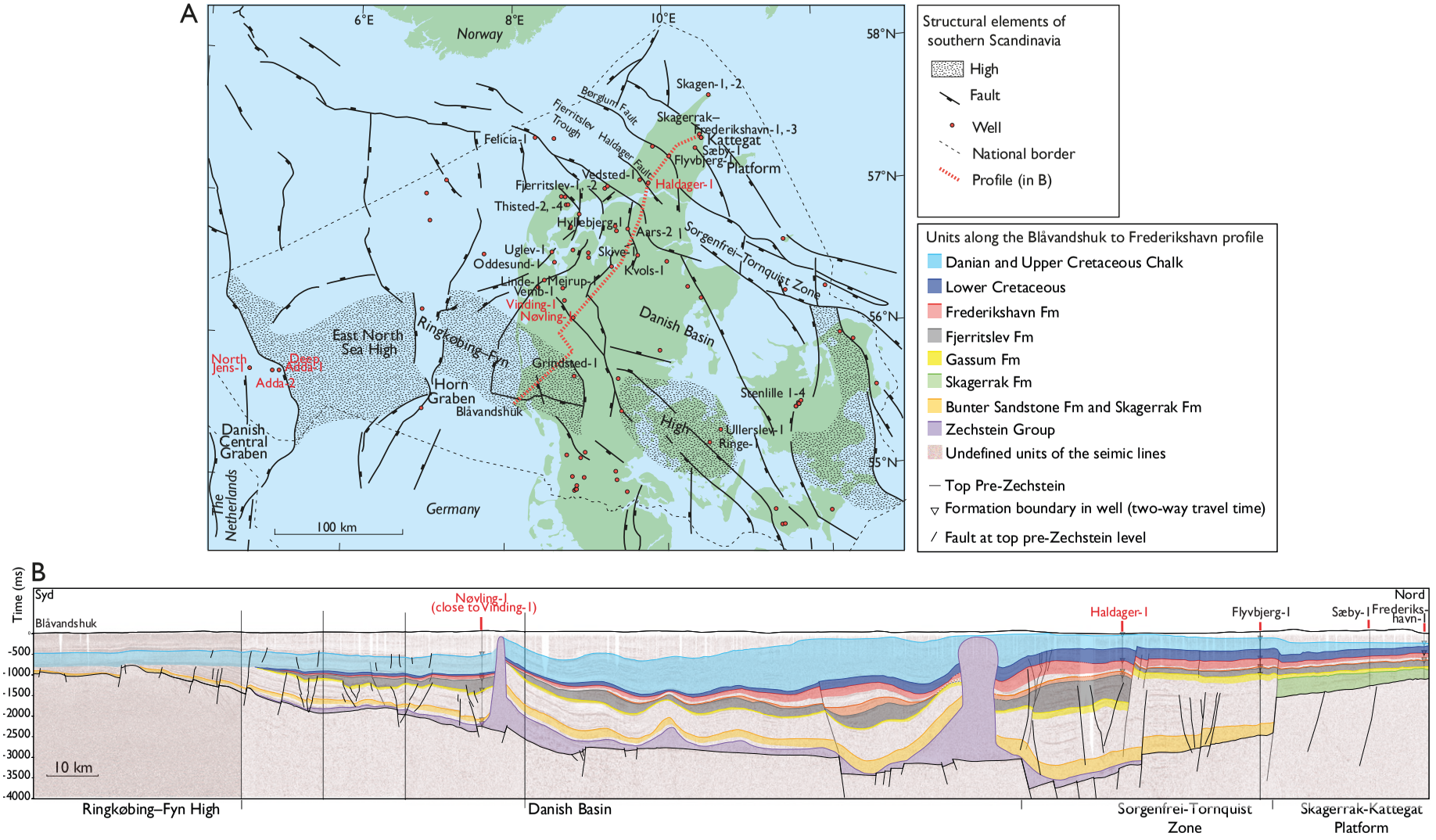


Fig. 1. A: Map of the Danish Basin highlighting the relevant wells, structural highs, faults, and the location of the profile illustrated in B. The Vinding-1, Haldager-1 and Nøvling-1 wells under focus here are indicated in red. The North Jens, Adda-2 and Deep Adda wells from the Danish Central Graben mentioned in the text are also shown in red. **B:** Seismic profile from Blåvandshuk in the south to Frederikshavn in the north (Vosgerau *et al.* 2016); the location of the profile is indicated in Fig. 1A. The profile is derived from the geothermal potential maps at https://dybgeotermi.geus.dk and used with permission. Lower Cretaceous is shown in dark blue. Nøvling-1 is close to Vinding-1 and they both appear on the same side of the fault.

Table 1. Stratigraphy and main lithologies of the onshore Lower Cretaceous in North-west Europe compared to Vinding-1 from the Danish Basin.

		Stage	Formations: Danish Central Graben	Formations: Danish Basin	Vinding-1	Denmark (outcrops)	NW Germany (outcrops)	Helgoland, Dünen Island (partly outcropping)	NE England (outcrops)	S England (outcrops)
Lower Cretaceous	**Albian**	late	Rødby Fm		Chalk				Poorly lithified mudstones and calcareous mudstones. Greensand common around the Aptian/Albian boundary	
		early				*Ammonites of early Albian age in the Lower Cenomanien Arnager Greensand conglomerate indicate previous deposits on Bornholm*	Condensed section			
	Aptian	late	Sola Fm	Vedsted Fm			Dark laminated clays	Laminated dark clays (Fishschiefer) and pale clays		Sandstone and grey clay
		early			Marly chalk, slightly marly chalk and marlstone					
	Barremian	late					Finely laminated clay	Dark grey clays and marly clays	Clay and marl beds, mid-Barremian Cementstone	Dark grey to black laminated clays and marls beds, mid-Barremian cementstone
		early	Tuxen Fm		Marly chalk					
	Hauterivian	late			Glauconitic marlstone and marlstone		Clay		Clay	
		early	Valhall Fm		Silt and sandy shale					
	Valanginian	late			*Not studied*		Clay, sandstone horizons and sideritic nodules		Phosp nodule bed	
		early	Leek Mb							
	Berriasian/ Volgian	late	Mandal Fm	Frederikshavn Fm/ Børglum Fm		Sand, silt and clay with plantfragments	Mud, sandstone and coal		Clay, ironstone, nodular beds	
		early								

The upper Vedsted Formation is time equivalent to the Tuxen Formation, the succeeding Sola Formation and the Rødby Formation in the Danish Central Graben. Outcrops of Lower Cretaceous age in Denmark are rare. Early Albian on Bornholm are in italics because the unit is only confirmed as early Albian ammonites in a Cenomanian conglomerate. The north-west Germany data are from Ruffel (1991); Mutterlose (1992); Mutterlose & Böckel (1998); Löb & Mutterlose (2012). The lower Albian is represented by a condensed section and the upper Albian is not present in Germany (Ruffel 1991; Vejbæk et al. 2010). Data on Dünen Island, Helgoland, are from Bishoff & Mutterlose (1998). Data from Speeton, NE England are from Ruffel (1991).

earliest Valanginian nearshore and terrestrial deposits of the Rabekke, Robbedale and Jydegård Formations (Gravesen *et al.* 1982; table 1). These formations are older than the North Sea Tuxen and Sola formations and are possibly time-equivalent with the lowermost Vedsted Formation. In southern Sweden, Lower Cretaceous strata (50–300 m thick) are encountered in deep boreholes in fault-bounded basins. These Valanginian to Hauterivian deposits are dominated by argillaceous sandstones, locally calcareous and rich in glauconite and phosphate (Lindström & Erlström 2011). The Arnager Greensand Formation crops out on Bornholm; the lower part comprises a phosphatic conglomerate that contains reworked nodule clasts yielding a rich early Albian ammonite fauna enclosed in a glauconitic sandstone matrix containing a foraminifera and ammonite fauna suggesting a Cenomanian age (Kennedy *et al.* 1980). This indicates that the Bornholm area was transgressed in earliest Albian time and the deposits were subsequently eroded, phosphatised and relict clasts deposited during a subsequent transgression in the Cenomanian (Kennedy *et al.* 1980). There is no record on Bornholm of deposits from the Barremian–Aptian period.

Vinding-1 well

Brief well history

The Vinding-1 well was only the second deep-test well drilled in the Danish Basin. It was drilled in 1947 and is situated to the south-east of Holstebro (08°41′56″E and 56°17′26″N; Fig. 1). The cored section from 4615′–4262′ (1409.7 to 1299.1 m) spanning cores 25 to 29 (Fig. 2) is Early Cretaceous in age according to Fazekas (1947). The present study focuses on the 4278′–4262′ interval (1303.9 to 1299.1 m) of core 25. Geological descriptions of Vinding-1 are found in an unpublished completion report (Fazekas 1947). The report can be downloaded from GEUS' homepage (frisbee.geus.dk, search for Vinding).

Measurements of the $CaCO_3$ content of the Lower Cretaceous deposits were carried out using the titration method (Fazekas 1947). $CaCO_3$ content ranges from 1–13% in beds older than late Hauterivian and 42– 69% in the lowermost Barremian part (Fig. 2). In the lower Aptian strata, the $CaCO_3$ content ranges from 62–82% and in the upper Albian from 79–88%.

Planktonic and benthic foraminifera were identified for biostratigraphic purposes at the drill site (Fazekas 1947). Ammonites from 4406′6″–4399′ dated this interval as being of early Hauterivian age (Fazekas 1947). O.B. Christensen identified the ostracods in the late 1960s, but the data were never published or included in any of the existing databases at the Geological Survey of Denmark and Greenland (GEUS). Identifications were written directly onto the microscope slides and these notes have been incorporated into the present study.

Chronostratigraphy

Early work carried out on Vinding-1 suggested the presence of 452′ (137.8 m) of Lower Cretaceous deposits as follows: 'Neocomian' (old term for Berriasian, Valanginian and partly Hauterivian) from 4707′–4540′ (1434.7–1383.8 m), Hauterivian from 4540′–4280′ (1383,8–1304,5 m), lower Barremian from 4280′–4277′ (1304.5–1303.6 m) and upper Albian from 4277′–4255′ (1303.6–1296.9 m; Fazekas 1947). The lack of upper Barremian, Aptian, lower and middle Albian was believed to be due to a regional unconformity based on correlation with several other cores in the Danish Basin (Larsen 1966).

The present study confirms the presence of Hauterivian strata from 4540′–4280′ in Vinding-1 and

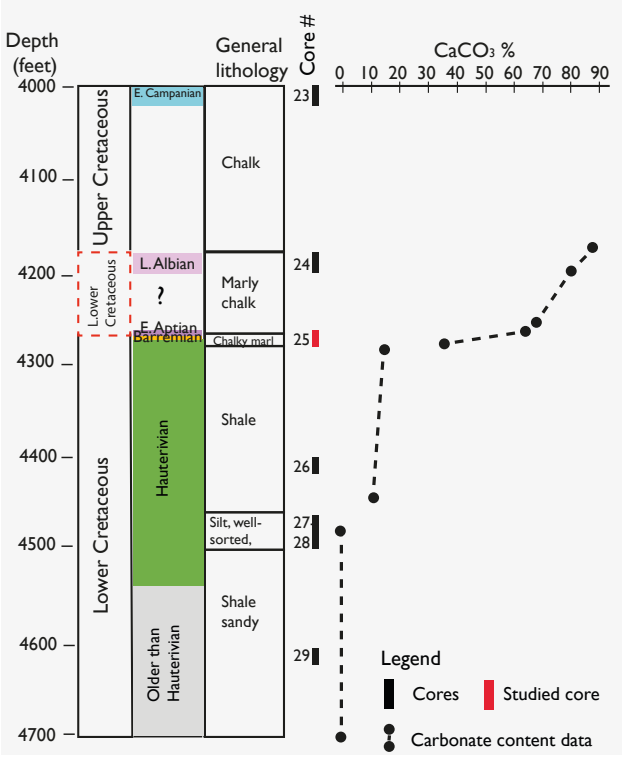
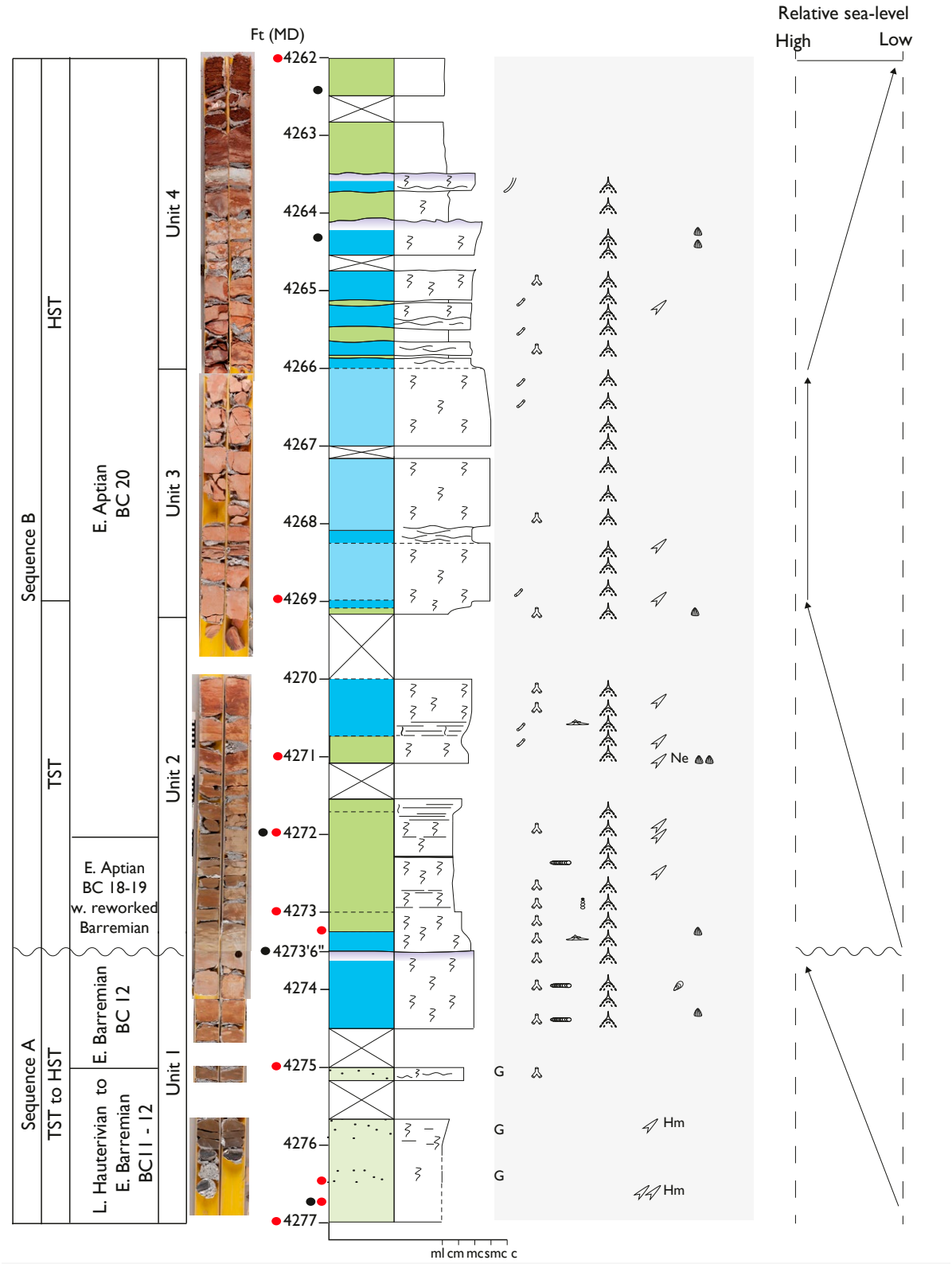


Fig. 2. Revised dating (new Aptian and Albian data from Lower Cretaceous; previously dated as Santonian), general lithology (from the original core descriptions) and $CaCO_3$ content of the Lower Cretaceous and the lower part of the Upper Cretaceous of the Vinding-1 well. The $CaCO_3$ content was analysed in nine selected samples (Fazkas 1947).


Relative sea-level
High
Low
Ft (MD)
4262
4263
4264
4265
4266
4267
4268
4269
4270
4271
4272
4273
4273'6"
4274
4275
4276
4277
Sequence B
HST
TST
Sequence A
TST to HST
E. Aptian BC 20
E. Aptian BC 18-19 w. reworked Barremian
E. Barremian BC 12
L. Hauterivian to E. Barremian BC11 - 12
Unit 4
Unit 3
Unit 2
Unit 1
Ne
G
G
G
Hm
Hm
ml cm mc sm c
Lithofacies
LF4 Slightly marly chalk
LF3 Marly chalk
LF2 Glauconitic marlstone
LF1 Marlstone
G Glauconite
SEM sample (black)
Nannofossil sample (red)
Bed boundaries
Well-defined
Diffuse/ gradational
Non deposition and erosion
Structures
Structureless
Intense bioturbation
Weak bioturbation
Parallel lamination (primary)
Wavy/irregular solution seams
Hardground/firmground
Trace fossils
Skolithos
Planolites
Thalassinoides
Taenidium
Zoophycos
Teichichnus
Chondrites
Macrofossils
Belemnite
Hm, Hibolites minutus
Ne, Neohibolites ewaldi
Brachiopod
Bivalve

a succession older than Hauterivian from 4707′–4540′, as previously suggested (Fazkas 1947). However, a revised interpretation of the Barremian, Aptian and Albian successions is presented here based on new nannofossil biostratigraphy and previously unpublished foraminifera and ostracod biostratigraphic data. The revised data suggest upper Hauterivian to lower Barremian from 4277–4275′ (1303,6–1303 m); lower Barremian at 4274′ (1302,7 m); lower Aptian from 4273′2″–4262′ (1302.5–1299.1 m) and upper Albian deposits from 4195′–4180′ (1278.6–1274.1 m; Fig. 2). The revised ages are discussed in the paragraph on biostratigraphy and palaeoecology. Our new data suggest a revised thickness of the Lower Cretaceous in Vinding-1 of at least 512′ (156.1 m), since neither the Lower to Upper Cretaceous boundary nor the Upper Jurassic to Lower Cretaceous boundaries are confirmed in this study. Beds with the revised age of late Albian in this study were previously dated as Santonian (Fazekas 1947).

Unfortunately, wireline log data do not exist for the Vinding-1 well. In the original studies only a general lithological description of the Lower Cretaceous succession based on cuttings along with measured $CaCO_3$-percentages were produced (Fig. 2).

Material and methods

The original Vinding-1 material consists of rock samples, cuttings, and prepared microfossil samples (ostracods and foraminifera, both benthic and planktonic) and is generally of good quality. The newly slabbed core from 4277′–4262′ (15′ or 4.57 m; Fig. 3) is important for improving our understanding of the Lower Cretaceous strata of the Danish Basin and for comparison with the Danish Central Graben.

The seven original foraminifera slides have been restudied for the 4277′–4260′ interval. Ostracod taxonomy undertaken by O.B. Christensen has been reviewed in this study and compared with published data of Neale (1973) and Slipper (2009). Ten new nannofossil samples were selected from a variety of facies for the present study (Fig. 3). Nannofossil smear slides were prepared using the techniques described by Bown & Young (1998) and analysed using a Leica DM 2500 P microscope, applying the simple relative abundance counting technique. The BC nannofossil zonation scheme of Bown *et al.* (1998) and the LK scheme of Jeremiah (2001) were applied. Additional nannofossil identification was carried out using scanning electron microscope (SEM) images.

A detailed core description was made at a scale of 1:5 for the 4277′–4262′ (1303.6–1299.1 m). The core had 94% recovery (Fig. 3). Macrofossils were identified directly from the core material and trace fossils were described from the slabbed core surface.

Polished slabs embedded in epoxy were made for scanning electron microscopy (SEM) studies of selected facies. The SEM laboratory at GEUS is equipped with a ZEISS Sigma 300VP field emission SEM, which uses a Bruker energy dispersive x-ray (EDX) analytical system. High-resolution backscattered electron (BSE) images were obtained from selected representative samples. Selected sites on the samples were chosen for SEM-EDX spot micro-analysis and element mapping including identification of the different clay minerals. For all analyses, SEM parameters remained constant and a set of fixed magnifications were used to provide optimal conditions for comparative studies of textures, nannofossils and mineralogy.

Biostratigraphy and palaeoecology

Nannofossils

Ten core samples were collected for nannofossil biostratigraphy from the 4277′–4262′ interval (Fig. 4). The samples were taken from red and olive-green marlstone, chalky marlstone, marly chalk and from slightly marly chalk lithologies.

The samples generally reveal high abundance and diversity nannofossil assemblages. The stratigraphically lowermost samples (4277′–4275′) are dominated by *Watznaureria barnesiae* and *Zeugrhabdotus noeliae*. *Zeugrhabdotus scutula* and *Assipetra infracretacea* are consistently present. A late Hauterivian to early Barremian (BC11–12, LK21–20D) age is indicated, tentatively supported by the absence of *Nannoconus abundans*, the marker species for the overlying nannofossil zone (Fig. 4).

A single sample at 4274′ is dated as BC12 (LK20D; early Barremian) based on the co-occurrence of *Assipetra terebrodentarius, Nannoconus pseudoseptentrionalis* and *Rhagodiscus pseudoangustus* and the absence of

◀ **Fig. 3.** Sedimentological log of Vinding-1, including core photos and distribution of facies, structures, trace fossils and macrofossils. The abbreviations: ml is marl, cm is chalky marl, mc is marly chalk, smc is slightly marly chalk and c is chalk. The units and the relative sea-level changes refer to the depositional history explained in the text. The biozones are based on nannofossils. The samples taken for nannofossil biostratigraphy are indicated by the red dots and for detailed SEM studies with black dots.

Fig. 4. Nannofossil biostratigraphic distribution chart (percentage distribution) for the late Hauterivian to early Aptian of the Vinding-1 well. Thickness of blue boxes indicates relative proportion (percentage) of each taxa in each sample. In addition, palaeoenvironmental indicators are grouped as percentages of the whole nannofossil assemblage. Nannoconids - green, coastal indicators - lilac, warm water indicators - red, high fertility indicators - orange.

the marker for BC13 (*N. abundans)*. A single specimen of *Rhagodiscus gallagheri* (FO in the early Aptian) was recorded. Given the consistent Barremian floral assemblage, and sedimentological continuity with the underlying core (see description below), this rare record of an Aptian affinity is considered an artefact, probably due to sample contamination or bioturbation.

The sample at 4273.17′/4273′2″ (Fig. 4) comprises a mixed nannofossil assemblage with elements from the Barremian or older (*Ethmorhabdus hauterivianus*, *Perissocyclus plethotretus*, *Micrantholithus brevis*) and those indicative of the Aptian (*Rhagodiscus gallagheri*, *Lithraphidites houghtonii*). It is interpreted as being early Aptian in age, BC18–19 (LK13–14) with reworked older material. This is compatible with the position of the sample immediately above a hardened, erosional surface (Figs 4; 9).

The samples from 4272′–4262′ include *Broinsonia signata*, *Grantarhabdus coronadventis*, *Radiolithus laingii*, *Flabellites oblonga*, *Rhagodiscus angustus*, *Braarudospahera hockwoldensis*, *Lithraphidites morayfirthensis*, *Lithraphidites houghtonii* and common *Rhagodiscus gallagherii*, dating this section as early Aptian (BC20, LK13).

The biostratigraphic data indicate a hiatus between 4274′ and 4273′ 2″ spanning mid to late Barremian zones BC13 to BC17 (LK20C–15).

Foraminifera, ostracods and macrofossils

The low diversity and high abundance foraminifera assemblage of the 4272′–4262′ interval was originally dated as Albian and an early–middle Barremian age was assigned to the 4277′– 4272′ level (Fazekas 1947). The original foraminifera slides have been restudied in the current project and the biostratigraphic results of these support the present nannofossil biostratigraphy. *Lenticulina muensteri* and *Gavelinella sigmoicosta* in the sample from the 4278′–4275′ interval indicate an early Barremian age. *Hedbergella delrioensis*, and *Hedbergella planispira* together with *Gavelinella barremiana* in the sample from the 4260′–4265′ interval suggest an early Aptian age.

A Barremian age is assigned to the 4277′1″–4276′7″ interval due to occurrences of the ostracod *Cythereis acuticostata* (Neale 1973). *Pontocyriella rara* is assigned an Aptian and Albian age and dates the 4272′5″–4262′ interval (Slipper 2009). *Pontocyriella rara* is assigned an Aptian and Albian age and date the 4272′5′–4262″ interval (Slipper 2009). A Barremian age is assigned to the 4277′1″–4276′7″interval due to occurrences of *Cythereis acuticostata* (Neale 1973). The following species were also found in the 4277′–4262′ interval: *Eocytheropteron* sp., *Schuleridea* sp., *Neocythere* (*Physocythere*) sp., *Eucythere* sp., but none of them have any biostratigraphic relevance. The ostracod data thus supports the nannofossil biostratigraphy.

Three specimens of the belemnite *Hibolithes minutus* were found in the marlstone from 4277′–4276′ (Fig. 5A) indicating an early Barremian to earliest Aptian age (Mutterlose 1998; Alsen & Mutterlose 2009). The *H. minutus* occurring in Vinding-1 is believed to represent the Barremian dwarf morphotype as described by Alsen & Mutterlose (2009). *H. minutus* is recorded from the Barremian beds of the Speeton Clay (Rawson & Mutterlose 1983). A specimen of the belemnite *Neohibolites ewaldi* (Stolley 1911) was found in the marlstone at 4271′1″ (Fig. 5B). This earliest Aptian to early late Aptian species (Mutterlose 1998) has a wide distribution in north-western Europe (Mutterlose 1992; Mutterlose & Wiedenroth 2009; Malkoc *et al*. 2010). Other belemnites encountered in the core from 4276′6″ to 4262′ are too fragmented to identify. The belemnite data support the nannofossil ages.

Palaeoecology

Nannofossils, foraminifera and belemnites are included in the palaeoecological analysis. The samples from 4277′–4275′ display high abundances of the nannofossil *Zeugrhabdotus noeliae* suggesting relatively high nutrient levels in the surface waters. However, species richness remains relatively high (17–25) indicating that surface waters were not eutrophic (Fig. 4). From 4274′–4269′, *Z. noeliae* is very low in abundance indicating oligotrophic surface waters at this level. *Rhagodiscus asper* (a warm-water indicator) remains stable, with low values throughout the section (Fig. 4). *Micrantholithus* spp. are suggested to be coastal indicators; these are only found in low numbers attesting to the relative offshore location of Vinding-1 during the Barremian to Early Aptian (Fig. 4).

Samples 4278′–4275′, 4275′–4270′ and 4270′–4265′ are conspicuous by the absence of planktonic foraminifera and their diverse calcareous benthic fauna including *Lenticulina* spp., *Dentalina* spp., *Conorboides* spp., *Saracenaria* spp. and common *Gavelinella* spp. A

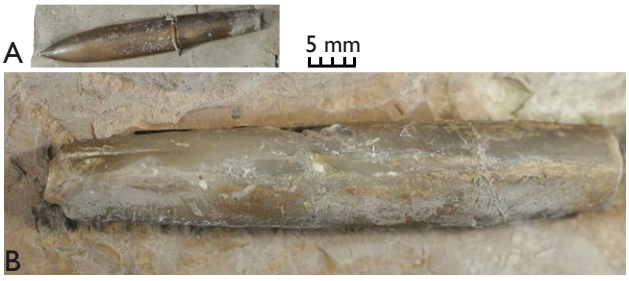
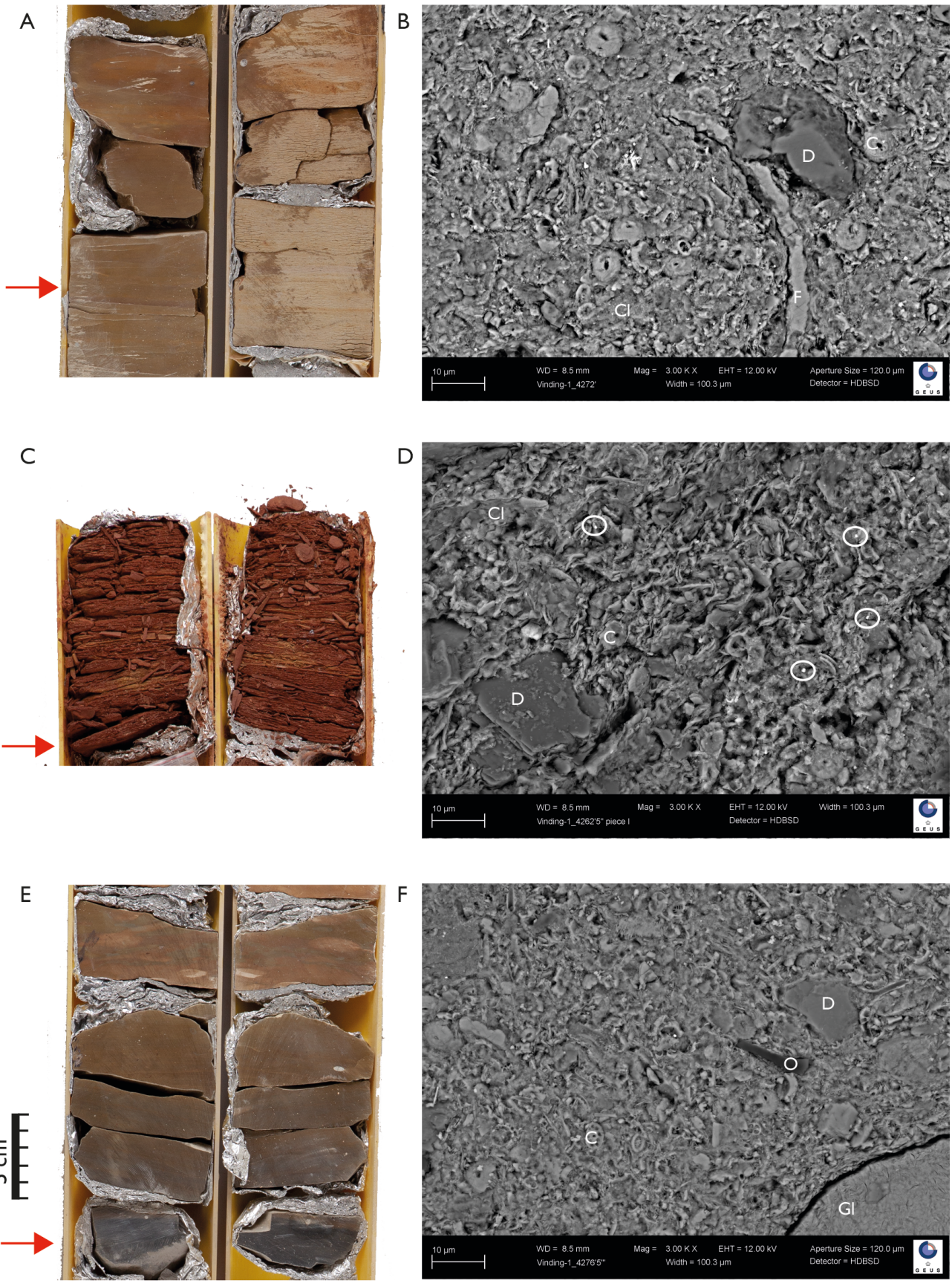


Fig. 5. A: *Hibolithes minutus* at 4276′6″–4277′. **B:** Fragments of possible *Neohibolites ewaldi* at 4271′1″.


A
B
C
D
E
F
5 cm
Cl
C
D
F
O
Gl
10 µm
WD = 8.5 mm
Vinding-1_4272'
Mag = 3.00 K X
Width = 100.3 µm
EHT = 12.00 kV
Aperture Size = 120.0 µm
Detector = HDBSD
Vinding-1_4262'5" piece I
Vinding-1_4276'5"

lack of planktonic foraminifera can be attributed to very shallow water depths (e.g. Gibson 1989), but in the Vinding-1 well case, facies analysis suggests that this explanation is unlikely. These samples contain *Gavelinella* spp. and *Lenticulina* spp. whose relatively common occurrence indicates well oxygenated sea-floor conditions and open marine circulation (King *et al.* 1989, Koutsoukos *et al.* 1990). It is therefore suggested that the paucity of planktonic formaminfera is probably not a primary signal but may be due to dissolution of their fragile tests compared with the more robust tests of benthic foraminifera (Nguyen *et al.* 2009).

Gavelinella spp. and *Lenticulina* spp. occupied epifaunal and shallow infaunal habitats and their relatively common occurrence indicates well oxygenated sea-floor conditions (Koutsoukos *et al.* 1990).

Samples from 4265'–4260' include the planktonic foraminifera *Hedbergella delrioensis* and *Hedbergella planispira*. These are indicative of open marine but relatively shallow water, marginal epicontinental seas, with water depths of less than 100 m (Leckie 1987). This sample also contains the benthic foraminifera *Arenobulimina* spp. and *Gavelinella* spp, suggesting open circulation with oxygenated botttom waters (King *et al.* 1989).

The presence of the Tethyan belemnite genus *Neohibolites* represented by *N. ewaldi* in Vinding-1 represents a signal of the early Aptian sea-level rise recorded globally, as discussed in the introduction, and as indicated locally by the cored section (see below). The early Aptian is described as a period of marked turnover, from the belemnite family Oxyteuthididae to the belemnite genus *Neohibolites* (Mutterlose 1998).

Facies analysis and depositional history

The 15 ft (4.57 m) thick cored section is composed of four lithofacies that together describe the spectrum from marlstone to slightly marly chalk (Fig. 3). The occurrence of these facies in the cored section defines four depositional units recording two discrete transgressive–regressive cycles.

Lithofacies

LF1 Marlstone

This facies ranges from dark greenish-grey to deep brick-red in colour and includes both marlstone and chalky marlstone lithologies (Fig. 6A–D). It dominates units 2 and 4; the marlstone facies either passes gradually into marly chalk (LF3, Fig. 3, unit 2), or is interbedded with marly chalk on a scale of 2–15 cm, with abrupt boundaries (Fig. 3, unit 4). Though typically thoroughly bioturbated, primary horizontal lamination is evident in places, particularly in unit 2. *Chondrites* is the dominant ichnofossil in the marlstone facies, often a diminutive form with a diameter of 0.2–0.5 mm; *Thalassinoides*, *Taenidium* and *Planolites* are present in places, particularly in chalky marlstones at the transition into the marly chalk facies. Previous studies have measured a relative $CaCO_3$ content of 35–62% (Fazkas 1947). Glauconite grains occur locally. Macrofossils are rare and only belemnites of the species *Neohibolites ewaldi* and indeterminable brachiopods have been found.

Microscopically, the facies has a high clay content of predominantly smectite to illite and a detrital mineral content of quartz, K-feldspar, rutile and mica (Fig. 6B, D). The amount of coccolithic debris and other fossil fragments is relatively small. Finely distributed hematite is abundant, locally colouring this facies red, and appears also as larger grains (Fig. 6D). Pyrite is absent and carbonate cement is rare. The facies is slightly compacted and in parts porous.

LF2 Glauconitic marlstone

This facies is restricted to the lower two feet of the core (Fig. 3; 4277–4275'), which are unfortunately fragmentary and not fully recovered. It includes marlstone and chalky marlstone and differs from LF1 by its content of very fine sand – silt and abundant glauconite grains in the sand fraction (Fig. 6E–F). The facies is varicoloured,

◀ **Fig. 6.** Core photographs and SEM micrographs of marlstone (LF1) and glauconitic marlstone (LF2) facies. Note that the annotations on the SEM micrographs only indicate one example of each component: coccolith (C), foraminifera (F), detrital grains (D), clay (Cl), glauconite (Gl), organic matter (O). The scale bar is applicable to all core pieces. **A, B:** Yellow brown chalky marl (SEM level 4272', location indicated by red arrow on core photo). Completely bioturbated with local lamination. Finely distributed clay (Cl; predominantly smectite–illite) and glauconite are common, carbonate cement is rare. **C, D:** Dark red marl (SEM level 4262' 5'', location indicated by red arrow on core photo); often appears bioturbated but lamination locally recognisable. The facies has a high clay and detrital mineral content and only small amounts of fragmented coccoliths. Finely distributed haematite (white circles) contributes to the red colour. **E, F:** Green-grey glauconitic marl (SEM from 4276'10'', location indicated by red arrow on core photo). The bioturbation is intense and the lamination absent weak lamination occurs in places. Glauconitic grains are present macro- and microscopic. The clay and detrital mineral contents are moderately high and the coccoliths are well preserved.

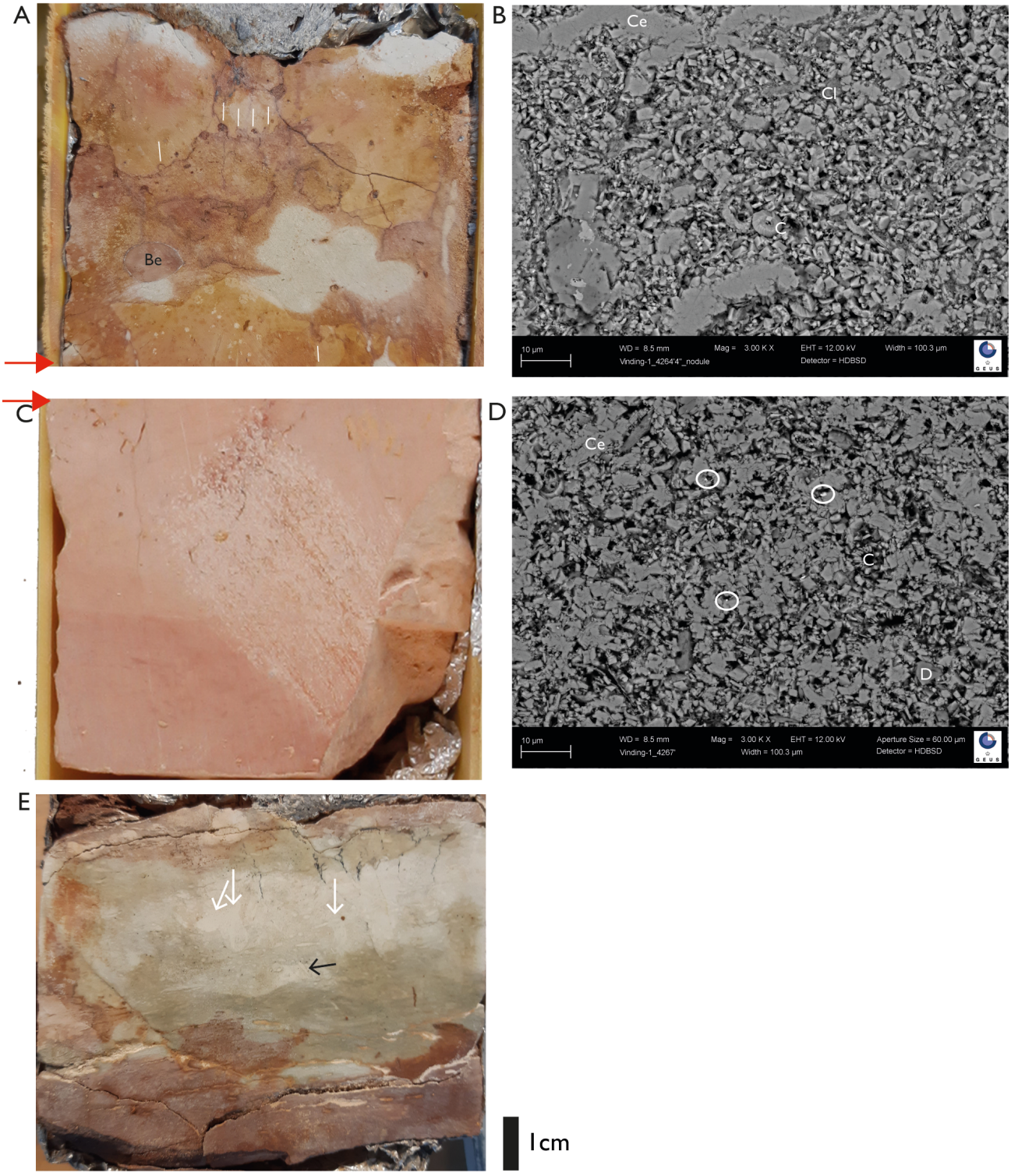


Fig. 7. Core photographs and SEM micrographs of the marly chalk (LF3; A, B, E) and slightly marly chalk (LF4; C, D) lithofacies. Note that the annotations on the SEM micrographs only indicate one example of each component; coccolith (C), cement (Ce), detrital grains (D), and clay (Cl), The scale bar is applicable to all core pieces. **A, B**: Marly chalk (SEM from 4264'4", location indicated by red arrow on core photo). The sample is completely bioturbated with many cross-cutting burrows. Irregular chalk nodules occur locally (4264'2") and are bored in places (indicated by white lines). The nannofossils (C) are well preserved but fragmented. Clay (Cl) is rare. Carbonate cement (Ce) is common. **C, D:** Slightly marly chalk (SEM from 4267', location indicated by red arrow on core photo). The sample appears very homogenous and completely bioturbated. The red colour is due to finely distributed hematite (marked with white circles). The nannofossils (C) are strongly recrystalised and chalk cement (Ce) is common. Detrital grains (D) are rare. **E:** A hardground developed in marly chalk at level 4263'6". The hardground appears completely bioturbated, vertical burrows (*Skolithos?;*white arrows) occurs locally. *Chondrites is* also common (black arrow).

from dark greenish grey to olive green-grey, locally mottled with reddish patches. The relative $CaCO_3$ content of this facies is approximately 33%, as measured in the previous study (Fazkas 1947). Lamination is absent and the structureless nature is probably due to thorough bioturbation; discrete trace fossils are rare, however. Macrofossils are predominantly belemnites of the dwarf species *Hibolithes minutus*, bivalves and vertebrate fragments.

Microscopically, the facies differs from the marlstone facies with respect to the presence of abundant micron to mm-sized grains of glauconitic and phosphatic-calcitic composition and abundant framboidal and euhedral pyrite (Fig. 6F). Some organic material is also preserved. The clay and detrital mineral contents are lower than in LF1, but still moderately high. The coccoliths are well preserved.

LF3 Marly chalk

This lithofacies ranges in colour from dark red to reddish mid-brown, locally pale yellowish brown (Fig. 7A–B). Well-defined ichnofabrics are developed with prominent *Thalassinoides*, *Planolites* and *Taenidium* traces, though *Chondrites* networks dominate overall. *Zoophycos* is also possibly present. *Skolithos* occurs at a hardground at level 4263'6'' (Fig. 7E). *Chondrites* occurs both as diminutive forms, < 0.5 mm in diameter, in the background marly chalk, but also as larger forms (1–2 mm diameter) within the fill of *Thalassinoides*. The clay component is disseminated in the marly chalk facies in the lower half of the section (below 4270') but commonly forms discrete solution seams in the upper core (Fig. 3). Locally, nodular chalk fabrics, hardgrounds, and erosional surfaces (Figs 8A–B, E; 9) occur. The irregular nodules have microscopic borings indicating exposure on the sediment surface (Fig. 7A). The inferred hardground and major hiatus at 4273'6'' is clearly observed at the macroscopic scale (Fig. 8A–B). However, in the SEM the change across the boundary is insignificant and observed as an increase in nannofossils (including nannoconids) and a change from small clay grains in between the coccolithic debris to larger pieces of clay in the youngest sample (Fig. 8E). The relative $CaCO_3$ content is 69–80% measured in a previous study (Fazkas 1947). Macrofossils are indeterminable belemnites, brachiopods and pectinid bivalves.

Microscopically the marly chalk is homogenous and relatively porous with a high preservation of coccoliths and coccospheres. Carbonate cement is common. Clays are finely distributed; no pyrite and only little hematite was encountered.

LF4 Slightly marly chalk

This facies forms a discrete interval (4269'–4266') of pale reddish pink, homogeneous chalk that is completely bioturbated (Fig. 7C–D). *Chondrites* traces are observed throughout, distinguished by their slightly darker fill. Deformation bands ('hairline fractures') are common in this cleaner chalk facies. Fazkas (1947) reported a relative $CaCO_3$ content of more than 80% in this lithology. Indeterminable belemnites are found.

Microscopically, the slightly marly chalks are very homogenous and more porous than the marly chalks (Fig. 7D). The nannofossils are strongly recrystalised and carbonate cement is common. The facies contains very little clay and quartz. Finely distributed hematite colours the facies red.

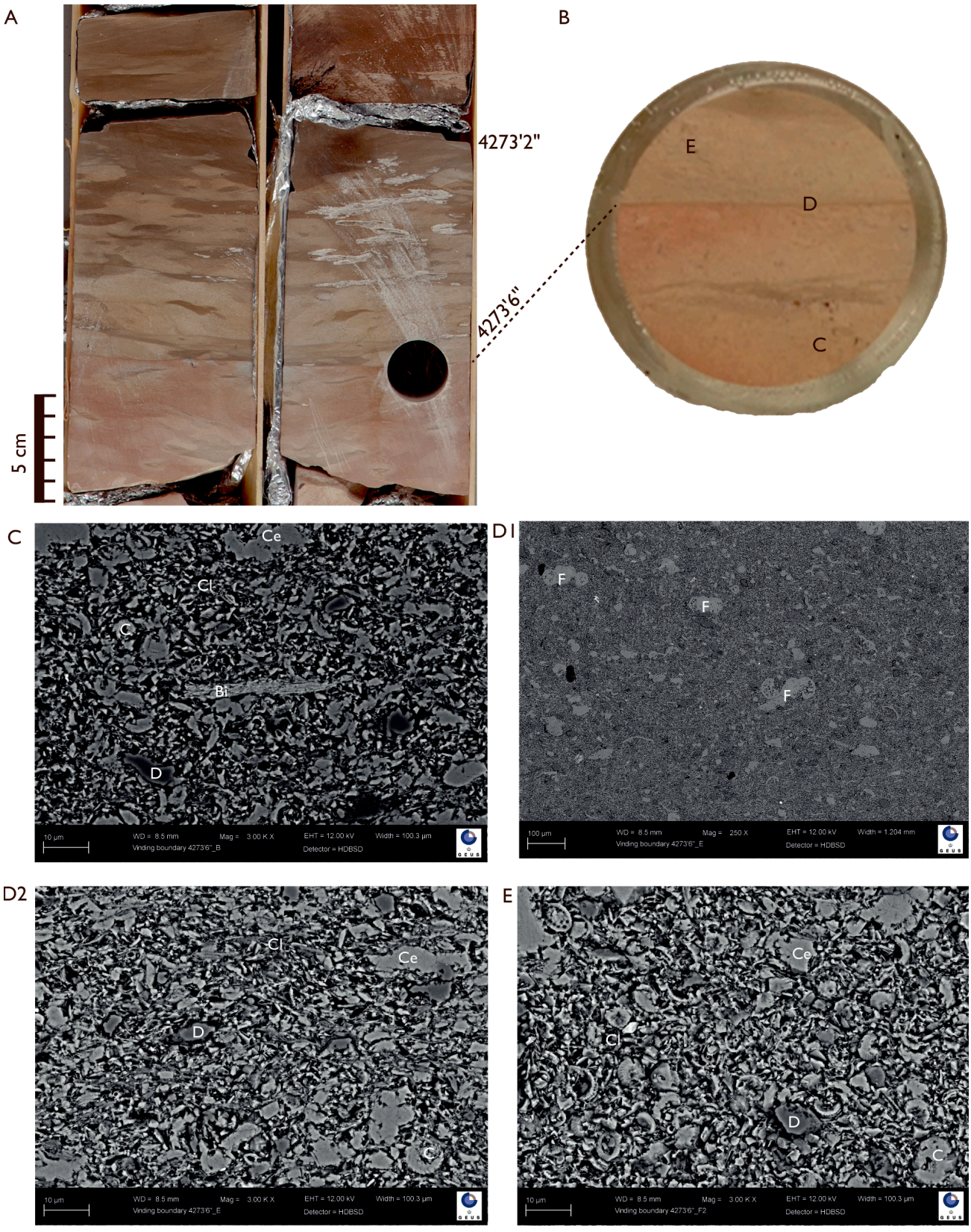
Facies succession and depositional history

The four lithofacies described above (Fig. 3) record a marine depositional environment in which the pelagic production of carbonate sediment was significant, at times dominating over the hemipelagic supply of mud in this setting in the central part of the Danish Basin. The alternation of clay-rich and clay-poor facies, constrained by the integrated biostratigraphic data, allows us to infer the sea-level history of this condensed Hauterivian–Aptian section and to relate this to the evolution of the wider North Sea region.

Unit 1 (4277'–4273'6''; late Hauterivian, BC11–12 to early Barremian, BC12)

Although the lower levels of the core are fragmentary, the existing material shows an upward transition from sandy, glauconitic marlstone (LF2) to bioturbated marly chalk (LF3), capped by an erosion surface. This transition from LF2 to LF3 is accompanied by an upward increase in the density and diversity of trace fossils. Lamination is locally weakly preserved in the glauconitic marlstones, but the scarcity of depositional structures overall suggests a bioturbated fabric. The succeeding marly chalk, in contrast, shows a complex well-defined biogenic fabric of cross-cutting *Thalassinoides*, the fill of which is re-burrowed by *Taenidium* and *Chondrites*. Intervening 'matrix' chalk is crowded by diminutive *Chondrites* networks. The capping erosional surface abruptly truncates the biogenic fabric of the marly chalk (Fig. 8). It has a gently scoured relief of a few millimetres and a thin dark, red-stained coating (< 1 mm thick). Possible borings were locally noted at this surface, but not confirmed in the SEM.

Interpretation. The gradual shift from hemipelagic


A
4273'2"
4273'6"
5 cm
B
E
D
C
C
Ce
Cl
C
Bi
D
10 µm
WD = 8.5 mm
Mag = 3.00 K X
EHT = 12.00 kV
Width = 100.3 µm
Vinding boundary 4273'6"_B
Detector = HDBSD
D1
F
F
F
100 µm
WD = 8.5 mm
Mag = 250 X
EHT = 12.00 kV
Width = 1.204 mm
Vinding boundary 4273'6"_E
Detector = HDBSD
D2
Cl
Ce
D
C
10 µm
WD = 8.5 mm
Mag = 3.00 K X
EHT = 12.00 kV
Width = 100.3 µm
Vinding boundary 4273'6"_E
Detector = HDBSD
E
Ce
Cl
D
C
10 µm
WD = 8.5 mm
Mag = 3.00 K X
EHT = 12.00 kV
Width = 100.3 µm
Vinding boundary 4273'6"_F2
Detector = HDBSD

siliciclastic mud-dominated to pelagic carbonate mud-dominated sedimentation is suggestive of a relative rise in sea-level resulting in drowning and/or lateral translation of sediment sources and basinal facies belts (Fig. 3). Alternatively, a decrease of run-off can also be due to a shift towards more arid conditions. This change is also in accordance with the change to a more arid climate during the period, as reported in the literature (e.g. Ineson 1993; Copestake *et al.* 2003). The ubiquity of glauconite grains in the marlstone facies is indicative of a reduced background sedimentation rate in this setting (e.g. Odin & Matter 1981), and the complex cross-cutting and biogenically reworked ichnofabric in the marly chalk facies records increasing condensation (e.g., Taylor *et al.* 2003). The dominance of the living chambers (*Thalassinoides*) of an active epifauna in the upper marly chalks may reflect an increasingly favourable benthic environment as hemipelagic siliciclastic mud supply decreased. The erosional surface capping unit 1 corresponds to an inferred hiatus accounting for much of the Barremian stage (see discussion under biostratigraphy) and records a significant relative sea-level fall. It is not clear whether the erosional processes were submarine or subaerial in nature, though the absence of evidence of meteoric diagenesis on the subjacent carbonates favours submergent, shallow-marine processes. Staining and potential boring of the erosional surface, and the nature of the trace fossil fabric in the succeeding sediments, following but never penetrating the surface, is indicative of a hardened, cemented horizon, possibly a marine hardground.

Unit 2 (4273'6''–4269'; early Aptian (BC18–19, with reworked Barremian) and early Aptian (BC20))

This interval comprises a thin basal marly chalk bed (LF 3) that grades rapidly up into a marlstone package (LF1) that dominates the unit. The carbonate component increases upwards and chalky marls and marly chalks dominate the upper levels (Fig. 3). Incomplete core recovery obscures much of the upper part of the unit. The marly chalks and chalky marlstones show a more diverse trace fossil assemblage, characterised particularly by *Thalassinoides*, whilst the marlstones though often fully bioturbated, exhibit an impoverished *Chondrites* ichnofauna. As noted earlier, the burrows immediately above the basal erosion surface follow but never penetrate the surface. Primary lamination is noted locally, particularly in the marlstone facies.

Interpretation. Marly chalks and marlstones in the lower 6 inches of the unit, immediately above the stained erosional surface, yielded an enigmatic biostratigraphic result, showing diagnostic nannofossil elements of several Barremian biozones (BC14–17) in addition to Early Aptian taxa (BC 18–19; see biostratigraphy above). Given the gradational, conformable transition upwards into marlstones that give a consistent early Aptian (BC20) age, it is considered likely that the lowermost bed is of early Aptian age (BC18–19) but contains a range of reworked Barremian nannofossils deposited during the initial onlap of the eroded surface. The upward transition to facies rich in pelagic carbonate (upper unit 2, unit 3) is indicative of progressive deepening, following the initial onlap (Fig. 3).

Unit 3 (4269'–4266', early Aptian, BC20)

This unit comprises a uniform succession of pink, slightly marly chalk (LF4), interbedded locally with thin marly chalk beds (LF3; Figs 4; 8C–D). The chalk is intensively bioturbated though recognisable trace fossils are largely restricted to *Chondrites*.

Interpretation. This metre-thick interval of clay-poor chalk of early Aptian age is indicative of an essentially uninterrupted period of pelagic carbonate accumulation, with limited dilution by siliciclastic mud. It prob-

◀ **Fig. 8**. Core photographs and SEM micrographs of bioturbated marly chalk showing a sharp erosional surface with gently scoured relief (4273'6''); this surface probably represents a hardground and is a major hiatus. Note that the annotations on the SEM micrographs only indicate one example of each component: coccolith (C), foraminifera (F), detrital grains (D), clay (Cl), cement (Ce), biotite (Bi). The scale bar is applicable to all core pieces. **A**: Core piece from 4273'–4274'. A biostratigraphic sample at 2474' yielded an early Barremian age (BC12) whereas a sample from 4273'2'' indicates an early Aptian age (BC18–19) with reworked Barremian nannofossils. These data indicate a major hiatus at the hardened erosional surface at 4273'6''. **B:** Plug spanning the hiatal surface at 4273'6''. Positions of SEM samples (C–E) are indicated on the plug photo. **C:** Abundant coccoliths both as fragments and complete shields; clay, predominantly kaolinite, between the coccoliths. Quartz, mica (biotite), and carbonate cement with small amounts of Mn and Mg present. **D1, D2:** Very similar to sample C, differing only in the presence of foraminifera and skeletal debris. The boundary is not evident on the SEM and no microscopic borings are identified on the pictures. **E:** This sample displays a marked increase in recognisable coccolith elements compared to samples C and D and exhibits higher nannofossil diversity and a relative increase in nannoconid elements.

ably represents the peak in relative sea level recorded in this core section (Fig. 3).

Unit 4 (4266'–4262'; early Aptian, BC20)

The uppermost unit of the core comprises interbedded marly chalks (LF3) and marlstones (LF1), the carbonate beds becoming thinner upwards such that the upper 2 ft of the core is dominated by dark brick-red marlstones. Hardground/firmground surfaces are developed capping marly chalk beds at two levels.

Interpretation. Unit 4 records a gradual shift from predominantly pelagic carbonate sedimentation to a hemipelagic siliciclastic mud-dominated regime. This probably reflects the basin-ward progradation of siliciclastic facies belts accompanying progressive shallowing of the basin (Fig. 3). It is possible that the chalk hardground surfaces at 4264'2'' and 4263'7'' represent depositional breaks, albeit shorter than the temporal resolution of the biostratigraphy (Fig. 7A–B).

Sequence stratigraphy

Based on the preceding analysis of lithofacies and the depositional history of the Vinding-1 cored section, the succession can be analysed in sequence stratigraphic terms (Fig. 3). The major hiatal surface at 4273'6'' indicated

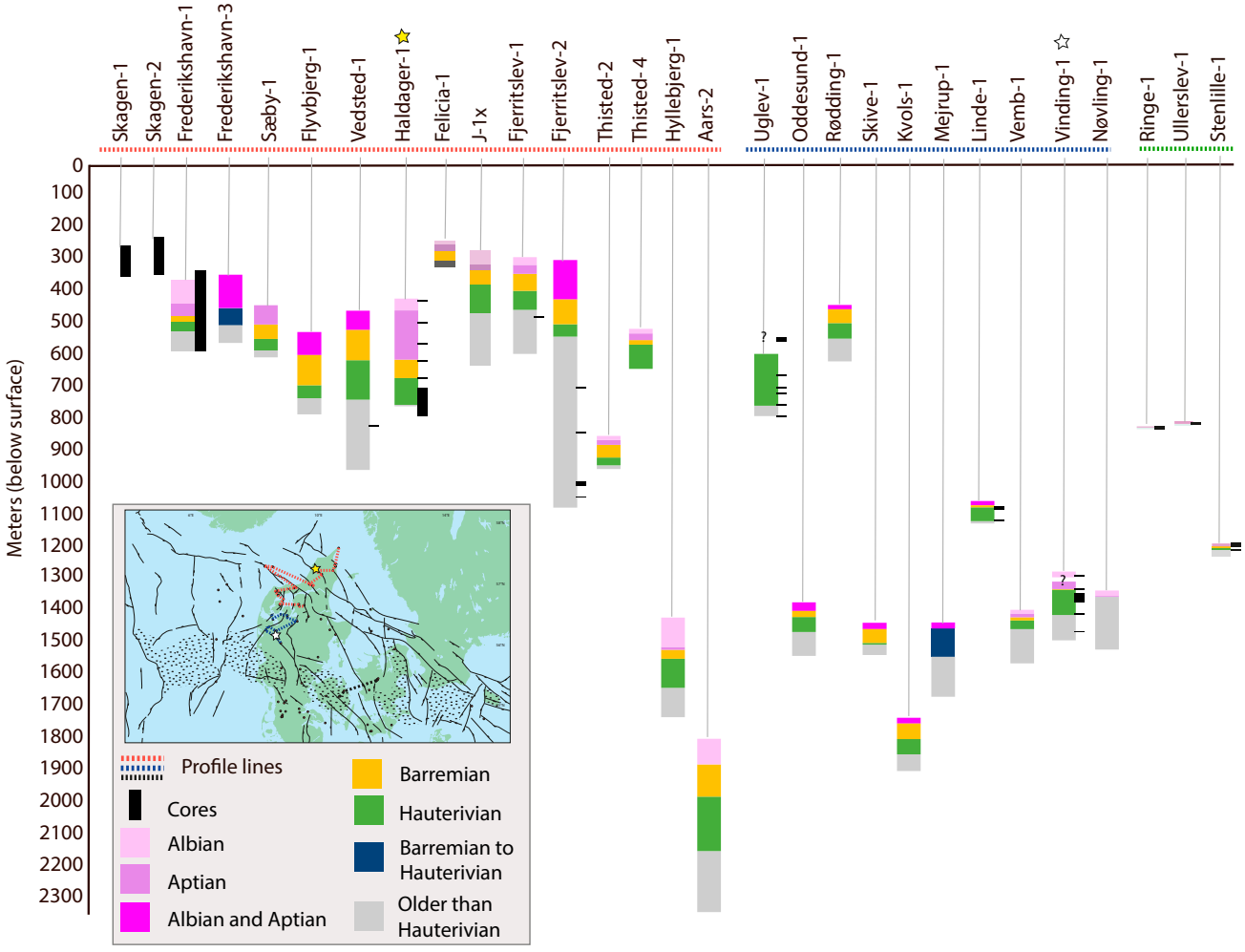


Fig. 9. Wells including strata of Early Cretaceous age in Jylland, north of the Ringkøbing –Fyn High. They are listed from north to south and then west to east, compiled in three profiles. Their positions is shown on fig. 1. The ages are based on data from well completion reports, geophysical logs and revised biostratigraphic data based on nannofossil data produced in this study. The inserted map shows the positions of the different profiles. The position of Haldager-1 is indicated with a yellow star, and the position of Vinding-1 with a white star. Ringe-1, Ullerslev-1 and Stenlille-1 are included for comparison. Core material, if present, is indicated in each of the wells (black bars). It is evident that very little core material is available. The question-marks in Vinding-1 and Uglev-1 refer to inadequate dating of boundaries.

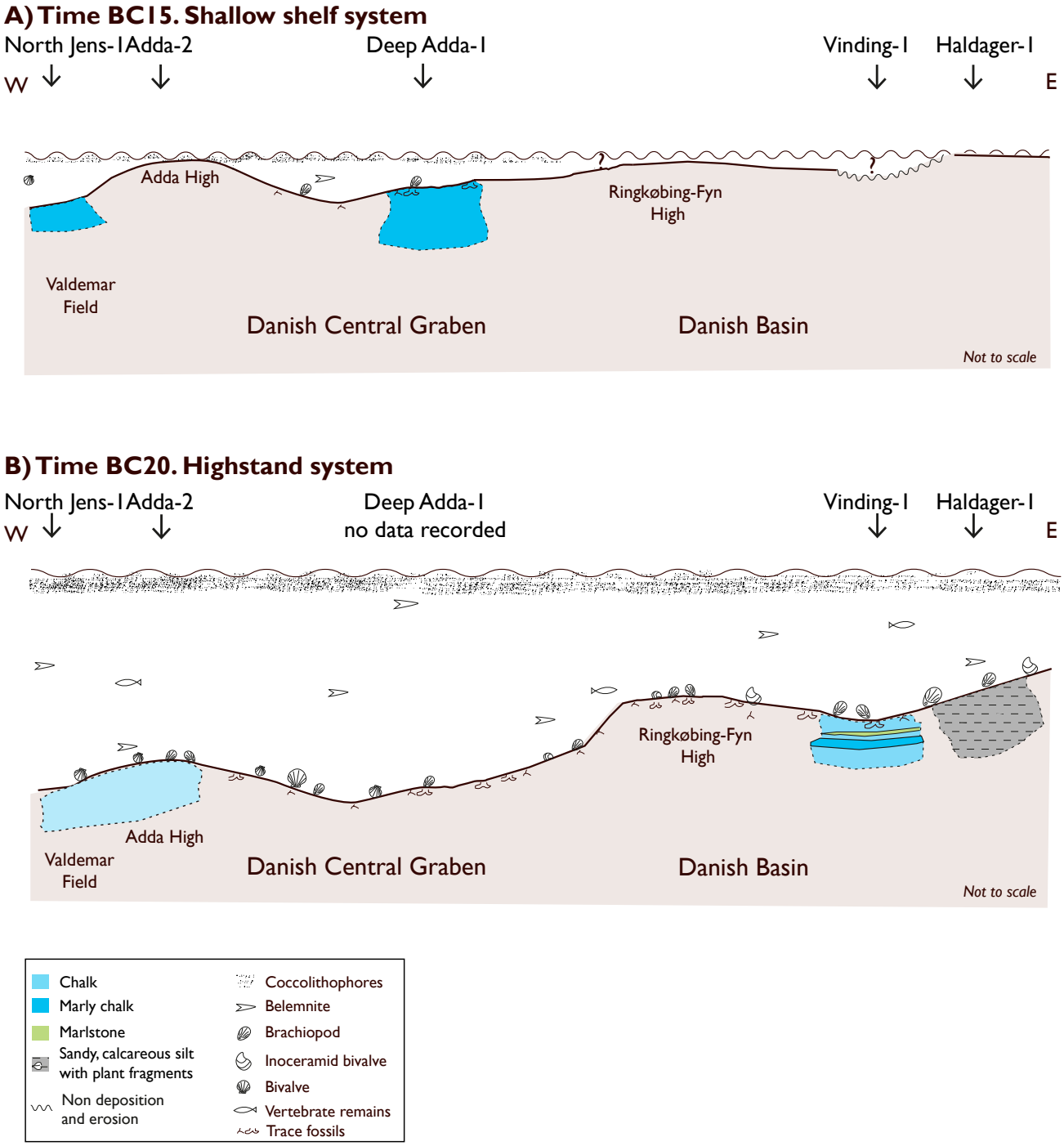


Fig. 10. Palaeoenvironmental reconstructions along a profile line from the Danish Basin (Haldager-1 and Vinding-1) in the east to the Danish Central Graben (Deep Adda-1, Adda-2, and North Jens-1) in the west. **A:** During lowstands (exemplified by BC15, late Barremian) land-derived sediments prograded basin-wards and deposition of marly chalk occurred in the Danish Central Graben (e.g. Valdemar Field and Deep Adda-1). Structural highs experienced winnowing or erosion and sediment accumulation was limited or absent (*e.g.* Adda High and Danish Basin). The Adda High was potentially within wavebase influence, but submergent. The Ringkøbing –Fyn High was shallow and possibly locally exposed. The question marks refer to our lack of coccolith data. **B:** During highstands (exemplified by BC20, early Aptian) siliciclastic sediments were sequestered in more marginal settings (*e.g.* sandy calcareous siltstones and slightly marly chalk to marl in the Danish Basin) and carbonate-rich deposition was favoured in distal parts of the basin (e.g. chalk deposition in the Valdemar Field area and on the Adda High).

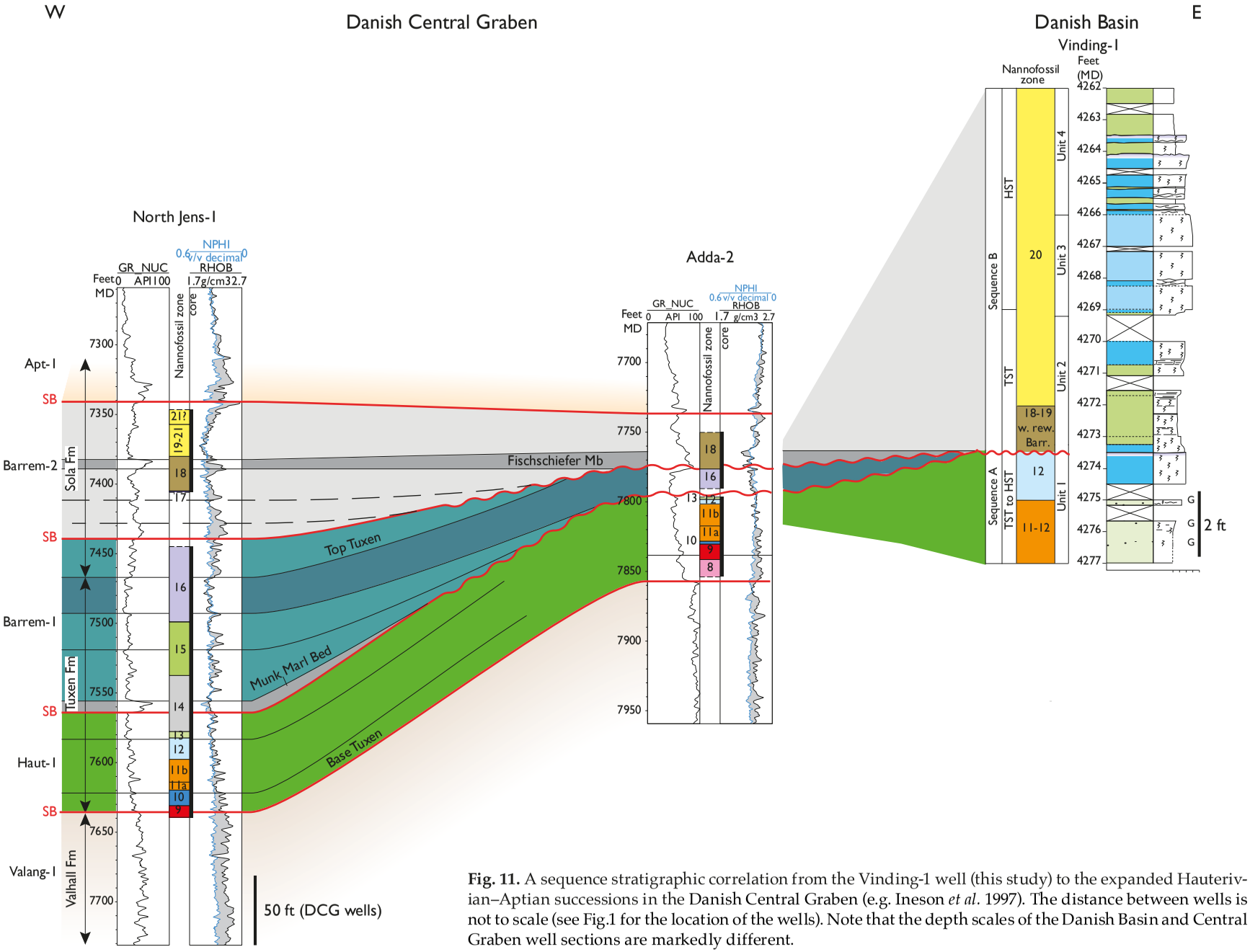


Fig. 11. A sequence stratigraphic correlation from the Vinding-1 well (this study) to the expanded Hauterivian–Aptian successions in the Danish Central Graben (e.g. Ineson *et al.* 1997). The distance between wells is not to scale (see Fig.1 for the location of the wells). Note that the depth scales of the Danish Basin and Central Graben well sections are markedly different.

by the combined biostratigraphic and sedimentological evidence clearly represents an important sequence boundary, recording relative sea-level fall and erosion. Correlation to the expanded Hauterivian–Aptian succession in the Danish Central Graben indicates that this boundary, though overtly a simple hardened erosion surface, probably represents a composite surface, the amalgamated result of several relative sea-level excursions (see discussion below).

The lower partial sequence (4277'–4273'6'', unit 1), referred to here as Sequence A, shows an upward transition from glauconitic marlstones to intensely bioturbated marly chalks. Showing characteristic features of condensation, this interval is tentatively referred to the transition from the transgressive (TST) to the early highstand (HST) systems tracts. This is compatible with the sequence stratigraphic interpretation of the coeval (BC 11–12) strata in the Danish Central Graben (see discussion below).

The upper partial sequence (4273'6''–4262', units 2–4), referred to as Sequence B, shows a tripartite development: a marl-dominated lower portion (unit 2), 'cleaning up' into a clay-poor chalk succession (unit 3) that is capped by an interbedded marly chalk – marlstone unit (unit 4) that becomes increasingly marl-dominated upwards. This partial sequence is readily subdivided into the TST and HST (Fig. 3), the latter recording the early highstand (unit 3) when siliciclastics were sequestered landward and pelagic carbonate production dominated the distal reaches of the basin, and the late highstand (unit 4) when the rate of relative sea-level rise waned and mud-rich siliciclastics prograded basin-ward.

Pelagic carbonates in other parts of the Danish Basin

Previous studies concluded that sediment accumulation was continuous, although not uniform throughout the Danish Basin from the Late Jurassic to the Early Cretaceous (e.g. Larsen 1966). The subdivision of Lower Cretaceous strata onshore Denmark is based on a combination of petrophysical and biostratigraphic data but not many wells are fully cored (Fig. 9). The Frederikshavn-1, Haldager-1 and Ringe-1 wells have recently been re-dated using nannofossils and contain material from BC10 to BC20 (late Hauterivian to early Aptian). The data are unpublished. The Vedsted-1, Gassum-1, Uglev-1, Linde-1, Ullerslev-1, and Stenlille-1 wells have previously been dated and reported to contain strata from the upper Hauterivian to the lower Aptian. New nannofossil biostratigraphy is needed to confirm this. The Uglev-1 well is situated on a top of a salt diapir and has experienced an atypical structural history. The Lower Cretaceous sections in Ullerslev-1, Ringe-1 and Stenlille-1 are highly condensed (Fig. 9). The Frederikshavn-1 well represents the proximal part of the basin in the Early Cretaceous and exhibits some non-marine units; the cores in this well are very fragmented and encased in drilling mud so correlation with the listed wells is problematic.

New nannofossil data from the Haldager-1 well correlate with the Vinding-1 biostratigraphy (Fig. 9). Core pieces from the 2307'6''–2280' interval of Haldager-1 are dated as BC10–13 (late Hauterivian to early Barremian) and the core section from 2195'–2180' is dated as BC18–21 (early to late Aptian). No core is present from 2280' to 2195' so this interval is not dated. The Hauterivian to Barremian beds comprise sandy silt with well-preserved plant fragments. The Aptian cored interval of Haldager-1 is represented by sandy, calcareous silt with intercalations of very fine sand. Previous studies of this core piece gave an average value of 40% $CaCO_3$. The equivalent section from the early Aptian in Vinding-1 (BC20) has an average $CaCO_3$ content of 75%.

The carbonate content of the other Lower Cretaceous wells in the Danish Basin has not been studied in detail and was not consistently measured when the wells were drilled. Only scattered data are published by Larsen (1966): Skagen-2 (around 20%), Børglum-1 (20–50%), Vedsted-1 (60%), Haldager-1 (10–70%), Gassum-1 (around 20%), Ullerslev-1 (20–85%), Rødby-1 (60–80%) and Lavö-1 (20–40%).

The SEM study of Vinding-1 samples indicates that the high carbonate content is due to the high abundance of nannofossils and carbonate cement derived from dissolution of nannofossils during diagenesis (Figs 7; 8). It is most likely that the high carbonate content in other parts of the Danish Basin can also be related to pelagic carbonates.

The study demonstrates that in the late Hauterivian – early Aptian, the Vinding area was situated in a pelagic-dominated carbonate system with minor benthic influence on carbonate production. Macrofossils are very rare in the Haldager-1 and Vinding-1 cores. Only two belemnite species and a few unidentified bivalves and brachiopods were found in Vinding-1. In Haldager-1, a few bivalves and plant fragments were found. None of the macrofossils display the typical morphological adaptations for soft substrate that are commonly seen amongst Upper Cretaceous benthic chalk fossils (e.g. Surlyk 1972; Lauridsen & Surlyk 2008): adaptations such as a split pedicle in brachiopods, thick and heavy lower valves in bivalves and brachiopods, or spines on valves to avoid sinking into the chalk mud as developed in bivalves and serpulids. Soft chalk was still a relatively new substrate in the Early Cretaceous, which could explain the relatively low diversity of benthic fauna in the Lower Cretaceous deposits compared with the Upper Cretaceous.

Stratigraphic ties between the Vinding-1 well and the Danish Central Graben

The alternation of chalk-rich and marl-rich intervals in the studied Vinding-1 core section reflects the interplay between pelagic carbonate supply and land-derived siliciclastic input under a regime of changing relative sea level. Climatic changes, such as variations in temperature, precipitation and humidity may also have affected the amount of run-off to the basin. Two scenarios can be envisaged, as depicted in Fig. 10. During lowstands, land-derived siliciclastic sediments prograde basin-wards, distal structural highs may experience submarine erosion or be emergent (*e.g.* Adda High and Ringkøbing–Fyn High), and pelagic carbonate productivity in shelf situations (such as in the Danish Basin) may be inhibited by turbidity or excessive nutrient supply. The late Barremian (BC15) provides a potential example of this scenario when an unconformity developed at the Vinding-1 location and on the Adda High (Fig. 10). During relative sea-level highstands, siliciclastic sediments are sequestered landwards, and pelagic carbonate production dominates in distal basin settings, particularly if structurally elevated and hence sheltered from siliciclastic input. The early Aptian (BC20) chalks in the Vinding-1 section exemplify such a scenario with the deposition of slightly marly chalk in Vinding-1 (Fig. 10).

The studied core section from the Vinding-1 well in the Danish Basin can be compared with the better-known and stratigraphically expanded Hauterivian–Aptian succession in the Danish Central Graben (Jensen & Buchardt 1987; Ineson 1993; Jakobsen *et al.* 2004, 2005; Mutterlose & Bottini 2013; van Buchem *et al.* 2017). The latter succession is referred to the Tuxen and Sola Formations (Jensen *et al.* 1986) and is best represented by the intensively cored and well-studied North Jens-1 well where the equivalent Hauterivian–Aptian section is about 260 ft (80 m) thick (Fig. 11). The Tuxen Formation comprises a heterogenous layered succession of chalks and argillaceous chalks interbedded with greenish grey to dark grey marlstones. The formation ranges in age from late Hauterivian (BC9) to late Barremian (BC16) and is subdivided into two discrete chalk units by the lower Barremian (BC14) Munk Marl Bed, about 2 m thick interval of finely laminated dark grey – black organic-rich chalky marlstones.

The succeeding Sola Formation is marlstone dominated overall but includes a basal marly chalk and chalky marlstone unit of late Barremian age (BC16) and a discrete chalk unit of early Aptian age (BC19–21) higher in the formation (Fig. 11). A discrete organic-rich marker bed, the lower Aptian (BC18) Fischschiefer Member immediately underlies the upper chalk packet and is the North Sea representative of the OAE 1a (*e.g.* Malkoc *et al.* 2010).

The conformable Hauterivian–Aptian succession in North Jens-1 and Adda-2 is subdivided into three depositional sequences (Haut-1, Barrem-1, Barrem-2 on Fig. 11); this sequence stratigraphic subdivision is modified from the preliminary subdivision of Ineson (1993) and more recent subdivisions by Jakobsen *et al.* (2004, 2005) and van Buchem *et al.* (2017). Using the detailed biostratigraphic constraints of the Central Graben and Danish Basin well sections, the Haut-1 sequence of the Danish Central Graben is correlated with Sequence A of the Vinding-1 well whilst the Barrem-2 sequence is correlated with Sequence B. The Barrem-1 sequence of the North Jens-1 well comprising the upper Tuxen Formation and lowermost Sola Formation, representing most of the Barremian stage, is partly present in Adda-2 as burrowed massive to laminated marly chalk, and entirely absent in the Vinding-1 well; this period is represented by the hiatal surface separating Sequences A and B. Resumption of sedimentation in the Aptian at the Vinding-1 location post-dated deposition of the Fischschiefer Member in the Central Graben which is generally interpreted to represent a transgressive peak, and to include the maximum flooding surface (e.g. van Buchem *et al.* 2017). The inferred transgressive systems tract (TST) of Sequence B in Vinding-1 appears to be anomalous in a regional context, therefore, though the succeeding highstand chalks in Vinding-1 correlate well with the Aptian reservoir chalks of the Sola Formation (Fig. 11), referred to the highstand system tract by van Buchem *et al.* (2017).

Conclusions

The renewed focus on Lower Cretaceous carbonate reservoirs has emphasised the need for more predictive models and a refined depositional and paleogeographic understanding of these complex layered heterogenous chalk-marl reservoirs in Denmark. One of the things to be studied is the relative roles of pelagic and benthic carbonate production. The study of Vinding-1 has increased our understanding of the Early Cretaceous shallow shelf system and the role of benthic carbonate production in the Danish Basin by studying vintage wells in the core storage at GEUS. Apparently, the Danish Basin was during late Hauterivian to early Aptian dominated by siliciclastic deposition but had a pelagic-dominated carbonate component demonstrated by the presence of chalks. But the area was not a benthic carbonate platform since

macrofossils are relatively rare with only belemnites commonly encountered. The scarcity of benthic macrofossils could be due to the lack of specialised boreal chalk fauna. They commonly occur on the soft chalk substrate in the Late Cretaceous, but since the chalk sediment was a relatively new substrate in the Early Cretaceous, morphological adaptations among the macrofauna had not yet evolved.

A revised biostratigraphy of the Vinding-1 is presented based on calcareous nannofossils and foraminifera. The new ages are confirmed by previously unpublished studies of ostracods from the core. Four lithofacies describe the spectrum from marlstone to slightly marly chalk, characterising four depositional units recording two discrete transgressive–regressive cycles. Unit 1 dated as late Hauterivian to early Barremian (BC11 to 12) was deposited during a relative sea-level rise and is truncated by an erosional surface recording a relative fall in sea level and the development of a hiatus accounting for much of the Barremian stage (BC13 to 17). The lower part of unit 2 comprises a marly chalk and is dated as early Aptian (BC18–19) but contains reworked nannofossils from the early Barremian which were deposited during the initial onlap of the eroded surface topping unit 1. The upper part of unit 2 shows a gradual change from chalky marl to marly chalk representing a sea-level rise. Unit 3 (BC 20) is of early Aptian age and the presence of slightly marly chalk is indicative of pelagic chalk accumulation with a limited supply of siliciclastic material. It probably represents the highest relative sea level recorded in the studied section. Unit 4 (BC20) is also of early Aptian age and contains more marly facies compared to unit 3. It records a gradual shift to a progressive shallowing of the basin associated with basin-ward progradation of siliciclastic facies.

The study provides a depositional record that permits sequence stratigraphic correlation to the Valdemar and Adda Fields in the Central Graben and a sequence stratigraphic model is developed.

Acknowledgements

This research received funding from the Danish Hydrocarbon Research and Technology Centre (DHRTC) under the Tight Reservoir Development program. Gunver Krarup Pedersen is thanked for useful discussion regarding Lower Cretaceous drill cores from the Danish Basin. Jörg Mutterlose is thanked for inspiring discussions on belemnites. Anders Mathiesen, GEUS are thanked for permission to use the seismic profile from 'DYB GEOTERMI – webgis portalen' illustrated in Fig. 1b.Laboratory technicians Bjørn Christensen, Carsten Guvad, Annette Ryge and Charlotte Olsen kindly helped in the laboratory and Jette Halskov is thanked for technical assistance with the illustrations. Constructive and detailed comments by journal referees Morten Bjerager and Jörg Mutterlose helped to improve the manuscript.

References

Alsen, P. & Mutterlose, J. 2009: The Early Cretaceous of North-East Greenland: A crossroads of belemnite migration. Palaeogeography, Palaeoclimatology, Palaeoecology 280, 168–182. https://doi.org/10.1016/j.palaeo.2009.06.011

Bischoff, G. & Mutterlose, J. 1998: Calcareous nannofossils of the Barremian/Aptian boundary interval in NW Europe: biostratigraphic and palaeoecologic implications of a high-resolution study. Cretaceous Research 19, 635–661. https://doi.org/10.1006/cres.1998.0123

Bown, P.R., Rutledge, D.C., Crux, J.A. & Gallagher, L.T. 1998. Lower Cretaceous. In: Bown, P.R. (ed.): Calcareous Nannofossil Biostratigraphy, 86–131. British Micropalaeontological Society Series. London: Chapman and Hall, London. https://doi.org/10.1007/978-94-011-4902-0_5

Bown, P.R. & Young, J. 1998: Techniques. In: P.R. Bown (ed.): Calcareous Nannofossil Biostratigraphy, 16–28. British Micropalaeontological Society Publication Series. Cambridge: Chapman & Hall/Kluwer Academic. https://doi.org/10.1007/978-94-011-4902-0_2

Copestake, P., Sims, A.P., Crittenden, S., Hamar, G.P., Ineson, J.R., Rose, P.T. & Tringham, M.E. 2003: Lower Cretaceous. In: Evans, D., Graham, C., Armour, A. & Bathurst, P. (eds): The Millennium atlas: petroleum geology of the central and northern North Sea, 191–211. London: Geological Society.

Fazekas, J.E. 1947: Completion report Vinding-1. Unpublished report, Danish American Prospecting CO, Geological division. 196 pp.

Gibson, T. 1989: Planktonic benthonic foraminiferal ratios: Modern ratios and Tertiary applicability. Marine Micropalaeontology 15, 29–52. https://doi.org/10.1016/0377-8398(89)90003-0

Gravesen, P., Rolle, F. & Surlyk, F. 1982: Lithostratigraphy and sedimentary evolution of the Triassic, Jurassic and Lower Cretaceous of Bornholm, Denmark. Geological Survey of Denmark Series B 7, 51 pp. https://doi.org/10.34194/serieb.v7.7062

Haq, B.U. 2014: Cretaceous eustasy revisited. Global and Planetary Change 113, 44–58. https://doi.org/10.1016/j.gloplacha.2013.12.007

Hardenbol, J., Thierry, J., Farley, M.B., Jacquin, T., de Graciansky. P-C & Vail, P.R., 1998: Mesozoic and Cenozoic sequence chronostratigraphic framework of European Basins. In: de Graciansky, P.-C. *et al.* (eds.): Mesozoic and Cenozoic sequence stratigraphy of European basins. SEPM Special Publication, 60, 3–13. https://doi.org/10.2110/pec.98.02.0003

Heilmann-Clausen, C. 1987. Lower Cretaceous dinoflagellate in the Danish Central Trough. Danmarks Geologiske Undersøgelse Serie A 12, 89 pp. https://doi.org/10.34194/seriea.v17.7036

Ineson, J.R. 1993: The Lower Cretaceous chalk play in the Danish Central Trough. Geological Society, London, Petroleum Geology Conference series 4, 175–183. https://doi.org/10.1144/0040175

Ineson, J.R., Jutson, D.J. & Schiøler, P. 1997: Mid-Cretaceous sequence stratigraphy in the Danish Central Trough. Danmarks og Grønlands Geologiske Undersøgelse Rapport 1997/109, 60 pp.

Jakobsen, F., Ineson, J. R., Kristensen, L. & Stemmerik, L. 2004: Characterization and zonation of a marly chalk reservoir: The Lower Cretaceous Valdemar Field of the Danish Central Graben. Petroleum Geoscience 10, 1–12. https://doi.org/10.1144/1354-079303-584

Jakobsen, F., Ineson, J.R, Kristensen, L., Nytoft, H.P. & Stemmerik, L. 2005: The Valdemar Field, Danish Central Graben: field compartmentalization and regional prospectivity of the Lower Cretaceous chalk play. In: Doré, A.G. & Vining, B.A. (eds): Petroleum Geology: North-West Europe and Global Perspectives – Proceedings of the 6th Petroleum Geology Conference, 177–186. https://doi.org/10.1144/0060177

Jensen, T.F, Holm, L., Frandsen, N. & Michelsen, O. 1986: Jurassic-Lower Cretaceous Lithostratigraphic Nomenclature for the Danish Central Trough. Danmarks Geologiske Undersøgelse Serie A 12, 65 pp. https://doi.org/10.34194/seriea.v12.7031

Jensen, T.F. & Buchardt, B. 1987: Sedimentology and geochemistry of the organic-rich Lower Cretaceous Sola Formation (Barremian–Albian), Danish Central Trough. In: Brooks, J. & Glennie, K. (eds): Petroleum Geology of North West Europe, 469–481. London: Graham & Trotman.

Jeremiah, J. 2001: A Lower Cretaceous nannofossil zonation for the North Sea Basin. Journal of Micropalaeontology 20, 45–80. https://doi.org/10.1144/jm.20.1.45

Kennedy, W.J., Hancock, J.M. & Christensen, W.K. 1980: Albian and Cenomanian ammonites from the island of Bornholm (Denmark). Bulletin of the Geological Society of Denmark 29, 203–244.

King, C., Bailey, H.W., Burton, C.A. & King, A.D. 1989: Cretaceous of the North Sea. In: Jenkins, D.G. & Murray, J.W. (eds): Stratigraphic atlas of fossil Foraminifera, 372–417. Chichester: Ellis Horwood.

Kougtosoukos, E.A.M., Leary, P.N., & Hart, M.B. 1990: Latest Cenomanian to earliest Turonian low oxygen tolerant benthonic foraminifera: a case study from the Sergipe Basin (N. E. Brazil) and the western Anglo Paris Basin (southern England). Palaeogeography, Palaeoclimatology, Palaeoecology 77, 145–177. https://doi.org/10.1016/0031-0182(90)90130-Y

Larsen, G. 1966: Rhaetic Jurassic Lower Cretaceous sediments in the Danish Embayment. Danmarks Geologiske Undersøgelse II række 91, 127 pp. https://doi.org/10.34194/raekke2.v91.6882

Lauridsen B.W. & Surlyk, F. 2008: Benthic faunal response to late Maastrichtian chalk – marl cyclicity at Rørdal, Denmark. Palaeogeography, Palaeoclimatology, Palaeoecology 269, 38–53. https://doi.org/10.1016/j.palaeo.2008.07.001

Leckie, M. 1987: Paleoecology of Mid-Cretaceous planktonic foraminifera: A comparison of open ocean and epicontinental sea assemblages. Micropalontology 33, 2, 164–176. https://doi.org/10.2307/1485491

Lindström, S. & Erström, M., 2011: Basin analysis of the uppermost Triassic to Lower Cretaceous, Danish Basin. Biostratigraphy and log correlation. Danmarks og Grønlands Geologiske Undersøgelse Rapport 2011/82, 72 pp.

Löb, C. & Mutterlose, J. 2012: The onset of anoxic conditions in the early Barremian of the Boreal Realm evidenced by benthic foraminifera. Review of Micropalaeontology 55, 113–126. https://doi.org/10.1016/j.revmic.2012.06.001

Malkoc, M., Mutterlose, J. & Pauly, S. 2010: Timing of the Early Aptian ?13C excursion in the Boreal Realm. Newsletter on Stratigraphy. 43, 251–273. https://doi.org/10.1127/0078-0421/2010/0043-0251

Mogensen, T.E. & Korstgård, J.A. 2003: Triassic and Jurassic transtension along part of the Sorgenfrei-Tornquist Zone in the Danish Kattegat. Geological Survey of Denmark and Greenland Bulletin 1, 439–458. https://doi.org/10.34194/geusb.v1.4680

Mutterlose, J. 1992: Migration and evolution patterns of floras and faunas in marine Early Cretaceous sediments of NW Europe. Palaeogeography, Palaeoclimatology, Palaeoecology 94, 261–282. https://doi.org/10.1016/0031-0182(92)90123-M

Mutterlose, J. 1998: The Barremian–Aptian turnover of biota in northwestern Europe: evidence from belemnites. Palaeogeography, Palaeoclimatology, Palaeoecology 144,161–176. https://doi.org/10.1016/S0031-0182(98)00081-9

Mutterlose, J. & Böckel, B. 1998: The Barremian to Aptian interval in NW Germany: a review. Cretaceous Research 19, 539–568. https://doi.org/10.1006/cres.1998.0119

Mutterlose, J. & Bottini, C. 2013: Early Cretaceous chalks from the North Sea giving evidence for global change. Nature communications 4, 1686. https://doi.org/10.1038/ncomms2698

Mutterlose, J. & Wiedenroth, K. 2009: Neue Tagesaufschlüsse der Unter-Kreide (Hauterive – Unter-Apt) im Großraum Hannover – Braunschweig: Stratigraphie und Faunenführung. Berliner paläobiologische Abhandlungen 10, 257–288.

Neale, J.W. 1973: Ostracoda as means of correlation in the Boreal Lower Cretaceous, with special reference to the British marine Ostracoda. In: Casey, R. & Rawson, P.F. (eds): The Boreal Lower Cretaceous. Geological Journal Special Issue 5, 169–184.

Nielsen, L.H. 2003: Late Triassic – Jurassic development of the Danish Basin the Fennoscandian Border Zone, Southern Scandinavia. Geological Survey of Denmark and Greenland Bulletin 1, 459–526. https://doi.org/10.34194/geusb.v1.4681

Nguyen, T.M.P., Petrizzo, M.P.M & Speijer, R.P. 2009: Experimental dissolution of a fossil foraminiferal assemblage (Paleocene–Eocene Thermal Maximum, Dababiya, Egypt):

Implications for paleoenvironmental reconstructions. Marine Micropaleontology 73, 241–258. https://doi.org/10.1016/j.marmicro.2009.10.005

Odin, G.S. & Matter, A. 1981: De Glauconiarum Origine. Sedimentology 28, 611–641. https://doi.org/10.1111/j.1365-3091.1981.tb01925.x

Rawson, P.F & Mutterlose, J. 1983: Stratigraphy of the Lower B and basal Cement Beds (Barremian) of the Speeton Clay, Yorkshire, England. Proceedings of the Geologists' Association 94, 133–146. https://doi.org/10.1016/S0016-7878(83)80005-4

Ruffel, A. 1991: Sea-level events during the Early Cretaceous in Western Europe. Cretaceous Research 12, 527–551. https://doi.org/10.1016/0195-6671(91)90006-X

Slipper, I. 2009: Marine Lower Cretaceous. In: Whittaker, J.E. & Hart, M.B. (eds): Ostracods in British Stratigraphy, 309-343. London: The Micropalaeontological Society. https://doi.org/10.1144/TMS003.13

Sorgenfrei, T. & Buch, A. 1964: Deep Tests in Denmark 1935–1959. Danmarks Geologiske Undersøgelse III række 36, 146 pp. https://doi.org/10.34194/raekke3.v36.6941

Stolley, E. 1911: Beiträge zur kenntnis der Cephalopoden der Norddeutschen Unteren Kreide I. Die Belemniteden der Norddeutschen Unteren Krede. 1. Die Belemniten des Norddeutschen Gaults (Aptiens und Albiens). Geologische und Palæontologische Abhandlingen 14(3), 95 pp.

Surlyk, F. 1972: Morphological adaptations and population structures of the Danish chalk brachiopods. Det Kongelige Danske Videnskabernes Selskab, Biologiske Skrifter 19, 57 pp.

Taylor, A., Goldring, R. & Gowland, S. 2003: Analysis and application of ichnofabrics. Earth-Science Reviews 60, 227–259. https://doi.org/10.1016/S0012-8252(02)00105-8

Thomsen, E. 1987: Lower Cretaceous calcareous nannofossil biostratigraphy in the Danish Central Trough, Danmarks Geologiske Undersøgelse Serie A 12, 89 pp. https://doi.org/10.34194/seriea.v20.7039

van Buchem, F.S.P, Smit, F.W.H., Buijs, G.J.A., Trudgill, B. & Larsen, P.-H. 2017: Tectonostratigraphic framework and depositional history of the Cretaceous–Danian succession of the Danish Central Graben (North Sea) – new light on a mature area. In: Bowman, M. & Levell, B. (eds): Petroleum geology of NW Europe: 50 years of learning, 1–38. Proceedings of the 8th Petroleum Geology Conference. https://doi.org/10.1144/PGC8.24

Vejbæk, O.V. 1989: Effects of asthenospheric heat flow in basin modelling exemplified with the Danish Basin. Earth and Planetary Science Letters 95, 97–114. https://doi.org/10.1016/0012-821X(89)90170-2

Vejbæk, O.V. 1997: Dybe strukturer i danske sedimentære bassiner. Geologisk Tidsskrift 4, 1–31.

Vejbæk, O.V., Andersen, C., Dusar, M., Herngreen, W., Krabbe, H., Leszczynski, K., Lott, G.H., Mutterlose, J. & van der Molen A.S. 2010. Cretaceous In: Doornenbal, J.C. & Stevenson, A.G. (eds): Petroleum geological atlas of the southern Permian Basin area, 195–209. Houten: European Association of Geoscientists and Engineers.

Vosgerau, H, Mathiesen, A, Andersen, M.S., Boldreel, L.O., Hjuler, M.L., Kamla, E., Kristensen, L., Pedersen, C.B., Pjetursson, B. & Nielsen, L.H. 2016: WebGIS portal for exploration of deep geothermal energy based on geological and geophysical data. Geological Survey of Denmark and Greenland Bulletin 35, 23–26. https://doi.org/10.34194/geusb.v35.4633

Mapping Cretaceous faults using a convolutional neural network

– A field example from the Danish North Sea

MADS C. L. LORENTZEN[1, 3, *], KENNETH BREDESEN[1], FLORIAN W. H. SMIT[1], TORSTEN H. HANSEN[2], LARS NIELSEN[3], AND KLAUS MOSEGAARD[4]



Geological Society of Denmark
https://2dgf.dk

Received 31 January 2022
Accepted in revised form
20 June 2022
Published online
15 August 2022

© 2022 the authors. Re-use of material is permitted, provided this work is cited. Creative Commons License CC BY: https://creativecommons.org/licenses/by/4.0/

Lorentzen, M. C. L., Bredesen, K., Smit, F. W. H., Hansen, T. H., Nielsen, L. and Mosegaard, K. 2022: Mapping Cretaceous faults using a convolutional neural network – A field example from the Danish North Sea. Bulletin of the Geological Society of Denmark, Vol. 71, pp. 31–50. ISSN 2245-7070.
https://doi.org/10.37570/bgsd-2022-71-03

The mapping of faults provides essential information on many aspects of seismic exploration, characterisation of reservoirs for compartmentalisation and cap-rock integrity. However, manual interpretation of faults from seismic data is time-consuming and challenging due to limited resolution and seismic noise. In this study, we apply a convolutional neural network trained on synthetic seismic data with planar fault shapes to improve fault mapping in the Lower and Upper Cretaceous sections of the Valdemar Field in the Danish North Sea. Our objective is to evaluate the performance of the neural network model on post-stack seismic data from the Valdemar Field. Comparison with variance and ant-tracking attributes and a manual fault interpretation shows that the neural network predicts faults with more details that may improve the overall geological and tectonic understanding of the study area and add information on potential compartmentalisation that was previously overlooked. However, the neural network is sensitive to seismic noise, which can distort the fault predictions. Therefore, the proposed model should be treated as an additional fault interpretation tool. Nonetheless, the method represents a state-of-the-art fault mapping tool that can be useful for hydrocarbon exploration and CO_2 storage site evaluations.

Keywords: Machine learning, fault detection, cap-rock integrity, reservoir modelling, Cretaceous, Danish North Sea.

[1]*Department of Geophysics and Sedimentary Basins, Geological Survey of Denmark and Greenland (GEUS), Øster Voldgade 10, 1350 Copenhagen, Denmark.* [2]*Department of Geoscience, Aarhus University, Høegh-Guldbergs Gade 2, Aarhus C, Denmark.* [3]*Department of Geosciences and Natural Resource Management, University of Copenhagen, Øster Voldgade 10, 1350 Copenhagen, Denmark.* [4]*Niels Bohr Institute, University of Copenhagen, Blegdamsvej 17, 2100 Copenhagen, Denmark.* [*]*Correspondence: mlo@geus.dk.*

Fault mapping is a crucial seismic interpretation task that provides valuable structural information for prospect evaluation, seal integrity studies, and drilling operations targeting reservoirs in hydrocarbon and green energy applications. As faults may act as potential migration pathways of pore-fluids or baffles to fluid flow, it is important to outline their spatial network, density, and connectivity (Sorkhabi & Tsuji 2005; Fossen 2016; Smit *et al*. 2018). Furthermore, fault mapping and visualisation in 2D section and map view provide insights into the tectonic evolution of an area. If vertical displacements are larger than the seismic resolution, faults may appear as discontinuities in the layered reflectivity, and their presence may scatter the energy and distort the seismic imaging. Manual interpretation of faults can be a tedious and time-consuming process, and their location and extent are not always clearly apparent in seismic data. To highlight these discontinuities, a standard procedure is to use some edge detection seismic attributes such as semblance (Marfurt *et al*. 1998), coherency (Marfurt *et al*. 1997), and variance (van Bemmel & Pepper 2000;

Randen *et al*. 2001). These attributes rely on lateral changes in seismic reflection (dis)continuity as well as alterations in the frequency content (Chopra & Marfurt 2007). However, a pitfall of these methods for fault interpretation is that these attributes also highlight lithological or stratigraphical facies variations and seismic noise.

In recent years, machine learning methods have successfully been implemented in the geoscience domain for a wide range of applications, such as horizon tracking, salt dome identification, facies classification and fault mapping (Dramsch 2020). The fault mapping challenge can generally be regarded as a basic image segmentation task by pixel-wise classifying the input seismic data as either background (seismic data) or fault location. The pixel dimensions correspond to the dimensions of the acquisition setup in terms of inline and crossline spacing and sample interval.

In a supervised learning framework, a convolutional neural network (CNN) approach can be used to identify the location of faults in seismic data based on a synthetic training set or manual or automated fault picks in seismic data. Therefore, this CNN approach does not require the calculation of seismic attributes to identify the location of potential fault zones (Wu *et al*. 2019; Wrona *et al*. 2020). Previous studies have successfully implemented and demonstrated applications of neural networks for fault mapping and delineation. A supervised learning system to map simple fault networks in the subsurface using raw seismic recordings was proposed by Araya-Polo *et al*. (2017). Their neural network model was trained and tested on 3D synthetic seismic data and they concluded that more complex fault structures were required in the synthetic data to enhance the mapping quality. It was demonstrated by Wrona *et al*. (2020) how cropped 2D samples with manually labelled faults from large 2D seismic sections from the northern North Sea could be used in a supervised learning framework for identifying faults in 2D sections. They compared two different CNN models: (1) a simple 2D CNN model that downsamples the cropped input image and classifies it, and (2) a 2D U-Net model (based on the work of Long *et al*. 2015; Ronneberger *et al*. 2015) that labels the cropped input image pixel-wise. Both approaches had similar fault mapping accuracy in the seismic section but differed significantly in computation time for these test predictions (2 hours for the simple CNN versus 5 seconds for the U-Net).

It was demonstrated by Wu *et al*. (2019) with limited computational resources, how a simplified version of the U-Net structure could accurately predict faults

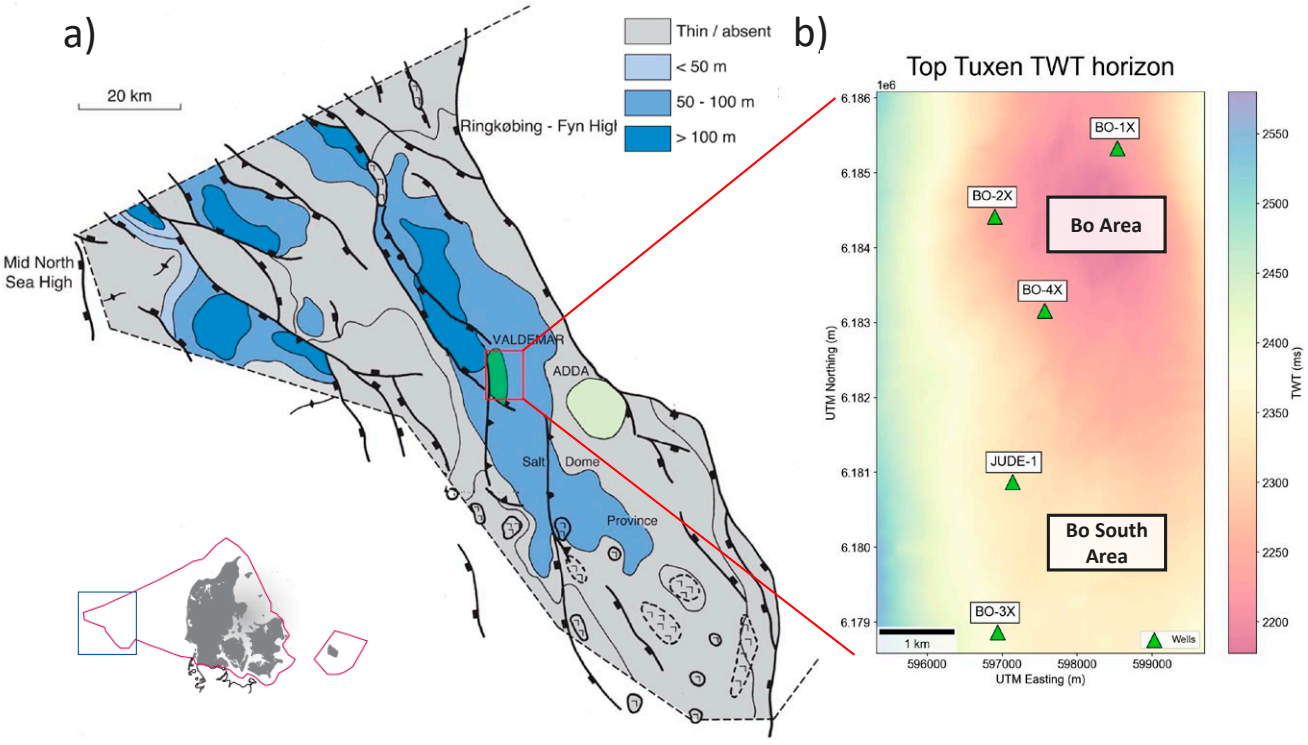


Fig. 1: a) Location of the Danish Central Graben and thickness map of the Sola and Tuxen formation. The Valdemar Field with the various Bo wells is outlined in the red rectangle (modified figure from Jakobsen *et al*. 2004). **b)** Map of the Bo and Bo South areas (part of the larger structure, Bo-Jens Ridge) in the Valdemar Field with Top Tuxen two-way traveltime (TWT) structure and relevant well locations.

in 3D seismic data by training on synthetic data. In their study, the trained U-Net CNN outlines realistic fault interpretations in various 3D seismic surveys including the Netherlands F3 Block and a subduction zone at the Costa Rica margin. Following that work a fault detection machine learning competition was held in 2020 by the Norwegian Petroleum Directorate (Bormann *et al*. 2020). The competition used synthetic seismic data and non-optimal real seismic data from the Itchys Field located on the NW Shelf of Australia for training and testing different supervised learning models. The fault mapping results were rated by human interpreters to assess the quality of the mapping, and none of the competitors was given a significantly high score. It was suspected that the low success rate was related to migration artifacts remained in the seismic data due to sub-optimal processing that was used for the test phase.

Other studies have modified the CNN structure proposed by Wu *et al*. (2019) and used it as a state-of-the-art benchmark model for automatic fault interpretations trained on either synthetic data, real data with interpretations or a combination of the two. A suite of models including the U-Net CNN was used in a study by An *et al*. (2021). By applying the models on two real test data sets, Inner Moray Firth (UK North Sea sector) and Thebe Gas Field (NW Shelf of Australia), they demonstrated that the test predictions of the U-Net CNN could be improved by implementing image augmentation methods and manually labelled field data in the training data. In a study by Dou *et al*. (2021), they show how a combination of 3D synthetic data and 2D labelled real data from the Shengli Oilfield in China could be used in the training process to improve the U-Net CNN model performance and ability to generalise to other seismic surveys.

In all the former cases, the U-Net CNN model seems in agreement with traditional fault-enhancing attributes and other proposed machine learning models, which indicates a good generalisation ability across seismic surveys of varying quality and with different faulting systems (Wu *et al*. 2019; An *et al*. 2021; Dou *et al*. 2021).

In this study, we apply the open-source U-Net CNN (hereafter referred to as 'CNN') model by Wu *et al*. (2019) that has been trained on synthetic seismic data generated by a convolutional model with planar-shaped faults on post-stack data from the Valdemar Field located in the Danish North Sea (Fig. 1a). We focus on Cretaceous succession comprising an upper and lower part. Fig. 2 shows a stratigraphic column covering the Cretaceous section in the Danish Central Graben (DCG). Whereas the Upper Cretaceous (UC) is regionally composed of thicker high-porosity pure chalk reservoir intervals, the Lower Cretaceous (LC),

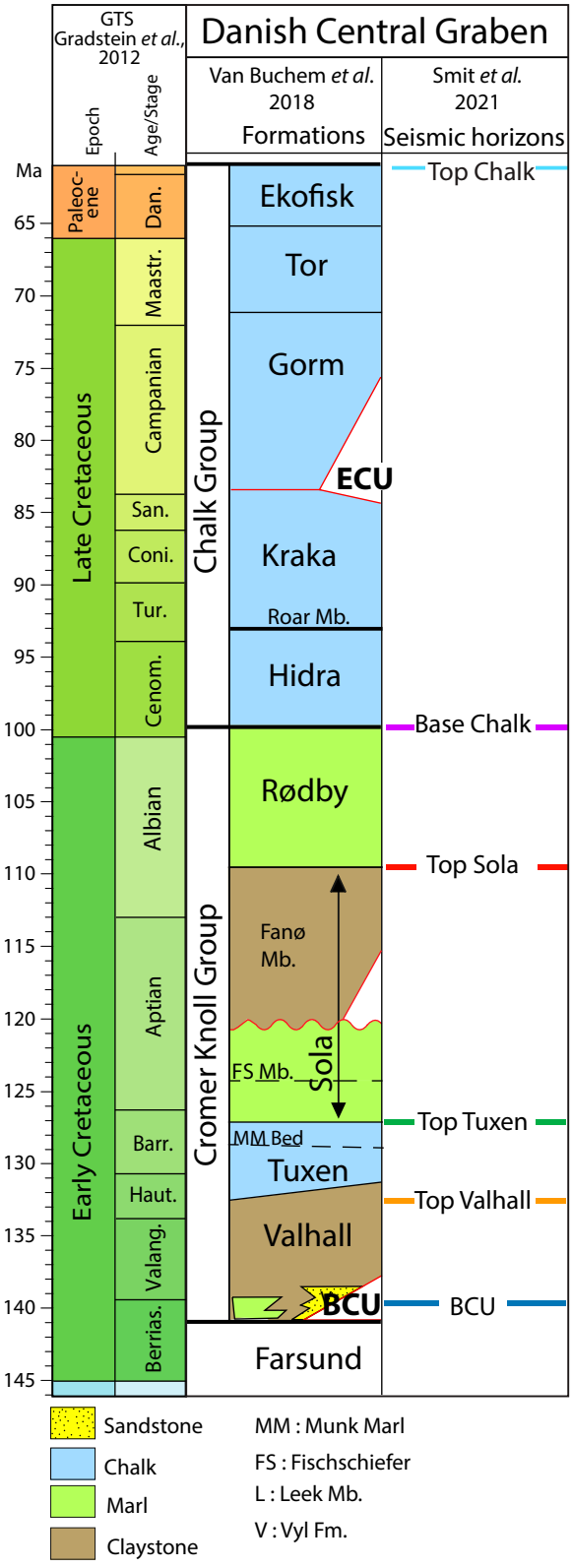


Fig. 2: Stratigraphic column scheme of the Cretaceous succession in the Danish Central Graben adapted from van Buchem *et al*. (2018). Coloring of the key seismic horizons used throughout the study from Smit *et al*. (2021) can be seen in the right section of the figure.

which also contains reservoir layers, is thinner and more heterogeneous with marly chalks and low matrix permeabilities (Jakobsen *et al*. 2004). The fine-grained shale can potentially be integrated in fault zones of the LC succession and work as barrier to fluid flow (Fossen 2016). Seismic interpretation and coherency studies of the Valdemar Field was conducted by Madsen & Britze (1999) as a part of the multi-institutional PRIORITY research programme (1997–2002) and they concluded that conventional fault mapping methods were insufficient to map the fault complexity of the field in the complete Cretaceous succession. More recently, Bredesen *et al*. (2021) performed a quantitative seismic interpretation study to outline reservoir quality variations and to boost the resolution of the LC succession in the Valdemar Field. Their study showed that the seismic image of the LC interval was characterised by limited resolution and by interfering multiple energy from the overlying UC chalk succession. This is caused by the chalk succession having a higher seismic velocity than the LC mudstones and chalks, which generates scattering, interfering multiples and converted waves (Vidalie *et al*. 2012; Montazeri *et al*. 2018).

The objective of this study is to evaluate the performance of the CNN model by Wu *et al*. (2019) on the Valdemar Field data and review the outlined faults by comparison to manually interpreted faults and a simple industrial standard workflow procedure with variance and intelligent ant-tracking (Pedersen *et al*. 2002). Firstly, we review the structural geology in a regional and local setting. Secondly, we outline how the CNN model and its training process work and address the data conditioning steps of the seismic data from the Valdemar Field. Finally, we analyse the results and discuss some of the shortcomings of the study as well as delineate potential improvements.

Geological background

Regional framework

The Valdemar Field is located in the central part of the DCG, occurring in the westernmost part of the Danish offshore sector (Fig. 1a). The DCG comprises a complex of fault-bounded basins and highs and is part of the system of failed rifts that spans the North Sea area (Ziegler 1990). During the Late Jurassic, tectonic extension generated a series of roughly NW–SE-trending half-graben bounded by large normal faults in the area (Møller & Rasmussen 2003). As a result of Late Jurassic rifting, subsidence of these basins caused the accumulation of thick successions of largely marine shale, including organic-rich units that are modern-day sources of hydrocarbons (Fig. 2) (Ineson 1993; Ineson *et al*. 2003). In the DCG, rifting ceased around the onset of the Early Cretaceous (Møller & Rasmussen 2003), but the rift-related basin morphology persisted throughout the Early Cretaceous along with the deposition of the Cromer Knoll Group deposits (Vejbæk 1986).

During the Late Cretaceous and Paleogene, regional tectonic shortening caused basin inversion and relative uplift of former rift depocentres (Vejbæk & Andersen 2002; van Buchem *et al.* 2018). This generated several structural traps with Cretaceous reservoirs in the area.

Local structural framework

The Valdemar Field contains hydrocarbon within the Cretaceous successions and occurs on the crest of a large anticlinal fold (the Bo–Jens Ridge), which formed during Late Cretaceous inversion and strikes approximately North–South (Vejbæk & Andersen 2002; Hansen *et al*. 2021). Locally within the field perimeter, a saddle point separates two gentle structural highs near the wells North Jens-1 and Bo-1X at reservoir levels (Jakobsen *et al*. 2005). This configuration arose due to varying degrees of reactivation of, and folding along, rift-related faults below the reservoir (Hansen *et al*. 2021). Groups of small normal faults (some with offsets near the limit of seismic resolution) populate the crest of Bo–Jens Ridge at Cretaceous levels. These faults are interpreted by Hansen *et al*. (2021) as the result of a combination of outer-arc extension and gravitational collapse during inversion and folding. Fig. 1b shows the southern downflank of the southern Bo–Jens Ridge with marked well locations. This outlines the area of interest for our study as it remains an immature part of the Valdemar Field.

Convolutional neural network

In this research, we use the previously trained version of the CNN model by Wu *et al*. (2019) to predict the faults in a 3D post-stack survey from the Valdemar Field based on the work of Bredesen *et al*. (2021). Two seismic processing steps are introduced for this study to make it suitable for the CNN fault prediction. Firstly, the post-stack data are filtered using an automatic gain control (AGC) to increase the weak signals of the LC. The amplitudes are increased to make the CNN fault labelling more accurate, however, the noise will be amplified as well, and there is a potential risk of the CNN predicting faults in the noisy areas. Secondly, after the AGC process the seismic data are normalised

by subtraction of its mean value and division by its standard deviation to make the amplitude ranges consistent with the synthetic training from Wu *et al.* (2019).

The visual effects of the two-step conditioning on the seismic data are shown at Fig. 3. The AGC-filtered seismic will be used for all the following figures to

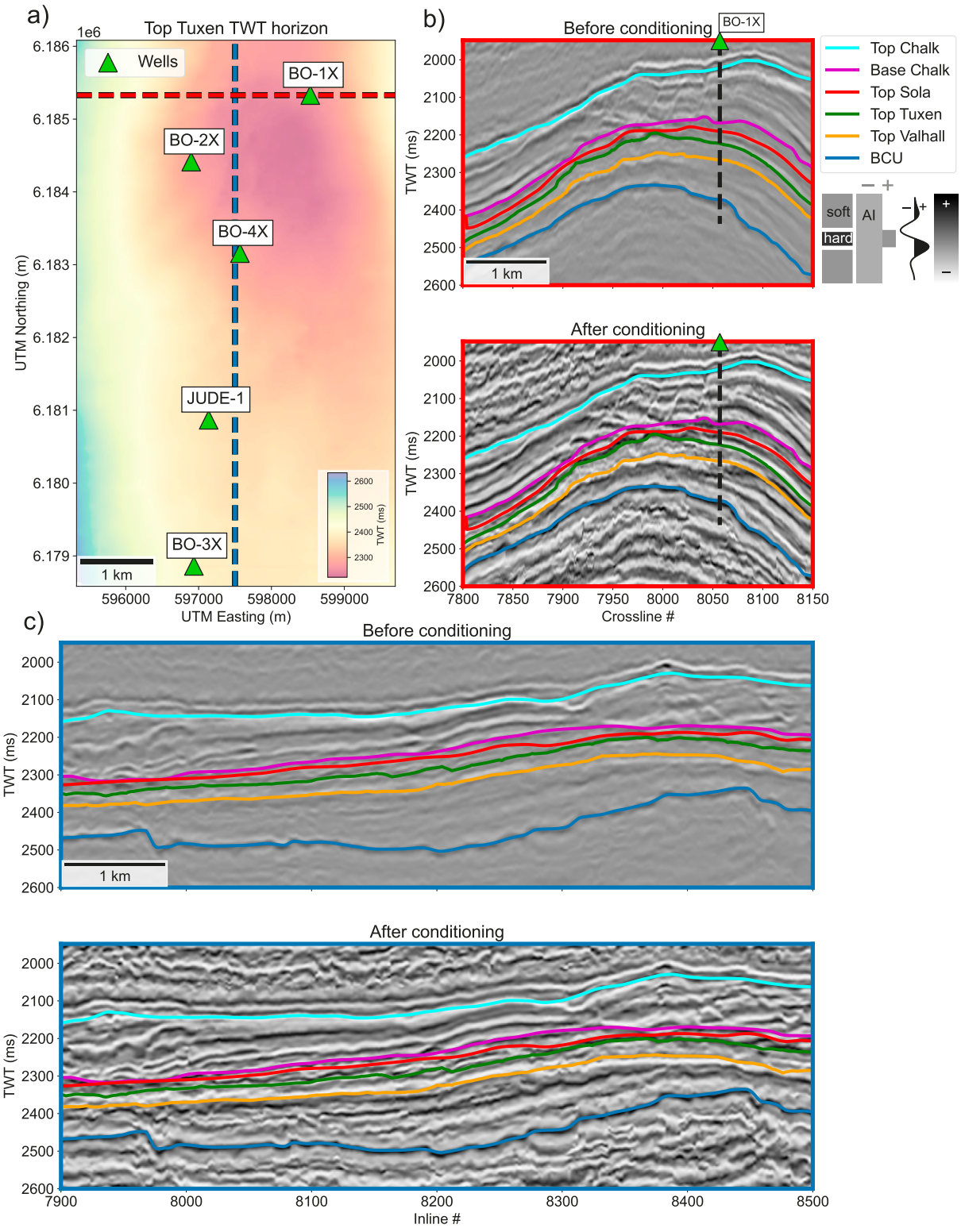


Fig. 3: a) Map of the Tuxen horizon in two-way traveltime (TWT) in the Valdemar Field with well locations. The dashed red and blue lines indicate the crossline and inline sections shown in **b)** and **c)**, respectively.

improve the visualisation of the LC succession. Note that inline and crossline sections shown throughout the study will be influenced by a vertical exaggeration. The European polarity convention shown in Fig. 3 will be used for all seismic data displayed in the study. The main horizons of the LC used in this study originate from the regional interpretation study by Smit *et al*. (2021).

A detailed description of the mathematics and architecture of the CNN model and its U-Net structure is beyond the scope of this study, and the reader is referred to the papers by Ronneberger *et al*. (2015) and Long *et al*. (2015). The main framework of the U-Net applied in this study is composed of two phases. Firstly, the 3D seismic volume is spatially reduced in steps to create a so-called feature vector. The feature vector contains filtered information from the seismic cubes through a series of matrix operations. Secondly, the downsampling process is followed by an upscaling operation, and the final feature layer holds extracted information from the seismic cube in terms of a fault cube of the same size as the original 3D seismic input.

The CNN model is trained using 200 synthetic seismic and fault cubes of dimensions (128×128×128) elements resembling seismic volumes of (1.6km×3.2km×512ms) by 12.5 meters inline and crossline spacing (considering every second crossline) and 4ms sample interval. The workflow for generating the synthetic data originates from Wu & Hale (2016). Here, they use a series of reflections between -1 and 1 includes folding structures and planar shearing to mimic true geological variations. Sequentially, planar faulting is generated in the cubes with dips ranging from 65°-85°, and the perturbed reflection cubes are convolved with a Ricker wavelet with pre-defined varying frequency content. Lastly, Gaussian noise is added to the synthetic cube yielding various signal-to-noise ratios. Compared to real seismic data, the synthetic data are convenient to use for CNN model training as they allow better control on the ground truth fault labels and thus avoid marking errors based on misinterpretations. The ground truth fault labels are located in binary cubes (zeros indicate non-fault, and ones indicate faults) of the same dimensions as the seismic cube. Moreover, using synthetic data render possible a great quantity of training data that can be difficult to obtain from real seismic data. To assess the similarity between the synthetic training data and the Valdemar Field data, Fig. 4a and 4b shows a training data slice and a cropped section of the

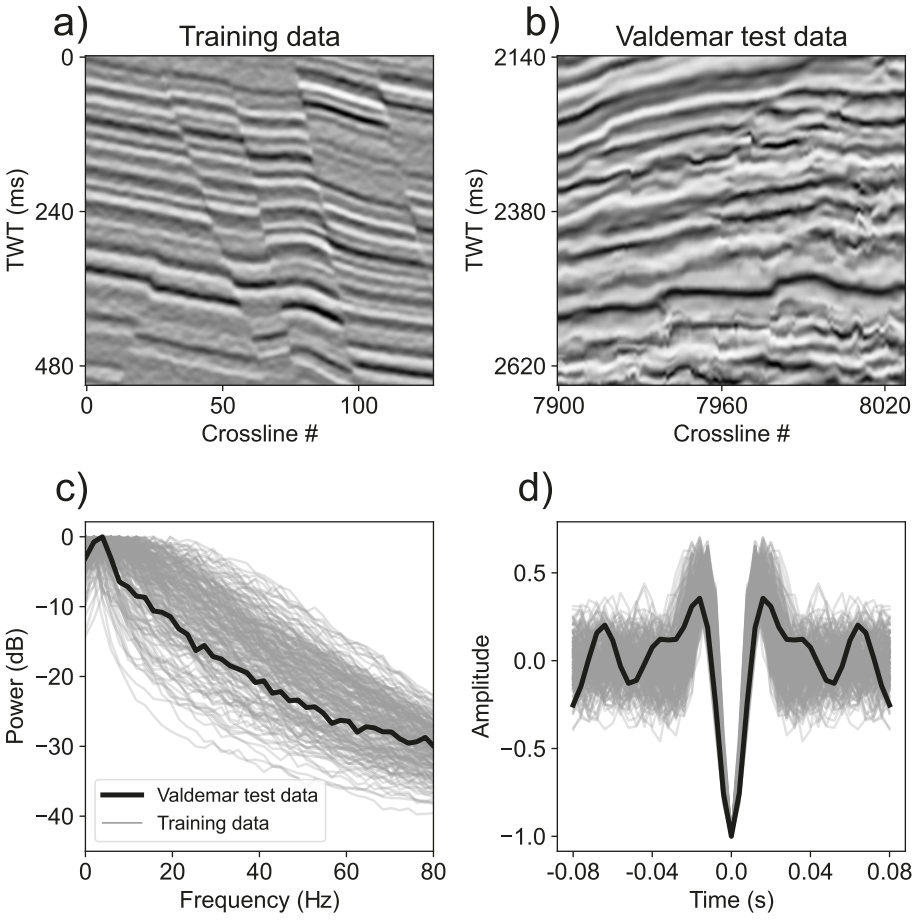


Fig. 4: Samples of crossline sections of **a)** synthetic training data and **b)** Valdemar Field data from the Cretaceous section (test data). The frequency spectrum of all 200 3D training cubes and the Valdemar test data is shown in **c)**, and their wavelets are shown in **d)**.

conditioned Valdemar test data from the Cretaceous section, respectively. Some visual discrepancies are observed between the training and test sample as the Valdemar data seems more blurred and distorted than the synthetic sample. This could be caused by noise left in the seismic volume after processing from e.g. interfering multiples. Nonetheless, Fig. 4c and 4d show the frequencies and wavelets of all training data 3D cubes versus the Valdemar Field Cretaceous test data, respectively, and indicate that the frequencies and wavelet form of the latter are well-represented in the training data.

The CNN training involves passing all the synthetic seismic cubes through the U-Net structure, estimating the error between the predicted fault labels and the ground truth faults, and adjusting the weights of the CNN accordingly. Hence, the training process can be regarded as an optimisation process that aims to minimise the difference between the predicted fault label and the ground truth fault label. The end result is a cube with an assigned CNN fault probability for each pixel. Fig. 5 shows a series of slices from the

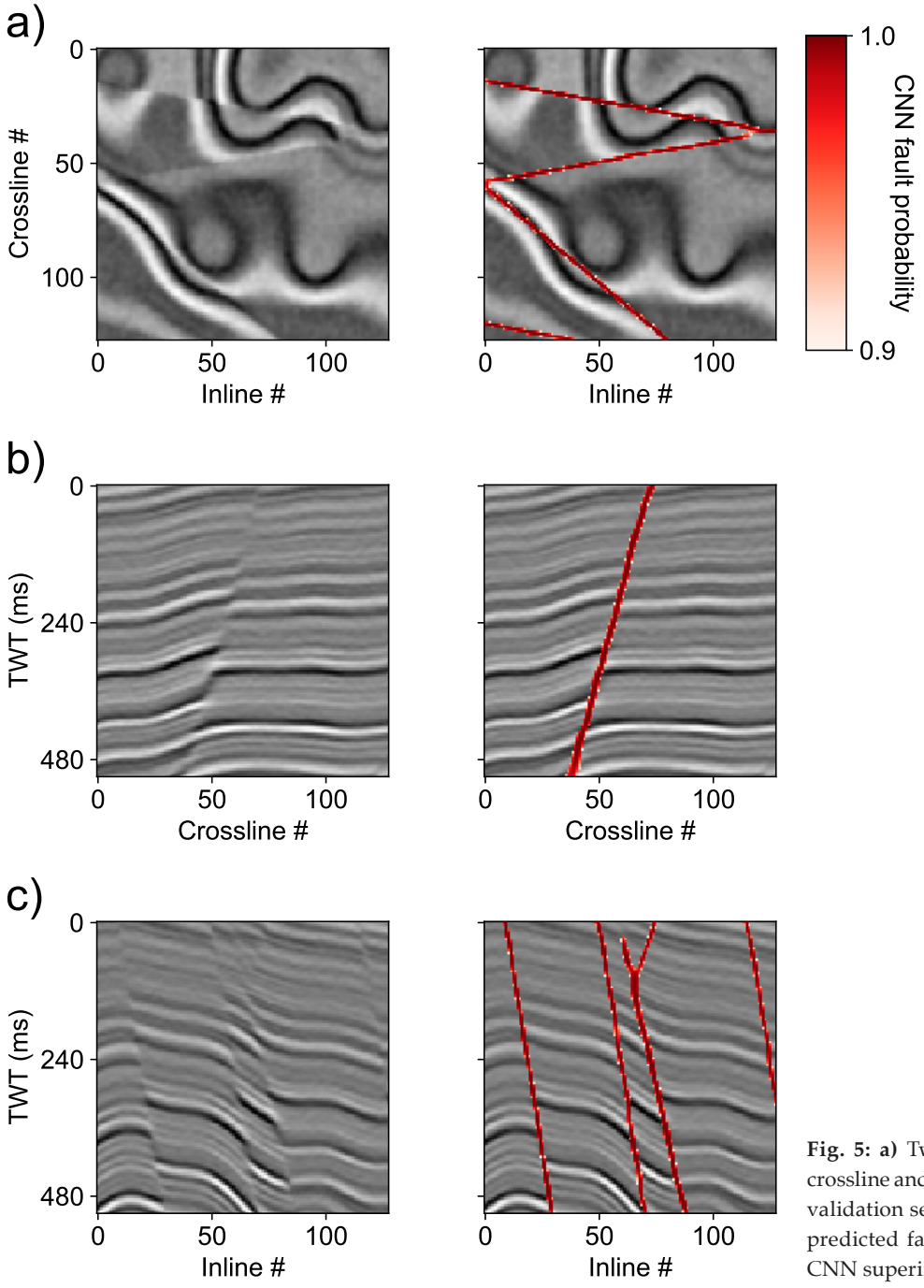


Fig. 5: a) Two-way traveltime (TWT), **b)** crossline and **c)** inline sections of a synthetic validation seismic cube in left column and predicted fault probability by the trained CNN superimposed in right column.

synthetic validation cube, which was not a part of the training process, with the fault predictions from the trained CNN model. We chose to show the > 90% of CNN fault probability throughout the study with the intention of ensuring a high level of confidence in the potential faults displayed. It should be stated that the CNN fault probability does not reflect true fault probability, but indicates the CNN model's posterior likelihood of a fault being present in a given dataset based on the learning and extracted features from the synthetic training data. Based on the synthetic samples used for training, the CNN model is applied to the conditioned seismic data from the Valdemar Field.

Variance and ant-tracking

The variance seismic attribute is a measure of spatial discontinuity. It is known as an edge detection process as it represents the lateral variability in a defined sample interval. The size of the sample interval determines the detail of fault features to be resolved, and the method is sensitive to both waveform and lateral changes of the reflection amplitude (Chopra & Marfurt 2007). For the interpreter, time slices of a variance volume or a similar edge attribute can be a great help when manually picking faults from vertical seismic sections. This makes it easier to stick to the same fault trace while scrolling through the data several inlines or crosslines at a time. Moreover, a so-called ant-tracking filter (Pedersen *et al*. 2002) can be applied to the variance attribute that further enhances surface-like features by a pre-defined set of orientation ranges and step sizes. This allows extracting features that resemble those of faults based on the variance while limiting the amount of random noise in the attribute. Both the variance attribute and ant-tracking filter will be used to compare with the CNN model predictions.

The post-stack seismic volume prior to the AGC-filtering as represented in upper plots of Fig. 3b and 3c is used as input for the variance attribute computation as the seismic attribute calculation does not require any pre-conditioning. From the variance attribute, the ant-tracking filter is applied. The details of the parameters for the variance and ant-tracking features are listed in Table 1.

Table 1. Input parameters of the variance and ant-tracking features. The Petrel E&P Software is used for the computations of the attributes.

Variance input parameters	
IL range	3
XL range	3
Vertical smoothing	15 samples (60 ms)
Window range	1 sample (4 ms)
Dip correction	off
Ant-tracking input parameters	
Ant mode	Passive
Initial ant boundary	7
Ant-track deviation	2
Ant step size	3
Illegal steps allowed	1
Legal steps required	3
Stop criteria (%)	5

Manual interpretations

A manual fault interpretation on the corresponding area from a regional 3D seismic volume (for details on this dataset, see Hansen *et al*. 2021) will be used to show what an interpreter with structural geological expertise would map in the area. It should be noted that the interpretation was performed on a depth-converted seismic volume that intersects with the Valdemar Field using both inlines, crosslines and variance maps of the Top Chalk, Base Chalk and Base Cretaceous Unconformity (BCU) horizons (Fig. 2). The fault offsets in the study area are relatively small compared to the vertical seismic resolution, which is around 30 meters for the section (Bredesen *et al*. 2021), and many show offsets that are near the limit of robust manual interpretation. It should be stated clearly that we do not consider the manual interpretation as a ground truth, but as an additional binary fault prediction attribute based on standard seismic attributes. The seismic attribute calculations and interpretations were achieved using another commercial software (Paleoscan) than what was used for the variance and ant-tracking features in this study. However, no major discrepancies are suspected, and the provided variance attribute as listed in Table 1 should be satisfying for the comparison purpose. In order to analyse the results, the depth of picked faults has been converted to two-way traveltime via the same velocity model that was used for generating the depth-converted volume.

CNN model results and comparison

A suite of the key Cretaceous horizons with superimposed CNN fault predictions can be seen in the following Figures: Top Chalk in Fig. 6, Base Chalk in Fig. 7, Sola horizon in Fig. 8, Tuxen horizon in Fig. 9, Valhall horizon in Fig. 10, and BCU horizon in Fig. 11.

Note that the seismic sections in the plots have slightly been brightened to contrast the superimposed

features. Both the manual interpretation and the CNN model are accompanied by a strike fault diagram to show the overall fault trends for the shown maps. According to the fault strike diagrams of both the manual interpretation and the CNN models, a general NE–SW-trend is dominating throughout the

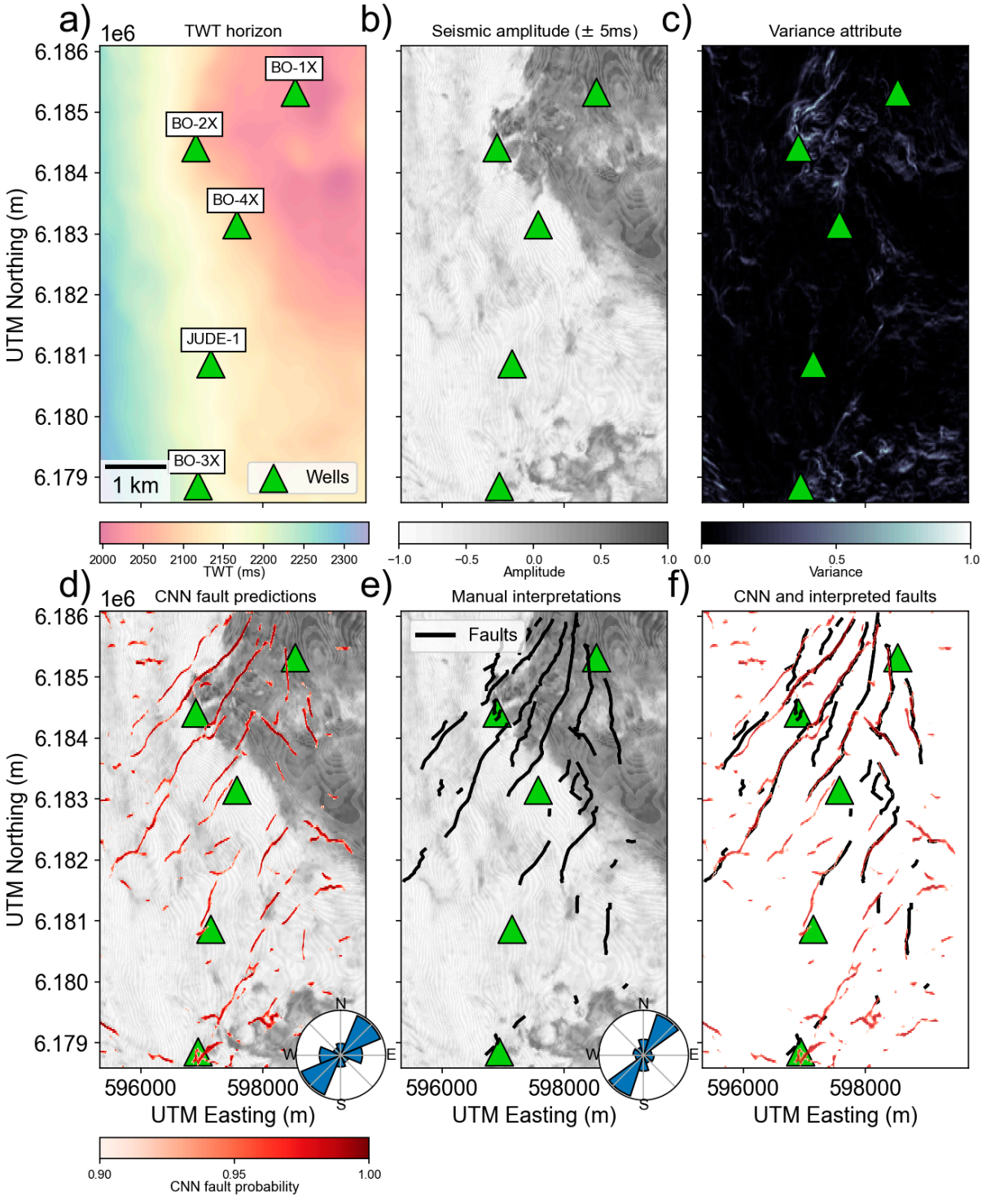


Fig. 6: a) Map of the Top Chalk horizon in two-way traveltime (ms). **b)** Averaged seismic amplitudes in a ± 5 ms window around the horizon. **c)** Variance attribute extracted along the horizon. **d)** CNN fault predictions (red colouring) and **e)** manual fault interpretations (black lines) along the horizon superimposed on the ± 5 ms seismic window with fault strike diagrams. **f)** CNN fault predictions superimposed with manual fault interpretations.

Cretaceous section in the Valdemar Field. The faults picked by the CNN model pose detailed and realistic interpretations when viewed on horizon maps. They are generally in agreement with the variance maps along the same horizons, in which relatively clear fault patterns are evident (e.g. Fig. 7 and Fig. 11).

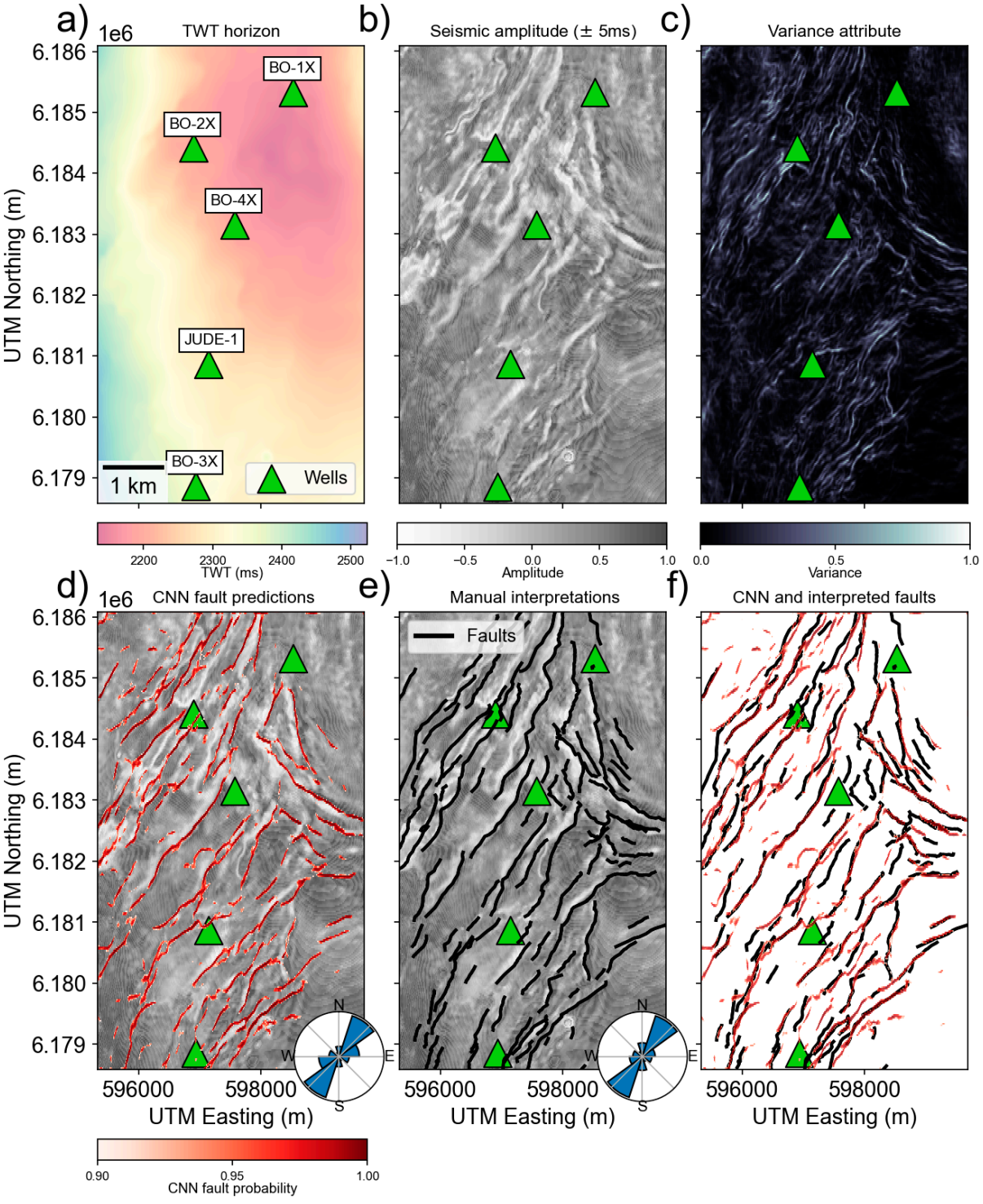


Fig. 7: a) Map of the Base Chalk horizon in two-way traveltime (ms). **b)** Averaged seismic amplitudes in a ± 5 ms window around the horizon. **c)** Variance attribute extracted along the horizon. **d)** CNN fault predictions (red colouring) and **e)** manual fault interpretations (black lines) along the horizon superimposed on the ± 5 ms seismic window with fault strike diagrams. **f)** CNN fault predictions superimposed with manual fault interpretations.

They also coincide well with the manually interpreted faults when viewed in this manner. A limited amount of manually interpreted faults are observed for the Top Tuxen and Top Valhall horzons (Fig. 9 and Fig. 10). It is suspected that this is related to interpretation was carried out using only the Top Chalk, Base Chalk and

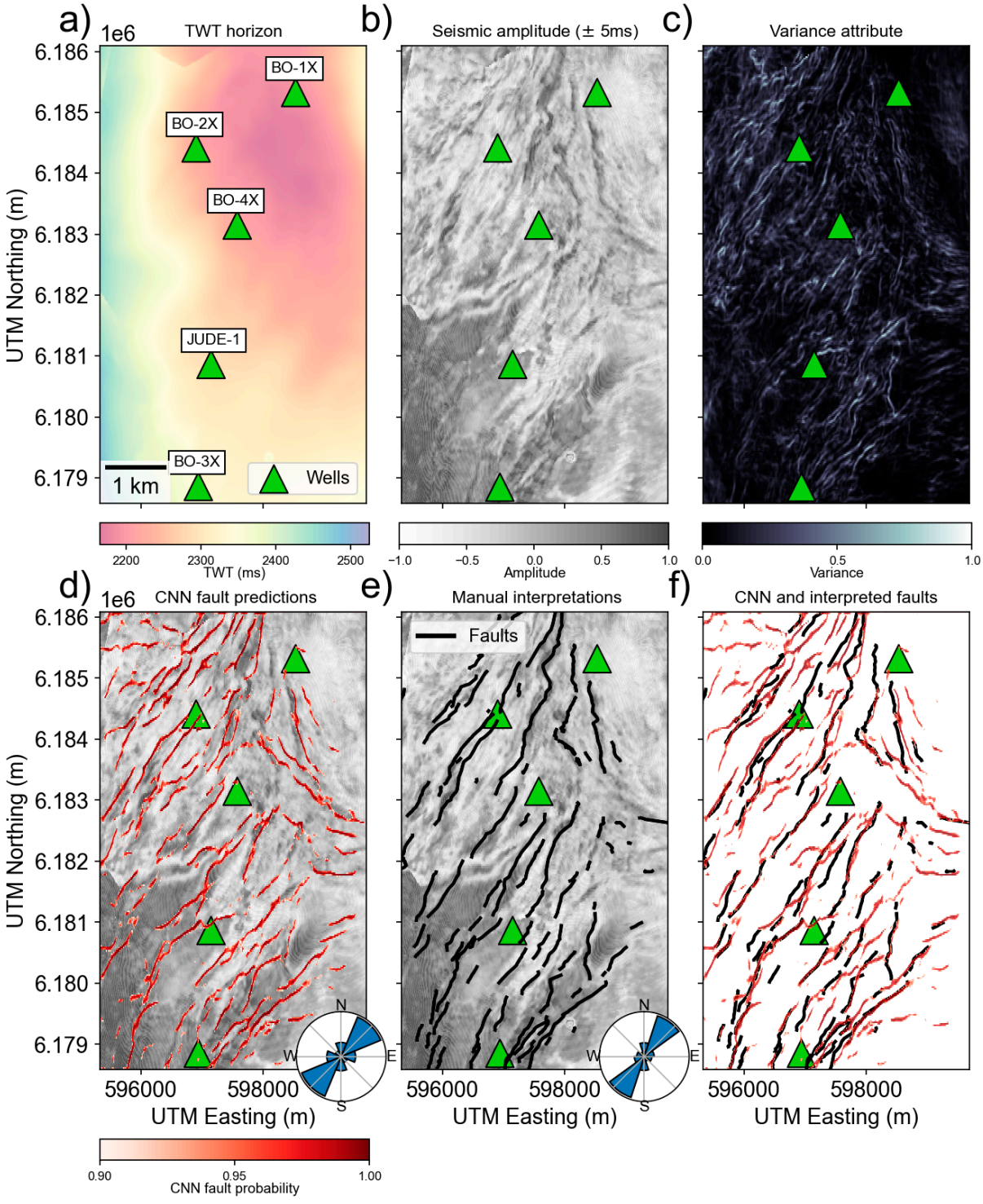


Fig. 8: a) Map of the Sola horizon in two-way traveltime (ms). **b)** Averaged seismic amplitudes in a ± 5 ms window around the horizon. **c)** Variance attribute extracted along the horizon. **d)** CNN fault predictions (red colouring) and **e)** manual fault interpretations (black lines) along the horizon superimposed on the ± 5 ms seismic window with fault strike diagrams. **f)** CNN fault predictions superimposed with manual fault interpretations.

BCU horizons, and therefore lacking details around the Tuxen and Valhall section of the survey. The CNN model provides a level of detail in the picked faults that surpasses that of the manual interpreter who only picks the faults from a fraction of the vertical seismic sections. Specifically, the close overlaps of individual

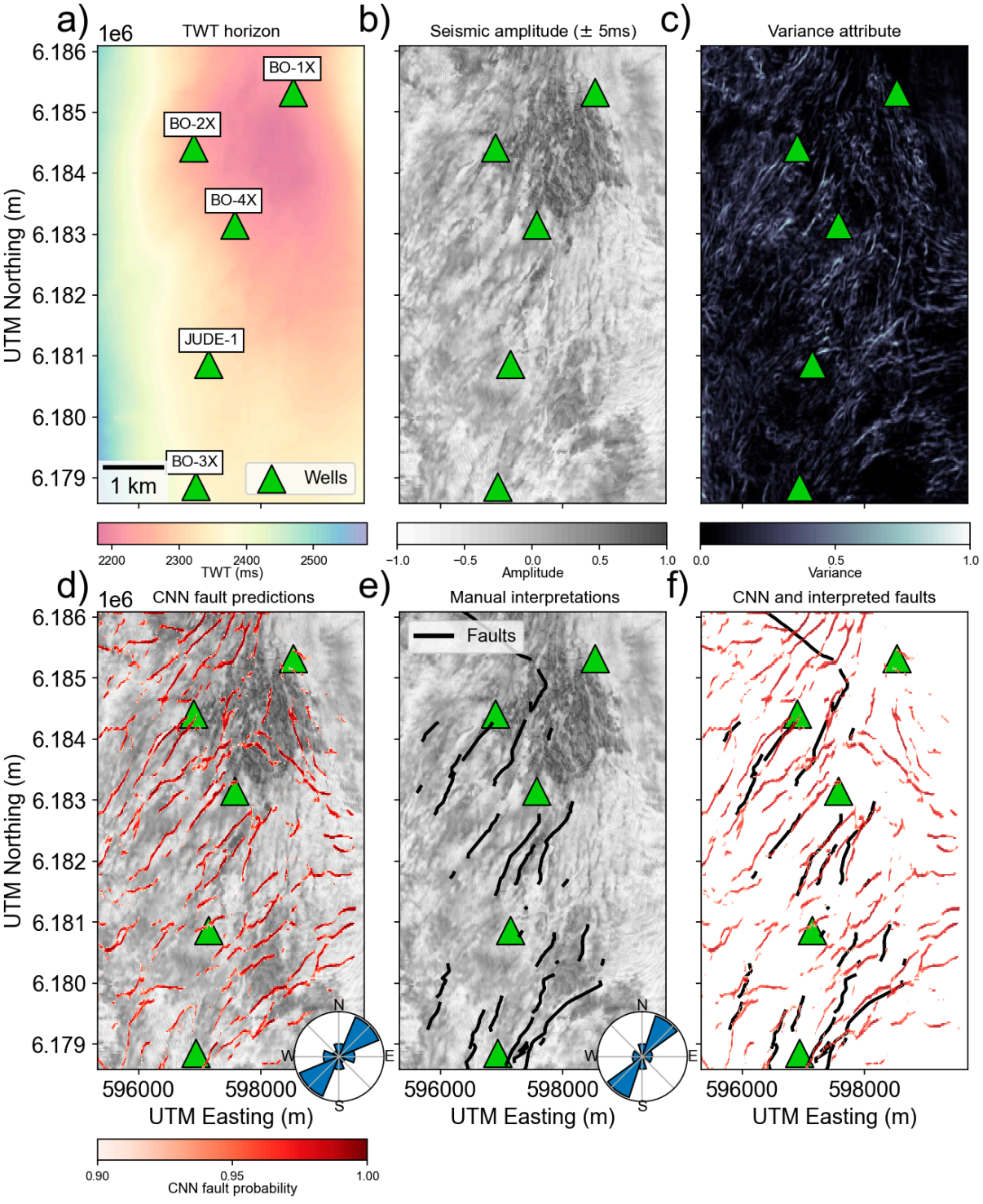


Fig. 9: a) Map of the Tuxen horizon in two-way traveltime (ms). **b)** Averaged seismic amplitudes in a ± 5 ms window around the horizon. **c)** Variance attribute extracted along the horizon. **d)** CNN fault predictions (red colouring) and **e)** manual fault interpretations (black lines) along the horizon superimposed on the ± 5 ms seismic window with fault strike diagrams. **f)** CNN fault predictions superimposed with manual fault interpretations.

faults and jogs in fault traces (caused by the merging of smaller fault segments during growth) are picked out nicely with good lateral consistency, whereas the manual interpreter would mostly pick only single linear fault segments across them. An example of this can be seen in (marked with blue circle in Fig. 11f)

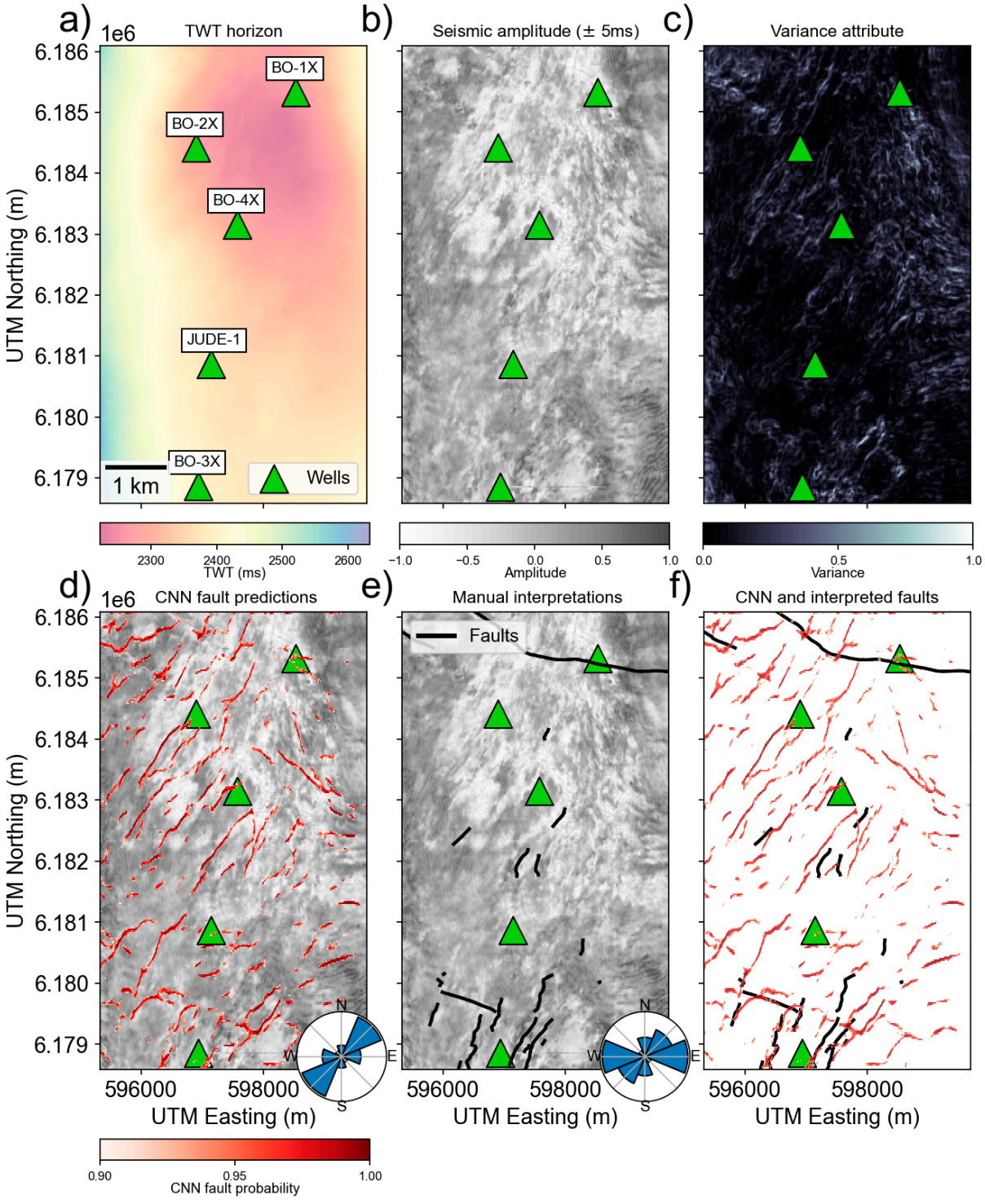


Fig. 10: a) Map of the Valhall horizon in two-way traveltime (ms). **b)** Averaged seismic amplitudes in a ± 5 ms window around the horizon. **c)** Variance attribute extracted along the horizon. **d)** CNN fault predictions (red colouring) and **e)** manual fault interpretations (black lines) along the horizon superimposed on the ± 5 ms seismic window with fault strike diagrams. **f)** CNN fault predictions superimposed with manual fault interpretations.

just below well Bo-4X. Here, the jogs where two faults have connected during lateral growth is mapped in detail by the CNN model, whereas neither the variance attribute nor the manual interpreter picks up

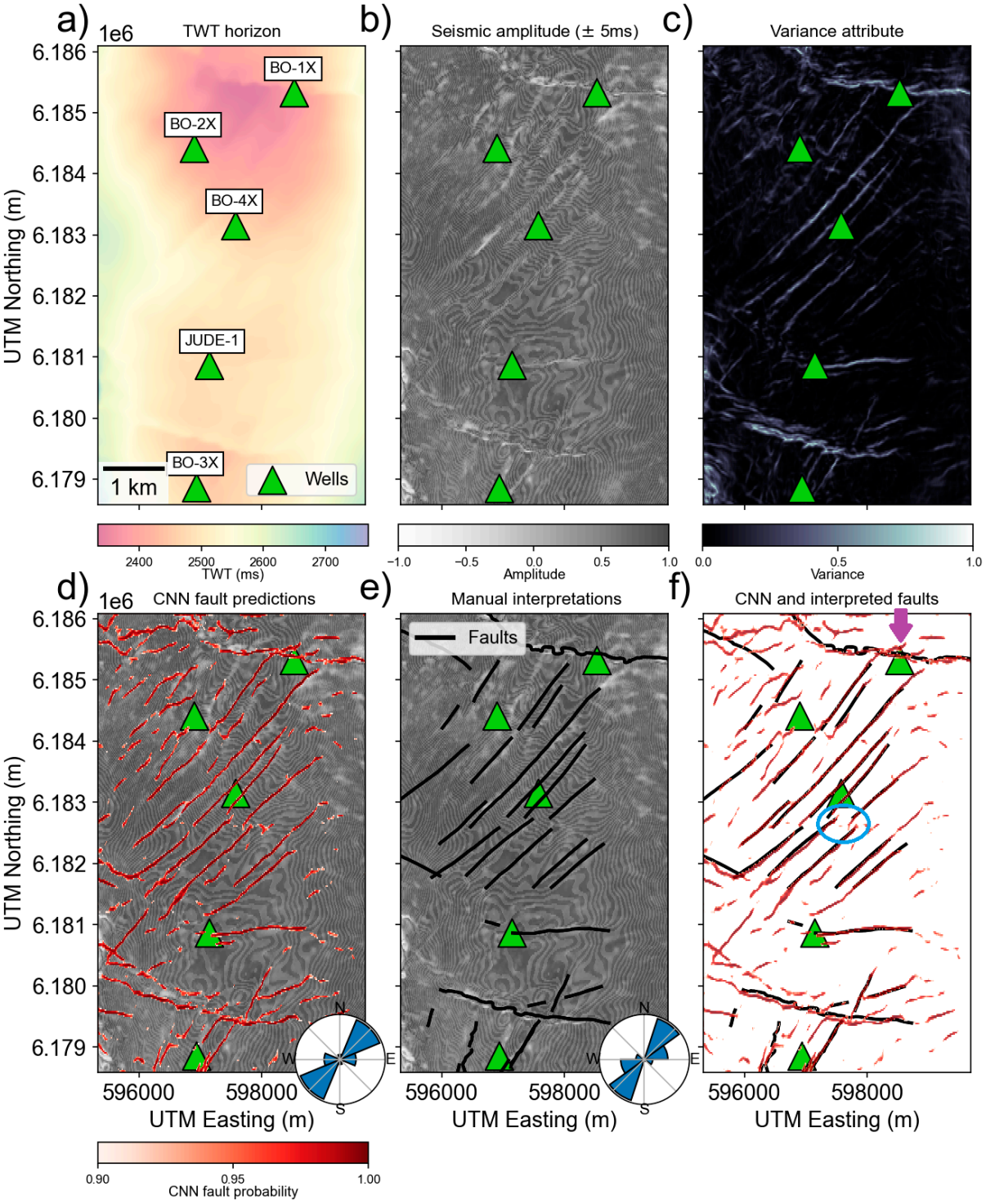


Fig. 11: a) Map of the Base Cretaceous Unconformity (BCU) horizon in two-way traveltime (ms). **b)** Averaged seismic amplitudes in a ± 5 ms window around the horizon. **c)** Variance attribute extracted along the horizon. **d)** CNN fault predictions (red colouring) and **e)** manual fault interpretations (black lines) along the horizon superimposed on the ± 5 ms seismic window with fault strike diagrams. **f)** CNN fault predictions superimposed with manual fault interpretations. The blue circle in f) highlights two jogs where faults have connected during lateral growth that are not represented in the variance attribute nor the manual interpretation.

this feature. Displayed upon stratigraphy-consistent horizons, the faults predicted by CNN appear realistic and overall in accordance with the manual interpretation and the seismic variance attribute.

Figures 12 and 13 show the crossline and inline sections displayed in Fig. 3 with superimposed results. The fault plots are accompanied by a dip attribute. It should be noted that the dip plots do not reflect the true angles due to the vertical exaggeration in the vertical sections. For simple planar fault segments in especially the Chalk Group (Fig. 2), the manual interpretation and the CNN model results seem to be in good agreement (green circles in Fig. 12c and Fig. 13c). However, some discrepancies are apparent between the dip angles of the CNN predictions and manual interpretations. In most cases, the CNN model predicts faults with larger dips than those of the manually interpreted faults, and less consistent, i.e. the CNN modelled faults often appear sinuous in the vertical sections (black circles in Fig. 12c and Fig. 13c). The most apparent detail in the CNN fault predictions and ant-tracking attribute of the crossline section (Fig. 12f) is in the lower-right region around the BCU horizon (marked with red circle). Here, the CNN predicts large areas to have a high probability of being faulted, and the same areas have high variance values (red circle in Fig. 13d). Considering the location of the crossline section (Fig. 3a, red dashed line), a WNW-ESE striking fault that runs sub-parallel to and intersects with the seismic section around Bo-1X has been outlined both manually and by CNN prediction at the BCU level (marked with purple arrow in Fig. 11f). Therefore, the faulting anomaly at BCU appears more as a plane rather than a line segment in the vertical section.

The ant-tracking filter agrees with the CNN model predictions in most cases as shown in Fig. 12f and Fig. 13f suggesting that the two methods track the same features in the seismic signals. Nonetheless, in the fault interpretation task of the Valdemar Field, the applied variance and ant-tracking filter can be problematic due to the ambiguity in the orientations of the fault features as well as outlining the extents of individual faults. A default set of input parameters was chosen for the variance and ant-tracking (Table 1), which shows the need to generate several iterations of variance and ant-tracking combinations in a trial and error fashion ideally limiting noise artefacts while preserving fault features. The CNN model does not require similar manual tuning as it is a part of the training process.

Discussion

The pre-trained CNN model from Wu *et al*. (2019) was used without any modifications of the model prior to applying it to the seismic data. It is important to have a healthy portion of scepticism about the training data that is put into the CNN model before making predictions in seismic data. This is due to the fact that the CNN model was trained on synthetic data, which raises a concern of to what extent the synthetic faults and seismic data represent the structural geology and seismic signals in the investigated area. It was suspected that the distortions observed in the Cretaceous succession of the Valdemar data originates from a combination of low signal-to-noise ratio and poor continuity of reflection events (Bredesen *et al*. 2021). Tailoring the synthetic data to resemble the seismic data from the Valdemar Field by e.g. using a statistical or deterministic wavelet from the seismic data instead of a Ricker wavelet and modifying the signal-to-noise ratio by adding or removing Gaussian noise could alter the fault predictions of the CNN model. It was seen in Fig. 4 that the wavelet and frequencies of the Valdemar data was well-represented in the training data. However, the cropped sections in Fig. 4a and 4b showed some visual dissimilarities with as the Valdemar data was more blurred and with poor reflection continuity. Data augmentation could be applied to make the training data more similar to the test data by implementing e.g. kernel filtering, resizing and rescaling and elastic (grid) deformation as a part of the training process. In the study by An *et al*. (2021), they conclude that vertical flip, emboss and elastic deformation substantially improves performance of the proposed machine learning models. The effect of the augmentation could be investigated by applying the CNN on the augmented data and, when trained, testing the new model on the Valdemar data and compare with the predictions presented in this research.

The pre-trained CNN has previously been applied on various seismic dataset representing different faulting systems with realistic fault predictions in agreement with other fault-enhancing seismic attributes and machine learning models, which indicates a good generalisation (Wu *et al*. 2019; An *et al*. 2021; Dou *et al*. 2021). However, it is questionable to what extent the trained CNN model is able to predict thrust and listric faults with low angle dips since these were not part of the training dataset. Low-angle faults were represented in the manual interpretation (Fig. 12a and 13a) whereas the CNN predicted faults were steeper (blue circles in Fig. 12c and 13c). The planar faulting in the synthetic data originating from Wu & Hale (2016) have dips ranging from 65°-85° corresponding to the seismic validation cube in Fig. 5. The high dip of the faults in

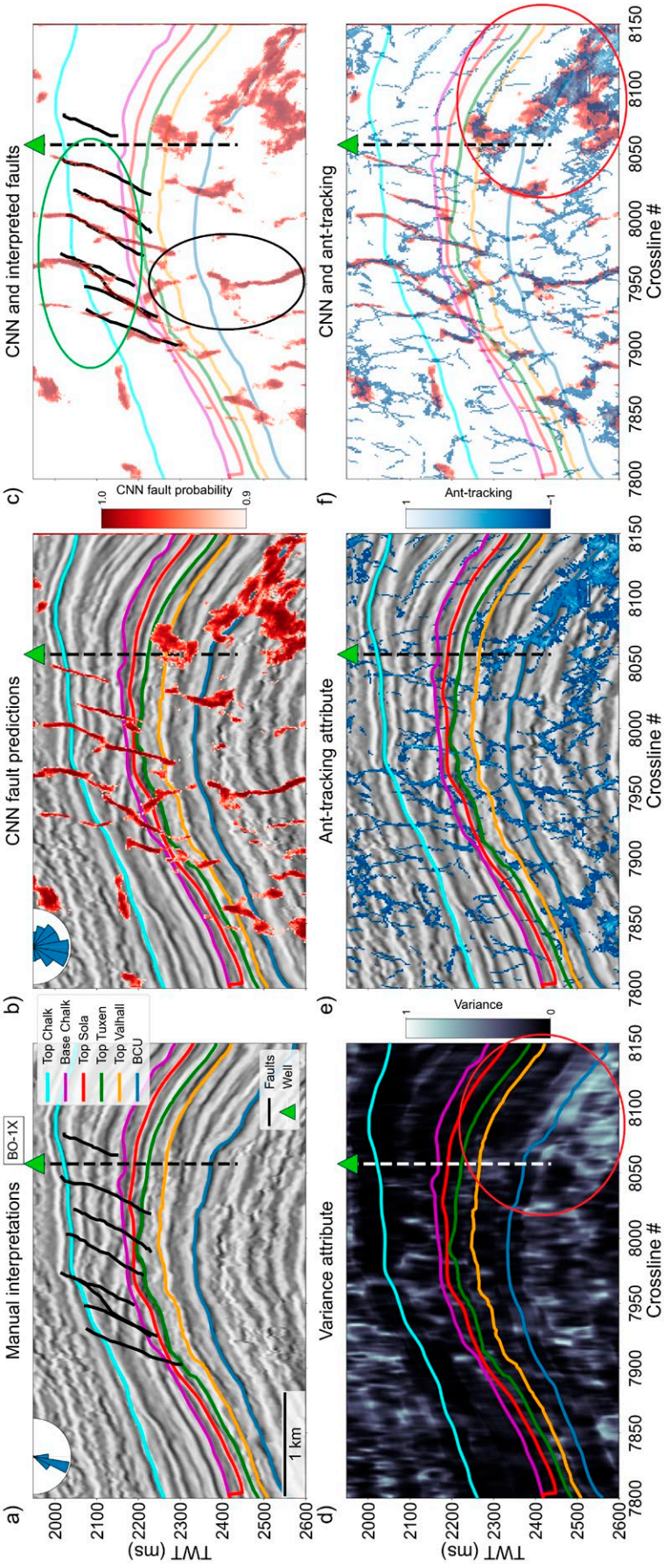


Fig. 12: Crossline section shown in Fig. 3a (dashed red) with **a)** intersecting manual interpretations and **b)** intersecting CNN predictions superimposed on the seismic section with dip attributes. **c)** CNN fault predictions superimposed with manual fault interpretations. The green circle highlights a good agreement between the two, and the black circle marks a discrepancy. **d)** Variance attribute and **e)** ant-tracking attribute extracted along the section superimposed on the seismic data. **f)** CNN fault predictions superimposed with ant-tracking attribute. The red circle indicates a parallel fault intersecting with the crossline section.

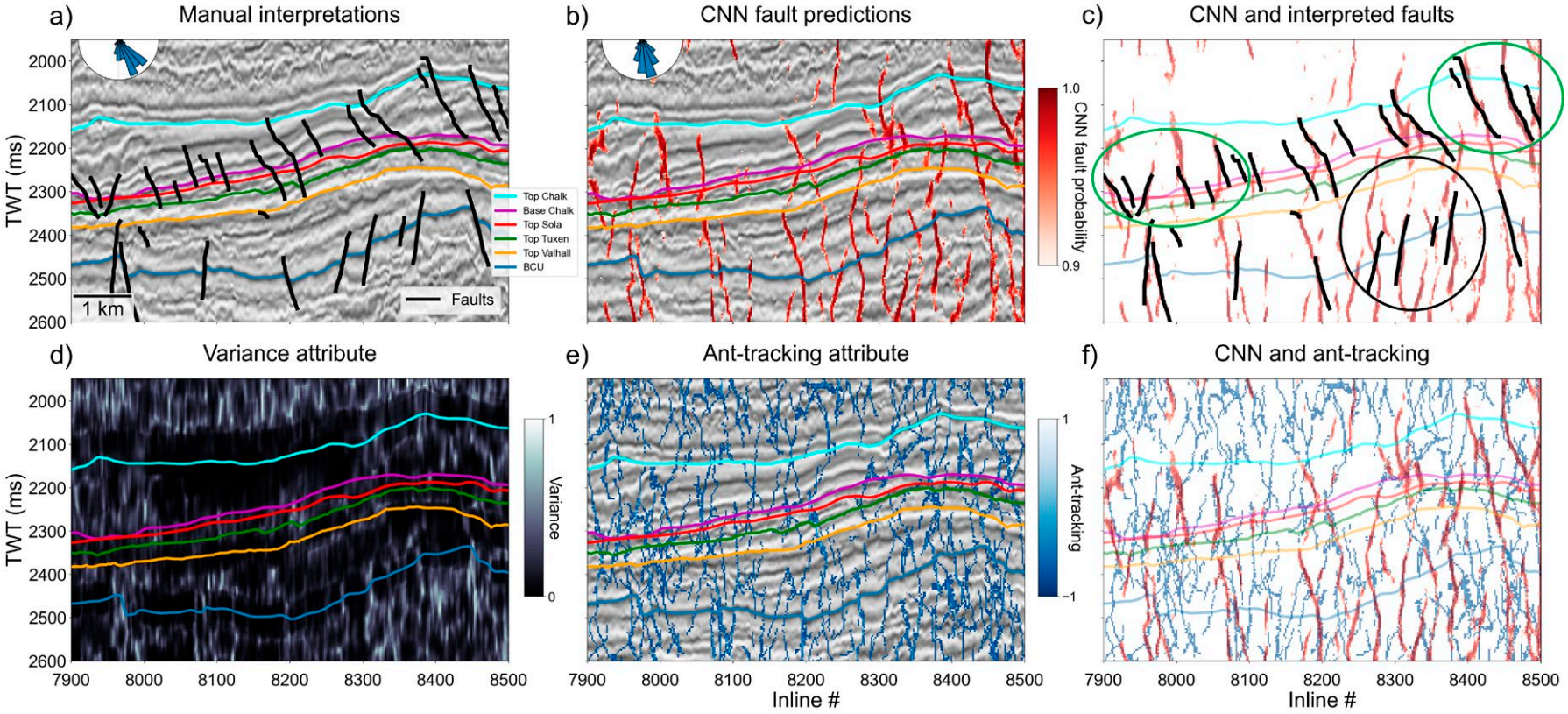


Fig. 13: Inline section shown in Fig. 3a (dashed blue) with **a)** intersecting manual interpretations and **b)** intersecting CNN predictions superimposed on the seismic section with dip attributes. **c)** CNN fault predictions superimposed with manual fault interpretations. The green circles highlight a good agreement between the two, and the black circle marks a discrepancy e) Variance attribute and **d)** ant-tracking attribute extracted along the section superimposed on the seismic data. **f)** CNN fault predictions superimposed with ant-tracking attribute.

the training data suggests that the CNN model has a bias towards predicting steeper faults limiting its ability to detect certain low-angle faults like thrust faults (Fossen 2016). One approach to test the hypothesis would be to apply the CNN model to a synthetic validation dataset with low-angle faults. Nonetheless, like a supervised learning approach, such as predicting faults with a CNN trained on synthetic fault dataset, the interpreter carries out the work with a given tectonic model in mind, which highlights the substantial degree of subjectivity and prior assumptions involved in manual seismic interpretation (Bond *et al.* 2012).

Different procedures exist that exploits a trained model and alter its learning towards a similar problem. A great number of fault attributes could be used in comparison to the CNN model results, but we chose some familiar structural attributes, namely variance (Marfurt *et al*. 1998) and ant-tracking (Pedersen *et al*. 2002). Other studies have utilised seismic attributes to guide fault modelling using supervised learning. Di *et al*. (2017) demonstrated how fault detection based on multi-attribute support vector machine classification and guided by manual interpretations could map faults in a 3D seismic cube. Such an approach could be implemented in a CNN model workflow, but the computational cost would be of concern due to the large increase of input data. In terms of using manual interpretations, Wrona *et al*. (2020) and An *et al*. (2021) demonstrated how manually labelled data could be used for fault predictions as mentioned in the introduction section. With regards to the challenge with limited seismic data quality, Cunha *et al*. (2020) demonstrated how transfer learning from a pre-trained neural network could utilise the learning obtained from synthetic seismic data into real data that significantly improved the overall scoring metrics for the fault predictions. Using transfer learning could potentially improve the fault mapping quality of the investigated area in this study.

The CNN model has provided new fault details in the Valdemar Field that may serve as an important input into building a robust static model or flow model. Moreover, due to the probability feature, the CNN model fault predictions are easier to interpret than the variance and ant-tracking attributes. The observed disagreements between the geometries of the fault systems in the CNN results and the manual interpretation shown in the vertical sections motivate for a re-interpretation of structural features occurring within the Cretaceous succession in Valdemar Field at a finer scale. Here, the CNN model predicts faults that are generally planar to slightly curved in nature, which suggests that the faults were deformed after their initial formation. These predictions could be erroneous due to the bias of steep faults in the training data and seismic noise, but the variance and ant-tracking attributes are to some extent in accordance with the CNN proposed fault patterns. Therefore, the CNN model should be treated as an additional fault interpretation tool for the interpreter to quality check in a critical manner. Identifying overlooked faults or adjusting previously interpreted faults may impact the fault mechanism that could influence the fluid migration in the Cretaceous succession (Smit *et al*. 2018). With decreasing commercial hydrocarbon exploration and production activities from the DCG, the proposed supervised learning approach to fault mapping and the results from this work can serve a purpose for prospect evaluation studies of exploiting the chalk fields for geological CO_2 storage (Frykman *et al*. 2009; Suicmez, 2019; Bonto *et al*. 2021).

Conclusion

A pre-trained convolution neural network is applied to the Cretaceous succession in the Valdemar Field, Danish North Sea, for improved fault predictions. The predicted faults show good consistency with the standard seismic attributes used for fault predictions and a manual interpretation. However, a comparison with the manual interpretations in vertical seismic sections show some fault geometry discrepancies in terms of dip angles and extents. As opposed to the manual interpretation, the neural network method suggest steeper and more curved fault geometries in accordance with the seismic variance and ant-tracking attribute. This sheds new light on the existing structural model and structural geological evolution in parts of the study area. The steeper dip angles proposed by the neural network could however be an artefact from the training data being composed of high-dipping planar faults. Moreover, like regular seismic attributes, the neural network is sensitive to seismic noise, which may distort the fault predictions. Hence, the method should be treated as an additional interpretation tool that needs quality checking. The method can yield valuable implications in reservoir characterisation and cap-rock integrity assessments for hydrocarbon exploration and CO_2 storage site evaluations.

Acknowledgements

This research has received funding from the Danish Offshore Technology Centre (DTU Offshore) under the Improved recovery from the tight Lower Cretaceous reservoir (LOCRETA) programme and is part of the PhD project of ML and THH. The authors kindly

acknowledge the Danish Underground Consortium (TotalEnergies E&P Denmark, Noreco and Nordsøfonden) for providing data and granting the permission to publish this work. The authors would like to thank the Software Underground community (SWUNG) for inspiring discussions regarding the machine learning aspect of the study. THH thanks Eliis for generously providing an academic license for the interpretation software, Paleoscan, which was used for the manual fault interpretation. Special thanks should be given to Shahjahan Laghari for the valuable technical support that greatly improved the quality of the study. Lastly, the authors would like to thank the reviewers for their thoughtful comments and efforts towards improving the manuscript.

References

An, Y., Guo, J., Ye, Q., Childs, C., Walsh, J., & Dong, R. 2021: Deep convolutional neural network for automatic fault recognition from 3D seismic datasets. Computers & Geosciences 153, 104776, doi:10.1016/j.cageo.2021.104776.

Araya-Polo, M., Dahlke, T., Frogner, C., Zhang, C., Poggio, T. & Hohl, D. 2017: Automated fault detection without seismic processing. Leading Edge 36, 208–214, doi:10.1190/tle36030208.1.

Bond, C. E., Lunn, R. J., Shipton, Z. K. & Lunn, A. D. 2012: What makes an expert effective at interpreting seismic images? Geology 40, 75–78, doi:10.1130/G32375.1.

Bonto, M. *et al*. 2021: Challenges and enablers for large-scale CO2 storage in chalk formations. EarthScience Reviews 222, 103826, doi:10.1016/j.earscirev.2021.103826.

Bormann P., Aursand P., Dilib F., Dischington P. & Manral S. 2020: FORCE Machine Learning Competition, url:https://github.com/bolgebrygg/ Force-2020-Machine-Learning-competition/.

Bredesen, K., Lorentzen, M., Nielsen, L. & Mosegaard, K. 2021: Quantitative seismic interpretation of the Lower Cretaceous reservoirs in the Valdemar Field, Danish North Sea. Petroleum Geoscience 27, petgeo2021-016, doi:10.1144/petgeo2021-016.

Chopra, S. & Marfurt, K. J. 2007: Seismic attributes for prospect identification and reservoir characterization, 1st edition, 457 pp. Society of Exploration Geophysicists and European Association of Geoscientists and Engineers.

Cunha, A., Pochet, A., Lopes, H. & Gattass, M. 2020: Seismic fault detection in real data using transfer learning from a convolutional neural network pretrained with synthetic seismic data. Computers and Geosciences 135, 104344, doi:10.1016/j.cageo.2019.104344.

Di, H., Shafiq, M. A. & AlRegib, G. 2017: Seismic-fault detection based on multiattribute support vector machine analysis. In 2017 SEG International Exposition and Annual Meeting. OnePetro, 2039–2044, doi:10.1190/segam2017-17748277.1.

Dou, Y., Li, K., Zhu, J., Li, T., Tan, S. & Huang, Z. 2021: Efficient Training of 3D Seismic Image Fault Segmentation Network under Sparse Labels by Weakening Anomaly Annotation, arXiv, doi: 10.48550/arXiv.2110.05319.

Dramsch, J. S. 2020: 70 Years of Machine Learning in Geoscience in Review. Advances in Geophysics 61, 1–55, doi:10.1016/bs.agph.2020.08.002.

Fossen, H. 2016: Structural Geology, 2nd edition, 524 pp., Cambridge University Press, doi:10.1017/9781107415096.

Frykman, P., Bech, N., Sørensen, A. T., Nielsen, L. H., Nielsen, C. M., Kristensen, L. & Bidstrup, T. 2009: Geological modeling and dynamic flow analysis as initial site investigation for large-scale CO2 injection at the Vedsted structure, NW Denmark. Energy Procedia 1, 2975–2982, doi:10.1016/j.egypro.2009.02.074.

Hansen, T. H., Clausen, O. R. & Andresen, K. J. 2021: Thick-and thin-skinned basin inversion in the Danish Central Graben, North Sea-the role of deep evaporites and basement kinematics. Solid Earth 12, 1719–1747, doi:10.5194/se-12-1719-2021.

Ineson, J. R. 1993: The Lower Cretaceous chalk play in the Danish Central trough. Petroleum Geology Conference Proceedings, 4. Geological Society of London, 175–183, doi:10.1144/0040175.

Ineson, J. R., Bojesen-Koefoed, J. A., Dybkjær, K. & Nielsen, L. H. 2003: Volgian-Ryazanian 'hot shales' of the Bo Member (Farsund Formation) in the Danish Central Graben, North Sea: Stratigraphy, facies and geochemistry. Geological Survey of Denmark and Greenland Bulletin 1, 403–436, doi:10.34194/geusb.v1.4679.

Jakobsen, F., Ineson, J. R., Kristensen, L. & Stemmerik, L. 2004: Characterization and zonation of a marly chalk reservoir: The Lower Cretaceous Valdemar field of the Danish Central Graben. Petroleum Geoscience 10, 21–33, doi:10.1144/1354-079303-584.

Jakobsen, F., Ineson, J. R., Kristensen, L., Nytoft, H. P. & Stemmerik, L. 2005: The Valdemar field, Danish central graben: Field compartmentalization and regional prospectivity of the Lower Cretaceous chalk play. In Petroleum Geology Conference Proceedings, 6. Geological Society of London, 177–186, doi:10.1144/0060177.

Long, J., Shelhamer, E. & Darrell, T. 2015: Fully Convolutional Networks for Semantic Segmentation. 2015 IEEE Conference on Computer Vision and Pattern Recognition, 3431–3440, doi: 10.1109/CVPR.2015.7298965.

Madsen, L. & Britze, P. 1999: PRIORITY - Improved oil recovery and productivity from Lower Cretaceous Carbonates – EFP-97. Sub-project 1.4.a: Seismic interpretation of the Cretaceous in the Valdemar Area. The Geological Survey of Denmark and Greenland.

Marfurt, K. J., Sudhakar, V., Gersztenkorn, A., Crawford, K. D. & Nissen, S. E. 1997: Coherency calculations in the presence of structural dip. 1997 SEG Annual Meeting 64, 566–569, doi:10.1190/1.1885964.

Marfurt, K. J., Kirlin, R. L., Farmer, S. L. & Bahorich, M. S. 1998:

3-D seismic attributes using a semblance-based coherency algorithm. Geophysics 63, 1150–1165, doi:10.1190/1.1444415.

Møller, J. J. & Rasmussen, E. S. 2003: Middle Jurassic–Early Cretaceous rifting of the Danish Central Graben. Geological Survey of Denmark and Greenland Bulletin 1, 247–264, doi:10.34194/geusb.v1.4654.

Montazeri, M., Uldall, A., Moreau, J. & Nielsen, L. 2018: Pitfalls in velocity analysis for strongly contrasting, layered media – Example from the Chalk Group, North Sea. Journal of Applied Geophysics 149, 52–62, doi:10.1016/j.jappgeo.2017.12.003.

Pedersen, S. I., Randen, T., Sønneland, L. & Steen, Ø. 2002: Automatic fault extraction using artificial ants. In SEG Technical Program Expanded Abstracts. Society of Exploration Geophysicists 21, 512–515, doi:10.1190/1.1817297.

Randen, T., Pedersen, S. I. & Sønneland, L. 2001: Automatic extraction of fault surfaces from three-dimensional seismic data. 2001 SEG Annual Meeting. Society of Exploration Geophysicists, 551–554, doi:10.1190/1.1816675.

Ronneberger, O., Fischer, P., & Brox, T. 2015: U-net: Convolutional networks for biomedical image segmentation. International Conference on Medical image computing and computer-assisted intervention 9351, 234-241, doi:10.1007/978-3-319-24574-4_28.

Smit, F. W., van Buchem, F. S. , Holst, J. C., Lüthje, M., Anderskouv, K., Thibault, N., Buijs, G. J., Welch, M. J. & Stemmerik, L. 2018: Seismic geomorphology and origin of diagenetic geobodies in the Upper Cretaceous Chalk of the North Sea Basin (Danish Central Graben). Basin Research 30, 895–925, doi:10.1111/bre.12285.

Smit, F. W., Stemmerik, L., Lüthje, M. & van Buchem, F. S. 2021: Characterization and origin of large Campanian depressions within the Chalk Group of the Danish Central Graben – implications for hydrocarbon exploration and development. Geological Society Special Publication 509, 249–282, doi:10.1144/SP509-2019-126.

Sorkhabi, R. & Tsuji, Y. 2005: Faults, Fluid Flow, and Petroleum Traps. Faults, Fluid Flow, and Petroleum Traps, 1st edition, 343 pp. American Association of Petroleum Geologists Memoir 85, doi:10.1306/m851033.

Suicmez, V. S. 2019: Feasibility study for carbon capture utilization and storage (CCUS) in the Danish North Sea. Journal of Natural Gas Science and Engineering 68, 102924, doi:10.1016/j.jngse.2019.102924.

van Bemmel, P. & Pepper, R. E. F. 2000: Seismic signal processing and apparatus for generating a cube of variance values. U.S. Patent 6151555.

van Buchem, F. S., Smit, F. W., Buijs, G. J., Trudgill, B. & Larsen, P. H. 2018: Tectonostratigraphic framework and depositional history of the Cretaceous-Danian succession of the Danish Central Graben (North Sea) - new light on a mature area. In Petroleum Geology Conference Proceedings, 8. Geological Society of London, 9–46, doi:10.1144/PGC8.24.

Vejbæk, O. V. 1986: Seismic stratigraphy and tectonic evolution of the Lower Cretaceous in the Danish Central Trough, Danmarks Geologiske Undersøgelse Serie A 11, 1-46, doi:10.34194/seriea.v11.7030.

Vejbæk, O. V. & Andersen, C. 2002: Post mid-Cretaceous inversion tectonics in the Danish Central Graben - regionally synchronous tectonic events? Bulletin of the Geological Society of Denmark 49, 129–144, doi:10.37570/bgsd-2003-49-11.

Vidalie, M., van Buchem, F., Schmidt, I. & Uldall, A. 2012: Seismic stratigraphy of the Lower Cretaceous Valhall Formation, Danish Graben, North Sea. 74th European Association of Geoscientists and Engineers Conference and Exhibition, 5327–5331, doi:10.3997/2214-4609.20148747.

Wrona, T., Pan, I., Bell, R. E., Gawthorpe, R. L., Fossen, H. & Brune, S. 2020: Deep learning of geological structures in seismic reflection data. Geophysics (submitted), doi: 10.31223/X5S88B.

Wu, X. & Hale, D. 2016: 3D seismic image processing for faults. Geophysics 81, IM1– IM11, doi:10.1190/GEO2015-0380.1.

Wu, X., Liang, L., Shi, Y. & Fomel, S. 2019: FaultSeg3D: Using synthetic data sets to train an end-to-end convolutional neural network for 3D seismic fault segmentation. Geophysics 84, IM35–IM45, doi:10.1190/geo2018-0646.1.

Ziegler, P. 1990: Geological Atlas of Western and Central Europe, Shell Internationale Petroleum Maatschappij B.V., the Hauge, 238 pp.

Facies and depositional processes of Lower Cretaceous carbonates, Danish Central Graben

MADS E. JELBY, JON R. INESON, NICOLAS THIBAULT, STÉPHANE BODIN, CARLETTE N. BLOK, NIKLAS EDVARDSEN, TATJANA S. CLEMMENSEN, TOMS BULS & KRESTEN ANDERSKOUV

Geological Society of Denmark
https://2dgf.dk

Received 16 February 2022
Accepted in revised form
1 July 2022
Published online
26 August 2022

© 2022 the authors. Re-use of material is permitted, provided this work is cited. Creative Commons License CC BY: https://creativecommons.org/licenses/by/4.0/

Jelby, M.E., Ineson, J.R., Thibault, N., Bodin, S., Blok, C.N., Edvardsen, N., Clemmensen, T.S., Buls, T. & Anderskouv, K. 2022: Facies and depositional processes of Lower Cretaceous carbonates, Danish Central Graben. Bulletin of the Geological Society of Denmark, Vol. 71, pp. 51–74. ISSN 2245-7070. https://doi.org/10.37570/bgsd-2022-71-04

The Lower Cretaceous Tuxen (lower Hauterivian – upper Barremian) and Sola (upper Barremian – Albian) Formations in the Danish Central Graben (North Sea) constitute one of the oldest chalk successions recorded globally, but have received little attention with regards to sedimentary facies and depositional processes. This study presents the first comprehensive carbonate facies analysis of the succession, retrieved from seven drill cores from the Valdemar and Adda Fields. A total of 50 facies are identified, based on a continuum of six lithologies ranging from chalk to marlstone and tuffaceous siltstone to sandstone that display eight different sedimentary structures or fabrics, and two redox-associated lithological color variations (green and red) in the Adda Field. The eight sedimentary structures record: (i) comprehensive bioturbation of homogeneous sediment during fully oxygenated benthic conditions and low sedimentation rates; (ii) a similar bioturbation process but in heterogeneous sediment with lithological contrasts permitting visible burrows to form, perhaps due to rhythmic alternation between pelagic (clay-poor) and hemipelagic (clay-rich) sedimentation; (iii) pelagic to hemipelagic suspension settling in dysoxic to anoxic bottom-water conditions; (iv) patchy cementation of the shallow sea bed during incipient hardground formation; (v) reworking of bioclasts and chalk intraclasts by bottom or wave-induced currents and cohesive debris flows; (vi) pressure solution during late burial diagenesis; (vii) shear deformation by intense plastic deformation of unlithified sediment from limited lateral displacement; and (viii) silicification during burial diagenesis. The facies distribution indicates that active tectonism took place prior to the onset of anoxia that resulted in deposition of the Munk Marl Bed, which in the Valdemar Field was followed by tectonic waning and repeated anoxia. The Valdemar Field constituted a basinal depocenter and was flanked to the east by an early inversion high in the Adda Field characterized by condensation and bypass. The Fischschiefer Member represents a return to prevailing anoxia, consistent with global records of the early Aptian Oceanic Anoxic Event 1a (OAE-1a).

Keywords: Aptian, Barremian, chalk, marlstone, Sola Formation, Tuxen Formation.

Mads E. Jelby [madsjelby@gmail.com], Department of Geosciences and Natural Resource Management, University of Copenhagen, Øster Voldgade 10, DK-1350 Copenhagen K, Denmark. Jon R. Ineson [ji@geus.dk], Geological Survey of Denmark and Greenland (GEUS), Øster Voldgade 10, DK-1350 Copenhagen K, Denmark. Nicolas Thibault [nt@ign.ku.dk], Department of Geosciences and Natural Resource Management, University of Copenhagen, Øster Voldgade 10, DK-1350 Copenhagen K, Denmark. Stéphane Bodin [stephane.bodin@geo.au.dk] and Carlette N. Blok [carletteblok@geo.au.dk], Department of Geoscience, Aarhus University, Høegh-Guldbergs Gade 2, DK-8000 Aarhus C, Denmark. Niklas Edvardsen [niklas.edvardsen@gmail.com], Tatjana S. Clemmensen [tatjanasc@gmail.com], Toms Buls [toms.buls@gmail.com] and Kresten Anderskouv [ka@ign.ku.dk], Department of Geosciences and Natural Resource Management, University of Copenhagen, Øster Voldgade 10, DK-1350 Copenhagen K, Denmark.

The Lower Cretaceous Tuxen (lower Hauterivian – upper Barremian) and Sola (upper Barremian – Albian) Formations of the Boreal North Sea Basin constitute one of the oldest chalk successions recorded globally (e.g. Mutterlose & Bottini 2013; van Buchem *et al.* 2018). Previously referred to as the 'Barremian limestones' (e.g. Damtoft *et al.* 1992), this Lower Cretaceous carbonate succession is widespread in the Danish Central Graben (DCG) in the westernmost offshore sector of Denmark (Fig. 1), and comprises a heterogeneous stratigraphy of pelagic white and marly chalk interbedded with marlstone and mudstone (Ineson 1993). The succession was deposited during a time of relatively frequent and pronounced global climatic and carbon-cycle perturbations, culminating with the crisis of the well-known early Aptian Oceanic Anoxic Event 1a (OAE-1a) (e.g. Malkoč *et al.* 2010; Mutterlose & Bottini 2013; Mutterlose *et al.* 2014; Blok *et al.* 2022 and references therein).

Due to a lower economic interest for the succession, the Tuxen and Sola Formations have received less attention than their Upper Cretaceous – Danian counterparts of the Chalk Group characterized by homogeneous, clean white chalk (Surlyk *et al.* 2003).

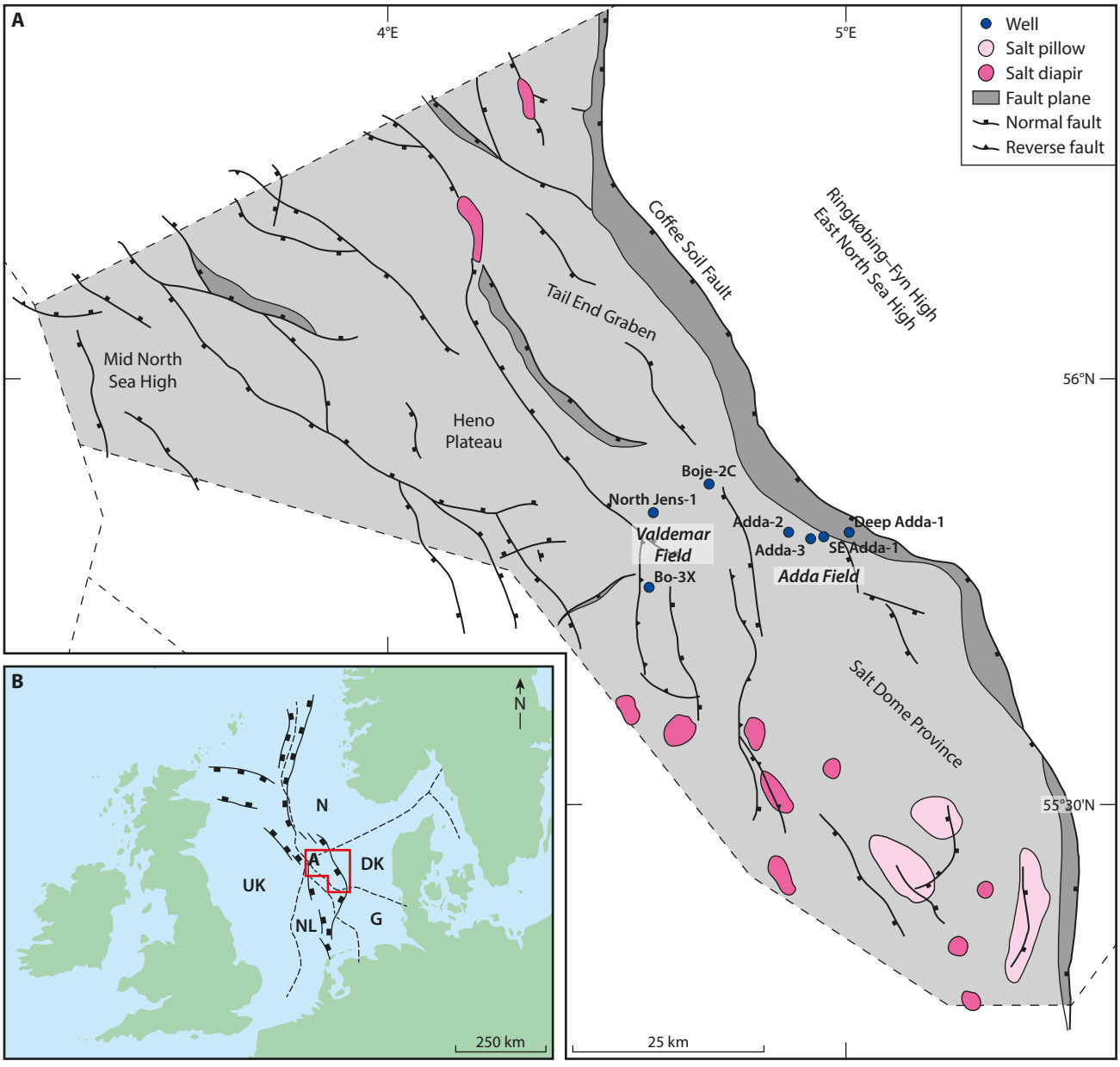


Fig. 1. Simplified maps of the structural configuration (modified from Japsen *et al.*, 2003, Møller & Rasmussen, 2003 and van Buchem *et al.*, 2018) of the DCG (A) in the larger North Sea Basin (B), including the well positions of the seven studied cores from the Valdemar and Adda Fields (A). DK, Denmark; G, Germany; N, Norway; NL, Netherlands; UK, United Kingdom.

Notable exceptions include studies on the general sedimentology (Jensen & Buchardt 1987; Ineson 1993), lithostratigraphy (Jensen *et al.* 1986; van Buchem *et al.* 2018), biostratigraphy (Heilmann-Clausen 1987; Thomsen 1987; Mutterlose & Bottini 2013), stratigraphic architecture and sequence stratigraphy (Vejbæk 1986; Kühnau & Michelsen 1994; Ineson *et al.* 1997; van Buchem *et al.* 2018), as well as reservoir characterization and zonation (Jakobsen *et al.* 2004, 2005). However, no detailed systematic accounts have been given of the sedimentary facies and corresponding depositional processes of the succession.

Thus, the primary objective of this study is to present the first coherent description and interpretation of the full range of carbonate facies of the Tuxen and Sola Formations, based on detailed sedimentological investigations of seven drill cores from the Valdemar and Adda Fields in the Danish Central Graben (Fig. 1A). In combination with a relatively robust lithostratigraphic framework of the cores (e.g. Jensen *et al.* 1986; Ineson 1993; Kühnau & Michelsen 1994; Jakobsen *et al.* 2004; van Buchem *et al.* 2018), this allows new inferences to be drawn for the Early Cretaceous basin development in this area of the DCG.

Regional setting and stratigraphy

Early Cretaceous basin configuration of the Danish Central Graben

In the Early Cretaceous, the North Sea Basin (Fig. 1B) formed part of a regionally extensive, but enclosed, epicontinental sea (Fig. 2) with a general low-gradient ramp physiography dissected centrally by a N–S-trending deeper-water graben system. The basin had relatively narrow connections to the open ocean to the north (Fig. 2A), and progressively to the south during post-Barremian times (Fig. 2B). Prior to the Aptian, however, the southern margin of the basin was closed from Tethyan influence (Tyson & Funnell 1987; Mutterlose 1992; Ineson 1993). Early Cretaceous sedimentation in the DCG is recorded by the Cromer Knoll Group, a marine mudstone-dominated succession up to 1 km thick (Fig. 3). The upper part of the Cromer Knoll Group in the DCG includes chalk-rich intervals within the Tuxen and Sola Formations, representing a gradual change from siliciclastic-dominated to carbonate-dominated sedimentation attributed to an overall sea-level rise that culminated in the Late Cretaceous eustatic highstand (Michelsen *et al.* 1987; Thomsen 1987; Thomsen & Jensen 1989; van Buchem *et al.* 2018).

The DCG consists of a complex series of NNW–SSE-trending half-grabens bounded by the Coffee Soil Fault and Ringkøbing-Fyn High to the east and by the Mid North Sea High to the west (Fig. 1; e.g. Japsen *et al.* 2003). Formation of the DCG commenced during repeated regional rifting and corresponding fault-controlled subsidence, which was initiated in the Callovian and continued into the Ryazanian (Møller & Rasmussen 2003). In the Early Cretaceous, the active rift phase was replaced by regional thermal subsidence centered on the axial graben system of the DCG, although differential subsidence of Late Jurassic half-grabens persisted from the Ryazanian to the mid-Hauterivian (Vejbæk 1986). Subsidence rates were lower than during the Late Jurassic and decreased further in the late Hauterivian with the initiation of uplift along inversion axes, which introduced regional subsidence patterns more characteristic of the Late Cretaceous and controlled the distribution of late Early Cretaceous depocentres (Vejbæk & Andersen 1987).

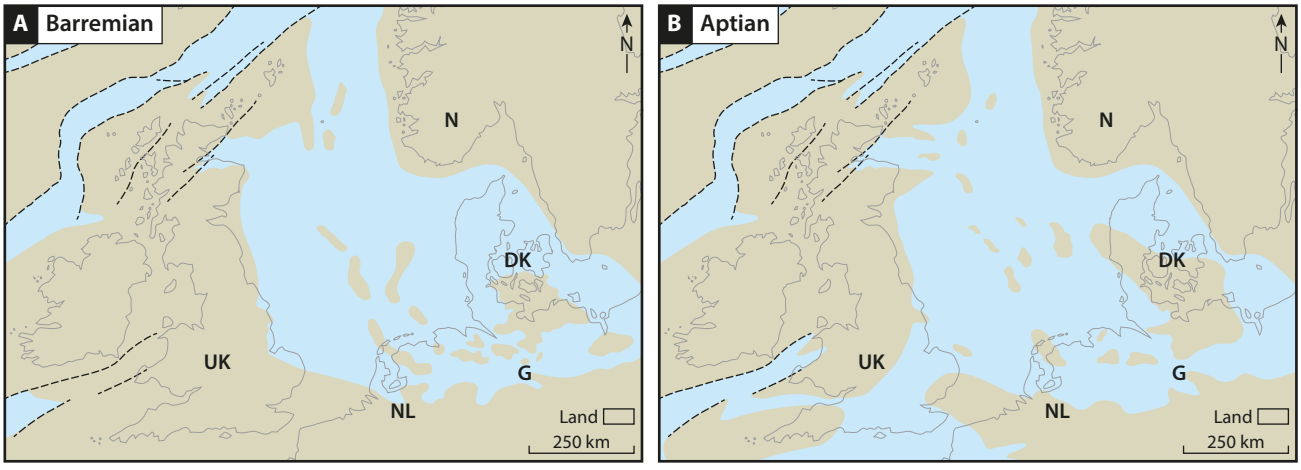


Fig. 2. Simplified Barremian (A) and Aptian (B) palaeogeographic reconstructions of the North Sea Basin (modified from Rückheim *et al.*, 2006). DK, Denmark; G, Germany; N, Norway; NL, Netherlands; UK, United Kingdom.

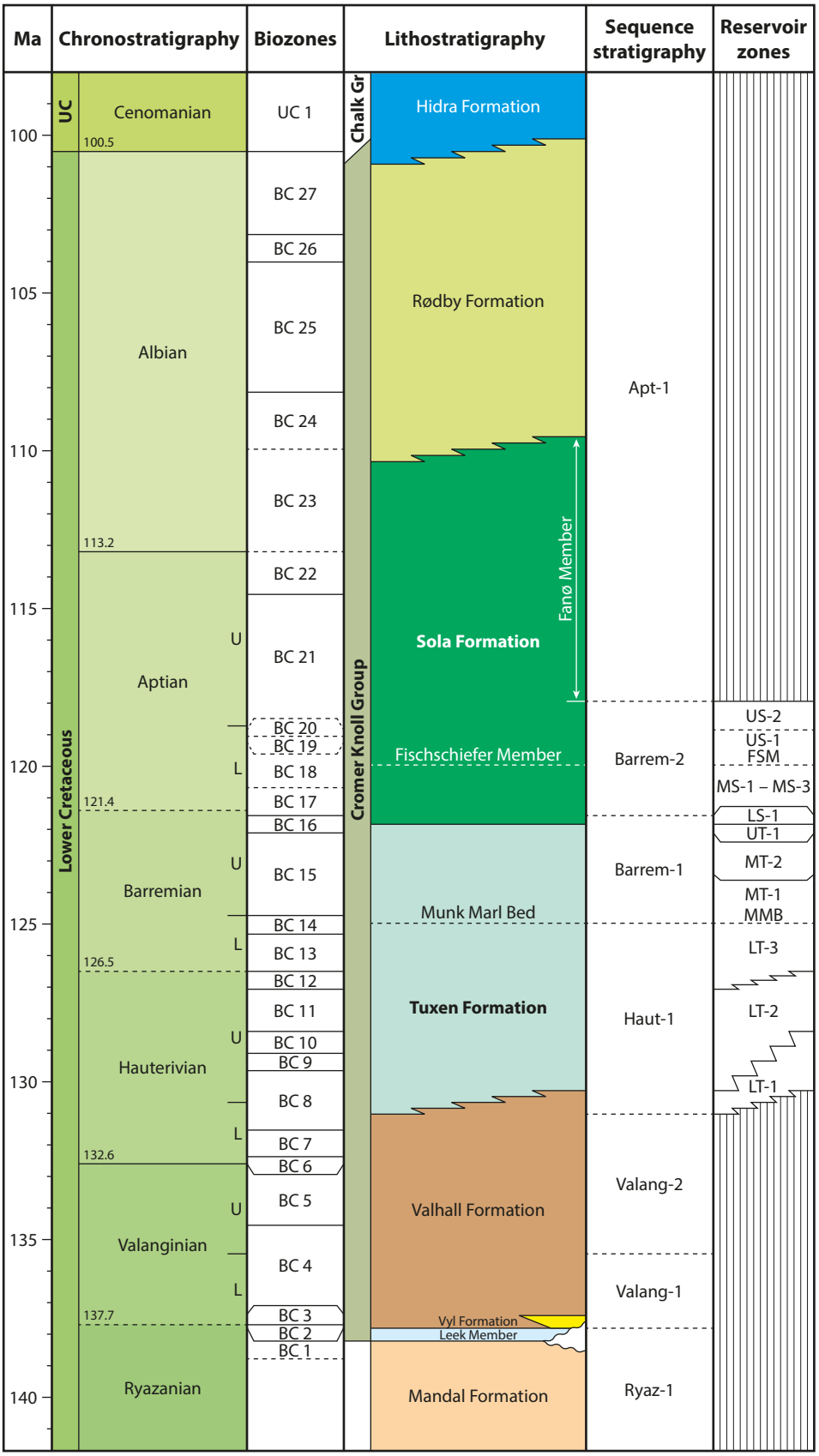


Fig. 3. Stratigraphic chart of the Lower Cretaceous Cromer Knoll Group in the DCG, including the Tuxen and Sola Formations and their depositional sequences and reservoir zones Lower Tuxen-1 (LT-1) to Upper Tuxen-1 (UT-1) and Lower Sola-1 (LS-1) to Upper Sola-2 (US-2). The chart is based on the Geological Time Scale 2020 (GTS2020; Gale *et al.* 2020), and compiled from Ineson (1993), Jakobsen *et al.* (2004) and van Buchem *et al.* (2018). UC, Upper Cretaceous.

The Valdemar and Adda Fields are located in the central part of the Danish Central Graben bounded to the north by the Heno Plateau and Tail End Graben and to the south by the Salt Dome Province (Fig. 1A). The Valdemar Field is situated on the crest of a N–S-elongated inversion ridge (the Jens–Bo Ridge), with the North Jens and Bo areas of this field separated by a saddle point (Jakobsen *et al.* 2004). The Adda Field lies at the north-western end of the Adda–Tyra–Igor ridge system, an inversion structure that was initiated in the late Valanginian – Hauterivian, but is primarily of Late Cretaceous age (Vejbæk & Andersen 1987).

Stratigraphy of the Tuxen and Sola Formations

The Tuxen Formation (lower Hauterivian – upper Barremian) is *c.* 20–80 m (65–260 ft) thick in the DCG (Jensen *et al.* 1986). The formation predominantly consists of white to off-white intensely bioturbated and commonly argillaceous coccolith chalk interbedded with bioturbated to laminated gray to green-gray marlstone (Fig. 4) of inferred pelagic and hemipelagic origin (Ineson 1993). The formation is characterized by two discrete chalk-dominated units separated by an up to 2 m (7 ft) thick unit of dark-gray to black, laminated, organic-rich marlstone of early Barremian age, named the 'Munk Marl Bed' (Jensen *et al.* 1986). The Munk Marl Bed is readily identified in most Lower Cretaceous well sections across the DCG by a clear break in petrophysical log patterns (Ineson 1993; Kühnau & Michelsen 1994), including a characteristic double peak in GR values (Fig. 4). In sequence and reservoir stratigraphic terms, the Tuxen Formation is equivalent to Sub-sequences K34–K36 of Copestake *et al.* (2003) and incorporates the reservoir zones Lower Tuxen-1 to Upper Tuxen-1 of Jakobsen *et al.* (2004) (Figs 3, 4). Whereas the two chalk-dominated, mainly bioturbated units broadly represent transgressive to highstand systems tracts and deposition in relatively well-oxygenated conditions, the laminated and organic-rich Munk Marl Bed has been postulated to record a protracted period of sea-floor anoxia due to sea-level lowstand and resulting basin isolation (Ineson *et al.* 1997; van Buchem *et al.* 2018). The carbonate content of the formation overall increases upwards with the cleanest chalk and best reservoir quality observed in the Upper Tuxen-1 reservoir zone in the top of the succession (Fig. 4; Jakobsen *et al.* 2004).

The Sola Formation (upper Barremian – Albian) is *c.* 20–40 m (65–130 ft) thick in the DCG (Jensen *et al.* 1986). The formation generally displays a laterally and vertically heterogeneous facies development of mainly gray-green to buff marlstone and claystone, dark-gray to black laminated marlstone and claystone (Fig. 4), as well as pale chalk and argillaceous chalk, and local siltstone and sandstone (Jensen & Buchardt 1987; Ineson 1993). Alternating pelagic and hemipelagic processes dominated deposition, with fluctuation of bottom-water oxygen levels and terrestrially derived sediment input (Jensen & Buchardt 1987). The Fischschiefer Member, a prominent laminated, organic-rich marlstone unit up to 2.5 m thick (8 ft), forms a distinctive stratigraphic and petrophysical well-log marker within the Sola Formation (Fig. 4) and time-equivalent formations elsewhere in the North Sea (Ainsworth *et al.* 2000). The uppermost part of the Sola Formation is constituted by the claystone-dominated Fanø Member (Fig. 3; van Buchem *et al.* 2018), previously referred to as the 'Albian shales'. The Sola Formation is equivalent to Sub-sequence K38 and Sequences K40–K50 of Copestake *et al.* (2003) and incorporates the reservoir zones Lower Sola-1 to Upper Sola-2 (Figs 3, 4; cf. Jakobsen *et al.* 2004). The formation has largely been attributed to lowstand and highstand systems tracts, with the base of the Fanø Member demarcating an important sequence boundary (Fig. 3; Ineson *et al.* 1997; van Buchem *et al.* 2018). The Fischschiefer Member corresponds to the globally recorded early Aptian OAE-1a (e.g. Malkoč *et al.* 2010; Mutterlose & Bottini 2013; Mutterlose *et al.* 2014), and has consequently been interpreted to record a maximum flooding surface possibly coinciding with partial oceanographic reconnection southwards with marine Tethyan basins (Malkoč *et al.* 2010; Pauly *et al.* 2013; van Buchem *et al.* 2018).

Material and methods

A total of 287 m (943 ft) of sedimentological logs were measured on drill cores from seven wells, namely the Bo-3X, Boje-2C and North Jens-1 wells of the Valdemar Field, and the Adda-2, Adda-3, Deep Adda-1 and SE Adda-1 wells of the Adda Field (Table 1; Fig. 1A). These wells are distributed across a *c.* 25 km long, roughly W–E-oriented transect (Fig. 1A). Collectively, the studied cores represent *c.* 11 m (35 ft) of the upper part of the Valhall Formation (Ryazanian – lower Hauterivian), 186 m (610 ft) of the entire Tuxen Formation, and *c.* 91 m (298 ft) of most of the Sola Formation with the exception of the upper part of the Upper Sola-2 reservoir zone and the Fanø Member (Table 1; Fig. 5). The cores are in moderate to excellent condition, and generally display a relatively continuous succession, although the uppermost Tuxen and lowermost Sola Formations are generally underrepresented (Fig. 5). Slickensided fractures are recorded locally in most core sections, often concentrated in marlier intervals.

Documentation of structural features in relation to facies and stratigraphy of the North Jens-1 core is presented in Glad *et al.* (2022).

Core description was carefully performed bed-by-bed at a scale of 1:5, and included descriptions of body and trace fossil assemblages and characteristics of bioturbation. The lithology (e.g. chalk, slightly marly chalk, chalky marlstone, etc.) was classified using a Tiffen® Q-13 Color Separation Guide and Gray Scale (Small), and several facies-representative intervals of the cores were treated with light, transparent oil in order to enhance the visual appearance of sedimentary

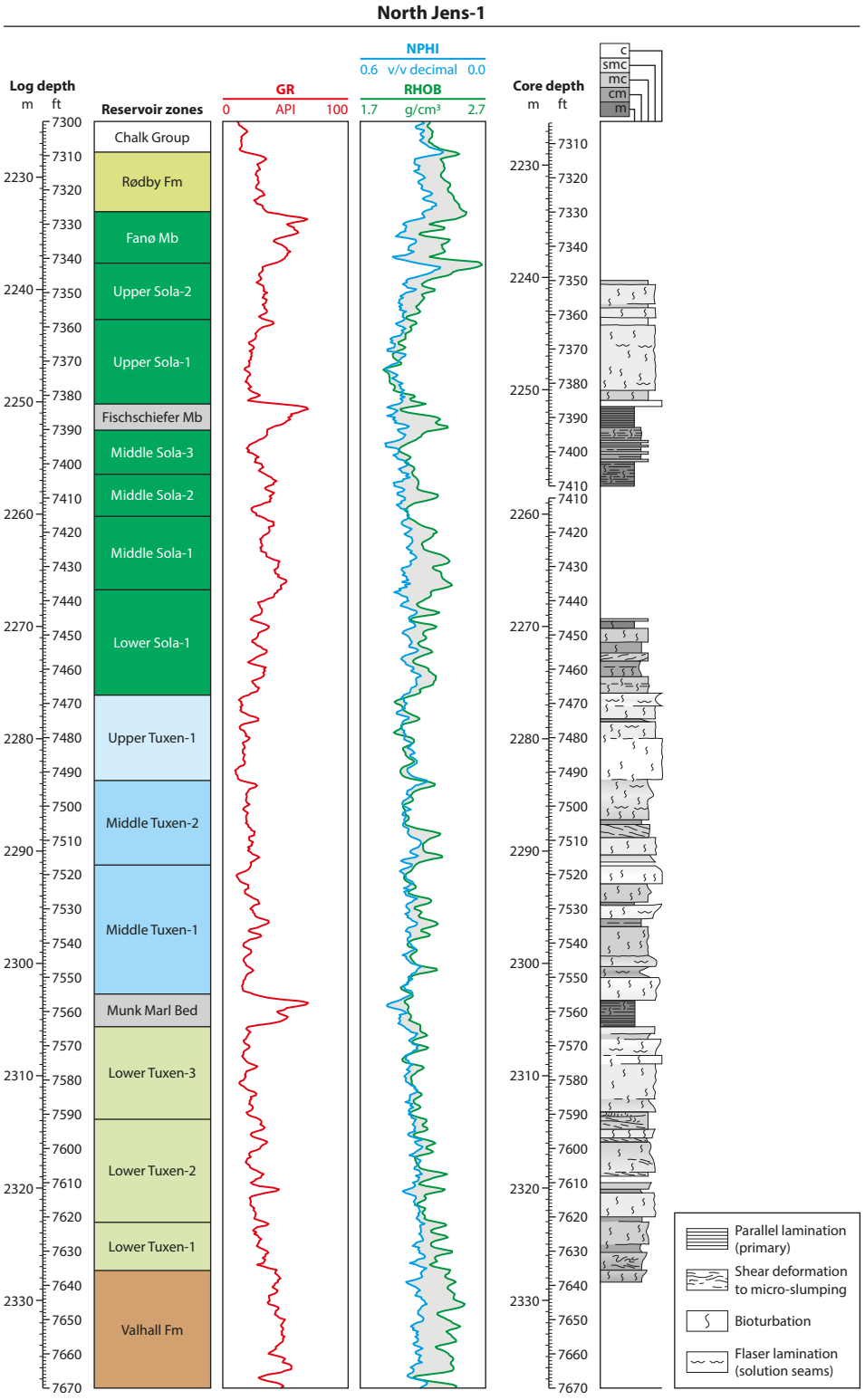


Fig. 4. General stratigraphy of the Cromer Knoll Group exemplified by the North Jens-1 well core, including reservoir zonation (Jakobsen *et al.* 2004), sedimentological log (this study), and petrophysical gamma-ray (GR), neutron porosity (NPHI) and density (RHOB) logs. The minor gap in the depth of the sedimentological log around 7410 ft results from different core:log depth-shifts between the upper core (*c.* 4 ft) and the lower cores (no significant shift). Lithological abbreviations refer to: c, chalk; smc, slightly marly chalk; mc, marly chalk; cm, chalky marlstone; m, marlstone.

Table 1. Depth, well stratigraphic thickness (including core gaps) and logged thickness (excluding core gaps) of studied core intervals, including the Valhall, Tuxen and Sola Formations

	Depth				Well stratigraphic thickness				Logged core thickness			
	Valhall Fm	Tuxen Fm	Sola Fm	Total	Valhall Fm	Tuxen Fm	Sola Fm	Total	Valhall Fm	Tuxen Fm	Sola Fm	Total
Valdemar Field												
Bo-3X	–	2580.13–2546.60 m	–	2580.13–2546.60 m	–	33.53 m	–	33.53 m	–	26.68 m	–	26.68 m
	–	8465 ft 0 in – 8355 ft 0 in	–	8465 ft 0 in – 8355 ft 0 in	–	110 ft 0 in	–	110 ft 0 in	–	87 ft 7 in	–	87 ft 7 in
Boje-2C	2623.41–2616.40 m	2616.40–2556.36 m	2556.36–2544.17 m	2623.41–2544.17 m	7.01 m	60.05 m	12.19 m	79.25 m	6.96 m	55.99 m	12.15 m	75.10 m
	8607 ft 0 in – 8584 ft 0 in	8584 ft 0 in – 8387 ft 0 in	8387 ft 0 in – 8347 ft 0 in	8607 ft 0 in – 8347 ft 0 in	23 ft 0 in	197 ft 0 in	40 ft 0 in	260 ft 0 in	22 ft 10 in	183 ft 9 in	39 ft 11 in	246 ft 6 in
North Jens-1	2328.37–2326.54 m	2326.54–2275.94 m	2275.94–2240.28 m	2328.37–2240.28 m	1.83 m	50.60 m	35.66 m	88.09 m	1.83 m	48.22 m	35.55 m	85.60 m
	7639 ft 0 in – 7633 ft 0 in	7633 ft 0 in – 7467 ft 0 in	7467 ft 0 in – 7350 ft 0 in	7639 ft 0 in – 7350 ft 0 in	6 ft 0 in	166 ft 0 in	117 ft 0 in	289 ft 0 in	6 ft 0 in	158 ft 2 in	116 ft 8 in	280 ft 10 in
Adda Field												
Adda-2	–	2393.59–2370.73 m	2370.73–2362.20 m	2393.59–2362.20 m	–	22.86 m	8.53 m	31.39 m	–	17.89 m	7.70 m	25.59 m
	–	7853 ft 0 in – 7778 ft 0 in	7778 ft 0 in – 7750 ft 0 in	7853 ft 0 in – 7750 ft 0 in	–	75 ft 0 in	28 ft 0 in	103 ft 0 in	–	58 ft 9 in	25 ft 3 in	84 ft 0 in
Adda-3	2404.90–2402.94 m	2402.94–2377.29 m	2377.29–2363.42 m	2404.90–2363.42 m	1.96 m	25.65 m	13.87 m	41.48 m	1.91 m	20.78 m	13.87 m	36.56 m
	7890 ft 1 in – 7883 ft 8 in	7883 ft 8 in – 7799 ft 6 in	7799 ft 6 in – 7754 ft 0 in	7890 ft 1 in – 7754 ft 0 in	6 ft 5 in	84 ft 2 in	45 ft 6 in	136 ft 1 in	6 ft 3 in	68 ft 2 in	45 ft 6 in	119 ft 11 in
Deep Adda-1	–	2450.52–2446.02 m	–	2450.52–2446.02 m	–	4.50 m	–	4.50 m	–	4.29 m	–	4.29 m
	–	8039 ft 9 in – 8025 ft 0 in	–	8039 ft 9 in – 8025 ft 0 in	–	14 ft 9 in	–	14 ft 9 in	–	14 ft 1 in	–	14 ft 1 in
SE Adda-1	–	2413.25–2396.24 m	2396.24–2374.39 m	2413.25–2374.39 m	–	17.02 m	21.84 m	38.86 m	–	12.12 m	21.44 m	33.56 m
	–	7917 ft 6 in – 7861 ft 8 in	7861 ft 8 in – 7790 ft 0 in	7917 ft 6 in – 7790 ft 0 in	–	55 ft 10 in	71 ft 8 in	127 ft 6 in	–	39 ft 9 in	70 ft 4 in	110 ft 1 in
				TOTAL	10.80 m	214.21 m	92.09 m	317.10 m	10.70 m	185.97 m	90.71 m	287.38 m
					35 ft 5 in	702 ft 9 in	302 ft 2 in	1040 ft 4 in	35 ft 1 in	610 ft 3 in	297 ft 8 in	943 ft 0 in

structures, and subsequently photographed using a fixed-position camera with precisely calibrated white and color balances.

In order to validate that the classification of lithologies was accurately determined by using the color (i.e. grayscale) of the sediments, a total of 246 geochemical data points were acquired from the Boje-2C core by X-ray fluorescence (XRF) on powdered samples using an Innov-x Olympus DELTA Premium 6000 Handheld XRF Analyzer with a 4W X-ray Rh tube in a stationary setup in combination with Innov-x DELTA PC software. The $CaCO_3$ content was estimated using a calibration of the Ca concentration measured by the XRF to reference powders (Ullmann 2013). Concurrently, lithological grayscale values were measured of the powdered samples using a conventional flatbed scanner.

The core depths are reported in imperial units, which were directly transcribed during core description and subsequently converted to metric units, with both units employed throughout this manuscript in order to preserve accurate relationships to the primary drilling data.

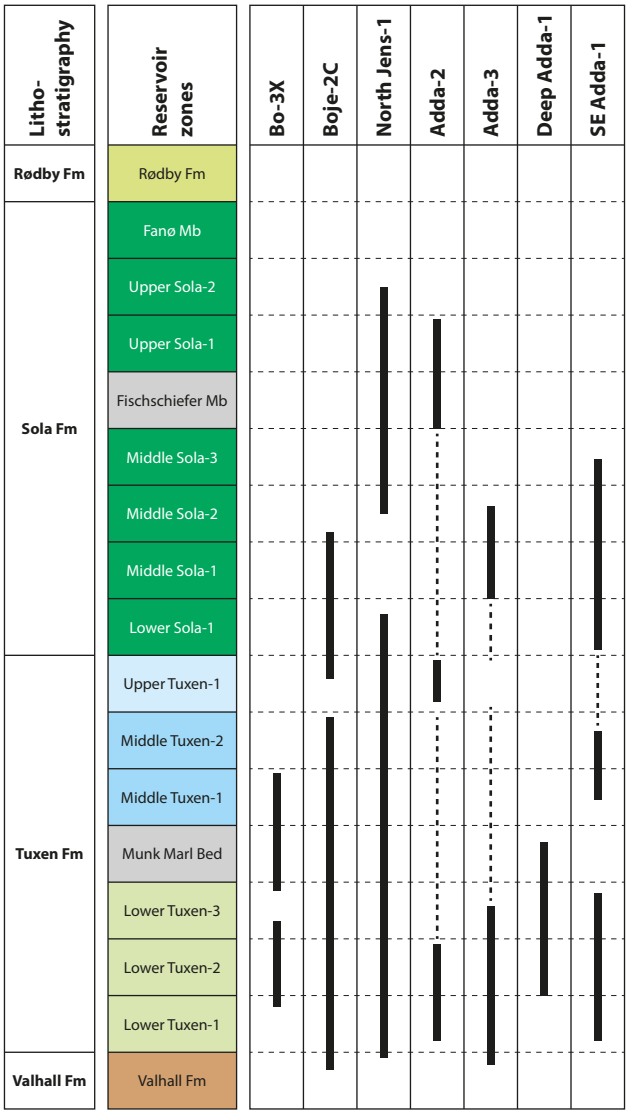


Fig. 5. Range and distribution of lithostratigraphic units, reservoir zones and hiati (dashed lines) in each of the seven well cores (black bars) investigated in this study.

Facies

Classification and definition

A total of 50 facies are defined and annotated according to: (i) six lithologies; (ii) eight different sedimentary structures (or fabrics); and (iii) two lithological color variations. First, the lithologies (1–6) include chalk (1), slightly marly chalk (2), marly chalk (3), chalky marlstone (4), marlstone (5; including shaly, silty and sandy marlstone and mudstone) and tuffaceous siltstone to sandstone (6), with the total thickness, proportion and number of units of each lithology varying between the studied cores (Table 2). Lithologies 1–5 constitute a color continuum from white (chalk) to dark-gray and black (marlstone), which correlates with a high and low carbonate content, respectively, and correspondingly low and high content of detrital mud, pyrite and/or organic matter. The exception is the Munk Marl Bed, which is anomalously dark compared to lithologies of similar carbonate content (Fig. 6), probably largely due to its high organic-matter content. Second, sedimentary structures (a–e and x–z) include homogeneous bioturbation (a), mottled bioturbation (b), parallel lamination (c), nodular fabric (d), matrix-rich conglomerate (e), flaser lamination (x), shear deformation structures (y) and silicified fabric (z) (Figs 7, 8). Third, lithological color variations include green (*g*) and red (*r*) redox-associated nuances of slightly marly chalk to marlstone (lithologies 2–5). This color-differentiated group of facies is confined to the Adda-2, Adda-3 and SE Adda-1 cores. In some cases, this facies classification and annotation results in a particular carbonate being described by three facies labels; for example, a facies of marly chalk (lithology 3) that is both biomottled (sedimentary structure b) and red-colored (color *r*) is referred to as 'F3b*r*' (Fig. 7).

Facies defined by sedimentary structures a–e are 'classical' facies, representing fabrics that either relate to depositional processes directly (e.g. grading, lamination etc.) or to processes within the surficial sediment that are directly linked to the depositional interface (i.e. bioturbation, early diagenetic nodular

cementation etc.). Facies comprising sedimentary structures x–z, in contrast, represent subsequent modifications of the depositional fabric under progressive burial by processes controlled by basin morphology or tectonics and the burial history. Facies that comprise sedimentary structures x–z thus constitute a heterogeneous group of fabrics formed in the shallow subsurface due to gravitational instability (i.e. shear-deformed fabrics), and fabrics that are of later, diagenetic origin (i.e. solution seams and silicified fabrics). It should be noted that deformation bands (*sensu lato* hairline fractures; Wennberg *et al*. 2013) are recorded in a range of facies (Glad *et al*. 2022). Given their facies-crossing nature and probable compactional origin (Wennberg *et al*. 2013), however, deformation bands are not considered here as a criterion for facies differentiation, though their abundance in certain facies is noted.

Recurring facies arrangements of the eight different sedimentary structures allow identification of fundamentally different depositional processes, which are thus outlined in detail below.

Table 2. Lithological distribution in cores

	Lithology 1	**Lithology 2**	**Lithology 3**	**Lithology 4**	**Lithology 5**	**Lithology 6**	**TOTAL**
	Chalk	Slightly marly chalk	Marly chalk	Chalky marlstone	Marlstone	Tuff	All lithologies
Bo-3X							
Units (N)	3	51	34	37	28	1	154
Cumulative thickness (m)	0.41	19.36	3.52	2.17	1.20	0.02	26.68
Content (%)	1.54	72.56	13.19	8.13	4.50	0.07	100.00
Boje-2C							
Units (N)	1	115	137	118	66	1	438
Cumulative thickness (m)	0.15	31.64	24.39	12.04	6.87	0.01	75.10
Content (%)	0.20	42.13	32.48	16.03	9.15	0.01	100.00
North Jens-1							
Units (N)	17	65	90	49	24	0	245
Cumulative thickness (m)	8.56	24.69	35.30	10.02	7.03	0.00	85.60
Content (%)	10.00	28.84	41.24	11.71	8.21	0.00	100.00
Adda-2							
Units (N)	7	37	60	29	18	0	151
Cumulative thickness (m)	0.92	4.07	13.89	2.60	4.11	0.00	25.59
Content (%)	3.60	15.90	54.28	10.16	16.06	0.00	100.00
Adda-3							
Units (N)	2	12	30	35	11	0	90
Cumulative thickness (m)	1.16	2.39	8.40	4.34	20.27	0.00	36.56
Content (%)	3.17	6.54	22.98	11.87	55.44	0.00	100.00
Deep Adda-1							
Units (N)	12	0	10	0	4	1	27
Cumulative thickness (m)	2.11	0.00	0.56	0.00	1.41	0.21	4.29
Content (%)	49.18	0.00	13.05	0.00	32.87	4.90	100.00
SE Adda-1							
Units (N)	2	15	19	18	4	0	58
Cumulative thickness (m)	3.40	1.84	4.40	5.56	18.36	0.00	33.56
Content (%)	10.13	5.48	13.11	16.57	54.71	0.00	100.00
TOTAL							
Units (N)	44	295	380	286	155	3	1163
Cumulative thickness (m)	16.71	83.99	90.46	36.73	59.25	0.24	287.38
Content (%)	5.81	29.23	31.48	12.78	20.62	0.08	100.00

Homogenously bioturbated facies

Description

A total of 12 homogeneously bioturbated facies are recognized (Fig. 7). Facies units are common and generally a few decimeters thick, but range between 1–200 cm (0.5 in – 6 ft 5 in). The facies are characterized by intense bioturbation with a relatively structureless fabric, faint biomottling (often only recognizable on clean, polished surfaces), and lack of physical sedimentary structures. The facies are commonly recognized in intervals displaying little lithological variation of either chalk (F1a), slightly marly chalk (F2a, F2a*g* and F2a*r*), marly chalk (F3a, F3a*g* and F3a*r*), chalky marlstone (F4a, F4a*g* and F4a*r*) or marlstone (F5a and Fa*r*) (Figs 7–9). The bioturbated fabric is predominantly devoid of recognizable trace fossils, but conspicuous burrows occur sporadically in low numbers and limited diversity, dominated by *Chondrites* and *Planolites* with rare *Nereites*, *Palaeophycus*, *Teichichnus*, *Thalassinoides* and *Zoophycos*. The facies units also commonly display deformation bands, and less commonly indistinct parallel lamination, shear banding, chalk nodules, pyrite, and sporadic sand-grade chalk clasts, as well

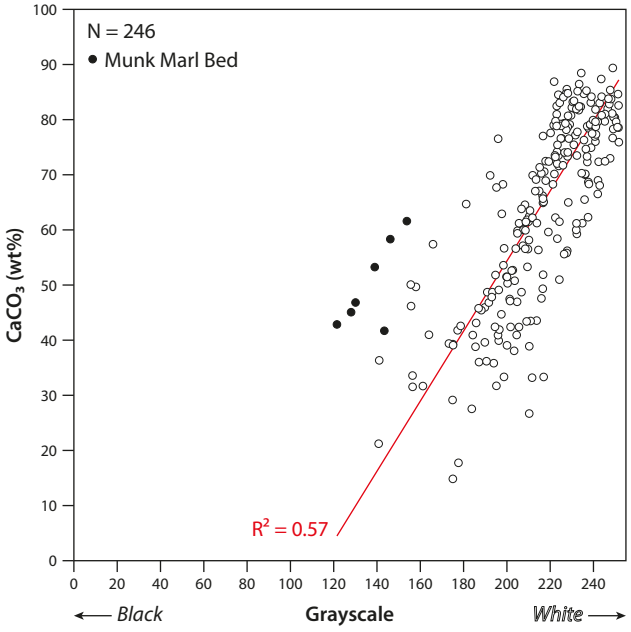


Fig. 6. Cross-plot of grayscale and XRF-determined carbonate ($CaCO_3$) percentage (wt%) of 246 samples in the Boje-2C core, showing that white (i.e. chalk-dominated) and dark-gray to black (i.e. marlstone-dominated) facies correlate with higher and lower carbonate percentage, respectively (except for the seven samples of the Munk Marl Bed, being anomalously dark compared to lithologies of similar carbonate content). The grayscale unit corresponds to a subdivision of the white–black spectrum into 256 shades.

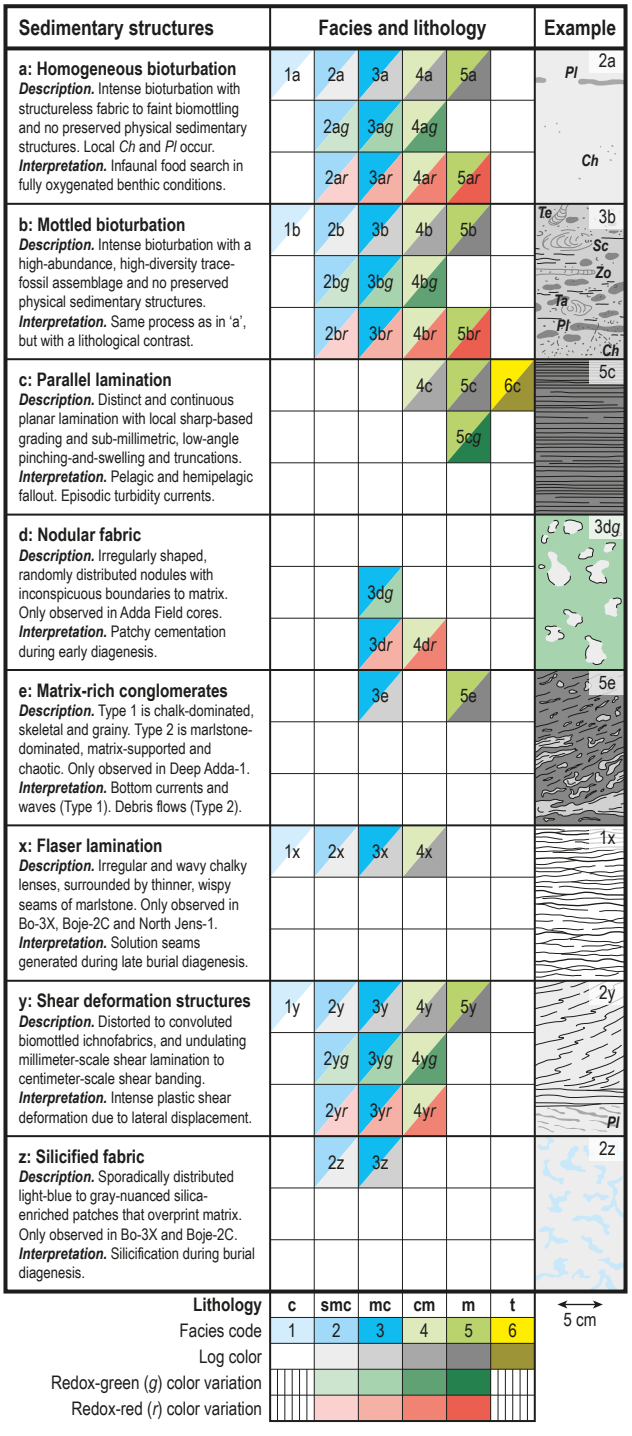


Fig. 7. Summary and representative line drawings of facies, annotated according to the six lithologies (1–6), eight different sedimentary structures (a–e and x–z), and two redox-associated color variations (green and red; *g* and *r*). Lithological abbreviations refer to: c, chalk (lithology 1); smc, slightly marly chalk (lithology 2); mc, marly chalk (lithology 3); cm, chalky marlstone (lithology 4); m, marlstone (lithology 5); t, tuff (lithology 6). Trace-fossil abbreviations refer to: *Ch*, *Chondrites*; *Pl*, *Planolites*; *Sc*, *Scolicia*; *Ta*, *Taenidium*; *Te*, *Teichichnus*; *Zo*, *Zoophycos*.

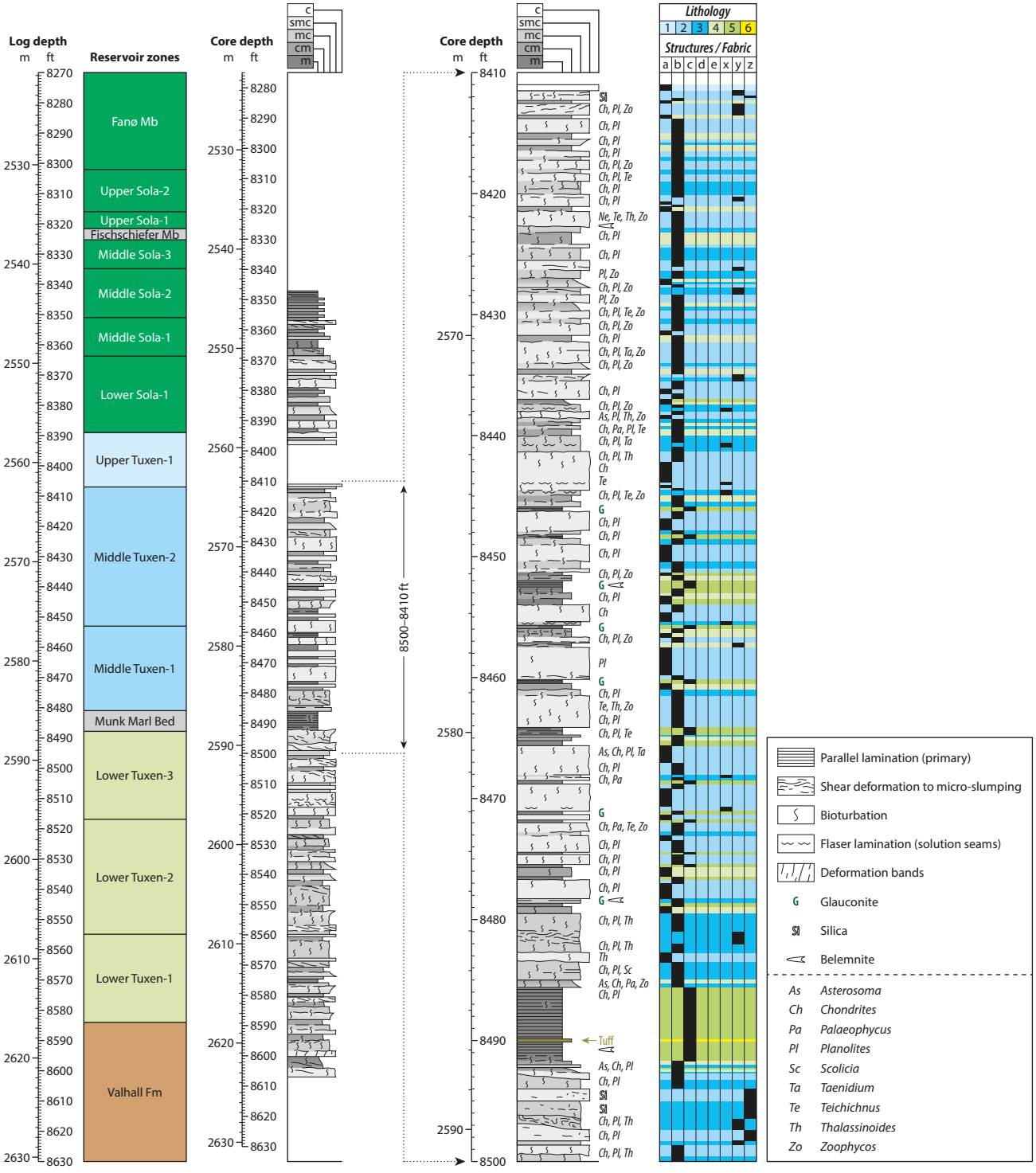


Fig. 8. Representative sedimentological log and accompanying reservoir zonation of the Tuxen and Sola Formations in the Boje-2C core, including detailed inset log of a heterolithic interval in the Tuxen Formation with corresponding facies plot of lithologies (chalk to marlstone, 1–5, and tuff, 6) and sedimentary structures (a–e and x–z), which highlights their stratigraphic distribution. Note the core:log depth-shift of *c.* 5 ft. Lithological abbreviations refer to: c, chalk; smc, slightly marly chalk; mc, marly chalk; cm, chalky marlstone; m, marlstone.

as belemnites, bivalves (including inoceramid shell fragments), crinoid stalks and rare ammonites. Lower boundaries of homogeneously bioturbated facies units are gradational, whereas upper boundaries are generally biomottled to irregular but may also be sharp (Fig. 9). Homogeneously bioturbated facies units are commonly interbedded with biomottled and shear-deformed facies units and subordinate flaser-laminated facies units (Fig. 9). Alternatively, the facies are either: (i) stacked as consecutive units of differing lithologies (e.g. F5a overlain by F3a and F4a); or (ii) forming bioturbated facies successions with lower biomottled and commonly marly divisions (e.g. F3b) cleaning upwards into chalkier and homogeneously bioturbated divisions (e.g. F2a).

Interpretation

The general lack of physical sedimentary structures and the completely bioturbated fabric indicate fully oxygenated benthic conditions and low sedimentation rates, which allowed the infauna to continuously exploit the sea bed in search for food, resulting in thorough obliteration of physical sedimentary structures. The subtle biomottling and the rarity of visible trace fossils probably reflects the homogeneity of the sediment and the resultant lack of color contrasts to define the biogenic structures. The destruction of the physical sedimentary structures inhibits precise determination of the precursor depositional process of the sediments, but low sedimentation rates are probably consistent with tranquil background deposition from pelagic (chalk to marly chalk) and hemipelagic (chalky marlstone and marlstone) fallout, although the episodic incursion of low-density turbidity currents and/or mudflows cannot be ruled out, as indicated by localized, dispersed sand-grade chalk clasts (e.g. Anderskouv & Surlyk 2011). The resulting units of such episodic flows would, however, probably be too thin to be preserved from subsequent bioturbation.

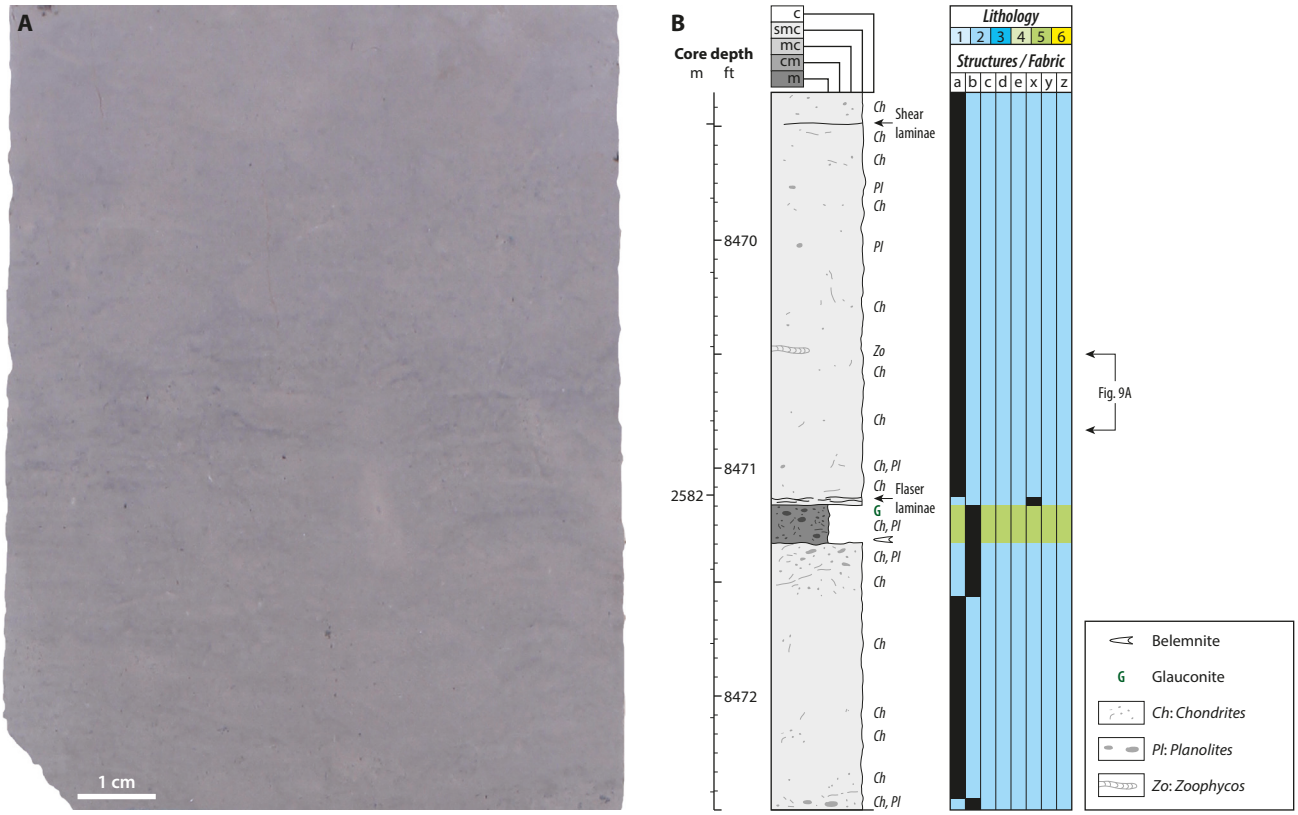


Fig. 9. Representative photograph (A) and detailed log (B) of homogeneous bioturbation (sedimentary structure a) in the Boje-2C core. The photograph shows completely homogenized slightly marly chalk (F2a) devoid of visible trace fossils, except some inconspicuous *Chondrites*. The photographed interval (A) has been treated with light oil for visual enhancement of sedimentary structures and corresponds to the middle part of the log, indicated to the right of the facies plot (B). Lithological abbreviations refer to: c, chalk (lithology 1); smc, slightly marly chalk (lithology 2); mc, marly chalk (lithology 3); cm, chalky marlstone (lithology 4); m, marlstone (lithology 5). Tuff corresponds to lithology 6.

Biomottled facies

Description

A total of 12 biomottled facies are recognized (Fig. 7). Facies units are dominant and generally a few decimeters thick, but range between 1–240 cm (0.5 in – 7 ft 11 in). The facies are characterized by a fully bioturbated fabric with a generally high-abundance, moderate to high-diversity trace-fossil assemblage and lack of physical sedimentary structures. The facies consist of slightly marly chalk (F2b, F2b*g* and F2b*r*), marly chalk (F3b, F3b*g* and F3b*r*), chalky marlstone (F4b, F4b*g* and F4b*r*), and locally chalk (F1b) and marlstone (F5b and F5b*r*), with the latter commonly being glauconitic in thin beds (Figs 7, 8, 10). Mottled bioturbation generally occurs in heterolithic intervals where it may form stacks of consecutive facies units of differing lithologies (e.g. F3b overlain

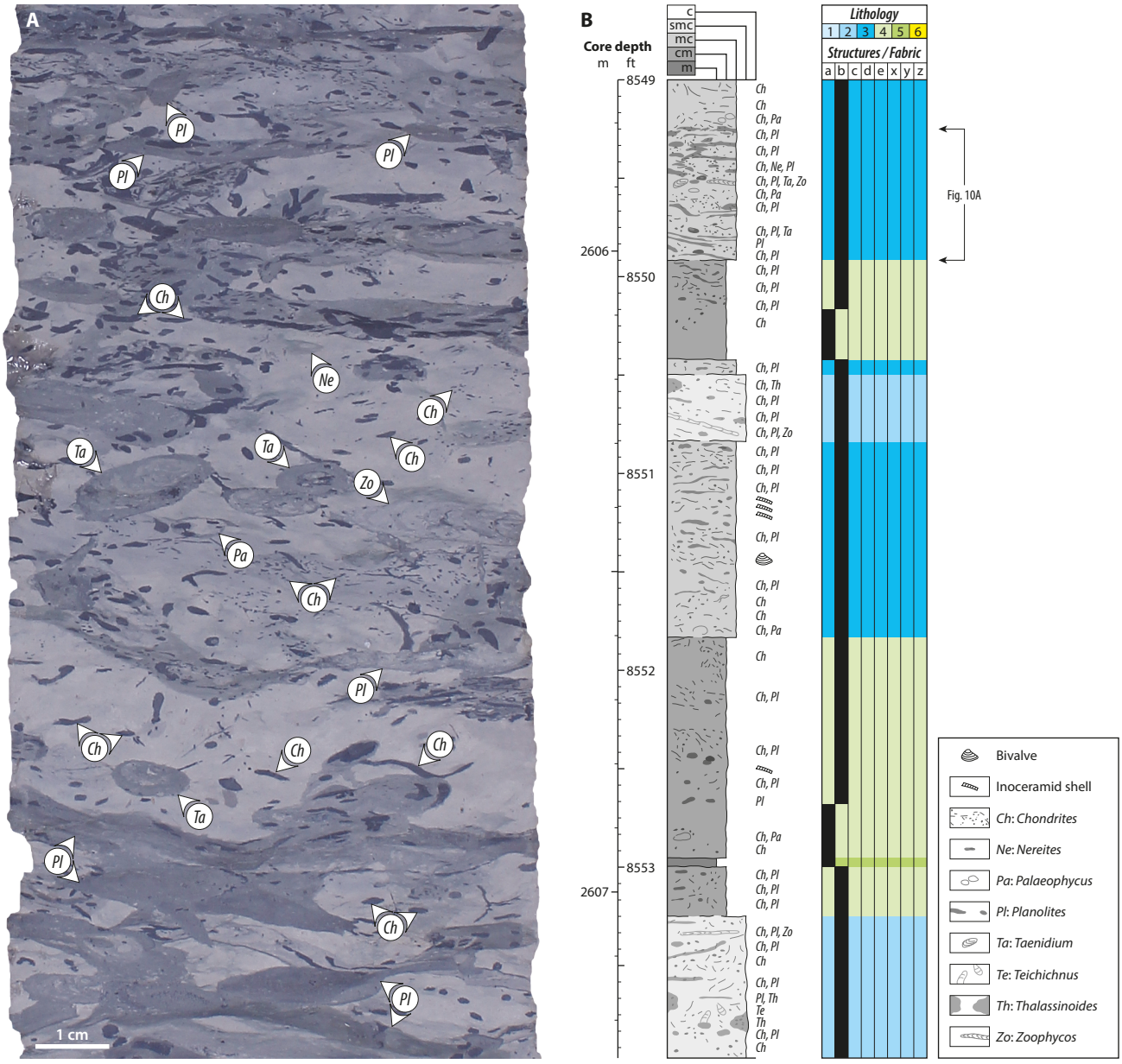


Fig. 10. Representative photograph (A) and detailed log (B) of mottled bioturbation (sedimentary structure b) in the Boje-2C core. The photograph shows thoroughly biomottled marly chalk (F3b), constituting a relatively high-abundance and moderate to high-diversity trace-fossil assemblage. The photographed interval (A) has been treated with light oil for visual enhancement of sedimentary structures and corresponds to the upper part of the log, indicated to the right of the facies plot (B). Lithological abbreviations refer to: c, chalk (lithology 1); smc, slightly marly chalk (lithology 2); mc, marly chalk (lithology 3); cm, chalky marlstone (lithology 4); m, marlstone (lithology 5). Tuff corresponds to lithology 6.

by F2b and F4b) up to 2.6 m (8 ft 6 in) thick. Trace fossils are generally clearly differentiated from the surrounding matrix, with chalk-dominated (i.e. chalk to marly chalk) units generally exhibiting the largest diversity of trace fossils. Trace-fossil assemblages are overwhelmingly dominated by *Chondrites* and *Planolites*, which are commonly the only ichnogenera present in a unit. Other trace fossils include common *Thalassinoides*, *Teichichnus*, *Scolicia* and *Zoophycos*, with lesser *Asterosoma*, *Palaeophycus*, *Taenidium*, *Nereites* and *Phycosiphon*, and very rare *Cosmorhaphe* (Figs 7, 8, 10). Larger burrows (e.g. *Planolites*, *Taenidium* or *Thalassinoides*) are typically exploited by smaller burrows (e.g. *Chondrites* and/or *Teichichnus*) (Fig. 10). Locally, biomottled facies units display relict parallel lamination, floating very coarse sand-grade to granule-sized chalk clasts, or slight inclination of the ichnofabric. Additional facies variations include: (i) local chalk nodules in the Adda-2, Adda-3 and SE Adda-1 cores, where the units may also consecutively shift between redox-associated green (*g*) and red (*r*) colors; and/or (ii) rare occurrences of bivalves (including inoceramid shell fragments), belemnites and ammonites, shear deformation structures (including shear lamination, shear banding and/or inclination and contortion of the ichnofabric), deformation bands, patchy silicified fabrics or flaser lamination, and pyrite nodules/- or cement. The boundaries of biomottled facies units are generally gradational to irregular or bioturbated, but rare cases of sheared to erosional or sharp boundaries do occur. The units are commonly interbedded with homogeneously bioturbated, parallel-laminated and shear-deformed facies units (Fig. 10), and more rarely silicified facies units.

Interpretation

Similar to homogeneous bioturbation, the thoroughly bioturbated fabric and general lack of physical sedimentary structures indicate fully oxygenated benthic conditions and dominantly low sedimentation rates compatible with pelagic (chalk to marly chalk) and hemipelagic (chalky marlstone and marlstone) fallout. However, the clearly distinguishable trace fossils probably reflect sufficient lithological contrasts in the burrowed sediments for well-defined burrows to be formed, and hence availability of heterolithic sediments. This suggests that dominantly pelagic (clay-poor) and hemipelagic (clay-rich) sedimentation may have alternated relatively rhythmically, perhaps due to recurring periods of heightened and lowered carbonate production and/or siliciclastic input, with the sediments subsequently mixed during bioturbation. The range of ichnogenera and the rarity of benthic fossils further indicate a relatively rich infauna and a restricted shelly epifauna, which suggests a high nutrient flux to the sea floor (Dayton & Oliver 1977; Bambach 1993; McKinney & Hageman 2006; Anderskouv & Surlyk 2011). In addition, the locally occurring chalk clasts may indicate episodic deposition from low-density turbidity currents (e.g. Anderskouv & Surlyk 2011).

Parallel-laminated facies

Description

Four parallel-laminated facies are recognized (Fig. 7). Facies units are generally a few centimeters thick, but range between 1–240 cm (0.5 in – 8 ft). The facies are predominantly characterized by relatively distinct and continuous planar lamination in clean to shaly and sandy marlstone (F5c and F5c*g*) and chalky marlstone (F4c), identified by sub-millimetric and millimetric variations between pale and dark laminae (Figs 7, 8, 11; Jensen & Buchardt 1987; Thomsen 1989a, b). In the Munk Marl Bed, the fine lamination is superimposed upon centimeter- to decimeter-scale diffuse banding defined by bulk color variations in the marlstone. Rare variations of the lamination include: (i) minute low-angle pinch-and-swell architecture, which may be associated with sub-millimetric truncations; or (ii) sets (3–10 mm thick) of three to five, sharp-based and graded or inversely graded laminae, for example by marlstone grading into marly chalk. In the Bo-3X core, a peculiar example of lamination (2553.5 m; 8377 ft 9 in) displays onlap against a small-scale (2 mm throw) fault scarp. Parallel-laminated facies units are commonly glauconitic and devoid of trace fossils, although small *Chondrites* and *Planolites*, typically confined to the top of the units, may occur (Figs 8, 11), as well as rare, isolated *Asterosoma*, *Teichichnus*, *Thalassinoides* or *Zoophycos*. Alternatively, the parallel-laminated facies units exhibit subtle shearing to contortion or small-scale overturning of the laminae, as well as scattered pyrite cement and/or nodules, siderite and rare chalk nodules, ammonites, belemnites, bivalves (including inoceramid shell fragments) and fish remains. Unit boundaries are predominantly sharp, with subordinate lower transitional and upper erosional boundaries, and the facies units are mainly interbedded with biomottled facies units and subordinately shear-deformed facies units (Figs 8, 11).

Rare occurrences of parallel lamination are recorded in tuffaceous siltstone to sandstone (F6c) within the Munk Marl Bed (Table 2), which in the Deep Adda-1 core forms a sharp-based graded bed with diffuse and spaced horizontal lamination defined by the concentration of coarse silt-grade grains.

Interpretation

The predominance of the distinctly planar lamination

in fine-grained marlstone (F5c) devoid of textural variations, cross-cutting relations and bioturbation indicates that the bulk of parallel-laminated facies reflects deposition in tranquil conditions from pelagic to hemipelagic suspension settling in dysoxic to anoxic bottom-water conditions (Jensen & Buchardt 1987; Ineson 1993). In the Munk Marl Bed, Thomsen (1989a, b) related the deposition to seasonal production variability and blooms of calcareous nannofossils resulting in the alternation of pale (calcareous nannofossil-rich) and dark (clay-rich) laminae. In comparison, the local presence of lamina truncations and grading probably reflects episodic sea-bed erosion and penecontemporaneous deposition from low-density turbidity currents. This notion is supported by the minute pinch-and-swell architecture of some laminae, which roughly mimics experimentally produced ripples formed from carbonate mud sediment that has flocculated into coarse silt to sand-sized particles capable of producing current ripples and associated cross-lamination comparable to those of siliciclastic deposits (Schieber *et al*. 2007, 2013; Ghadeer & Macquaker 2011). The localized examples of lamina disruption and small-scale draped scarps are attributed to minor slope creep.

The sharp-based tuffaceous siltstone to sandstone bed in the Munk Marl Bed of the Deep Adda-1 core is interpreted as a turbidite, with the lamination conforming to the T_b division of Bouma (1962).

Nodular facies

Description

Three nodular facies are recognized (Fig. 7). Facies units are decimeter-thick, ranging between 17–30 cm (6.5–12 in), and occur in the four Adda Field cores (Ta-

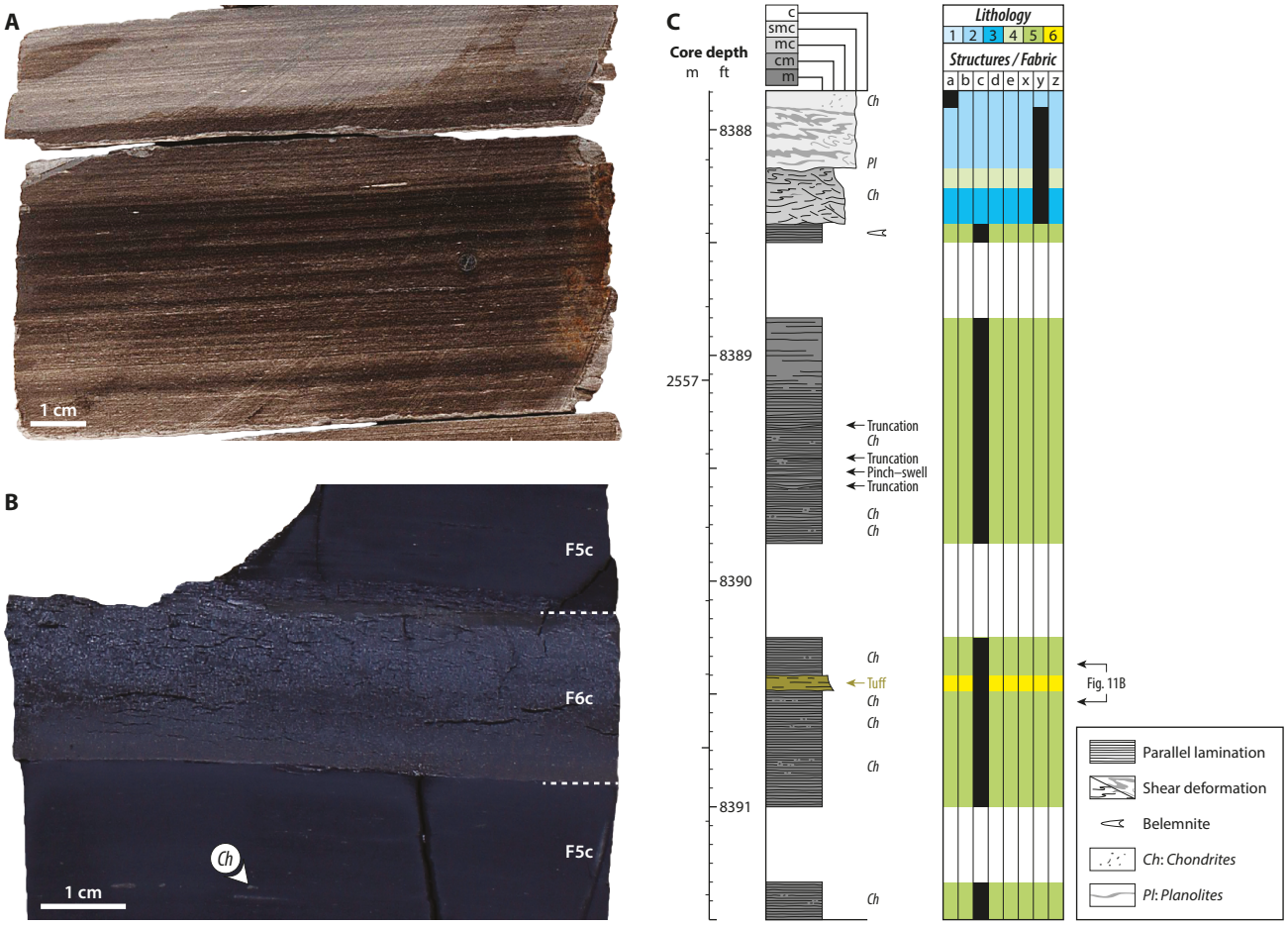


Fig. 11. Representative photographs (A, B) and detailed log (C) of parallel lamination (sedimentary structure c) in the Munk Marl Bed of the North Jens-1 (A; 2304.49–2304.41 m) and Bo-3X (B, C) cores. The photographs show distinctly laminated marlstone (A; F5c) and weakly graded tuff (B; F6c) with solitary *Chondrites* (*Ch*). The photographed interval in (B) has been treated with light oil for visual enhancement of sedimentary structures and corresponds to the lower part of the log, indicated to the right of the facies plot (C). Lithological abbreviations refer to: c, chalk (lithology 1); smc, slightly marly chalk (lithology 2); mc, marly chalk (lithology 3); cm, chalky marlstone (lithology 4); m, marlstone (lithology 5). Tuff corresponds to lithology 6.

ble 1). The facies are characterized by centimeter-scale chalk nodules floating in a matrix of redox-associated green-colored (F3d*g*) and red-colored (F3d*r*) marly chalk and red-colored chalky marlstone (F4d*r*) (Figs 7, 12). The nodules are generally randomly distributed, devoid of prevalent orientations, and irregularly shaped with inconspicuous to gradual boundaries to the surrounding matrix (Fig. 12). Nodular facies units are locally associated with faint sub-vertical deformation bands, biomottling, and rare bivalves and pyrite nodules. Unit boundaries are generally transitional to irregular, with the exception of upper boundaries in the Deep Adda-1 core that form conspicuous firmgrounds to hardgrounds. Nodular facies units are generally interbedded with biomottled and shear-deformed facies units.

Interpretation

The nodular fabric conforms to an early stage in the process that eventually leads to the formation of incipient hardgrounds. The nodules formed during relatively prolonged periods of sediment starvation and early diagenesis resulting in patchy cementation of the shallow sea bed (Kennedy & Garrison 1975). This interpretation is consistent with the position of the units below firmgrounds and hardgrounds in the Deep Adda-1 core.



Fig. 12. Representative photograph of nodular fabric (sedimentary structure d) in the Adda-3 core (2387.19–2386.99 m), showing various irregular shapes and indistinct boundaries of chalk nodules in dominantly red (F3d*r*) and green (F3d*g*) marly chalk. The interval has been treated with light oil for visual enhancement of sedimentary structures.

Matrix-rich conglomerate facies

Description

Two matrix-rich conglomerate facies are recognized (Fig. 7). Facies units are generally a few decimeters thick, but range between 1–38 cm (0.5–15 in). The facies occur only in the Deep Adda-1 core, where they constitute chalk-dominated and marlstone-dominated conglomerates (Figs 7, 13).

The chalk-dominated conglomerates (F3e) comprise centimeter-thick (1–15 cm; *c.* 0.5–6 in) beds in the lower Tuxen Formation below the Munk Marl Bed, which are primarily characterized by matrix-supported granule to pebble-sized, skeletal wackestone chalk clasts randomly floating in a matrix of marly chalk of skeletal wackestone grading into packstone and locally grainstone. The clasts are commonly accompanied by inoceramid, belemnite and more rarely ammonite shell fragments. The chalk-dominated conglomerates generally occur immediately above firmground to hardground surfaces and are interbedded with biomottled and nodular facies units, with the lower boundaries being sharp or irregular to erosional, whereas the upper boundaries are transitional.

The marlstone-dominated conglomerates (F5e) are represented by three decimeter-thick (10–38 cm; 4–15 in) beds in the Munk Marl Bed, which are primarily characterized by chaotic fabrics devoid of conspicuous sedimentary structures or textures, but with granule to cobble-sized chalk and marlstone clasts randomly dispersed in a structureless marlstone matrix (Figs 7, 13). Whereas the lower and upper beds are predominantly matrix-supported (Fig. 13), the middle bed is clast-supported. In addition, the middle and upper beds exhibit a low-angle oblique fabric defined primarily by the orientation of elongate clasts (Fig. 13). The clasts are predominantly characterized by being either: (i) nodular to spherical in shape with local bioerosion and glauconitic impregnation of the margins; or (ii) plastically deformed with lenticular and elongated to contorted shapes that may be associated with slight convolution of streaked-out marlstone matrix (Fig. 13). The marlstone-dominated conglomerates have sharp boundaries and are interbedded with parallel-laminated facies units.

Interpretation

The general occurrence of the chalk-dominated conglomerates (F3e) above irregular and erosional

firmground to hardground surfaces, and the absence of physical sedimentary structures in a skeletal and grainy fabric, collectively indicate that this facies represents reworking of locally derived bioclasts and chalk intraclasts by relatively intense bottom or wave-induced currents. The heterogeneous fabric of the facies units further suggests that they were subsequently subjected to intense biogenic reworking in concert with pelagic ooze fallout.

In contrast, the chaotic fabric and structureless, mud-grade matrix of the marlstone-dominated conglomerates (F5e) suggest that this facies represents gravity flows. The random distribution and plastic deformation of the clasts indicate that deposition was associated with freezing of the flows, and that these possessed a shear strength sufficiently large for the matrix to prohibit sorting and cause small-scale shearing. Such non-Newtonian flow conditions are well-documented features of cohesive debris flows (Postma 1986; Mulder & Alexander 2001), which were likely to have developed from nearby mass wastage.



Fig. 13. Representative photograph of matrix-rich conglomerate (sedimentary structure e) in the Deep Adda-1 core (2446.25–2446.05 m), showing a marlstone-dominated (F5e), relatively chaotic and low-angle oblique fabric that contains dispersed granule to cobble-sized, plastically deformed chalk clasts with lenticular and elongated to contorted shapes and slight lamina convolutions.

Flaser-laminated facies

Description

Four flaser-laminated facies are recognized (Fig. 7). Facies units are generally a few centimeters thick, ranging between 1–13 cm (0.5–5 in), and occur in the three Valdemar Field cores (Table 1). The facies constitute irregular and wavy lenses of predominantly chalk (F1x) and slightly marly chalk (F2x), and subordinately marly chalk (F3x) and chalky marlstone (F4x), surrounded by thinner, wispy seams of marlstone (Figs 7, 14). The facies generally occur as isolated beds, and are only rarely stacked as consecutive units of differ-

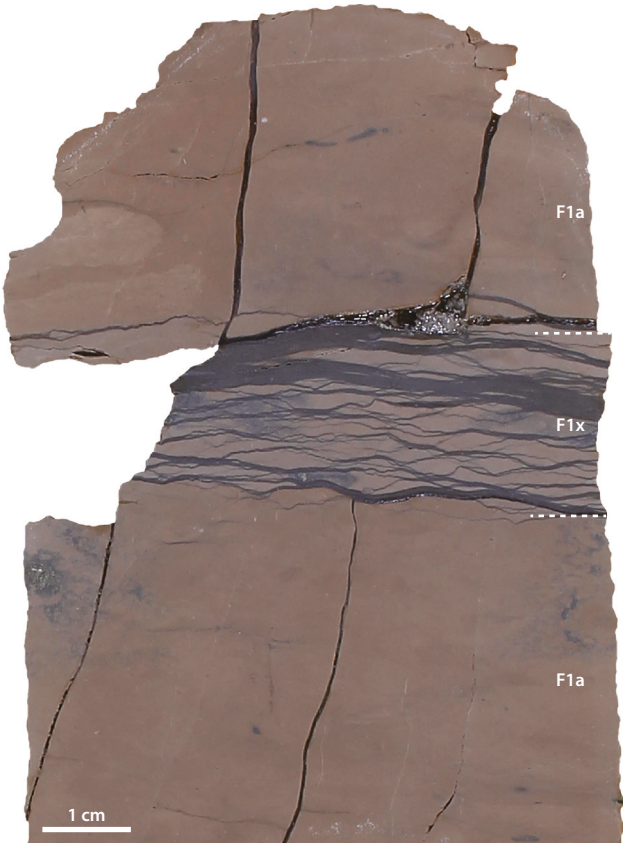


Fig. 14. Representative photograph of flaser lamination (sedimentary structure x) in the Bo-3X core (2568.83–2568.73 m), showing irregular and wavy lenses of chalk (F1x) surrounded by thinner wispy seams of marlstone. The flaser-laminated unit is intercalated between two homogeneously bioturbated chalk facies units (F1a). The interval has been treated with light oil for visual enhancement of sedimentary structures.

ing lithologies (e.g. F4x overlain by F3x). Boundaries are generally sharp and irregular conforming to the shape of the marlstone seams, and the facies units are generally interbedded with homogeneously bioturbated and biomottled facies units, and more rarely with shear-deformed facies units.

Interpretation
Flaser lamination in chalk generally represents solution seams generated during late burial diagenesis in response to mechanical compaction and pressure dissolution of the carbonate, as outlined by Garrison & Kennedy (1977). Following the interpretation of these authors, the dissolution mainly affected the coccolith-rich chalk matrix, and was probably most intense in the most argillaceous parts of the primary sediment.

Shear-deformed facies

Description
A total of 11 shear-deformed (*sensu lato* Anderskouv & Surlyk 2011) facies are recognized (Fig. 7). Facies units are generally a few decimeters thick, but range between 1–90 cm (0.5 in – 2 ft 10 in). The facies exhibit a relatively wide range of sedimentary structures in chalk (F1y), slightly marly chalk (F2y, F2y*g* and F2y*r*), marly chalk (F3y, F3y*g* and F3y*r*) and chalky marlstone (F4y, F4y*g* and F4y*r*), and more rarely in marlstone (F5y) (Figs 7, 8, 15). The sedimentary structures represent two common end-members, which typically co-occur within a single facies unit.

The first end-member displays a distorted to convoluted biomottled ichnofabric recognized by horizontal to inclined strain of relatively poorly preserved burrows and locally overturned relict lamination (Fig. 15). Individual burrows may display contorted to folded morphologies, although trace fossils can commonly be identified as *Chondrites* and *Planolites* with subordinate *Palaeophycus*, *Phycosiphon*, *Teichichnus*, *Thalassinoides* and *Zoophycos*. Locally, oblique imbrication of strained *Planolites* burrows mimic centimeter-scale thrusts above basal shear planes. Such micro-thrusted ichnofabrics may occur several times within a single facies unit and display opposing directions of displacement. Fine pebble-sized chalk clasts are locally present.

The second end-member is predominantly characterized by horizontal to sub-horizontal lamination and banding that deviates from primary parallel lamination by exhibiting minor undulations to significant pinching-and-swelling organized as either millimeter-scale (shear lamination) or centimeter-scale (shear banding) lamina sets (Fig. 15). Coarse sand-grade chalk clasts and/or cross-cutting relationships are locally present.

Shear-deformed facies units are commonly associated with irregular or conjugate deformation bands, and locally contain belemnites, bivalves (including inoceramid shell fragments), and silicified intervals, and more rarely pyrite (Fig. 15). Facies units are predominantly interbedded with biomottled facies units, and subordinately with homogeneously bioturbated, parallel-laminated, flaser-laminated or silicified facies units (Fig. 15). Alternatively, shear-deformed facies form stacks of consecutive units of differing lithologies (e.g. F2y*r* overlain by F4y*r* and F3y*r*) up to 2.5 m (8 ft 2 in) thick. Lower boundaries of the facies units are generally sharp, erosional or irregular, whereas upper boundaries are bioturbated, irregular or transitional. In some cases, lower erosional boundaries contain rip-up clasts and incipient rip-up clasts, the former generally recognized by base-detached, irregularly shaped clasts (some with unidirectional or bidirectional double tails), and the latter characterized by base-attached, angular clasts situated immediately above similarly shaped cavities.

Interpretation
The shear-deformed ichnofabrics and shear lamination/- and banding end-member configurations are strikingly similar to shear deformation or 'shredded' structures previously reported in Upper Cretaceous chalk (Kennedy 1980; Nygaard *et al.* 1983; Anderskouv & Surlyk 2011). Correspondingly, the configurations reported here were probably formed from plastic shear deformation of relatively unlithified sediment, including moderately intense deformation of biomottled sediment (first end-member configuration), and highly intense deformation of sediment where the precursor sedimentary structures are virtually indeterminable (second end-member configuration).

As emphasized by Anderskouv & Surlyk (2011), it is typically difficult to determine in core whether shear-deformed units occur *in situ* or allochthonously, for example as part of larger slumps or structurally deformed intervals of the succession. Indeed, a core section through a succession of thin recumbent folds with large aspect ratios would probably exhibit numerous laminae and only few fold hinges, thereby prohibiting recognition of the formative process of the shear deformation (Anderskouv & Surlyk 2011). However, the generally limited unit thickness, common interbedding with undisturbed facies (for example biomottled facies units) and lack of marked erosion surfaces collectively indicate that most of the deformation took place *in situ* as episodic events. Considering that only few of the observed shear-deformed facies units occur in association with deposits formed from events conspicuously capable of producing shear deformation (e.g. overriding slumps or debris flows; cf. Anderskouv & Surlyk 2011), the general deformation

is inferred to have been governed by relatively limited lateral displacement. The common co-occurrence of the different configurations within a single facies unit indicates that the different shear deformation styles acted penecontemporaneously, or that the unit was repeatedly deformed through different shear events. For example, basal shear planes beneath micro-thrusted *Planolites* ichnofabrics probably record highly intense ductile deformation that acted as minor 'décollement' surfaces bounding intervals that experienced less intense deformation.

Consequently, most of the shear deformation structures are suggestive of minor sediment creep at or close to the sediment surface. However, some beds that display shear-deformed, shredded ichnofabrics and folded lamination (such as in the North Jens-1 core; Fig. 4) probably record rare events when slope creep and *in situ* deformation resulted in failure and limited mass transport in the form of disconnected slumps transitional to debris flows (Anderskouv & Surlyk 2011).

Silicified facies

Description

Two silicified facies are recognized (Fig. 7). Facies units are generally a few decimeters thick, but range between 5–42 cm (2–16.5 in), and occur in the Bo-3X and Boje-2C cores. The facies are characterized by sporadically distributed light-blue to gray-nuanced silica-enriched patches that overprint the prevailing lithology of slightly marly chalk (F2z) and marly chalk (F3z) (Figs 7, 8, 16). The silica patches are generally irregularly shaped with indistinct boundaries, but may also mimic precursor sedimentary structures, such as shear deformation structures and biomottling

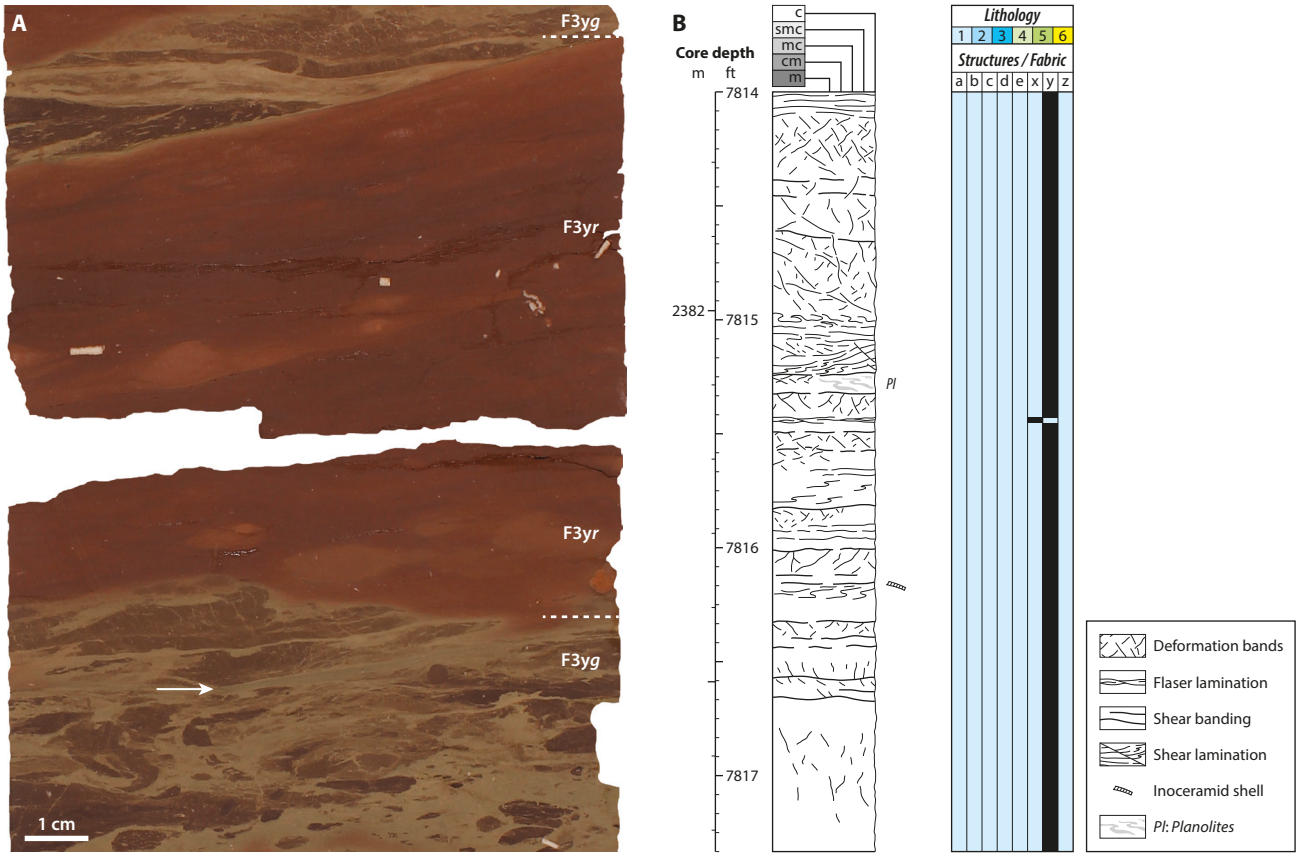


Fig. 15. Representative photograph (A) and detailed log (B) of shear deformation structures (sedimentary structure y) in the SE Adda-1 (2505.21–2505.08 m) and Adda-3 cores, respectively. The photograph shows a distorted to convoluted biomottled ichnofabric (first end-member configuration) recognized by horizontal to inclined strain and contortion of relatively poorly preserved burrows (most likely *Chondrites* and *Planolites*) in green (F3y*g*) and red (F3y*r*) marly chalk, with a single occurrence of shear lamination (second end-member configuration) indicated by the white arrow. The floating, white, angular grains are inoceramid shell fragments. The photographed interval has been treated with light oil for visual enhancement of sedimentary structures. Lithological abbreviations refer to: c, chalk (lithology 1); smc, slightly marly chalk (lithology 2); mc, marly chalk (lithology 3); cm, chalky marlstone (lithology 4); m, marlstone (lithology 5). Tuff corresponds to lithology 6.

with local relict *Chondrites* and *Planolites* (Fig. 16). Correspondingly, silicified facies units are predominantly interbedded with biomottled and shear-deformed facies units, as well as homogeneously bioturbated facies units, and exhibit transitional boundaries. Rarely, silicified facies form stacks of consecutive units of differing lithologies (e.g. F3z overlain by F2z) up to 0.7 m (2 ft 5 in) thick.

Interpretation

The overprinting of the silica on precursor sedimentary structures testifies to a post-depositional origin of these facies, namely precipitation of a stable silica phase during burial diagenesis. The silica was most likely sourced by dissolved, biogenic, amorphous silica (Clayton 1986; Madsen & Stemmerik 2010). The diffuse precipitation and lack of flint nodules may represent a lack of body (e.g. echinoids) and trace (e.g. *Thalassinoides*) fossils.

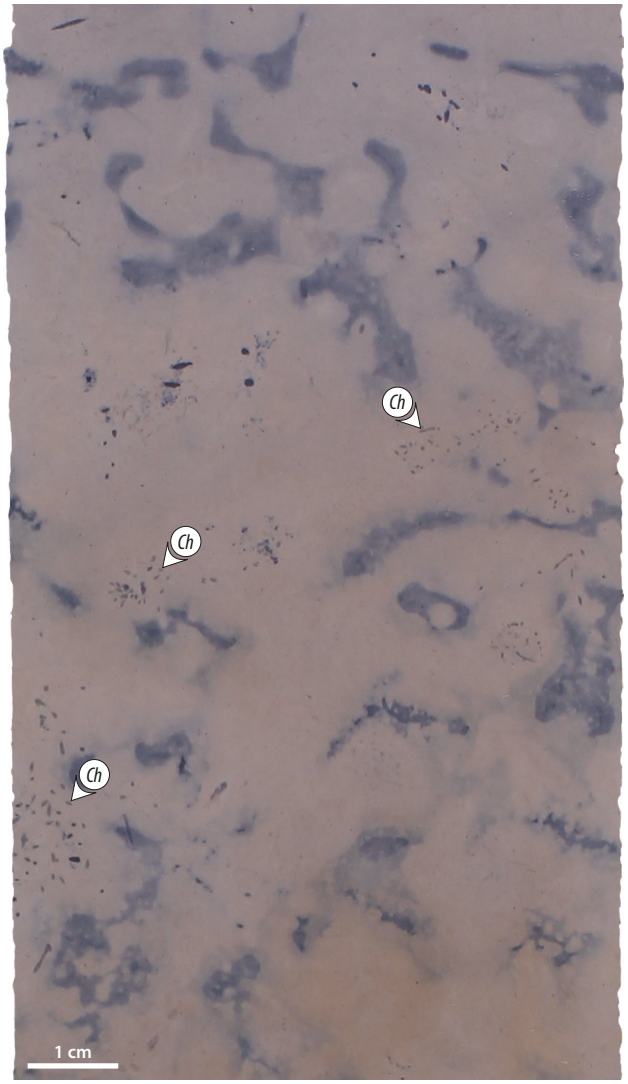


Fig. 16. Representative photograph of silicified fabric (sedimentary structure z) in the Bo-3X core (2558.15–2558.03 m), showing sporadically distributed, irregularly shaped light-blue silica-enriched patches that overprint the prevailing slightly marly chalk lithology (F2z). The interval has been treated with light oil for visual enhancement of sedimentary structures. *Ch*, *Chondrites*.

Facies distribution and implications for basin development

The facies distribution and stratigraphic development of the Tuxen and Sola Formations in the seven investigated cores generally conform to previous observations of the succession (Jensen & Buchardt 1987; Ineson 1993; Jakobsen *et al*. 2004). The Tuxen Formation predominantly comprises intensely bioturbated marly chalk and chalk, punctuated by parallel-laminated marlstone of the Munk Marl Bed, whereas the Sola Formation is significantly more marly and displays relatively thick parallel-laminated and bioturbated marlstone units, particularly in the Fischschiefer Member (Figs 4, 8, 17). However, a vertical and lateral variability in the distribution of facies is recorded throughout the study area, with important implications for understanding the Early Cretaceous basin evolution of the DCG. These are primarily observed in the Tuxen Formation, and include: (i) abundant shear-deformed facies units below the Munk Marl Bed (but a general absence above) (Figs 8, 17A); (ii) abundant thin, parallel-laminated marlstone facies units above the Munk Marl Bed (but a general absence below) (Figs 8, 17A); (iii) redox-associated green and red lithological color variations and associated nodular fabrics confined to the Adda Field (Fig. 17B); and (iv) matrix-rich conglomerates confined to the Deep Adda-1 core.

The general dominance of intense bioturbation in the Tuxen Formation indicates a continuously well-oxygenated depositional setting, with the alternation of the chalk- and marlstone-dominated facies reflecting the relative sediment flux from pelagic and terrestrial sources, respectively. In contrast, the Munk Marl Bed records a period of persistent sea-floor anoxia, postulated to have been caused, at least in part, by lowstand conditions (Jensen & Buchardt 1987; Ineson *et al*. 1997; van Buchem *et al*. 2018). In this scenario, the low relative sea-level may have led to isolation of the basin contributing to restricted ocean ventilation and/or potential lowering of the oxygen minimum zone to the seafloor. The predominance of shear-deformed facies units below the Munk Marl Bed (Figs 8, 17A), probably indicates that active tectonism took place prior to the onset of anoxic conditions in the basin. This is compatible with inferences from seismic observations

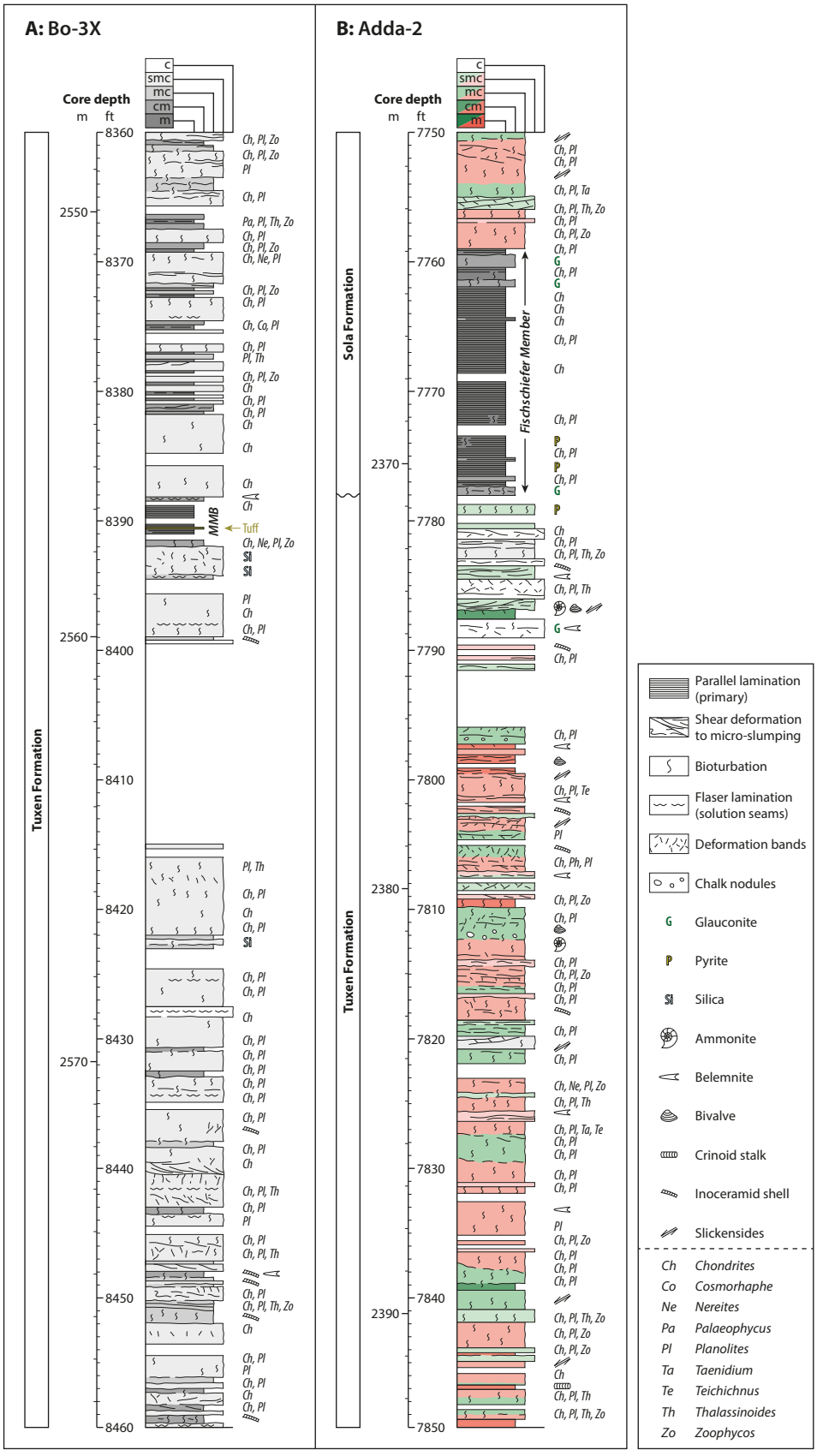


Fig. 17. Representative sedimentological logs of the Bo-3X (A) and Adda-2 (B) cores highlighting the most important characteristics of the vertical and lateral variability in the distribution of facies (see Fig. 1A for well positions). Notable facies-distribution characteristics include an upward increase in the marlstone content passing from the Tuxen Formation to the Sola Formation, exemplified here by the Fischschiefer Member (B); the presence of redox-associated green and red lithological color variations and nodular fabrics in the Adda Field (B), while these are absent in the Valdemar Field (A); abundant shear-deformed facies units below the Munk Marl Bed (MMB) in the Tuxen Formation (A); and abundant thin, parallel-laminated marlstone facies units above the Munk Marl Bed in the Valdemar Field (A). Lithological abbreviations refer to: c, chalk; smc, slightly marly chalk; mc, marly chalk; cm, chalky marlstone; m, marlstone.

of the initiation of inversion in the Adda Field in the late Valanginian – Hauterivian (Vejbæk & Andersen 1987). In the Valdemar Field, the general absence of shear-deformed facies units above the Munk Marl Bed suggests subsequent waning of gravitational instability (and hence tectonism) in that area. In addition, the abundant thin, parallel-laminated marlstone facies units above the Munk Marl Bed in the Valdemar Field reflect recurring episodes of anoxia.

Inversion and tectonic instability of the Adda Field area during the Hauterivian–Barremian is also supported by the thin and incomplete stratigraphic record in this area (Jensen & Buchardt 1987; van Buchem *et al.* 2018) when compared with the Valdemar Field cores (Figs 5, 17). The dominance of green and red redox-associated lithological color variations and the common occurrence of nodular fabrics in the Adda Field cores also indicate that this area was subject to condensation and perhaps sediment bypass. This facies evidence supports the bathymetric model of van Buchem *et al.* (2018) proposing that the Adda Field constituted a plateau at the eastern basin margin of the DCG in the Barremian, separated from the basinal depocenter of the Valdemar Field area. This model is compatible with the presence of matrix-rich conglomerates in the Munk Marl Bed of the Deep Adda-1 core, which suggest that steady pelagic and hemipelagic background sedimentation was occasionally interrupted by deposition from gravity-flow events, most likely sourced from the adjacent Coffee Soil Fault (Fig. 1A; Jensen & Buchardt 1987).

The relatively thick parallel-laminated marlstone facies units in the Fischschiefer Member (Figs 4, 8, 17B) represent a return to prevailing anoxic conditions during the early Aptian, consistent with global records of the OAE-1a (e.g. Mutterlose & Bottini 2013; Blok *et al.* 2022 and references therein).

Conclusions

Comprehensive carbonate facies analysis of cored sections of the Lower Cretaceous Tuxen and Sola Formations from seven wells in the Valdemar (Bo-3X, Boje-2C and North Jens-1) and Adda (Adda-2, Adda-3, Deep Adda-1 and SE Adda-1) Fields of the Danish Central Graben (DCG) has permitted: (i) the first detailed account of the range of lithologies, sedimentary structures and depositional processes in the succession; and (ii) new insights into the Early Cretaceous basin evolution of the DCG, drawn from the documentation of vertical and lateral variability in the distribution of facies.

- A total of 50 facies are defined by: (i) lithology, ranging from chalk to marlstone and tuffaceous siltstone to sandstone; (ii) eight different sedimentary structures (or fabrics); and (iii) two (green and red) redox-associated lithological color variations (confined to the Adda-2, Adda-3 and SE Adda-1 cores) of slightly marly chalk to marlstone.
- Homogeneous bioturbation represents fully oxygenated benthic conditions and low sedimentation rates, allowing the infauna to obliterate physical sedimentary structures.
- Mottled bioturbation records the same process as homogeneous bioturbation, but lithological contrasts in the burrowed sediments ensured that biogenic structures are well-defined, possibly reflecting a relatively rhythmic alternation between pelagic (clay-poor) and hemipelagic (clay-rich) sedimentation.
- Parallel lamination is predominantly recorded in marlstone within and above the Munk Marl Bed in the Tuxen Formation, and is common in the Sola Formation marlstones, and reflects deposition in tranquil conditions from pelagic to hemipelagic suspension settling in dysoxic to anoxic bottom-water conditions.
- Nodular fabrics are confined to the Adda Field cores, and represent patchy cementation of the shallow sea bed during early diagenesis as a precursor to the development of incipient and mature hardgrounds.
- Matrix-rich conglomerates are confined to the Deep Adda-1 core, and record: (i) reworking of locally derived bioclasts and chalk intraclasts by relatively intense bottom or wave-induced currents; and (ii) cohesive debris flows indicative of mass wastage, probably at the eastern margin of the graben.
- Flaser lamination represents solution seams generated during late burial diagenesis in response to mechanical compaction and pressure dissolution of clay-rich carbonate.
- Shear deformation structures are mainly recorded in the lower Tuxen Formation, below the Munk Marl Bed, and represent moderate to intense plastic shear deformation of relatively unlithified sediment, predominantly involving limited lateral displacement.
- Silicified fabrics reflect burial diagenesis.
- The vertical and lateral distribution of facies record that: (i) active tectonism, probably related to early inversion, created localized sediment instability prior to the onset of anoxic conditions that resulted in deposition of the Munk Marl Bed, which in the Valdemar Field was followed by tectonic waning and repeated episodes of anoxia in the basin; and (ii) the Valdemar Field area constituted the primary basinal depocenter in this part of the DCG and during the Barremian was flanked to the east

in the Adda Field area by an early inversion high characterized by condensation and bypass.
- The Fischschiefer Member represents a return to prevailing anoxic conditions during the early Aptian consistent with global records of the Oceanic Anoxic Event 1a (OAE-1a).

Acknowledgements

We gratefully acknowledge the Danish Underground Consortium (TotalEnergies E&P Denmark, Noreco and Nordsøfonden) for granting permission to publish this work. The study was funded by the Danish Offshore Technology Centre (DTU Offshore). We warmly thank reviewers Andy Gale and Henrik Tirsgaard and Editor Bodil Wesenberg Lauridsen for critical and constructive comments, which helped improve the outcome of this paper. Thomas Blume and the staff at the Total Core Laboratory in Copenhagen are kindly thanked for allowing access to the cores and for technical assistance. We also extend our thanks to Astrid Juel Bojsen-Møller for patient and meticulous core photography and photograph editing.

References

Ainsworth, N.R., Riley, L.A. & Gallagher, L.T. 2000: An Early Cretaceous lithostratigraphic and biostratigraphic framework for the Britannia Field reservoir (Late Barremian–Late Aptian), UK North Sea. Petroleum Geoscience 6, 345–367.

Anderskouv, K. & Surlyk, F. 2011: Upper Cretaceous chalk facies and depositional history recorded in the Mona-1 core, Mona Ridge, Danish North Sea. Geological Survey of Denmark and Greenland Bulletin 25, 60 pp.

Bambach, R.K. 1993: Seafood through time: changes in biomass, energetics, and productivity in the marine ecosystem. Paleobiology 19, 372–397.

Blok, C.N., Ineson, J., Anderskouv, K., Fantasia, A., Sheldon, E., Thibault, N., Jelby, M.E., Adatte, T. & Bodin, S. 2022: Latitude-dependant climate changes across the Aptian Oceanic Anoxic Event 1a. Palaeogeography, Palaeoclimatology, Palaeoecology 601, 111085.

Bouma, A.H. 1962: Sedimentology of Some Flysch Deposits: A Graphic Approach to Facies Interpretation. Elsevier, Amsterdam, 168 pp.

Clayton, C.J. 1986: The chemical environment of flint formation in Upper Cretaceous chalk. In: Sieveking, G. & Hart, M.B. (eds): The Scientific Study of Flint and Chert. Cambridge University Press, Cambridge, U.K., 43–54.

Copestake, P., Sims, A.P., Crittenden, S., Hamar, G.P., Ineson, J.R., Rose, P.T. & Tringham, M.E. 2003: Lower Cretaceous. In: Evans, D. *et al.* (eds): The Millennium Atlas: petroleum geology of the central and northern North Sea. The Geological Society, London, 191–211.

Damtoft, K., Nielsen, L.H., Johannessen, P.N., Thomsen, E. & Andersen, P.R. 1992: Hydrocarbon plays of the Danish Central Trough. In: Spencer, A.M. (ed.): Generation, Accumulation and Production of Europe's Hydrocarbons II. Special Publication of the European Association of Petroleum Geoscientists, Springer-Verlag, Berlin, Heidelberg, 35–58.

Dayton, P.K. & Oliver, J.S. 1977: Antarctic soft-bottom benthos in oligotrophic and eutrophic environments. Science 197, 55–58.

Gale, A.S., Mutterlose, J. & Batenburg, S. 2020: The Cretaceous Period. In: Gradstein *et al.* (eds): Geological Time Scale 2020. Elsevier, Boston, MA, 1023–1086.

Garrison, R.E. & Kennedy, W.J. 1977: Origin of solution seams and flaser structure in Upper Cretaceous chalks of southern England. Sedimentary Geology 19, 107–137.

Ghadeer, S.G. & Macquaker, J.H.S. 2011: Sediment transport processes in an ancient mud-dominated succession: a comparison of processes operating in marine offshore settings and anoxic basinal environments. Journal of the Geological Society, London 168, 1121–1132.

Glad, A.C., Amour, F., Welch, M.J., Clausen, O.R., Anderskouv, K., Ineson, J.R., Sheldon, E. & Nick, H.M. 2022: Natural fractures and discontinuities in a Lower Cretaceous chalk-marlstone reservoir, Valdemar Field, Danish North Sea. Marine and Petroleum Geology 136, 105445.

Heilmann-Clausen, C. 1987: Lower Cretaceous dinoflagellate biostratigraphy in the Danish Central Trough. Danmarks Geologiske Undersøgelse, Serie A, 17, 87 pp.

Ineson, J.R. 1993: The Lower Cretaceous chalk play in the Danish Central Trough. In: Parker, J.R. (ed.): Petroleum Geology of Northwest Europe: Proceedings of the 4th Conference. Geological Society, London, 175–183.

Ineson, J.R., Jutson, D.J. & Schiøler, P. 1997: Mid-Cretaceous sequence stratigraphy in the Danish Central Trough. Geological Survey of Denmark and Greenland Report 109, 86 pp.

Jakobsen, F., Ineson, J.R., Kristensen, L. & Stemmerik, L. 2004: Characterization and zonation of a marly chalk reservoir: the Lower Cretaceous Valdemar Field of the Danish Central Graben. Petroleum Geoscience 10, 21–33.

Jakobsen, F., Ineson, J.R., Kristensen, L., Nytoft, H.P. & Stemmerik, L. 2005: The Valdemar Field, Danish Central Graben: field compartmentalization and regional prospectivity of the Lower Cretaceous chalk play. In: Doré, A.G. & Vining, B.A. (eds): Petroleum Geology: North-West Europe and Global Perspectives—Proceedings of the 6th Petroleum Geology Conference. Geological Society, London, 177–186.

Japsen, P., Britze, P. & Andersen, C. 2003: Upper Jurassic – Lower Cretaceous of the Danish Central Graben: structural framework and nomenclature. Geological Survey of Denmark and Greenland Bulletin 1, 233–246.

Jensen, T.F. & Buchardt, B. 1987: Sedimentology and geochemistry of the organic carbon-rich Lower Cretaceous Sola Formation (Baremian–Albian), Danish North Sea. In: Brooks, J. &

Glennie, K. (eds): Petroleum Geology of North West Europe. Graham & Trotman, 431–440.

Jensen, T.F., Holm, L., Frandsen, N. & Michelsen, O. 1986: Jurassic - Lower Cretaceous lithostratigraphic nomenclature for the Danish Central Trough. Danmarks Geologiske Undersøgelse, Serie A, 12, 64 pp.

Kennedy, W.J. 1980: Aspects of chalk sedimentation in the southern Norwegian offshore. Symposium volume 'The sedimentation of the North Sea reservoir rocks'. Norwegian Petroleum Society, 29 pp.

Kennedy, W.J. & Garrison, R.E. 1975: Morphology and genesis of nodular chalks and hardgrounds in the Upper Cretaceous of southern England. Sedimentology 22, 311–386.

Kühnau, L. & Michelsen, O. 1994: Detailed log-stratigraphic study of the Lower Cretaceous in the Danish Central Trough, North Sea. Marine and Petroleum Geology 11, 467–477.

Madsen, H. & Stemmerik, L. 2010: Diagenesis of flint and porcellanite in the Maastrichtian chalk at Stevns Klint, Denmark. Journal of Sedimentary Research 80, 578–588.

Malkoč, M., Mutterlose, J. & Pauly, S. 2010: Timing of the Early Aptian $\delta^{13}C$ excursion in the Boreal Realm. Newsletters on Stratigraphy 43, 251–273.

McKinney, F.K. & Hageman, S.J. 2006: Paleozoic to modern marine ecological shift displayed in the northern Adriatic Sea. Geology 34, 881–884.

Michelsen, O., Frandsen, N., Holm, L., Jensen, T.F., Møller, J.J. & Vejbæk, O.V. 1987: Jurassic - Lower Cretaceous of the Danish Central Trough; – depositional environments, tectonism, and reservoirs. Danmarks Geologiske Undersøgelse, Serie A, 16, 44 pp.

Mulder, T. & Alexander, J. 2001: The physical character of subaqueous sedimentary density flows and their deposits. Sedimentology 48, 269–299.

Mutterlose, J. 1992: Migration and evolution patterns of floras and faunas in marine Early Cretaceous sediments of NW Europe. Palaeogeography, Palaeoclimatology, Palaeoecology 94, 261–282.

Mutterlose, J. & Bottini, C. 2013: Early Cretaceous chalks from the North Sea giving evidence for global change. Nature Communications 4, 1686.

Mutterlose, J., Bottini, C., Schouten, S. & Damsté, J.S.S. 2014: High sea-surface temperatures during the early Aptian Oceanic Anoxic Event 1a in the Boreal Realm. Geology 42, 439–442.

Möller, J.J. & Rasmussen, E.S. 2003: Middle Jurassic – Early Cretaceous rifting of the Danish Central Graben. Geological Survey of Denmark and Greenland Bulletin 1, 247–264.

Nygaard, E., Lieberkind, K. & Frykman, P. 1983: Sedimentology and reservoir parameters of the Chalk Group in the Danish Central Graben. Geologie en Mijnbouw 62, 177–190.

Pauly, S., Mutterlose, J. & Wray, D.S. 2013: Palaeoceanography of Lower Cretaceous (Barremian–Lower Aptian) black shales from northwest Germany evidenced by calcareous nannofossils and geochemistry. Cretaceous Research 42, 28–43.

Postma, G. 1986: Classification for sediment gravity-flow deposits based on flows conditions during sedimentation. Geology 14, 291–294.

Rückheim, S., Bornemann, A. & Mutterlose, J. 2006: Planktic foraminifera from the mid-Cretaceous (Barremian–Early Albian) of the North Sea Basin: Palaeoecological and palaeoceanographic implications. Marine Micropaleontology 58, 83–102.

Schieber, J., Southard, J. & Thaisen, K. 2007: Accretion of mudstone beds from migrating floccule ripples. Science 318, 1760–1763.

Schieber, J., Southard, J.B., Kissling, P., Rossman, B. & Ginsburg, R. 2013: Experimental deposition of carbonate mud from moving suspensions: importance of flocculation and implications for modern and ancient carbonate mud deposition. Journal of Sedimentary Research 83, 1025–1031.

Surlyk, F., Dons, T., Clausen, C.K. & Higham, J. 2003: Upper Cretaceous. In: Evans, D. *et al.* (eds): The Millennium Atlas: petroleum geology of the central and northern North Sea. The Geological Society, London, 213–233.

Thomsen, E. 1987: Lower Cretaceous calcareous nannofossil biostratigraphy in the Danish Central Trough. Danmarks Geologiske Undersøgelse, Serie A, 20, 88 pp.

Thomsen, E. 1989a: Seasonal variability in the production of Lower Cretaceous calcareous nannoplankton. Geology 17, 715–717.

Thomsen, E. 1989b: Seasonal variation in Boreal Early Cretaceous calcareous nannofossils. Marine Micropaleontology 15, 123–152.

Thomsen, E. & Jensen, T.F. 1989: Aptian to Cenomanian stratigraphy in the Central Trough of the Danish North Sea sector. Geologisches Jahrbuch, Reihe A, 113, 337–358.

Tyson, R.V. & Funnell, B.M. 1987: European Cretaceous shorelines, stage by stage. Palaeogeography, Palaeoclimatology, Palaeoecology 59, 69–91.

Ullmann, C.V. 2013: Isotopic and elemental proxies in mollusc and brachiopod calcite: diagenesis, vital effects and climatic trends. Unpublished PhD thesis, University of Copenhagen, 117 pp.

van Buchem, F.S.P., Smit, F.W.H., Buijs, G.J.A., Trudgill, B. & Larsen, P.-H. 2018: Tectonostratigraphic framework and depositional history of the Cretaceous–Danian succession of the Danish Central Graben (North Sea) – new light on a mature area. In: Bowman, M. & Levell, B. (eds): Petroleum Geology of NW Europe: 50 Years of Learning – Proceedings of the 8th Petroleum Geology Conference. Geological Society, London, https://doi.org/10.1144/PGC8.24.

Vejbæk, O.V. 1986: Seismic stratigraphy and tectonic evolution of the Lower Cretaceous in the Danish Central Trough. Danmarks Geologiske Undersøgelse, Serie A, 11, 57 pp.

Vejbæk, O.V. & Andersen, C. 1987: Cretaceous–Early Tertiary inversion tectonism in the Danish Central Trough. Tectonophysics 137, 221–238.

Wennberg, O.P., Casini, G., Jahanpanah, A., Lapponi, F., Ineson, J., Wall, B.G. & Gillespie, P. 2013: Deformation bands in chalk, examples from the Shetland Group of the Oseberg Field, North Sea, Norway. Journal of Structural Geology 56, 103–117.

Early Cretaceous stratigraphic and basinal evolution of the Danish Central Graben: a review

JON R. INESON*, HENRIK, I. PETERSEN, CLAUS ANDERSEN, MORTEN BJERAGER, FINN C. JAKOBSEN, LARS KRISTENSEN, FINN MØRK & EMMA SHELDON

Geological Society of Denmark
https://2dgf.dk

Received 14 January 2022
Accepted in revised form
7 September 2022
Published online
26 September 2022

© 2022 the authors. Re-use of material is permitted, provided this work is cited. Creative Commons License CC BY: https://creativecommons.org/licenses/by/4.0/

Ineson*, J.R., Petersen, H.I., Andersen, C., Bjerager, M., Jakobsen, F.C., Kristensen, L., Mørk, F. & Sheldon, E. 2022: Early Cretaceous stratigraphic and basinal evolution of the Danish Central Graben: a review. Bulletin of the Geological Society of Denmark, Vol. 71, pp. 75–98. ISSN 2245-7070.
https://doi.org/10.37570/bgsd-2022-71-05

An integrated seismic–stratigraphic study of the Lower Cretaceous Cromer Knoll Group was undertaken as part of a recent comprehensive analysis of the Upper Jurassic – lowermost Cretaceous petroleum system in the Danish Central Graben. This study of the basal group of the post-rift package yielded an updated regional assessment of the distribution of the Valhall, Tuxen, Sola and Rødby Formations. This is documented by four high resolution isochore maps (presented here) that record temporal shifts in subsidence patterns from the latest Ryazanian to the earliest Cenomanian. The distribution and thickness variation of the mud-dominated Valhall Formation (latest Ryazanian – early Hauterivian) at the base of the group attests to the progressive fill of inherited syn-rift morphology. The dominant depositional theme is thus ponding in, and onlap from, the main inherited depocentres, although growth faults and incipient inversion locally controlled stratigraphic architecture, and new depocentres were initiated in the east of the graben (Ål and Outer Rough Basins). The isochores for the succeeding, increasingly chalk-rich Tuxen, Sola and Rødby Formations (Hauterivian – earliest Cenomanian) document the regional weakening of syn-rift patterns but emphasize the shift in sedimentation patterns controlled by accelerating inversion activity in the east (Adda–Tyra area, Søgne Basin) and increased local subsidence. The latter sometimes coincided with syn-rift depocentres, such as the Roar Basin and the Arne-Elin Graben, but was also significant in the new Early Cretaceous depocentres in the west of the graben, particularly the Outer Rough Basin. The evolution of the Early Cretaceous basin recorded by this dataset reveals significant shifts in the subsidence pattern in the late Valanginian – early Hauterivian, in large part due to early inversion in the east, and during the late Aptian – early Albian when subsidence was focussed in central and western sub-basins, probably locally due to salt withdrawal. These events, in combination with sea-level change, had implications for the accumulation and preservation of Barremian and early Aptian reservoir chalks.

Corresponding author; email: ji@geus.dk

Keywords: Danish Central Graben, North Sea, Cromer Knoll Group, Lower Cretaceous, updated seismic mapping, lithostratigraphy, subsidence history.

Jon R. Ineson [ji@geus.dk], Henrik, I. Petersen [hip@geus.dk], Claus Andersen [ca@geus.dk], Morten Bjerager [mbj@geus.dk], Finn C. Jakobsen [fj@geus.dk], Lars Kristensen [lk@geus.dk], Finn Mørk [fm@geus.dk], Emma Sheldon [es@geus.dk], Geological Survey of Denmark and Greenland (GEUS), Øster Voldgade 10, DK-1350 Copenhagen K, Denmark.

Lower Cretaceous sediments of the Cromer Knoll Group are widely distributed in the Danish Central Graben where the succession has been drilled by numerous exploration wells (Nielsen & Japsen 1991). The sedimentary contrast to the underlying Upper Jurassic – lowermost Cretaceous syn-rift shales of the Farsund and Mandal Formations is striking and characterized by a significant fall in gamma-ray (GR) values (Jensen *et al*. 1986; Petersen & Jacobsen 2021). The lower Ryazanian – Albian post-rift succession though dominated by siliciclastic mudstones records the initial pulses of chalk accumulation (Ineson 1993; Mutterlose & Bottini 2013), heralding the development of the Chalk Sea that dominated NW Europe during the Late Cretaceous (Surlyk *et al*. 2003). The upper Ryazanian – Danian succession in the Danish Central Graben, North Sea, is thus carbonate-dominated overall and includes the highly prolific Upper Cretaceous – Danian chalk play (e.g. Hemmet 2005) (Figs 1, 2). Since production started in 1972, most of the Danish oil and gas production has been from Maastrichtian (Upper Cretaceous) and Danian (lower Paleocene) chalk reservoirs in fields primarily located in the Salt Dome Province in the central–southern part of the Danish Central Graben (Fig. 1). However, hydrocarbon production also occurs from low permeability marly chalk reservoirs in the Lower Cretaceous Tuxen and Sola Formations of the Valdemar Field (Jacobsen *et al*. 2004; Danish Energy Agency 2014; Ponsaing e*t al*. 2020a, b).

As part of an industrial multiclient study ('CRETSYS'; Skaarup *et al*. 2017), seismic mapping was integrated with in-house sedimentological data, a stratigraphic review and petrophysical analysis of the Cromer Knoll Group, and a consistent, well-constrained seismic-stratigraphic framework for the Lower Cretaceous succession was established to improve the regional understanding of the stratigraphy and basin development. The framework was validated with biostratigraphy based primarily on review and update of existing data, both from industrial and published sources.

The aim of this paper is to review the evolution of the Lower Cretaceous Cromer Knoll Group in the Danish Central Graben based on a systematic description of the lithostratigraphy, including an account of the key facies, within the updated seismic architectural framework. High resolution images of the seismic maps that form the basis of this review are included as Supplementary Data files.

Geological setting

The Danish Central Graben constitutes part of the Central Graben in the southern extension of the Jurassic North Sea rift complex, consisting of a series of NNW-SSE trending half-grabens bounded to the east by the Coffee Soil Fault towards the Ringkøbing-Fyn High and to the west by the Mid North Sea High (e.g. Møller 1986; Japsen *et al*. 2003; Møller & Rasmussen 2003) (Fig. 1). Jurassic extensional rifting and half-graben subsidence started in the Middle Jurassic and continued into the earliest Cretaceous (Andsbjerg & Dybkjær 2003; Japsen *et al*. 2003; Møller & Rasmussen 2003; Verreussel *et al*. 2018; Hansen *et al*. 2021). Marine transgression of the developing graben began in the deepest depocentres along the Tail End Graben in the late Middle Jurassic (Andsbjerg 2003; Andsbjerg & Dybkjær 2003), and the seaway expanded episodically during the Late Jurassic, flooding the entire Danish Central Graben and lapping westward onto the Mid North Sea High in Volgian–Ryazanian times (Johannessen 2003; Johannessen *et al*. 2010; Verreussel *et al*. 2018).

The upper boundary of the Upper Jurassic – lowermost Cretaceous syn-rift marine shale succession (Lola, Farsund and Mandal Formations) is defined by the regional seismic surface colloquially termed the 'Base Cretaceous Unconformity' (BCU). Although a true, often composite, unconformity on structural highs and in marginal areas, it is commonly seismically conformable in depocentres and stratigraphic continuity has been proposed in uncored well sections in such basin-centre locations (Rawson & Riley 1982). As indicated by Kyrkjebø *et al*. (2004), the BCU term is thus an over-generalisation but is entrenched in the literature and is retained here for pragmatic reasons. In depocentres in the Central Graben, the BCU seismic horizon marks a basinwide facies change in the latest Ryazanian from black shales deposited under oxygen-deficient/anoxic conditions to open-marine sediments of the Lower Cretaceous Cromer Knoll Group (Rawson & Riley 1982; Copestake *et al*. 2003; Kyrkjebø *et al*. 2004; Ineson *et al*. 2022a). The post-rift Cromer Knoll Group accumulated under early thermal subsidence infilling the basin-floor topography inherited from the Late Jurassic rifting stages in the Danish Central Graben. Although the general Late Jurassic structural basin configuration was maintained during the Early Cretaceous, subsidence along the Coffee Soil Fault at the eastern margin of the basin became less dominant with the development of a number of smaller depocentres, both along the axis of the Tail End Graben and westwards across the Danish Central Graben (Vejbæk 1986; Japsen *et al*. 2003). The total thickness of the Cromer Knoll Group locally exceeds 800 m in depocentres (Britze *et al*. 1995) and thicknesses over a kilometre may be present in undrilled parts of the Outer Rough Basin (Japsen *et al*. 2003).

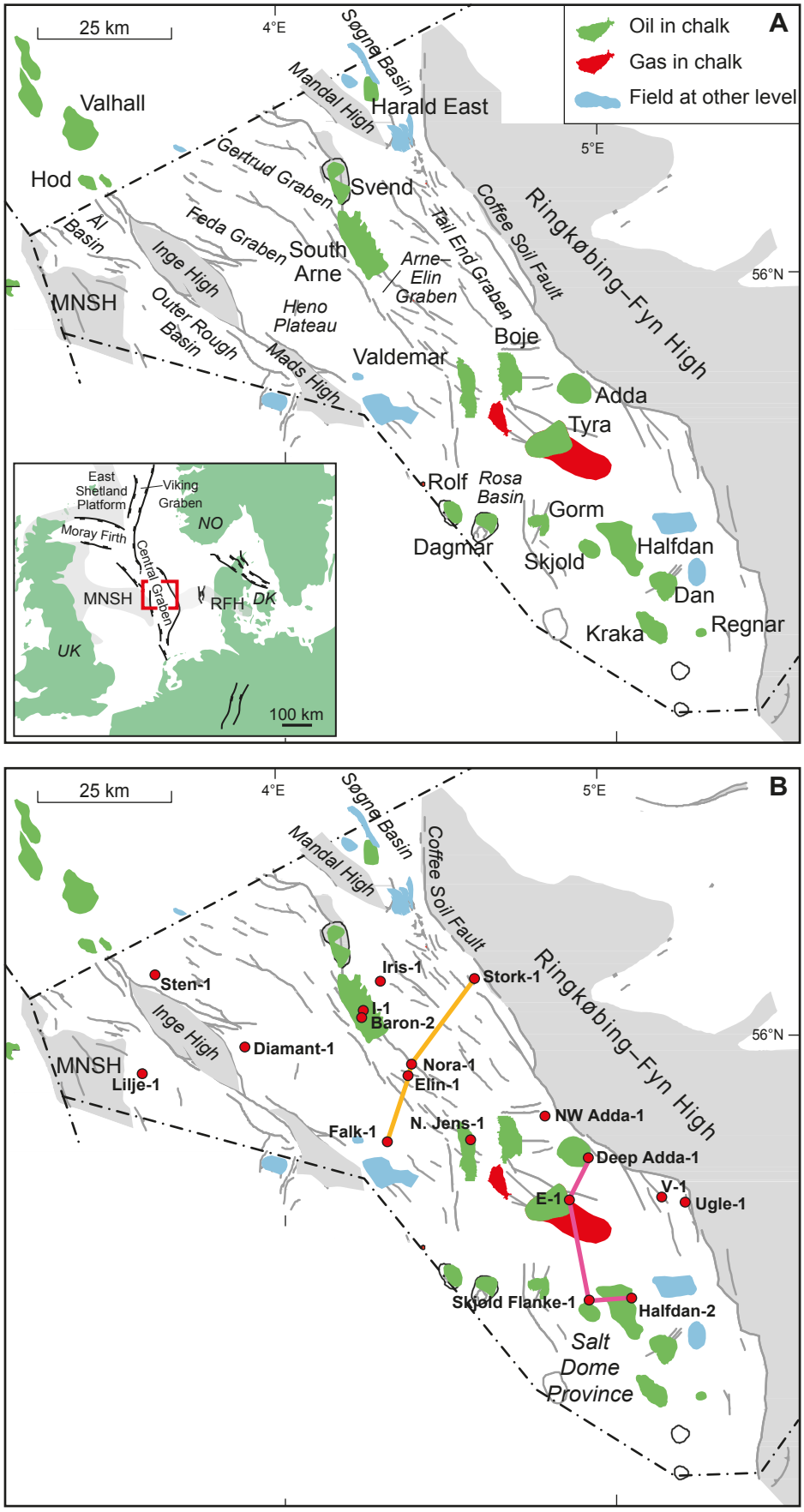


Fig. 1. (A) Early Cretaceous structural framework of the Danish Central Graben showing the main structural elements and chalk fields; the latter are concentrated in the Salt Dome Province. Insert map shows the location of the Danish sector within the North Sea rift complex. (**B**) Location of the wells discussed in the text and indicated on figured seismic profiles (Figs 12, 13). MNSH: Mid North Sea High; open circles (southern Danish Central Graben) indicate dry salt-cored structures at Cretaceous level.

Methodology

Seismic mapping

Final migration versions from eight separate 3D surveys of various vintages in the public domain were used. The datasets have an areal overlap of varying size but there is almost full 3D coverage of the entire Danish Central Graben. However, released 3D data is lacking in an area where the Coffee Soil Fault changes direction from NNW–SSE to WNW–ESE, north of the NW Adda-1 well (Fig. 1); structural interpretation and mapping in this area was reliant on vintage 2D data. The line orientations are SW–NE parallel to the general structural dips, apart from the southern surveys in the salt-structure dominated area where the in-line orientation is E–W. The data quality of the surveys in the Cretaceous section is generally fair to very good. A problem exists where a thick high-velocity chalk section directly overlies low-velocity Lower Cretaceous sediments. This gives rise to severe ringing and interbed multiples that mask the imaging of the uppermost Lower Cretaceous section. To mitigate the multiple problem on a couple of the surveys, an FK-filter that removed dips up to 1 ms/trace was applied post-stack on flattened volumes at Base Chalk to remove parallel events immediately below the Chalk Group. This improved the ability to pick dipping events in the upper part of the Lower Cretaceous although this robust treatment was at the expense of removing some of the subsurface data.

Five distinct reflectors that can be traced over most of the Danish Central Graben and tied to well sections were selected for regional interpretation and mapping of the Lower Cretaceous section (see below); an additional surface at top Leek Member – Vyl Formation (Fig. 2, CKG2) is only locally mappable and is not considered further here. The regional reflectors were used to define Lower Cretaceous seismic units with top and base delimited by seismic horizons. Locally, in areas of structural complexity and poor imaging, the interpretation was guided by stratigraphic data from wells. The five regionally interpreted horizons were used to create four time-isochore maps of the Lower

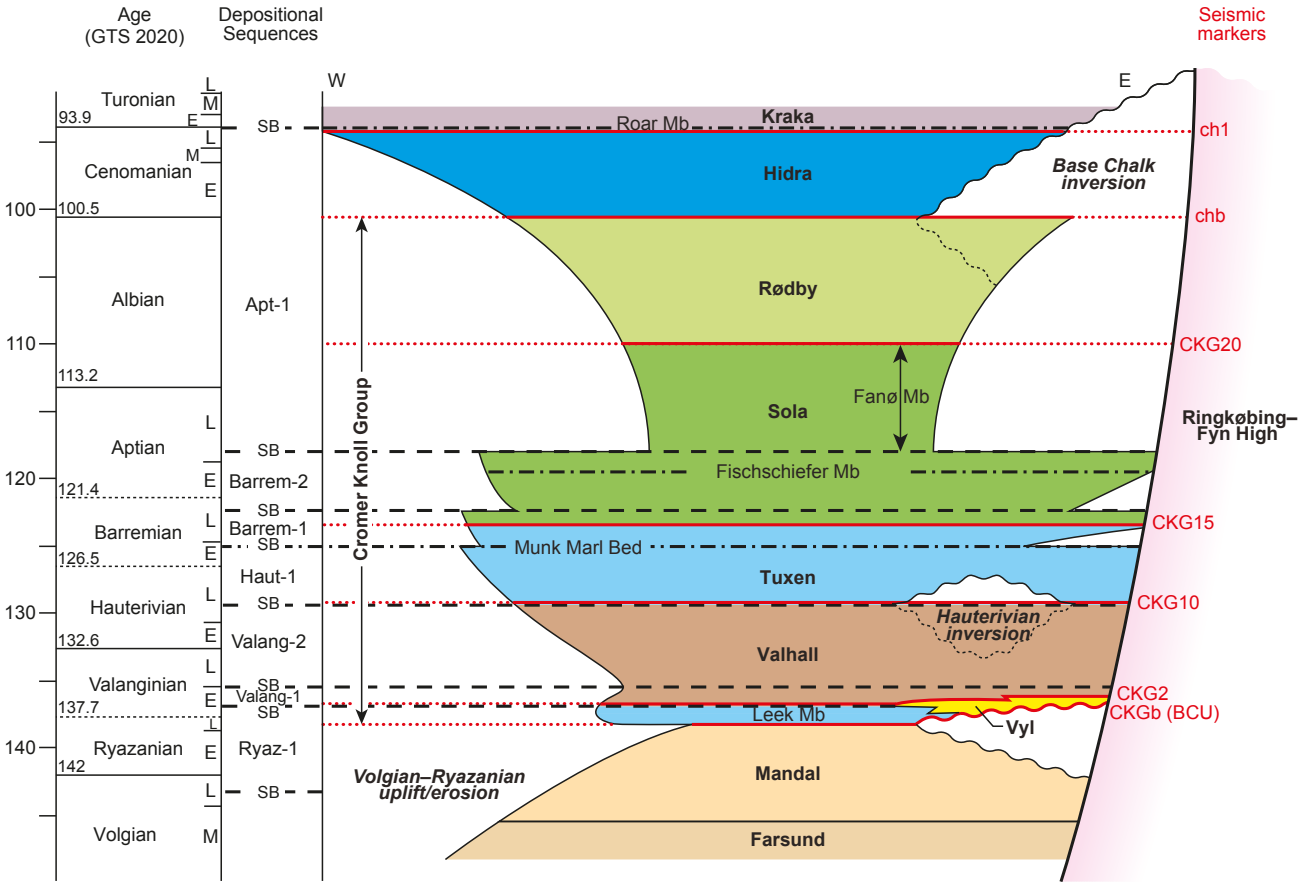


Fig. 2. Schematic representation of the Lower Cretaceous lithostratigraphy showing the relative lateral distribution of the formations in a W–E cross-section of the Danish Central Graben; local stratigraphic variations are not depicted. Key seismic horizons are shown, together with depositional sequences. Chronostratigraphy after Gale *et al.* (2020).

Cretaceous succession by simple subtraction of the relevant horizons. The four isochore maps correspond to the Valhall, Tuxen, Sola and Rødby Formations.

Biostratigraphy

All available biostratigraphic data were reviewed from 65 key wells covering a wide geographic area of the Danish Central Graben in order to provide seismic ties in key locations (see summary in Skaarup *et al.* 2017). The biostratigraphy was mainly based on nannofossils and microfossils (mostly foraminifera with some Radiolaria, diatoms and ostracods). The data were primarily extracted from industrial biostratigraphic consultancy reports but published data and unpublished in-house GEUS data were also incorporated (important published sources include Heilmann-Clausen 1987; Thomsen 1987; Jeremiah 2001; Dybkjær & Jutson 2003; Mutterlose & Bottini 2013; Ineson *et al.* 2022a, 2022b). Key biostratigraphic events (both micro- and nannofossils) were correlated to the current Cretaceous chronostratigraphic scheme (Ogg & Hinnov 2012, subsequently updated to the revised Gale *et al.* 2020 timescale, see Fig.2) and applied to constrain borehole lithostratigraphy (Fig. 2) and regional ties to seismic data.

Seismic stratigraphy and lithostratigraphic development

Seismic stratigraphic framework: key reflectors

The regionally interpreted five key seismic reflectors constituting the seismic stratigraphic framework have been used to delineate and map the distribution and thickness of the different Lower Cretaceous lithostratigraphic formations discussed below (Fig. 2). The reflectivity of the seismic reflectors and the seismic character of the various units vary within the Danish Central Graben.

Base Cretaceous Unconformity

The Base Cretaceous Unconformity (BCU; Fig. 3) marks the base of the Cromer Knoll Group in the Danish Central Graben. As noted above, the BCU

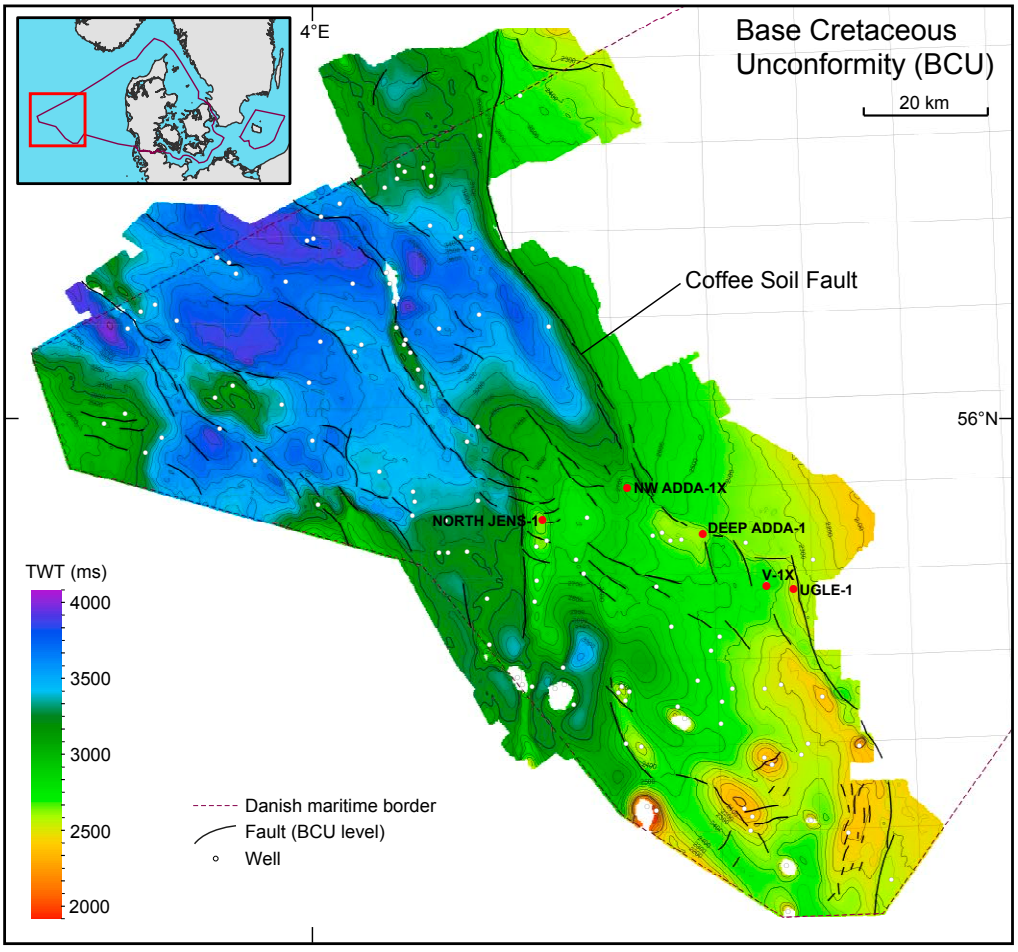


Fig. 3. Time-structure map (TWT, ms) of the Base Cretaceous Unconformity (BCU). Note the deepening of the BCU in the northern part of the Danish Central Graben. Wells discussed in the text specific to this map are named and highlighted in red; see Supplementary Data for high-resolution image, facilitating identification of all wells and detailed contouring.

seismic surface in basin-centre depocentres defines the boundary separating the Jurassic – lowermost Cretaceous syn-rift succession from the Cretaceous post-rift deposits. Regionally, the BCU represents a hiatus and/or a significant facies change that is clearly defined on wireline logs and has a distinct seismic character making it an important marker that can be correlated and mapped in major parts of the North Sea (Copestake *et al*. 2003). A distinct seismic reflector is also observed where Lower Cretaceous successions overlie pre-Jurassic strata.

In large parts of the Danish Central Graben where the BCU seismic horizon corresponds to the lithological change from the low impedance Upper Jurassic – lowermost Cretaceous syn-rift shales to the marly deposits of the lowermost Cromer Knoll Group (the Leek member of the Valhall Formation), the transition is associated with a characteristic distinct positive seismic reflector. In such basinal areas, this reflector corresponds broadly to a distinct shift in the well-log pattern representing the change from the organic-rich Upper Jurassic – lowermost Cretaceous Mandal/Farsund shales to the chalky marlstones of the lowermost Valhall Formation (Figs 2, 4; Petersen & Jacobsen 2021). The boundary is defined at the first significant upwards decrease in gamma ray (GR) response and a corresponding increase in sonic velocity related to the change in lithology (Jensen *et al*. 1986). A cored section in the North Jens-1 well spanning this key surface in a basinal setting was described recently by Ineson *et al*. (2022a).

Along the faulted margin (Coffee Soil Fault) of the Ringkøbing-Fyn High where the Upper Jurassic – lowermost Cretaceous succession includes gravity-flow silt-/sandstone intervals (the Poul Formation), the BCU reflector is less distinct, marking the boundary between Poul Formation sandstones and the overlying Cromer Knoll Group marlstones and shales. In a number of wells located in the fault zone (e.g. V-1, Ugle-1, Deep Adda-1), gravity-flow sandstones referred to the Vyl Formation by Jensen *et al*. (1986) are located above the seismic BCU marker and the sandstone interval is considered as part of the Cromer Knoll Group (Fig. 4). Biostratigraphic data from cored Vyl Formation sandstones in the Deep Adda-1 well suggest an early Valanginian age for these deposits (Fig. 2; Jutson 1997).

Seismic mapping at this level demonstrates the variable degree of stratigraphic truncation in the Danish Central Graben, dependent on the structural position within the basin. Although conformable or para-conformable in many depocentres, stratigraphic truncation increases in magnitude onto the flanks of the graben and on intrabasinal highs where the Cromer Knoll Group progressively overlaps older Jurassic and locally pre-Jurassic strata (Fig 5A). The relief inherited from the late syn-rift phase results in a similar supercrop pattern with basal Cromer Knoll Group sediments present in depocentres and progressive onlap of younger Cromer Knoll Group, and ultimately Upper Cretaceous strata, onto the BCU surface towards the graben flanks and onto intrabasinal highs (Fig. 5B).

CKG10
The top of the mudstone-dominated Valhall Formation, succeeded by Tuxen Formation marly chalks (Fig. 2), is picked in a continuous peak overlying a generally rather transparent interval with few continuous internal reflectors. The top Valhall Formation reflector shows basal onlap to the west but is truncated by the Base Chalk (chb) reflector towards the north in the Søgne Basin and along inversion ridges to the east in the central part of Danish Central Graben. The surface is itself a truncation surface locally in the east of the area, for example in the eastern Adda discovery where the Tuxen Formation unconformably overlies the lower Valhall Formation (Ineson *et al*. 2022b).

CKG15
This reflector is generally a strong seismic trough produced by the boundary between the chalks and marly chalks of the Tuxen Formation below and the marls and shales of the Sola Formation above (Fig. 2). The horizon has a more restricted extent than the CKG10 horizon towards the Søgne Basin and along inversion ridges to the east due to truncation by the Base Chalk Group (chb) reflector.

CKG20
This reflector is picked in a peak marking the transition from the mudstones and calcareous mudstones of the upper part of the Sola Formation (Fanø Member of van Buchem *et al*. 2018), to the marlstones and marly chalks of the overlying Rødby Formation (Fig. 2). The reflector can only be traced over restricted areas in the north-west, northernmost, and central-eastern parts of the Danish Central Graben where the overlying Rødby Formation is thick, allowing separation of CKG20 from the distinct Base Chalk reflector.

chb
The base of the Chalk Group (chb) is everywhere represented by a distinct strong amplitude peak marking the break from high impedance chalk above to lower velocity Cromer Knoll Group or older strata beneath.

Lithostratigraphy, facies and distribution

The Lower Cretaceous Cromer Knoll Group lithostratigraphy is based primarily on Jensen *et al*.

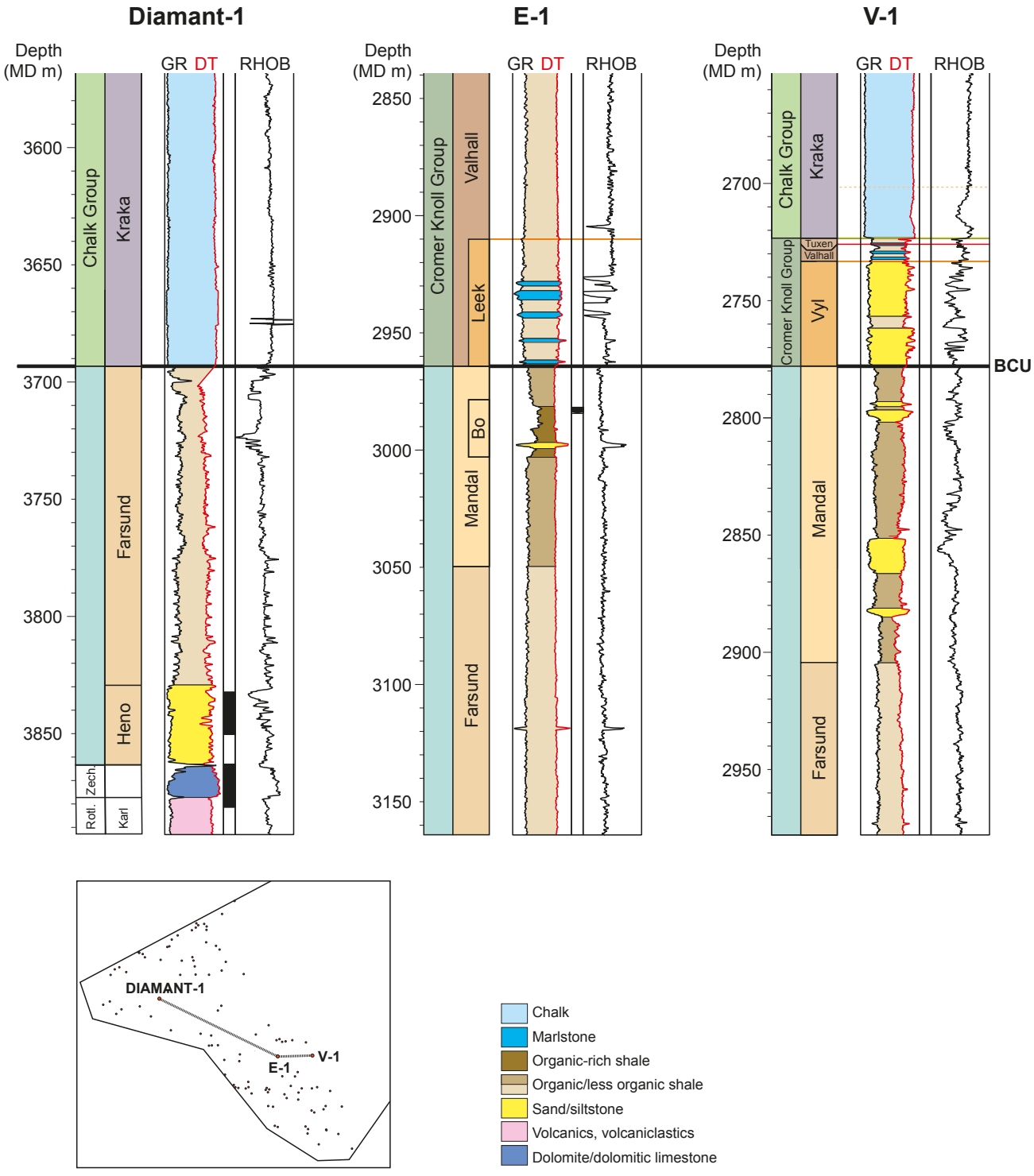


Fig. 4. NW–SE log correlation at the Base Cretaceous Unconformity (BCU) stratigraphic level showing three different scenarios; inset map shows the location of the three illustrated wells in the Danish sector of the Central Graben (see Fig. 1 for enlarged version). The **E-1** well represents a deep depocentre with a probable conformable relationship between the late syn-rift deposits (the Mandal Formation, including the organic-rich mudstones of the Bo Member) overlain by an expanded Leek Member (lowermost Valhall Formation) composed of thin marly chalks – chalky marlstones interbedded with marlstones. Increasing organic richness of the Farsund–Mandal mudstones is indicated by light/medium/dark brown shades. **V-1**, close to the Coffee Soil Fault at the eastern margin of the graben illustrates Vyl Formation gravity-flow sandstones at the base of the Valhall Formation; the indications of Barremian strata (Tuxen Formation) in this well are speculative and may reflect faunal/floral reworking at a base Chalk Group hiatal surface (lowermost Chalk Group absent). The **Diamant-1** well on the north-western Heno Plateau illustrates the western pinch-out of the Cromer Knoll Group on truncated Upper Jurassic syn-rift strata; note that the lowermost Chalk Group is also absent here. GR: Gamma-ray log; DT: Sonic log; RHOB: Density log; Rotl.: Rotliegendes; Zech.: Zechstein.

(1986) with modifications by Riley *et al*. (1992) and more recently by van Buchem *et al*. (2018) (Fig. 2). These modifications included changes to the Sola Formation, whereby the informal Fischschiefer bed was defined as a member (Riley *et al*., 1992) and the new Fanø Member replaced the informal 'Albian Shale' unit in the upper part of the formation (van Buchem *et al*., 2018). Jensen *et al*. (1986) included five formations in the Cromer Knoll Group: Valhall, Vyl, Tuxen, Sola and Rødby. The Valhall Formation contains the carbonate-rich Leek Member. The Tuxen, Sola and Rødby Formations are also used in the Norwegian Central Graben and the formations are largely time-equivalent (Isaksen & Tonstad 1989; Copestake *et al*. 2003; Gradstein *et al*. 2016). The Valhall Formation was defined in the UK North Sea and is time-equivalent to part of the Åsgard Formation in the Norwegian North Sea (Deegan & Scull 1977; Isaksen & Tonstad 1989; Copestake *et al*. 2003; Gradstein *et al*. 2016).

Valhall Formation (uppermost Ryazanian – lower Hauterivian)

In complete sections, the uppermost Ryazanian – lower Hauterivian Valhall Formation is a uniform, mudstone-dominated marine succession; carbonate content in the formation decreases upwards above the basal carbonate-rich Leek Member (<5 m to *c*. 60 m thick) and increases again towards the top of the formation where transitional to the chalk-rich Tuxen Formation. Marlstones and thin argillaceous chalks are recorded in the lower and upper levels. In expanded, complete sections of the Valhall Formation, the GR log pattern reflects these trends, showing an overall upward increase in values to the middle of the formation reverting to a decrease up to the gradational base of the overlying chalk-dominated Tuxen Formation (Fig. 6). In such sections (e.g. E-1 (Fig. 4), Sten-1 (Fig. 6), Iris-1 and I-1 wells; see Fig. 1 for well locations), the spiky log pattern of the Leek Member at the base of the Valhall Formation reflects the interbedding of discrete thin carbonate-rich beds with calcareous shales or marlstones whereas in thinner, more condensed sections the member is commonly carbonate dominated, yielding a blocky GR log pattern.

The distribution and thickness of the Valhall Formation is mapped by the seismic interval BCU – CKG10. The isochore map reveals considerable thickness variations across the Danish Central Graben from

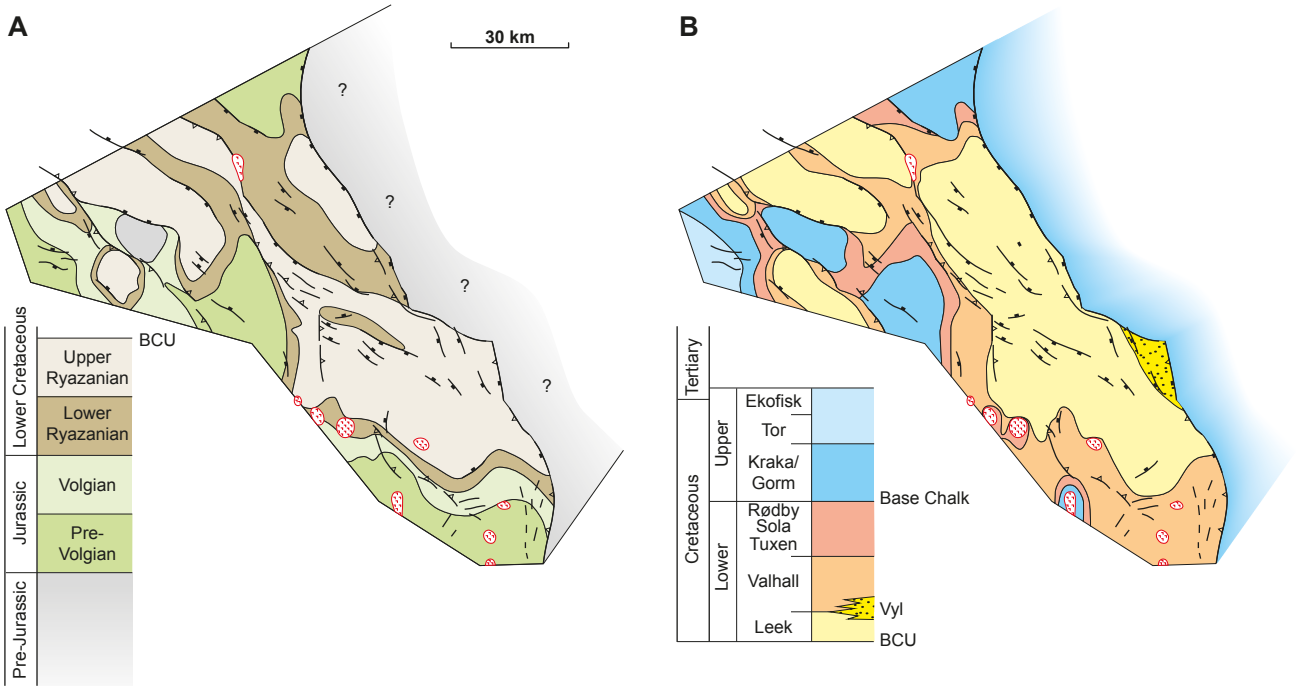


Fig. 5. (A) BCU sub-crop map with indications of the degree of truncation of the lowermost Cretaceous, Jurassic and older strata. Gentle truncation is associated with fault activity in the central part of the Danish Central Graben. On structural highs, deep erosion of the Jurassic is recognized. On the Ringkøbing–Fyn High and on the Inge High, the BCU reflector forms the top of Palaeozoic or older rocks (basement). **(B)** BCU super-crop map. Initial Cromer Knoll Group sedimentation (Leek Member) took place in the main depocentres; sandstones of the Vyl Formation were deposited in a narrow zone along the Ringkøbing–Fyn High. The depocentres expanded progressively during the early Cretaceous and prominent intrabasinal highs and the graben flanks were first onlapped in the Late Cretaceous.

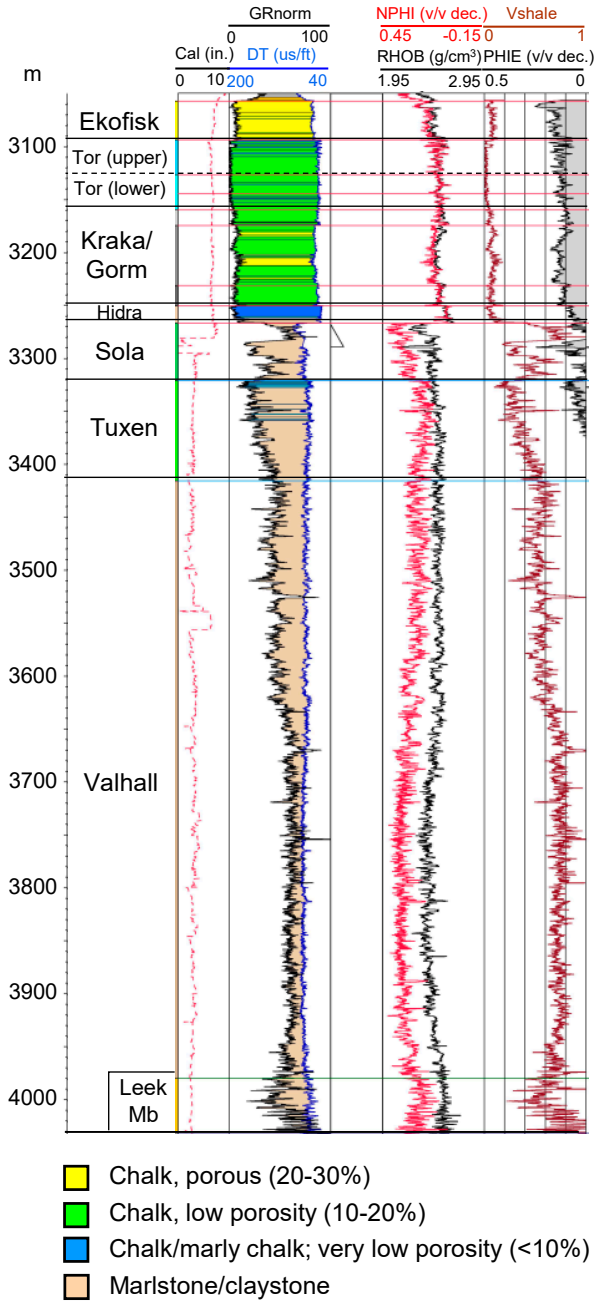


Fig. 6. The Sten-1 well in the Feda Graben illustrating the development of the Valhall, Tuxen and Sola Formations in a major Early Cretaceous depocentre. The low gamma-ray (GR) values at the base of the Valhall Formation correspond to the carbonate-rich Leek Member. The GR readings show an overall upward increase to the middle of the Valhall Formation due to increasing clay content, reverting to a decrease up to the gradational base of the overlying Tuxen Formation that comprises marly chalks and marlstones, displaying lower GR values. The Sola Formation includes clay-dominated intervals indicated by increased GR values, particularly in the lower half and upper levels of the formation. GRnorm: normalised Gamma-ray log; DT: Sonic log; NPHI: Neutron porosity log; PHIE: Effective porosity; RHOB: Density log; Vshale: Calculated shale volume.

absence on the Mid North Sea High, Inge High, Heno Plateau and in the Søgne Basin to thick sections in depocentres (Fig. 7A). The main depocentres with the thickest Valhall Formation are the Feda, Gertrud and Arne-Elin Grabens, and the Iris, Gulnare and Roar Basins (Fig. 7A). Drilled Valhall thicknesses range from less than 30 m to hundreds of meters with a maximum drilled thickness of 614 m in the Sten-1 well located in the Feda Graben (Fig. 6); thicknesses of up to a kilometre may be attained in the deepest subbasins (Jensen *et al*. 1986). Although largely representing the primary distribution of the formation, the distribution and thickness variation depicted on Fig. 7A are locally influenced by erosional truncation, either at base Tuxen (e.g. easternmost Adda discovery and Tyra Field) or at base Chalk Group (e.g. Søgne Basin area).

Vyl Formation (lower Valanginian)

Based on well penetrations, the lower Valanginian Vyl Formation is apparently restricted to a narrow zone adjacent to the Coffee Soil Fault against the Ringkøbing-Fyn High, particularly in the breached transfer zone intersected by the V-1, Deep Adda-1 and Ugle-1 wells in the south-eastern Danish Central Graben (Figs 1, 4). The distribution of the formation was not mapped seismically. This formation represents gravity-flow sandstones located stratigraphically above the BCU while comparable sandstones assigned to the upper Volgian – Ryazanian Poul Formation occur below the BCU (Petersen & Jakobsen 2021). Stratigraphic data suggest that the Vyl Formation may post-date much of the carbonate-dominated Leek Member of the Valhall Formation (Jutson 1997; Fig. 2). Deposition of the Vyl Formation may have been linked to active tectonism along the fault zone, as inferred for the Poul Formation by Petersen & Jakobsen (2021), suggesting that extensional fault activity along the Coffee Soil Fault zone persisted into the early Valanginian.

The formation comprises silty fine-grained sandstones and interbedded siltstones (Jensen *et al*. 1986); in the Deep Adda-1 core section through the upper Vyl Formation, the siltstones and silty fine sandstones are intensely bioturbated and contain bioclasts (Nielsen *et al*. 2015; succession erroneously referred to the uppermost Farsund Formation by these authors). Cuttings in the Ugle-1 well suggest that coarser, texturally and mineralogically immature facies are represented in the most proximal settings, close to the fault zone (Michelsen *et al*. 2003; Nielsen *et al*. 2015).

Tuxen Formation (Hauterivian – upper Barremian)

The Tuxen Formation is an important chalk reservoir unit in the producing Valdemar Field and in the Adda–Tyra area (Jakobsen *et al*. 2004; Fig. 1) but is recognized throughout the Danish Central Graben and extends

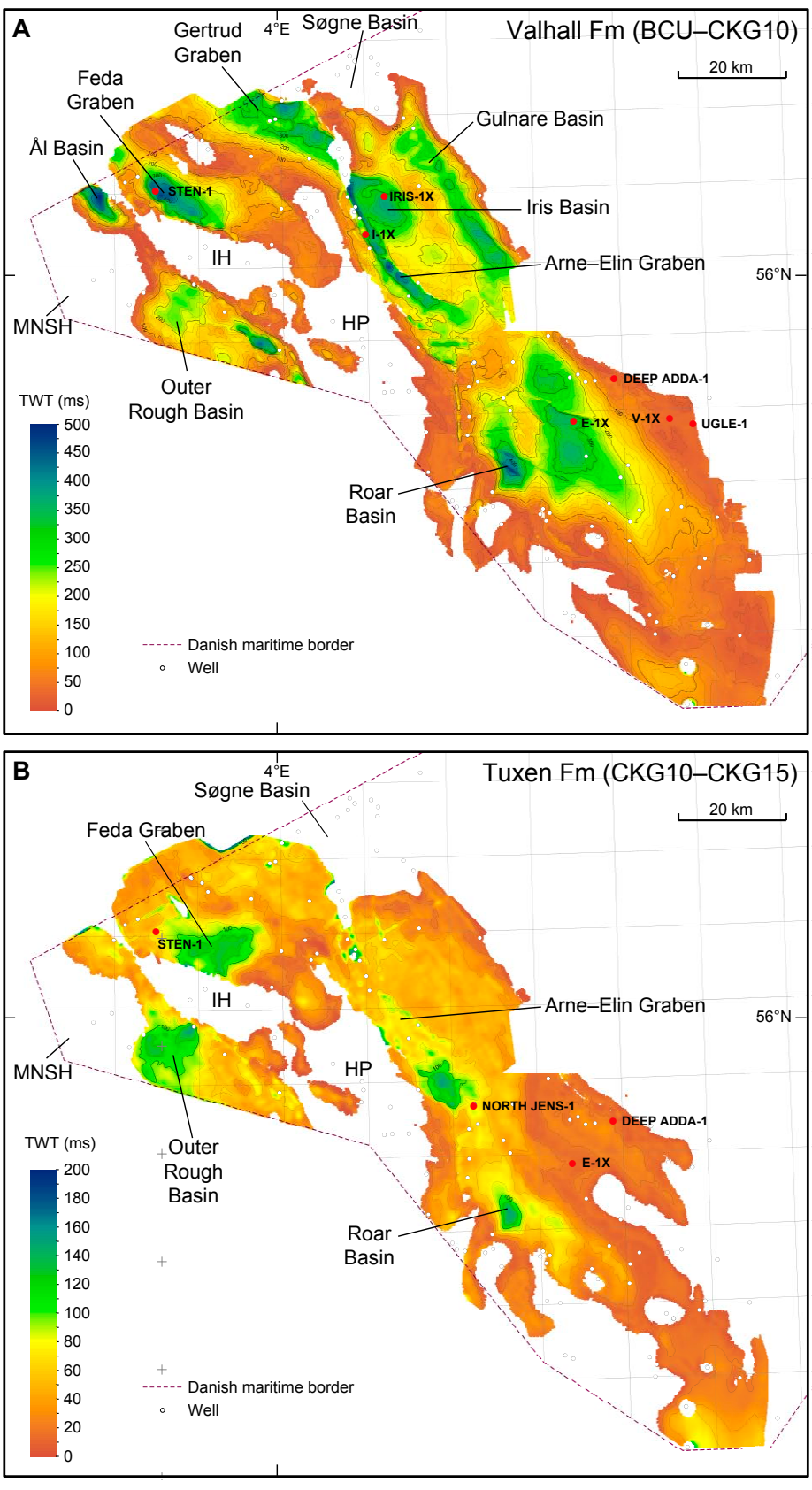


Fig. 7. Time-isochore maps (TWT, ms) of Lower Cretaceous formations with indication of the key structural highs and depocentres; wells discussed in the text specific to the mapped unit are named and highlighted in red. See Supplementary Data for high-resolution images to identify all wells and enlarge contouring details. **(A)** Valhall Formation (seismic interval BCU–CKG10). **(B)** Tuxen Formation (seismic interval CKG10–CKG15). **(C)** Sola Formation (seismic interval CKG15–CKG20). **(D)** Rødby Formation (seismic interval CKG20–chb). HP: Heno Plateau; IH: Inge High; MNSH: Mid North Sea High.

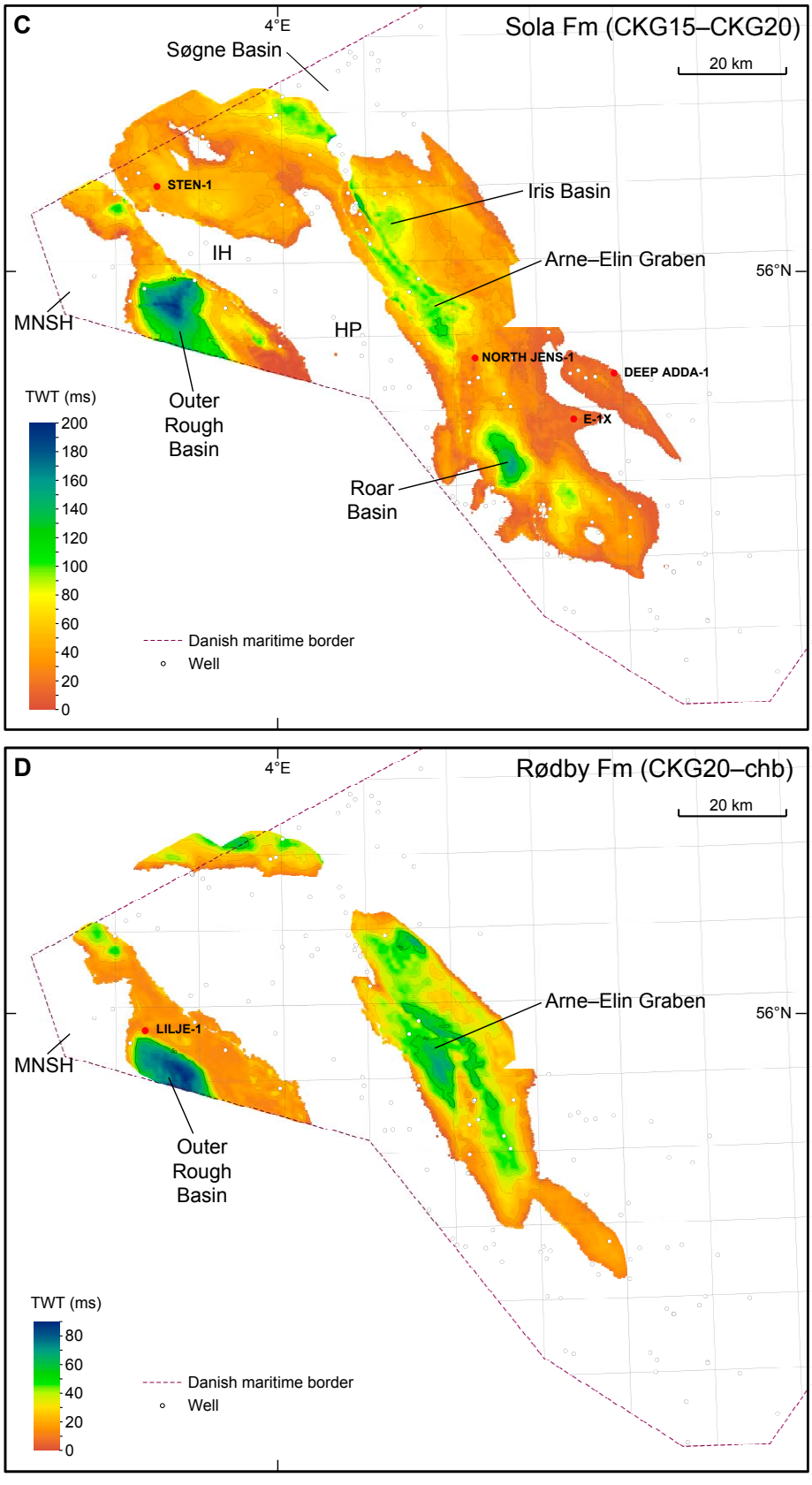


Fig. 7. Continued.

northwards into the southern Norwegian Central Graben. The formation is generally of late Hauterivian to late Barremian age, though the lowermost beds in the Adda area extend down into the lower Hauterivian due primarily to condensation and the earlier onset of carbonate-dominated sedimentation on the evolving Adda High.

In expanded sections, such as in the Valdemar Field (Ineson 1993: Jakobsen *et al.* 2004), the formation is subdivided by a prominent organic-rich marker bed, the Munk Marl Bed (MMB; Jensen *et al.* 1986), which forms a distinctive 'forked' GR peak recognized widely in the subsurface of the North Sea (Fig. 8; Crittenden *et al.* 1991; Copestake *et al.* 2003). The chalk-rich lower and upper Tuxen Formation units show similar 'cleaning-upward' trends, the cleanest, clay-poor chalks (with the lowest GR values) occurring at the top of the units (Figs 6, 8). The formation comprises a heterogeneous layered succession of bioturbated chalks and marly chalks interbedded with greenish grey (locally reddish) or dark grey-black marlstones; a detailed description of the lithofacies of the Tuxen and Sola Formations is presented by Jelby *et al.* (2022). Marly chalk constitutes nearly 75% of the Tuxen Formation in the Valdemar Field (Fig. 9A; Jakobsen *et al.* 2004) but marlstones dominate the lowermost Tuxen Formation. The dominant marly chalk facies is characterized by mid-grey to light yellowish-fawn chalk with a clear marl content in the form of burrow fills, marlstone flasers, solution seams and laminae; biogenic fabrics dominate and the definition of the trace fossils can be striking, particularly adjacent to darker marlstone beds (Fig 9A). *Chondrites* burrows are abundant and the best-defined trace, and clearly represent the last component of a tiered ichnofabric that includes *Planolites, Asterosoma*, and less commonly *Zoophycos, Teichichnus* and *Thalassinoides*.

At certain levels, particularly immediately beneath the MMB and at the top of the Tuxen Formation, off-white, pale yellow or cream-coloured chalk is prominent and forms the most important reservoir facies in the Valdemar Field. Although this facies contributes only 9% to the gross Tuxen Formation in this field, it forms 50% of the uppermost Tuxen Formation – the 'Upper Tuxen-1' reservoir zone of Jakobsen *et al.* (2004). It comprises chalk without significant marl content, with the exception of rare isolated marlstone flasers. The chalk is typically homogeneous and essentially structureless; faint bio-mottling may be recognized locally, and a diffuse pelleted fabric is evident in places. In the Adda–Tyra area, the Tuxen Formation is thin and stratigraphically condensed or incomplete; pebbly chalk beds occur locally in association with nodular chalks and hardgrounds (Jensen & Buchardt 1987; van Buchem *et al.* 2018; Jelby *et al.* 2022; Ineson *et al.* 2022b).

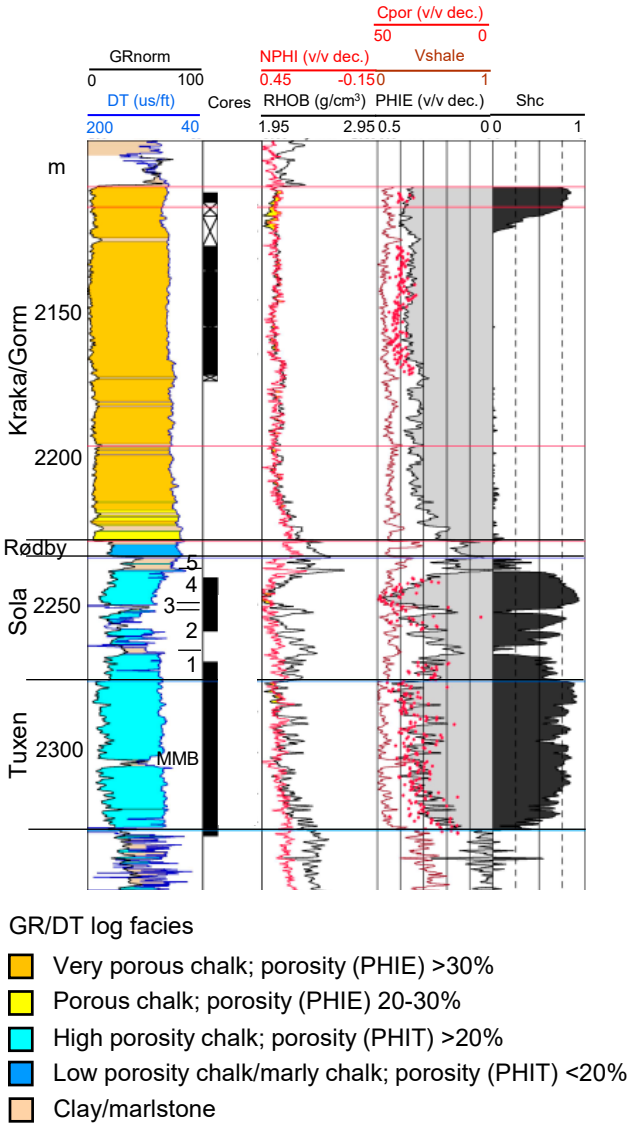


Fig. 8. Computer-processed interpretation (CPI) log of the North Jens-1 well (Valdemar Field; see Fig. 1 for location) showing high oil saturations exceeding 75% in high porosity chalk reservoirs of the Lower Cretaceous Tuxen and Sola Formations. Note minor oil saturations in the lower part of the Chalk Group (lower Kraka Formation) above the Tuxen and Sola accumulations. The five units (1–5) of the Sola Formation described in the text are indicated; MMB: Munk Mark Bed. Semi-quantitative log evaluation of reservoir facies (first column) utilized different parameters for the clay-poor Upper Cretaceous – Danian Chalk Group (PHIE, effective porosity) and the clay-rich Cromer Knoll Group chalks (PHIT, total porosity; for full methodology, see Skaarup *et al.* 2017). Cpor: core porosity, GRnorm: normalised Gamma-ray log; DT: Sonic log; NPHI: Neutron porosity log; PHIE: Effective porosity; RHOB: Density log; Shc: Hydrocarbon saturation. Vshale: Calculated shale volume.

The MMB, bisecting the Tuxen Formation (Figs 2, 8), is an interval of dark grey to black, finely laminated, organic-rich marlstone up to 2 m thick; the bed is locally absent or condensed on structural highs (e,g, Adda-2, Jensen & Buchardt 1987). The organic matter contains diagenetic bituminite and late-oil solid bitumen (Rudra *et al*. 2021). The lamination is commonly defined by an alternation of lighter-coloured carbonate-rich and darker clay-rich laminae (Fig. 9B; see also Jelby *et al*. 2022). As reported in detail by Thomsen (1989a, b), the carbonate-rich laminae are dominated by nannofossils and the coccoliths are spectacularly preserved. The lamination is typically parallel and undisturbed but weakly bioturbated levels (*Chondrites*) are recognized locally. Pyrite is common in this lithofacies, both disseminated and forming framboidal pyrite nodules up to ~2.5 cm across (Rudra *et al*., 2021). The marlstones are rich in organic carbon and Jensen & Buchardt (1987) recorded an average TOC value of 11.5 wt.% for the MMB in the E-1 well (Fig. 1 for location). Matrix-rich conglomerate beds up to 0.4 m thick, of debris flow origin, and thin graded marlstone turbidites occur interbedded with laminated marlstones in the MMB in the Deep Adda-1 well; these redeposited facies were probably derived from the fault-controlled eastern margin of the Danish Central Graben (Ineson *et al*. 2022b).

Log definition of the base of the formation is variable. In expanded sections, the apparently conformable boundary is transitional and picking a significant fall in GR values (increase in carbonate content) can be subjective (Fig. 6); in other cases, for example in the eastern Adda area, the boundary is abrupt and associated with seismic truncation at seismic marker CKG10 and a significant biostratigraphic hiatus (Ineson 1993; Copestake *et al*. 2003; Ineson *et al*. 2022b). The top of the formation is defined at a significant increase in GR values marking the incoming of the shale-dominated facies of the overlying Sola Formation (Figs 6, 8).

The preserved Tuxen Formation is somewhat less widespread than the underlying Valhall Formation, as indicated by the mapped seismic interval CKG10 – CKG15 (Fig. 7B), due to truncation in the Søgne Basin and in the southern part of the graben. The thickness of the Tuxen Formation in well penetrations generally ranges from ~10–90 m but the formation can exceed 100 m in thickness in depositional depocentres such as the Feda Graben (e.g. Sten-1 well; Fig. 6). As illustrated in Fig. 7A and B, discrete depocentres were more localised than during Valhall times, being restricted to the Feda Graben, the southern part of the Arne-Elin Graben and the south-western part of the Roar Basin (Fig. 7B), the latter depocentre possibly the result of salt withdrawal. The depositional depocentre in the Outer Rough Basin (Fig. 7B), which was initiated in Valhall Formation times, shows more definition in the Tuxen Formation isochore, a trend that developed strongly during deposition of the Sola and Rødby Formations (Fig. 7C, D). The eclipse of the Valhall depocenter east of the Roar Basin in the Hauterivian and Barremian

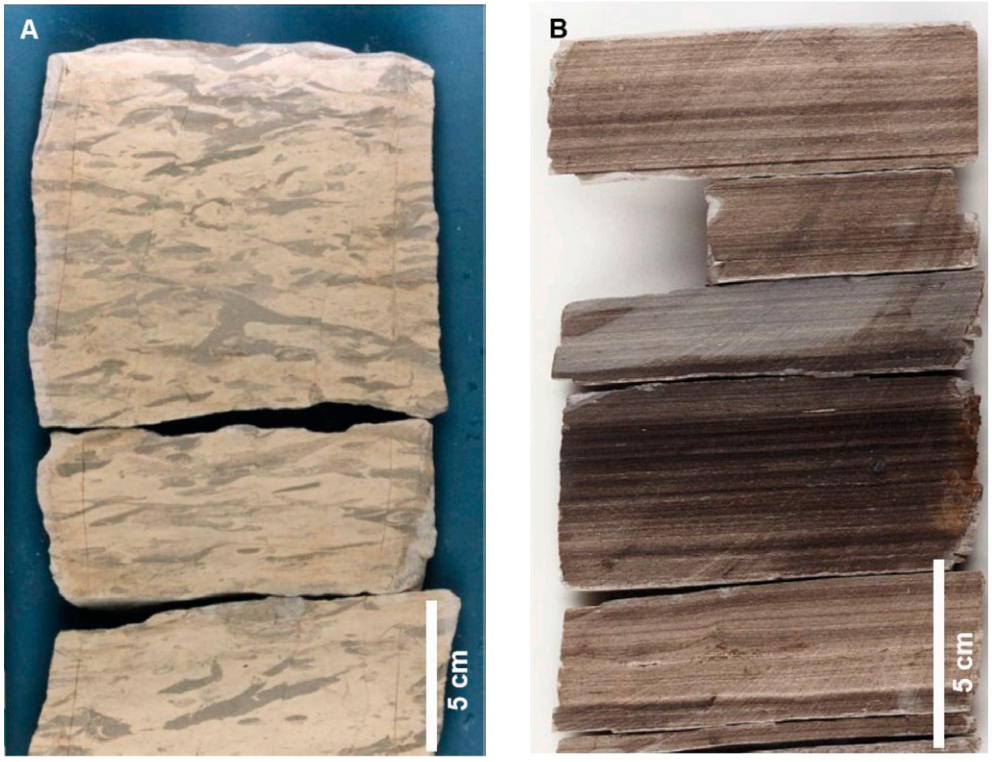


Fig. 9. (A) Bioturbated marly chalk, the typical facies in the central portion of the upper Tuxen Formation (North Jens-1 well, 7944 ft/2421.3 m), **(B)** Finely laminated marlstones of the Munk Marl Bed in the Tuxen Formation (North Jens-1 well, 7560 ft/2304.3 m). Note the absence of bioturbation, the delicate dark–light laminae and the superimposed gradual transitions from darker more clay-rich intervals to lighter chalkier intervals. Minor truncation and drape (lower left) is attributed to slope creep.

reflects beginning uplift along the trend of the subsequent Late Cretaceous Tyra–Igor and Adda inversion ridges (Vejbæk & Andersen 2002).

Sola Formation (upper Barremian – lower Albian)
The Upper Barremian – Lower Albian Sola Formation is dominated by fine-grained calcareous siliciclastics but also includes marly chalk interbeds; a discrete thin reservoir-quality chalk unit (*c.* 5–8 m thick) of late early Aptian age is present locally, notably in the Valdemar Field (Figs 1, 8).

Where fully developed (e.g. northern Valdemar Field; Ineson 1993; Jakobsen *et al.* 2004; Fig. 8), the formation comprises five units:

(1) The basal unit of late Barremian age (Lower Sola-1 of Jakobsen *et al.* 2004) is up to 8 m thick, although often absent or thinly developed. Lithologically it resembles the underlying Tuxen Formation, comprising thoroughly bioturbated chalky marlstones and marly chalks.

(2) Dark grey to black bioturbated or laminated marlstones dominate this interval (Middle Sola-1 to -3 of Jakobsen *et al.* 2004), though interbedded bioturbated chalky marlstones and marly chalks are represented in the upper levels. This upper Barremian to lowermost Aptian unit is *c.* 15 m thick in the northern Valdemar Field and up to 25 m thick in eastern Adda discovery wells.

(3) Black, finely laminated, organic-rich marlstones of the lower Aptian Fischschiefer Member, typically 2–5 m thick, create a distinctive log marker that is recognized widely in the North Sea region (see below),

(4) This unit (Upper Sola-1, -2 of Jakobsen *et al.* 2004) varies lithologically in the Danish Central Graben, being dominated by marlstones with subordinate marly chalk interbeds in most areas but forming a secondary chalk reservoir body in the northern Valdemar Field (Fig. 8) where it is *c.* 13 m thick and includes clay-poor chalk of reservoir quality in the lower half.

(5) The uppermost Sola Formation consists of a mid-Aptian – lower Albian variably calcareous claystone succession that varies in thickness from a few metres to nearly 100 metres in late Aptian – Albian depocentres. Previously referred to informally as the 'Albian Shale' (Jakobsen *et al.* 2004), this unit was defined formally as the Fanø Member of the Sola Formation by van Buchem *et al.* (2018) and interpreted to record lowstand deposition in a restricted, dysaerobic basin with reduced water circulation. The lower boundary is locally erosional, truncating the Aptian chalk reservoir beneath (e.g. southern Valdemar Field).

Complete sections including all five of these units are relatively scarce in the Danish Central Graben. The lower two units may be absent such that the Fischschiefer Member rests directly on the Tuxen Formation, exemplified by the Adda-2 well (Jensen & Buchardt 1987), whilst the upper Sola Formation (and the succeeding Rødby Formation) is typically only well developed in the central depocentres (e.g. the Roar Basin, Arne Elin Graben) and is more commonly highly condensed or absent.

The laminated organic-rich marker bed in the Sola Formation, the lower Aptian Fischschiefer Member, is recognized widely in the North Sea subsurface (Crittenden *et al.* 1991; Ainsworth *et al.* 2000; Riley *et al.* 1992; Copestake *et al.* 2003) and is commonly correlated with the globally recognized early Aptian anoxic event, OAE 1a (van Buchem *et al.* 2018; Blok *et al.* 2022). Although overtly resembling the MMB within the Tuxen Formation, Thomsen (1989b) demonstrated that the light-coloured, carbonate-rich laminae in the Fischschiefer Member are commonly composed of discrete coccolith-rich pellets, contrasting with the pristine, often monospecific nannofossil-rich laminae in the MMB (Thomsen 1989a, b). The Fischschiefer Member contains bitumen from migrated oil, degraded lamalginite and abundant framboidal pyrite (Rudra *et al.* 2021).

The areal extent and thickness variation of the Sola Formation is illustrated by the seismic interval CKG15–CKG20 (Fig. 7C). The formation has a reduced lateral extent in the south-south-eastern part of the Danish Central Graben due to truncation but otherwise the time-isochore map shows similarities to that of the Tuxen Formation with regard to the location of the main depocentres, i.e. the Arne-Elin Graben – Iris Basin and the south-eastern Roar Basin. Contrasts include the decrease in importance of the Feda Graben and the evidence of marked subsidence of the central part of the Outer Rough Basin during Sola Formation times, where based on seismic data the formation has a maximum thickness of more than 200 m (150 ms). In most wells the drilled thickness of the Sola Formation is ~10–60 m but exceeds 100 m in the Arne-Elin Graben and Iris Basin depocentres (Fig. 7C; Nielsen & Japsen 1991; van Buchem *et al.* 2018). It is deemed likely that much of the enhanced thickness in undrilled depocentres is attributable to the Fanø Member, recording centres of Late Aptian – Albian subsidence (see also Rødby Formation, Fig 7D; van Buchem *et al.* 2018).

Rødby Formation (early Albian – earliest Cenomanian)

The Lower Albian – lowermost Cenomanian Rødby Formation represents the upward transition from the mud-rich facies of the Sola Formation to the chalks of the Upper Cretaceous Chalk Group above, as reflected by the overall upward decrease in GR values. The formation typically consists of greyish marlstones with subordinate calcareous shales and chalky limestones (Jensen *et al*. 1986).

The CKG20 – chb seismic interval comprising the Rødby Formation is generally thinly developed and there is poor separation between the CKG20 and the distinct Base Chalk chb seismic horizon (Fig. 7D); the limited extent of this formation relative to those beneath (compare Fig. 7D with 7A–C) may thus be in part an artefact due to seismic resolution. The Outer Rough Basin is anomalous showing extraordinary thicknesses, but it is stressed that the central part of this basin is without well control, the only direct seismic tie being that of the Lilje-1 well, located at the western basin margin. In many wells, the Rødby Formation is condensed and in most wells the formation is <25 m thick or absent, but thicknesses over 60 m have been recorded in mid-Cretaceous depocentres (e.g. Nielsen & Japsen 1991) where the R1–R3 subdivisions of Crittenden *et al*. (1991) are often recognisable. In such expanded sections, where the succeeding chalks of the Hidra Formation are thickly developed and argillaceous, defining the location of the upper boundary of the Rødby Formation can be difficult. Compared to the underlying uppermost Sola Formation (Fanø Member) the sediments and microfossils of the Rødby Formation indicate a return to more open marine depositional conditions (van Buchem *et al*. 2018).

Discussion

The new stratigraphically well-constrained isochore maps presented here (Fig. 7, Supplementary Data) document the regional Early Cretaceous evolution of the Danish Central Graben in unprecedented detail; this is particularly the case for the Hauterivian–Albian portion of the basin fill that is the focus of much industrial and academic interest (e.g. Mutterlose & Bottini 2013; van Buchem *et al*. 2018; Blok *et al*. 2022; Ineson *et al*. 2022b). The shifting subsidence history revealed by these maps, and the interaction with eustatic sea-level events, have important implications for the stratigraphic development and lateral distribution of mid-Cretaceous chalk reservoirs, as stressed below, a subject relevant to optimizing ongoing hydrocarbon production and future storage potential.

Basin evolution and reservoir development

The depth to the base of the Cromer Knoll Group, the BCU surface, in the Danish Central Graben increases from south to north from about 2000 ms (equivalent to about 2340 m) to more than 3800 ms (equivalent to about 4800 m; Fig. 3). The southern area is dominated by Zechstein salt piercement structures and pillows giving rise to rather dramatic relief (Fig. 10). It is noteworthy that the BCU is shallower in the graben area along the south-eastern segments of the Coffee Soil Fault Zone than on the adjoining part of the stable Ringkøbing-Fyn High. This is the result of intra-Cretaceous compressional tectonism with minor thrust faults that propagate from the tips of former extensional basement-attached faults in the substrate. The major faults (both normal and reverse) affecting the BCU are highlighted in Fig. 11A.

The Cromer Knoll Group sediments were deposited during a post-rift thermal subsidence phase, and the main depocentres are mapped as elongate troughs or sub-basins parallel to the basin axis (Fig. 11B). The Roar Basin to the south was separated by a NE–SW trending threshold (Pollerne Ridge of Vejbæk 1986) from the northern sub-basins. The post-rift Valhall Formation depocentres are to a large extent coincident with the major depocentres of the late-rift deposits referred to the middle Volgian – upper Ryazanian Farsund/Mandal Formations, i.e. the Feda Graben, Gertrud Graben, Arne-Elin Graben and major parts of the former Tail End Graben (Fig. 11B). The Outer Rough Basin and Ål Basin developed as new structural elements that accumulated thick Lower Cretaceous sections (Fig. 10). The Cromer Knoll Group is, however, more limited in extent than the underlying Upper Jurassic – lowermost Cretaceous syn-rift deposits, being absent on the Mid North Sea High and the Heno Plateau, and in the Søgne Basin and the south-western part of the Salt Dome Province (Fig. 11B).

The lower Cromer Knoll Group basin-fill geometry in the northern sub-basins (e.g. Feda Graben, Arne-Elin Graben, Gulnare Basin) shows that the uppermost Ryazanian to lower Hauterivian Valhall Formation (rather seismically transparent BCU–CKG10 interval) onlaps onto the BCU along the basin margins (Fig. 12). The basin-fill geometry differs in the southern part of the Roar Basin where oblique reflectors dipping gently (1–2°) basinwards (westwards) have been interpreted to represent clinoforms that prograded towards the basin centre from east to west (Vidalie *et al*. 2014); these workers estimated that the maximum topographical relief on these gently dipping reflectors was in the order of 400 m.. Based on flattening at the Base Chalk Group, Vidalie *et al*. (2014) mapped a pattern of laterally continuous sequences over more than 20 km and

suggested that this records south-westward migration of a shelf, into the underfilled Early Cretaceous basin. An alternative interpretation, however, is that the dipping surfaces in this area represent gently tilted strata due to a progressive westward shift in the depocentre accompanying incipient inversion in the Adda–Tyra area, the latter being testified by hiatal surfaces at base Tuxen Formation and within both the Tuxen and Sola Formations (Jensen & Buchardt 1987; Copestake *et al.* 2003; van Buchem *et al.* 2018; Ineson *et al.* 2022b). Synsedimentary tectonic control during deposition of the interval is demonstrated in the Adda–Tyra area by a system of WNW–ESE oriented normal faults that show a vertical displacement of up to 150 m at BCU level (Fig. 13; Vidalie *et al.* 2014). Syndepositional growth on these faults peaked in the Valanginian,

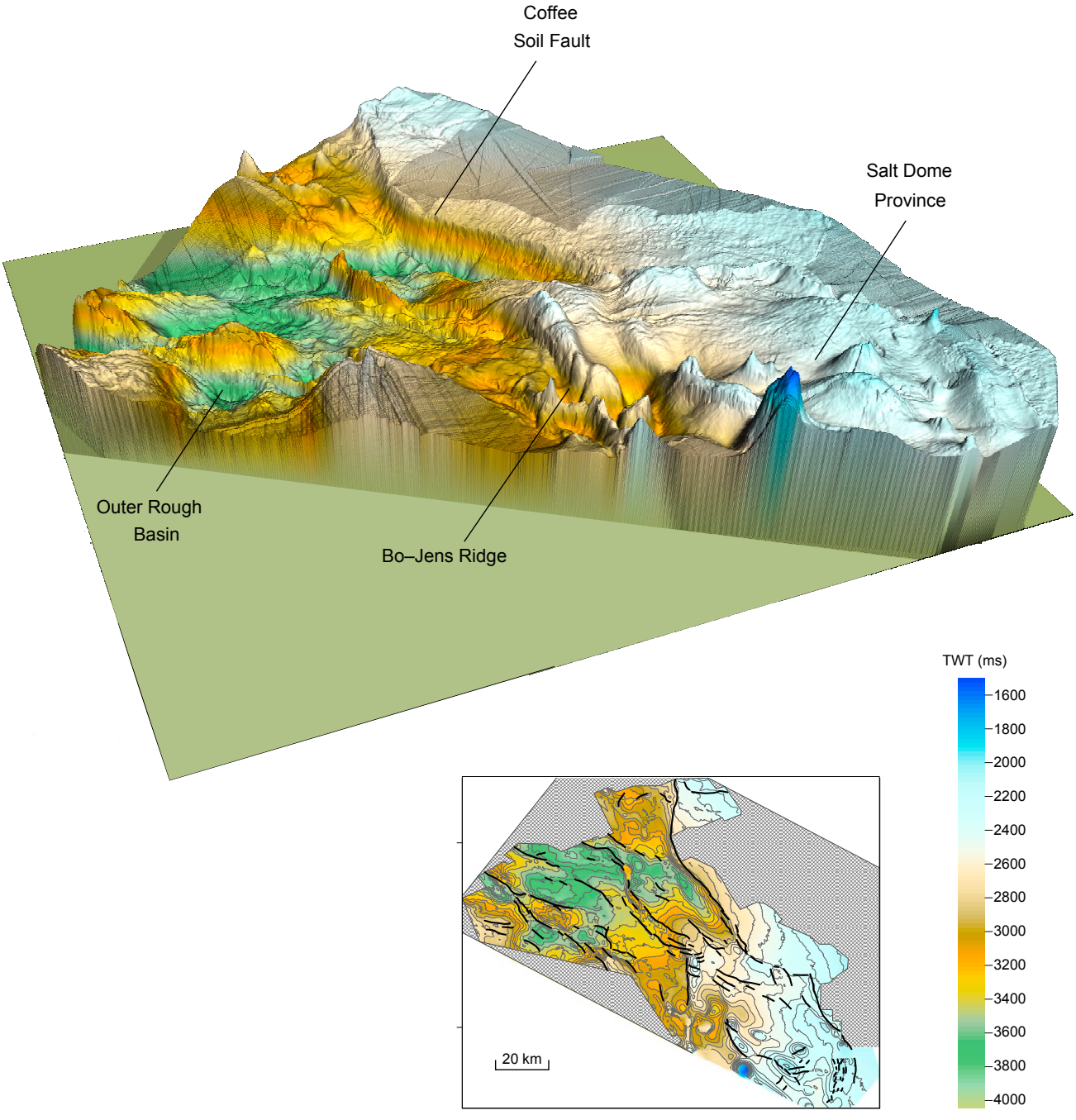


Fig 10. 3D presentation of the time-structure map of the BCU as viewed from the south towards the NNE; key features are indicated for reference. Insert map shows the BCU time-structure map of the Danish Central Graben to aid orientation (see also Fig. 3). 3D image produced by Christian Brogaard Pedersen (GEUS).

waned during the Hauterivian–Albian and the faults were apparently inactive by the Cenomanian (base Chalk Group level).

During deposition of the Tuxen Formation (seismic interval CKG10–CKG15) the basin configuration changed with pronounced subsidence in the Outer Rough Basin in the NW Danish Central Graben (Figs 7B; 10). The Tuxen Formation also marks a change from clay- to chalk-dominated deposition. The depositional setting of the Tuxen Formation is a subject of some debate. Although the chalks that dominate this formation are generally overwhelmingly dominated by nannofossils of pelagic origin, van Buchem *et al.* (2018) suggested a model of areally differentiated carbonate production comprising relatively shallow settings (50–100 m or less) where carbonate-rich sections accumulated separated by mud-dominated deeper water environments. Detailed consideration of this model will be presented elsewhere though regional well and seismic data document the persistence of the chalk-rich Tuxen Formation throughout the Danish Central Graben, albeit being thicker and marlier in depocentres (e.g. Fig. 6; Jakobsen *et al.* 2005). It is likely, however, that relatively shallow 'shelf-like' conditions prevailed locally on uplifted Early Cretaceous inversion structures such as the Adda–Tyra high – the site of the main 'Tuxen shelf' of van Buchem *et al.* (2018). The structural evolution of the basin in the Valdemar and Adda–Tyra areas during the late Hauterivian – Barremian strongly influenced both the facies development and the distribution and preservation of Tuxen Formation reservoir chalks (Ineson 1993; Jakobsen *et al.* 2004, 2005; Jelby *et al.* 2022; Ineson *et al.* 2022b). Protracted subsidence in the Valdemar area ensured the accumulation of continuous chalk–marl successions whereas early inversion of the Adda–Tyra structure resulted in thin, stratigraphically incomplete, condensed chalk deposits.

The succeeding Sola Formation records a significant shift in sedimentation style, being dominated by fine-grained siliciclastic sediment, the influx of mud probably resulting in part from two relative falls in sea level (Ineson 1993; Jakobsen *et al.* 2004; van Buchem *et al.* 2018). In stratigraphically complete sections (e.g. North Jens-1, see Ineson 1993; Copestake *et al.* 2003; Fig. 8), the organic-rich Fischschiefer Member marks the transition from dark bioturbated and laminated marlstones to chalk-rich facies, and has been interpreted to represent a maximum flooding surface that is equivalent to the global oceanic anoxic event OAE 1a characterized by transgression and the accumulation and preservation of organic matter (van Buchem *et al.* 2018; Blok *et al.* 2022). In contrast, the mud-rich upper part of the Sola Formation (the Fanø Member) was deposited under lowstand conditions in a more restricted basin and is considered to reflect a global sea-level fall in the latest Aptian – earliest Albian (van Buchem *et al.* 2018). The absence of the Aptian chalk reservoir (unit 4 of the Sola Formation, Fig. 8) in the southern Valdemar Field probably resulted from sub-

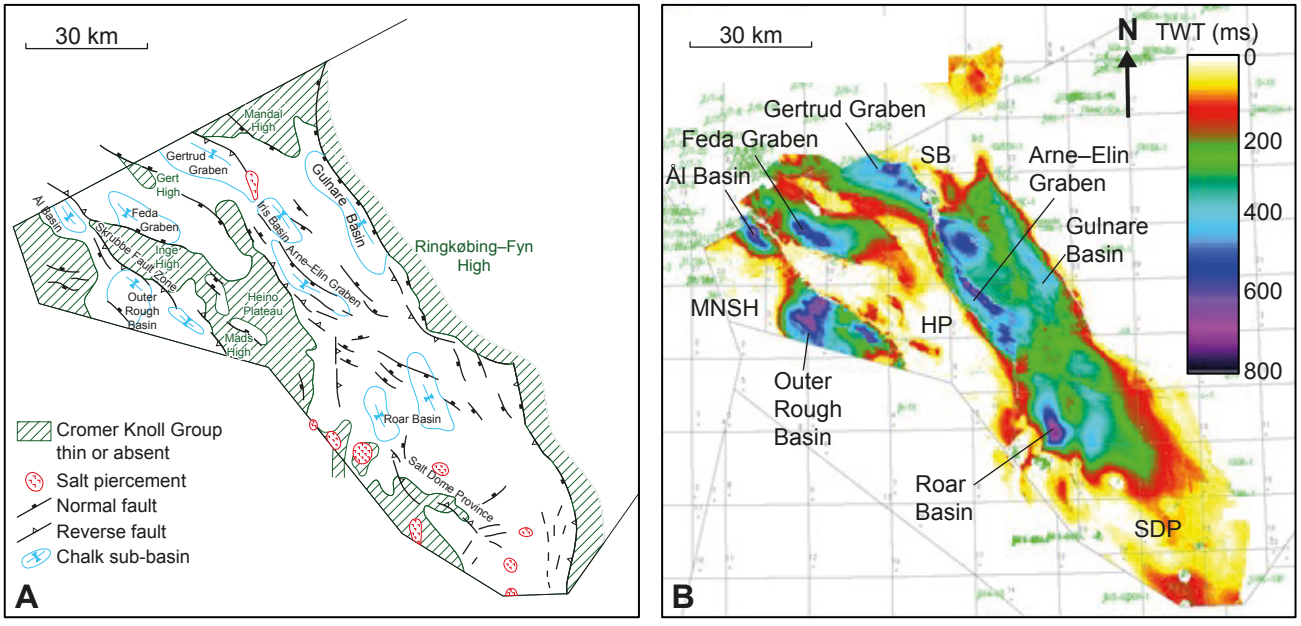


Fig. 11. (A) Lower Cretaceous structural elements with fault traces at the BCU level. Lower Cretaceous sub-basins are shown together with areas where the Cromer Knoll Group is thin or absent. Structural nomenclature partly after Britze *et al.* (1995) **(B)** Time-isochore map (TWT, ms) of the Lower Cretaceous Cromer Knoll Group. HP: Heno Plateau; MNSH: Mid North Sea High; SB, Søgne Basin; SDP: Salt Dome Province.

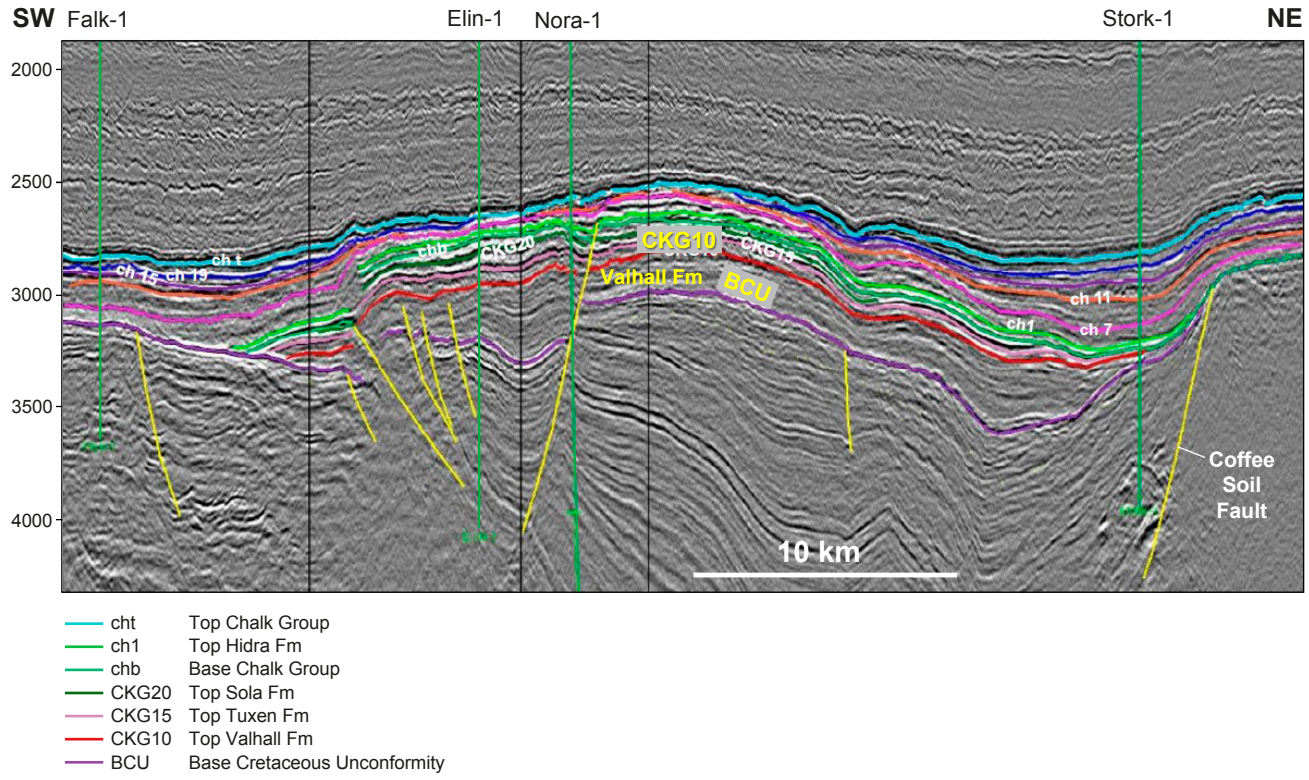


Fig. 12. SW–NE seismic structural profile across the Arne–Elin Graben and the Gulnare Basin (Early Cretaceous sub-basin of the Tail End Graben) to the east showing basal onlap of the lowermost Cretaceous Valhall Formation (seismic interval BCU–CKG10) onto the BCU. See Fig. 1 for location of seismic profile.

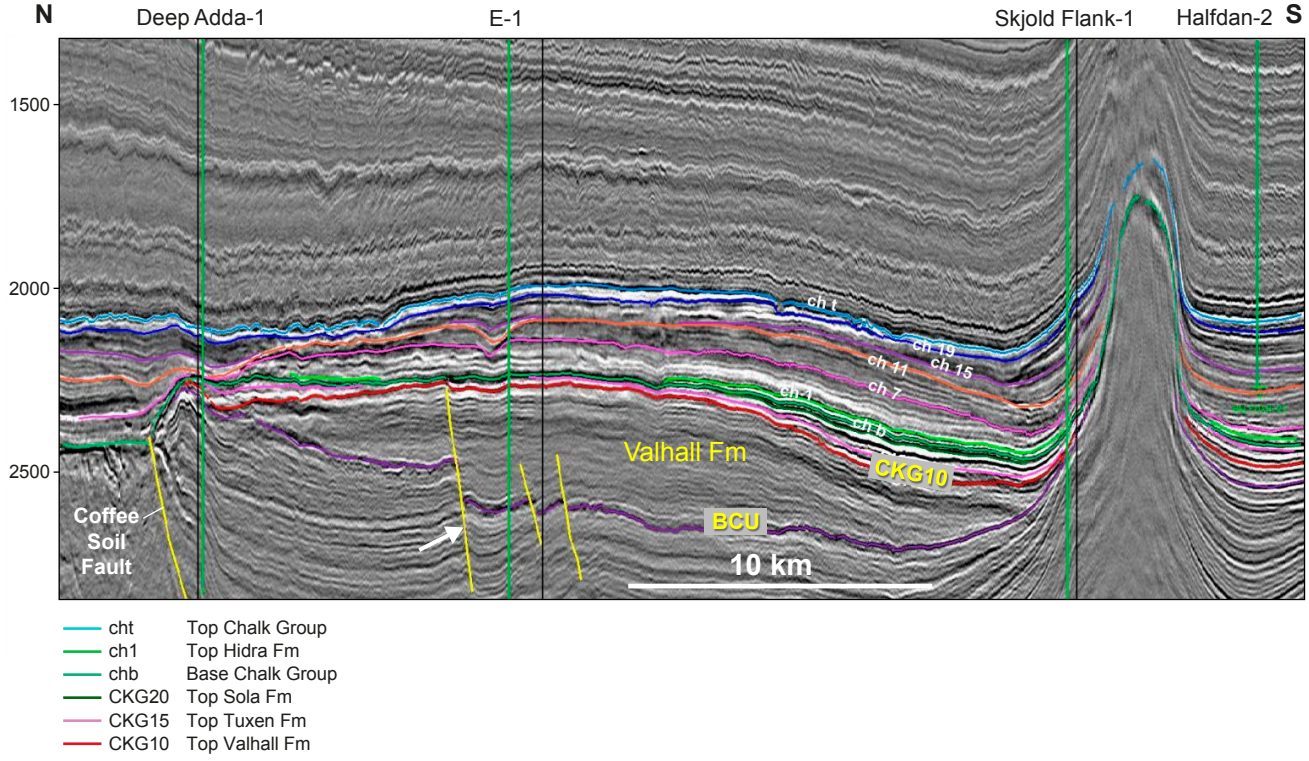


Fig. 13. N–S seismic structural profile showing faults active during the deposition of the Valhall Formation (seismic interval BCU–CKG10). An important Valanginian growth fault is arrowed. See Fig. 1 for location of seismic profile.

marine erosion accompanying this sea-level excursion.

The uppermost unit of the Cromer Knoll Group, the Rødby Formation (seismic interval CKG20 – chb; Fig. 7D), comprises a succession of marlstones and marly chalks that becomes increasingly carbonate-rich upwards, and represents a return to more open marine depositional conditions. It oversteps underlying deposits but is typically relatively thinly developed in the Danish Central Graben, often being beneath seismic resolution, though thickening to up to 60 m in local depocentres (e.g. Roar Basin, Outer Rough Basin). In such expanded sections, the fluctuating carbonate:clay content yields a distinctive log pattern that matches the 'type North Sea' development described by Crittenden *et al.* (1991) suggesting regional/global controls on facies development.

Hydrocarbon aspects

The Danish Central Graben is a mature petroleum producing basin in which the vast majority of the oil can be correlated to source rock facies of the Upper Jurassic – lowermost Cretaceous marine shales of the Farsund and Mandal Formations, i.e. Kimmeridge Clay Formation equivalents (Petersen *et al.* 2016; Petersen & Hertle 2021; Petersen & Jakobsen 2021). The source rock quality varies through space and time, but generally it increases through time and attains the best quality in the upper Volgian – Ryazanian Mandal Formation that includes the organic-rich 'hot shales' of the Bo Member (Ineson *et al.* 2003; Ponsaing *et al.* 2020a, b, 2021; Petersen & Hertle 2021; Petersen & Jakobsen 2021). Today, this upper, rich part of the source rock section is only mature in the northern part of the Danish Central Graben while the deepest buried part is gas mature to overmature. In contrast, in the southern part of the basin, the source rock section is thermally immature with regard to oil generation due to insufficient burial depth, thus suggesting a complex filling history of the chalk fields in the Salt Dome Province. The Upper Cretaceous – Danian Chalk Group contains the most successful and economically important play in the Danish Central Graben. Since the first discovery in 1966 and the initiation of production some years later, substantial amounts of hydrocarbons (oil and gas) have been produced from the Upper Cretaceous Tor and Danian Ekofisk Formations but also from the Tuxen (and Sola) Formations of the Cromer Knoll Group (e.g. Danish Energy Agency 2014). Hydrocarbon production started to decline in 2004, mainly due to gradual exhaustion of recoverable reserves in the ageing fields.

The chalk fields are mostly structural traps formed by salt halokinesis but other trapping mechanisms exist, including the inversion structures of the South Arne and Valdemar Fields and the large non-structural, stratigraphic/dynamic trap of the Halfdan Field (Albrechtsen *et al*. 2001; Megson & Tygesen 2005; Vejbæk & Rasmussen 2005; Fig. 1). The Halfdan Field illustrates the validity of more complex dynamic trapping mechanisms of hydrocarbons. In addition to the prolific chalk play, multiple sandstone plays exist in the Danish North Sea as shown by fields and discoveries in sandstone reservoirs in the Middle and Upper Jurassic (e.g. Søgne Basin fields and Hejre discovery; Petersen & Hertle 2018, 2021), Paleocene (e.g. Siri Fairway fields; Ohm *et al*. 2006) and Miocene (Lille John discovery; Danish Energy Agency 2015).

Recoverable hydrocarbons in the Lower Cretaceous Cromer Knoll Group are considered to be restricted to the chalk reservoirs of the Tuxen Formation, and locally the Sola Formation. Present production is primarily from the Valdemar Field though the Tuxen Formation reservoir is also present in the Adda discovery and across the Tyra Field (Jakobsen *et al*. 2004, 2005; Ponsaing *et al*. 2020a, b; Schovsbo *et al*. 2020; Figs 1, 8). (). Structurally trapped oil has been recorded in both the Hidra and Hod Formations in the lower part of the Chalk Group above accumulations in the Tuxen Formation (e.g. North Jens-1 well, Valdemar Field), either because the top-seal has leaked/breached or the hydrocarbons have migrated in porous layers from entry points outside the structural trap. These discoveries show that the chalk can act both as a reservoir and as a seal. The siliciclastic sediments of the Vyl Formation at the base of the Cromer Knoll Group, flanking the eastern margin of the Danish Central Graben (Fig. 2), have been the focus of some exploration interest though without success to date.

The Tuxen/Sola interval has traditionally been considered as a secondary, deeper exploration target below structural traps identified in the overlying Chalk Group. The reservoirs consist of pelagic chalk and marly chalk in the Tuxen Formation and to a lesser extent in the overlying Sola Formation. The interval is located above the rich Upper Jurassic source rocks and below the Upper Cretaceous hydrocarbon-bearing chalk reservoirs and is thus favourably positioned on the migration route via fractures and faults (Ponsaing *et al*. 2020a, b; Rudra *et al*. 2021). The highest porosity and hydrocarbon saturations in the Tuxen Formation are recorded in the central parts of the Danish Central Graben concentrated on the Bo-Jens and Adda inversion highs (Valdemar Field and Adda discovery, respectively) (Fig. 1); the northward decline in reservoir properties illustrated in Fig 14 supports the inverse relationship between chalk porosity and burial depth proposed by Jakobsen *et al.* (2005). The best reservoir properties in the Valdemar Field are obtained in chalk-dominated intervals with less than

20% clay (Jakobsen *et al*. 2004); the porosity in the chalk units is locally very high, up to 35–40% at *c*. 2500 m depth (Schovsbo *et al*. 2020; Fig. 8). The effective porosity decreases with increasing burial depth and clay content, and due to the very low permeability of the layers in the Lower Cretaceous (0.1–4 mD; Jakobsen *et al*. 2004), chalk production is challenged in some parts of the Valdemar Field where internal baffles also result in compartmentalization of the reservoir (Jakobsen *et al*. 2005; Danish Energy Agency 2014). The distribution of sub-seismic faults and natural fractures is considered an important factor in the productivity of these tight reservoirs (Glad *et al*. 2022; Lorentzen *et al*. 2022) though the difficult production conditions are mitigated by the use of horizontal wells and sand-propant fracture stimulation. Since the onset of hydrocarbon production about 50 years ago, the exploitation efficiency of such low permeability chalk reservoirs has significantly improved following the introduction in the mid-1980s of long horizontal wells and for some fields water or gas injection, which maintains the pressure and forces the oil towards the production wells. These technologies have increased the hydrocarbon recovery factor in tight chalk reservoirs from 5–10% to about 30% (Danish Energy Agency 2009).

Conclusions

The comprehensive seismic mapping program undertaken during an integrated petroleum system study incorporated all available 3D seismic data, constrained by lithostratigraphic and biostratigraphic review of 65 key boreholes. Although the lithostratigraphic framework and broad depositional evolution of the Cromer Knoll Group in the Danish Central Graben is well-established, this seismic–stratigraphic re-evaluation resulted in documentation of the regional subsidence history and depositional patterns in the Danish Central Graben at a scale previously unattained. This is especially pertinent for the mid-Cretaceous, where the Tuxen and Sola Formations command particular interest both in view of their productive chalk reservoirs and their palaeoceanographic significance as harbingers of the Chalk Sea of the Late Cretaceous (Mutterlose & Bottini 2013).

The time isochore maps illustrate the interplay between the dynamic subsidence history of the Early Cretaceous – due to inherited basin morphology, the development of new depocentres and incipient inversion uplift – and regional/global sea-level change. Significant shifts in the subsidence pattern can be

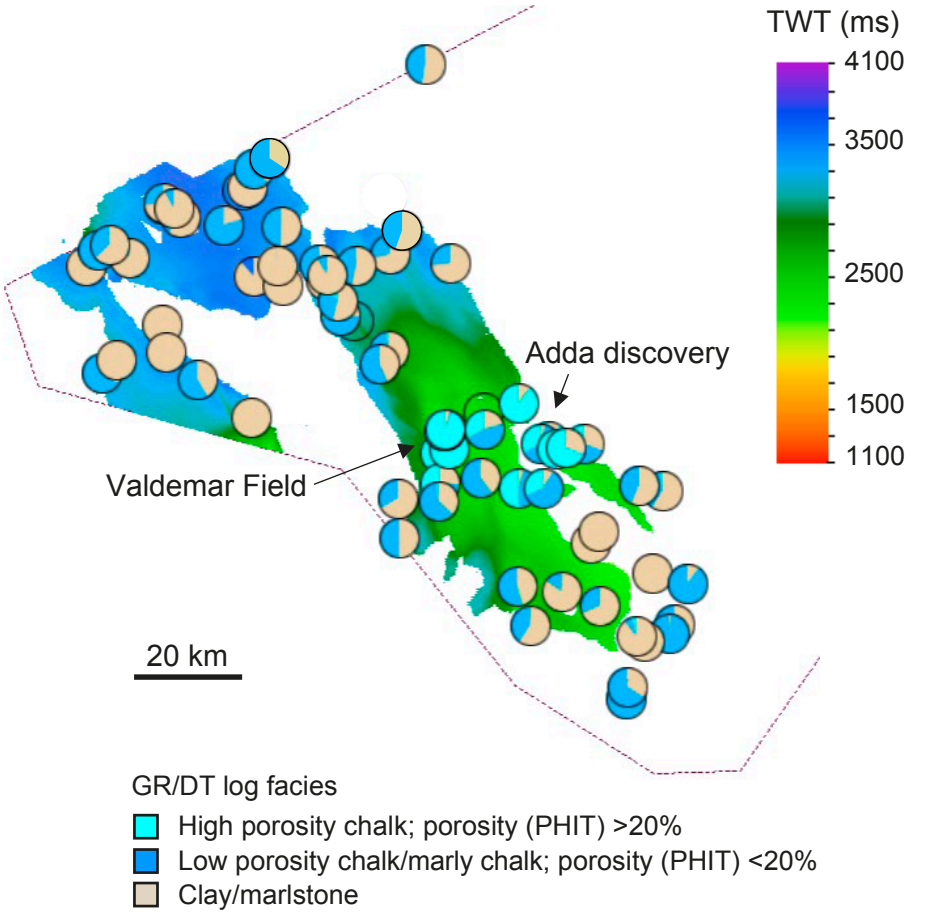


Fig. 14. Top Tuxen structure map (CKG15 reflector) overlain with pie diagrams showing the relative proportions of the main reservoir facies in the Tuxen Formation, based on semi-quantitative log evaluation (GR/DT facies, see Skaarup *et al*. 2017). The optimum chalk reservoir in the Tuxen Formation (highest porosity and net chalk) is recorded in the central parts of the Danish Central Graben concentrated on the Bo–Jens and Adda inversion ridges (Valdemar Field and Adda discovery, respectively; see Fig. 1 for location).

detected in the late Valanginian – early Hauterivian and the late Aptian – early Albian, the former due to the initiation of inversion in the east and the latter resulting from accelerating subsidence in central and western sub-basins. In concert with sea-level changes, these events influenced the facies development and gross thicknesses of the Barremian and lower Aptian chalk reservoirs.

Acknowledgements

The seismic–stratigraphic data presented here are derived from the industrial multiclient CRETSYS project conducted by GEUS; the subscribing companies (un-named for contractual reasons) are acknowledged for financial support. Jette Halskov (GEUS) is thanked for her professional graphical contribution; the 3D image in Figure 10 was produced by Christian Brogaard Pedersen (GEUS). We thank Thomas Blume and colleagues for assistance and hospitality at the Total Core Laboratory in Copenhagen, and we are grateful to Ole Vejbæk, an anonymous referee and the editor for their constructive critiques which significantly strengthened the paper. The paper is published with the permission of the Geological Survey of Denmark and Greenland (GEUS).

References

Ainsworth, N.R., Riley, L.A. & Gallagher L.T. 2000: An Early Cretaceous lithostratigraphic and biostratigraphic framework for the Britannia Field reservoir (Late Barremian – Late Aptian), UK North Sea. Petroleum Geoscience 6, 345–367. https://doi.org/10.1144/petgeo.6.4.345

Albrechtsen, T., Andersen, S.J., Dons, T., Engstrøm, F., Jørgensen, O. & Sørensen, F.W. 2001: Halfdan: Developing non-structural trapped oil in North Sea Chalk. SPE 71322, Society of Petroleum Engineers. https://doi.org/10.2118/71322-ms

Andsbjerg, J. 2003: Sedimentology and sequence stratigraphy of the Bryne and Lulu Formations, Middle Jurassic, northern Danish Central Graben. In: Ineson, J.R. & Surlyk, F. (eds): The Jurassic of Denmark and Greenland. Geological Survey of Denmark and Greenland Bulletin 1, 301–347. https://doi.org/10.34194/geusb.v1.4676

Andsbjerg, J. & Dybkjær, K. 2003: Sequence stratigraphy of the Jurassic of the Danish Central Graben. In: Ineson, J.R. & Surlyk, F. (eds): The Jurassic of Denmark and Greenland. Geological Survey of Denmark and Greenland Bulletin 1, 265–300. https://doi.org/10.34194/geusb.v1.4675

Blok, C.N., Ineson, J., Anderskouv, K., Fantasia, A., Sheldon, E., Thiabault, N., Jelby, M.E., Adatte, T. & Bodin, S. 2022: Latitude-dependant climate changes across the Aptian Oceanic Anoxic Event 1a. Palaeogeography, Palaeoclimatology, Palaeoecology 601, 111085. https://doi.org/10.1016/j.palaeo.2022.111085

Britze, P., Japsen, P. & Andersen, C., 1995: Geological map of Denmark. 1: 200,000: The Danish Central Graben. 'Base Cretaceous' and the Cromer Knoll Group (two-way-traveltime and depth, thickness and interval velocity). Danmarks Geologiske Undersøgelse Map Series 49, 7 pp. and 4 maps. https://doi.org/10.34194/geusb.v1.4653

Copestake, P., Sims, A.P., Crittenden, S., Hamar, G.P., Ineson, J.R., Rose, P.T. & Tringham, M.E. 2003: Lower Cretaceous. In: Evans, D. *et al*. (eds): The Millennium Atlas: petroleum geology of the central and northern North Sea, 191–211. London: Geological Society of London.

Crittenden, S., Cole, J.M. & Harlow, C. 1991: The Early to 'Middle' Cretaceous lithostratigraphy of the Central North Sea (UK sector). Journal of Petroleum Geology 14, 387–416. https://doi.org/10.1111/j.1747-5457.1991.tb00328.x

Danish Energy Agency 2009: Denmark's oil and gas production 08, 128 pp. Copenhagen: Danish Energy Agency.

Danish Energy Agency 2014: Oil and gas production in Denmark 2013, 106 pp. Copenhagen: Danish Energy Agency.

Danish Energy Agency 2015. Lille John-2 appraisal well encounters oil in the Danish North Sea. Danish Energy Agency press release February 10th, 2015.

Deegan, C.E & Scull, B.J. 1977: A standard lithostratigraphic nomenclature for the Central and Northern North Sea. Report Institute Geological Sciences 77/25, 36 pp.

Dybkjær, K. & Jutson D. 2003: Composite biostratigraphy of the Hauterivian–Ryazanian interval in the Iris-1 (5604/30b1) well, Danish Sector, North Sea. Courier Forschungsinstitut Senckenberg 244, 1–10.

Gale, A.S., Mutterlose, J. & Batenburg, S. 2020: The Cretaceous Period. In: Gradstein, F.M., Ogg, J.G. & Ogg, G.M. (eds): Geologic Time Scale 2020, 1023–1086. Amsterdam: Elsevier B.V. https://doi.org/10.1016/B978-0-12-824360-2.00027-9

Gradstein, F.M., Waters, C.N., Charnock, M., Munsterman, D., Hollerbach, M., Brunstad, H., Hammer, Ø. & Vergara, L. 2016: Stratigraphic guide to the Cromer Knoll, Shetland and Chalk Groups, North Sea and Norwegian Sea. Newsletters on Stratigraphy 49 (Supplement), 71–280. https://doi.org/10.1127/nos/2016/0071

Hansen, T.H., Clausen, O.R. & Andresen, K.J. 2021: Thick- and thin-skinned basin inversion in the Danish Cnetral Graben, North Sea – the role of deep evaporites and basement kinematics. Solid Earth 12, 1719–1747. https://doi.org/10.5194/se-12-1719-2021

Heilmann-Clausen, C. 1987: Lower Cretaceous dinoflagellate in the Danish Central Trough. Danmarks Geologiske Undersøgelse, Serie A, 12, 89 pp. https://doi.org/10.34194/seriea.v17.7036

Hemmet, M. 2005: The hydrocarbon potential of the Danish Continental Shelf. In: Doré, A.G. & Vining, B.A. (eds): Petroleum geology: North-West Europe and global per-

spectives – Proceedings of the 6th Petroleum Geology Conference, 85–97. London: Geological Society. https://doi.org/10.1144/0060085

Ineson, J.R. 1993: The Lower Cretaceous chalk play in the Danish Central Trough. In: Parker, J.R. (ed.): Petroleum geology of Northwest Europe: Proceedings of 4th Conference, 175–183. London: Geological Society. https://doi.org/10.1144/0040175

Ineson, J.R., Bojesen-Koefoed, J.A., Dybkjær, K. & Nielsen, L.H. 2003: Volgian–Ryazanian 'hot shales' of the Bo Member (Farsund Formation) in the Danish Central Graben, North Sea: stratigraphy, facies and geochemistry. In: Ineson, J.R. & Surlyk, F. (eds): The Jurassic of Denmark and Greenland. Geological Survey of Denmark and Greenland Bulletin 1, 403–436. https://doi.org/10.34194/geusb.v1.4679

Ineson, J.R., Sheldon, E., Dybkjær, K., Andersen, C., Alsen, P. & Jakobsen, F. 2022a: The 'Base Cretaceous Unconformity' in a basin-centre setting, Danish Central Graben, North Sea: A cored record of resedimentation and condensation accompanying transgression and basinal overturn. Marine and Petroleum Geology 137, 105489. https://doi.org/10.1016/j.marpetgeo.2021.105489

Ineson, J.R., Lauridsen, B.W., Lode, S., Sheldon, E., Sørensen, H.O., Wisshak, M. & Anderskouv, K. 2022b: A condensed chalk–marl succession on an Early Cretaceous structural high, Danish Central Graben: Implications for the sequence stratigraphic interpretation of the Munk Marl Bed. Sedimentary Geology 440 (in press). https://doi.org/10.1016/j.sedgeo.2022.106234

Isaksen, D. & Tonstad, K. 1989: A revised Cretaceous and Tertiary lithostratigraphic nomenclature for the Norwegian North Sea. Norwegian Petroleum Directorate Bulletin 5, 55 pp.

Jakobsen, F., Ineson, J.R., Kristensen, L. & Stemmerik, L. 2004: Characterization and zonation of a marly chalk reservoir: The Lower Cretaceous Valdemar Field of the Danish Central Graben. Petroleum Geoscience 10, 21–33. https://doi.org/10.1144/1354-079303-584

Jakobsen, F., Ineson, J.R., Kristensen, L., Nytoft, H.P. & Stemmerik, L. 2005: The Valdemar Field, Danish Central Graben: field compartmentalization and regional prospectivity of the Lower Cretaceous chalk play. In: Doré, A.G. & Vining, B.A. (eds): Petroleum geology: North-West Europe and global perspectives – Proceedings of the 6th Petroleum Geology Conference, 177–186. London: Geological Society. https://doi.org/10.1144/0060177

Japsen, P., Britze, P. & Andersen, C. 2003: Upper Jurassic – Lower Cretaceous of the Danish Central Graben: structural framework and nomenclature. In: Ineson, J.R. & Surlyk, F. (eds): The Jurassic of Denmark and Greenland. Geological Survey of Denmark and Greenland Bulletin 1, 233–246. https://doi.org/10.34194/geusb.v1.4653

Jelby, M.E., Ineson, J.R., Thibault, N., Bodin, S., Blok, C., Edvardsen, N., Clemmensen, T.S., Buls, T. & Anderskouv, K. 2022: Facies and depositional processes of Lower Cretaceous carbonates, Danish Central Graben. Bulletin of the Geological Society of Denmark 71, 51–74. https://doi.org/10.37570/bgsd-2022-71-04

Jensen, T.F. & Buchardt, B. 1987: Sedimentology and geochemistry of the organic-rich Lower Cretaceous Sola Formation (Barremian-Albian), Danish Central Trough. In: Brooks, J. & Glennie, K. (eds): Petroleum geology of North West Europe, 431–440. London: Graham & Trotman.

Jensen, T.F., Holm, L., Frandsen, N. & Michelsen, O. 1986: Jurassic – Lower Cretaceous lithostratigraphic nomenclature for the Danish Central Trough. Danmarks og Grønlands Geologiske Undersøgelse Serie A 12, 65 pp. https://doi.org/10.34194/seriea.v12.7031

Jensen, T.F., Holm, L., Frandsen, N. & Michelsen, O. 1986: Jurassic – Lower Cretaceous lithostratigraphic nomenclature for the Danish Central Trough. Danmarks Geologiske Undersøgelse Serie A 12, 65 pp. https://doi.org/10.34194/seriea.v12.7031

Jeremiah, J. 2001: A Lower Cretaceous nannofossil zonation for the North Sea Basin. Journal of Micropalaeontology 20, 45–80. https://doi.org/10.1144/jm.20.1.45

Johannessen, P.N. 2003: Sedimentology and sequence stratigraphy of paralic and shallow marine Upper Jurassic sandstones in the northern Danish Central Graben. In: Ineson, J.R. & Surlyk, F. (eds): The Jurassic of Denmark and Greenland. Geological Survey of Denmark and Greenland Bulletin 1, 367–402. https://doi.org/10.34194/geusb.v1.4678

Johannessen, P.N., Dybkjær, K., Andersen, C., Kristensen, L., Hovikoski, J. & Vosgerau, H. 2010: Upper Jurassic reservoir sandstones in the Danish Central Graben: new insights on distribution and depositional environments. In: Vining, B.A. & Pickering, S.C. (eds): Petroleum geology: from mature basins to new frontiers – Proceedings of the 7th Petroleum Geology Conference, 127–143. London: Geological Society. https://doi.org/10.1144/0070127

Jutson, D.J. 1997: Nannofloral analysis of the Lower Cretaceous of the Deep Adda-1 well. Danmarks og Grønlands Geologiske Undersøgelse Rapport 1997/99, 9 pp, 3 enclosures, 1 appendix.

Kyrkjebø, R., Gabrielsen, R.H. & Faleide, J.I. 2004: Unconformities related to the Jurassic-Cretaceous synrift – postrift transition of the northern North Sea. Journal of the Geological Society London 161, 1–17. https://doi.org/10.1144/0016-764903-051

Lorentzen, M.C.L., Bredesen, K., Smit, F.W.H., Hansen, T.H., Nielsen, L. & Mosegaard, K. 2022: Mapping Cretaceous faults using a convolutional neural network – A field example from the Danish North Sea. Bulletin of the Geological Society of Denmark 71, 31–50. https://doi.org/10.37570/bgsd-2022-71-03

Megson, J. & Tygesen, T. 2005: The North Sea Chalk: an underexplored and underdeveloped play. In: Doré, A.G. & Vining, B.A. (eds): Petroleum geology: North-West Europe and global perspectives – Proceedings of the 6th Petroleum Geology Conference, 159–168. London: Geological Society. https://doi.org/10.1144/0060159

Michelsen, O., Nielsen, L.H., Johannessen, P.N., Andsbjerg, J. &

Surlyk, F. 2003: Jurassic lithostratigraphy and stratigraphic development onshore and offshore Denmark. In: Ineson, J.R. & Surlyk, F. (eds): The Jurassic of Denmark and Greenland. Geological Survey of Denmark and Greenland Bulletin 1, 147–216. https://doi.org/10.34194/geusb.v1.4651

Mutterlose, J. & Bottini, C. 2013: Early Cretaceous chalks from the North Sea giving evidence for global change. Nature Communications 4:1686, 6 pp. https://doi.org/10.1038/ncomms2698

Møller, J.J. 1986: Seismic structural mapping of the Middle and Upper Jurassic in the Danish Central Trough. Danmarks Geologiske Undersøgelse Serie A 13, 37 pp. https://doi.org/10.34194/seriea.v13.7032

Møller, J.J. & Rasmussen, E.S. 2003: Middle Jurassic – Early Cretaceous rifting of the Danish Central Graben. In: Ineson, J.R. & Surlyk, F. (eds): The Jurassic of Denmark and Greenland. Geological Survey of Denmark and Greenland Bulletin 1, 247–264. https://doi.org/10.34194/geusb.v1.4654

Nielsen, L.H. & Japsen, P. 1991: Deep wells in Denmark 1935 – 1990. Lithostratigraphic subdivision. Danmarks Geologiske Undersøgelse Serie A, 177 pp. https://doi.org/10.34194/seriea.v31.7051

Nielsen, M.T., Weibel, R. & Friis, H. 2015: Provenance of gravity-flow sandstones from the Upper Jurassic – Lower Cretaceous Farsund Formation, Danish Central Graben. Marine and Petroleum Geology 59, 371–389. http://dx.doi.org/10.1016/j.marpetgeo.2014.09.016

Ogg, J.G. & Hinnov, L.A. 2012: Cretaceous. In: Gradstein, F.M. et al. (eds): The Geologic Time Scale 2012, 793–853. Amsterdam: Elsevier B.V. https://doi.org/10.1016/b978-0-444-59425-9.00027-5

Ohm, S.E., Karlsen, D.A., Roberts, A., Johannessen, E. & Høiland, O. 2006: The Paleocene sandy Siri Fairway: an efficient "pipeline" draining the prolific Central Graben? Journal of Petroleum Geology 29, 53–82.

Petersen, H.I. & Hertle, M. 2018: A review of the coaly source rocks and generated petroleums in the Danish North Sea: an underexplored Middle Jurassic petroleum system? Journal of Petroleum Geology 41, 135–154. https://doi.org/10.1111/jpg.12697

Petersen, H.I. & Hertle, M. 2021: Temporal and spatial distribution of original source rock potential in Upper Jurassic – lowermost Cretaceous marine shales, Danish Central Graben, North Sea. Journal of Petroleum Geology 44, 5–24. https://doi.org/10.1111/jpg.12776

Petersen, H.I., Hertle, M., Juhasz, A. & Krabbe, H. 2016: Oil family typing, biodegradation and source rock affinity of liquid petroleum in the Danish North Sea. Journal of Petroleum Geology 39, 247–268. https://doi.org/10.1111/jpg.12645

Petersen, H.I. & Jakobsen, F.C. 2021: Lithostratigraphic definition of the Upper Jurassic – lowermost Cretaceous (Upper Volgian – Ryazanian) organic-rich and oil-prone Mandal Formation in the Danish Central Graben, North Sea. Marine and Petroleum Geology 129, https://doi.org/10.1016/j.marpetgeo.2021.105116

Ponsaing, L., Petersen, H.I., Bojesen-Koefoed, J.A., Nytoft, H.P., Schovsbo, N.H. & Stemmerik, L. 2020a: Source rock quality variations of Upper Jurassic – lowermost Cretaceous marine shales and their relationship to oils in the Valdemar Field, Danish North Sea. Journal of Petroleum Geology 43, 49–74. https://doi.org/10.1111/jpg.12749

Ponsaing, L., Mathiesen, A., Petersen, H.I., Bojesen-Koefoed, J.A., Schovsbo, N.H., Nytoft, H.P. and Stemmerik, L. 2020b: Organofacies composition of Upper Jurassic – lowermost Cretaceous source rocks, Danish Central Graben, and insight into the correlation to oils in the Valdemar Field. Marine and Petroleum Geology 114. https://doi.org/10.1016/j.marpetgeo.2020.104239

Rawson, P.F. & Riley, L.A. 1982: Latest Jurassic – Early Cretaceous events and the 'Late Cimmerian Unconformity' in the North Sea area. American Association of Petroleum Geologists Bulletin 66, 2628–2648. https://doi.org/10.1306/03b5ac87-16d1-11d7-8645000102c1865d

Riley, L.A., Harker, S.D. & Green, S.C.H. 1992: Lower Cretaceous palynology and sandstone distribution in the Scapa Field, U.K. North Sea. Journal of Petroleum Geology 15, 97–110. https://doi.org/10.1111/j.1747-5457.1992.tb00868.x

Rudra, A., Sanei, H., Nytoft, H.P., Petersen, H.I., Blok, C., Bodin, S. & Bojesen-Koefoed, J.A. 2021: Organic matter characterization of the Lower Cretaceous tight reservoirs in the Danish North Sea. International Journal of Coal Geology 238. https://doi.org/10.1016/j.coal.2021.103714

Schovsbo, N.H., Jacobsen, F., Britze, P., 2020. Hydrocarbon play maps in the Danish Central Graben. Danmarks og Grønlands Geologiske Undersøgelse Rapport 2020/49, 30 pp.

Skaarup, N., Andersen, C., Bjerager, M., Dybkjær, K., Heijboer, T., Ineson, J.R., Jakobsen, F., Knudsen, H., Kristensen, L., Larsen, U., Lauridsen, L.P., Mathiesen, A., Nielsen, C.M., Mørk, F.M., Nytoft, H.P., Pedersen, C.B., Rasmussen, R., Schovsbo, N.H., Sheldon, E., Thomsen, E. & Esbensen, K.H. 2017: The Cretaceous Petroleum System in the Danish Central Graben (CRETSYS). Technical notes. Danmarks og Grønlands Geologiske Undersøgelse Rapport 2017/32, 203 pp. and Appendix.

Surlyk, F., Dons, T., Clausen, C.K. & Highham, J. 2003: The Upper Cretaceous. In: Evans, D. *et al*. (eds): The Millennium Atlas, petroleum geology of the central and northern North Sea, 213–233. London: Geological Society.

Thomsen, E. 1987: Lower Cretaceous calcareous nannofossil biostratigraphy in the Danish Central Trough, Danmarks Geologiske Undersøgelse, Serie A, 12, 89 pp. https://doi.org/10.34194/seriea.v20.7039

Thomsen, E. 1989a: Seasonal variability in the production of Lower Cretaceous calcareous nannoplankton. Geology 17, 715–717. https://doi.org/10.1130/0091-7613(1989)017<0715:SVITPO>2.3.CO;2

Thomsen, E. 1989b: Seasonal variation in Boreal Early Cretaceous calcareous nannofossils. Marine Micropaleontology 15, 123-152. https://doi.org/10.1016/0377-8398(89)90008-X

van Buchem, F.S.P., Smit, F.W.H., Buijs, G.J.A., Trudgill, B. & Larsen, P.-H., 2018: Tectonostratigraphic framework and depositional history of the Cretaceous–Danian succession of the Danish Central Graben (North Sea) – new light on a mature area. In: Bowman, M. & Levell, B. (eds): Petroleum Geology of NW Europe: 50 Years of Learning – Proceedings of the 8th Petroleum Geology Conference, 9–46. London: Geological Society. http://dx.doi.org/10.1144/PGC8.24

Vejbæk, O.V. 1986: Seismic stratigraphy and tectonic evolution of the Lower Cretaceous in the Danish Central Trough. Danmarks Geologiske Undersøgelse Serie A 11, 46 pp. https://doi.org/10.34194/seriea.v11.7030

Vejbæk, O.V. & Andersen, C. 2002: Post mid-Cretaceous tectonics in the Danish Central Graben – regionally synchronous tectonic events? Bulletin of the Geological Society of Denmark 49, 129–144. https://doi.org/10.37570/bgsd-2003-49-11

Vejbæk, O.V. & Rasmussen, R. 2005: Forward modelling of seismic response from North Sea Chalk. Geological Survey of Denmark and Greenland Bulletin 7, 17–20. https://doi.org/10.34194/geusb.v7.4824

Verreussel, R.M.C.H., Bouroullec, R., Munsterman, D.K., Dybkjær, K., Geel, C.R., Houben, A.J.P., Johannessen, P.N. & Kerstholt-Boegehold, S.J. 2018: Stepwise basin evolution of the Middle Jurassic – Early Cretaceous rift phase in the Central Graben area of Denmark, Germany and The Netherlands. Geological Society Special Publications (London) 469, 305–340. https://doi.org/10.1144/SP469.23

Vidalie, M., van Buchem, F., Schmidt, I. & Uldall, A. 2014: Seismic stratigraphy of the Lower Cretaceous Valhall Formation (Danish Graben, North Sea). First Break 32, 71–80. https://doi.org/10.3997/1365-2397.2014008

Clay mineral assemblages as a tool in source-to-sink studies: an example from the Lower Cretaceous of the North Sea Basin

CARLETTE N. BLOK, THIERRY ADATTE, JON R. INESON, EMMA SHELDON, MADS E. JELBY, FLORIAN W.H. SMIT, BODIL W. LAURIDSEN, KRESTEN ANDERSKOUV & STÉPHANE BODIN

Geological Society of Denmark
https://2dgf.dk

Received 29 May 2023
Accepted in revised form
26 September 2023
Published online
13 Oktober 2023

© 2023 the authors. Re-use of material is permitted, provided this work is cited. Creative Commons License CC BY: https://creativecommons.org/licenses/by/4.0/

Blok, C.N., Adatte, T., Ineson, J.R., Sheldon, E., Jelby, M.E., Smit, F.W.H., Lauridsen, B.W., Anderskouv, K. & Bodin, S. 2023. Clay mineral assemblages as a tool in source-to-sink studies: an example from the Lower Cretaceous of the North Sea Basin. Bulletin of the Geological Society of Denmark, Vol. 71, pp. 99–113. ISSN 2245-7070. https://doi.org/10.37570/bgsd-2023-71-06

The alternating marlstone and chalk of the Lower Cretaceous succession in the Danish Central Graben (DCG) are important for the understanding of the evolution of the larger North Sea Basin. This study focusses on the clay mineral assemblages of the upper Hauterivian – lower Aptian in the DCG and Danish Basin (DB) and their implications. Clay mineral assemblages are predominantly used to assess palaeoclimate. In this study, however, they were additionally used in a source-to-sink context. Kaolinite was found to form a dominant component of the clay mineral assemblage in the sampled wells of the DCG and in the DB, suggesting that a feldspar- or kaolinite-rich source was present and actively eroded in the region during the Early Cretaceous. Moreover, a decreasing gradient west to east of average kaolinite content is observed in the three studied wells for the early Hauterivian to late Barremian (BC9-BC17), with the highest content observed in the North Jens-1 well (av. 74%), followed by the Boje-2C well (av. 49%) and lastly in the Vinding-1 well (av. 39%). Due to the relatively rapid settling of kaolinite in marine environments compared to other clay minerals, this gradient suggests that the main clay mineral source was located in the south-western part of the DCG. Isochore maps, a new palaeogeographic map of the DCG and the western part of the German sector of the North Sea illustrates where Lower Cretaceous rocks are absent in this region, due to either erosion or non-deposition. Potential subaerially exposed highs included the distant Baltic Shield to the north, the Ringkøbing–Fyn High to the east and the Heno Plateau within the DCG, with the latter being located closest to the North Jens-1 well and containing feldspar-rich sandstones of the Heno Formation (upper Kimmeridgian – lowermost Volgian/Tithonian). During the Early Cretaceous, part of the Heno Formation was potentially subaerially exposed or subject to wave reworking/erosion in parts of the Danish and German sectors. The sandstones could weather into kaolinite and this structural high is therefore suggested to have been the main source area for this part of the DCG, with minor sediment influxes from the Ringkøbing–Fyn High and Baltic Shield. In addition, the overall decrease in kaolinite in the DCG from the late Hauterivian to the late Barremian indicates a climatic change towards drier conditions, with some minor, slightly more humid periods.

Keywords: Barremian, Danish Central Graben, Heno Plateau, kaolinite, source-to-sink, Tuxen Formation.

Carlette N. Blok [carletteb@unis.no], Department of Arctic Geology, The University Centre in Svalbard, P.O. Box 156, N-9171 Longyearbyen, Norway. Thierry Adatte [thierry.adatte@unil.ch], Institute of Earth Sciences (ISTE), University of Lausanne, 1015 Lausanne, Switzerland. Jon R. Ineson [ji@geus.dk], Emma Sheldon [es@geus.dk], Florian W.H. Smit [fs@geus.dk], Bodil W. Lauridsen [bwl@geus.dk], Geological Survey of Denmark and Greenland, Øster Voldgade 10, DK-1350 Copenhagen K, Denmark. Mads E. Jelby [mads.e.jelby@uib.no], Department of Earth Science, University of Bergen, Allégaten 41, P.O. Box 7803, N-5020 Bergen, Norway. Kresten Anderskouv [ka@ign.ku.dk], Department of Geosciences and Natural Resource Management, University of Copenhagen, Øster Voldgade 10, DK-1350 Copenhagen K, Denmark. Stéphane Bodin [stephane.bodin@geo.au.dk], Department of Geoscience, Aarhus University, Høegh-Guldbergs Gade 2, 8000 Aarhus C, Denmark.

The Lower Cretaceous succession in the Danish Central Graben (DCG) has been studied to better understand the tectonic (Vejbæk 1986; Japsen *et al.* 2003; van Buchem *et al.* 2017), palaeoecological (Jeremiah 2001; Mutterlose & Bottini 2013), palaeoceanographic (Mutterlose & Böckel 1998) and palaeoclimatic (Chenot *et al.* 2018; Blok *et al.* 2022) basin evolution. The succession is characterised by alternating marlstone and chalk, composed of pelagic calcareous nannofossils, micritic grains and hemipelagic detrital material (Ineson 1993). A systematic study of the carbonate facies has recently been conducted (Jelby *et al.* 2022). However, the exact geographic origin of the detrital material, specifically of the clay minerals that were transported into the DCG, remains largely unknown.

New high-resolution clay mineral data are presented here from the offshore Boje-2C well (DCG) and the onshore Vinding-1 well (Danish Basin; DB). Generally, clay mineral assemblages are used to interpret palaeoclimate, as the type of clay minerals formed in soils is influenced by climate. Illite, for example, is prone to form in dry conditions, whereas kaolinite normally forms in humid conditions (Singer 1984; Chamley 1989; Ruffell *et al.* 2002). In this study, however, the notably large amount of kaolinite permits these data to, in addition, be utilised as a tool in a source-to-sink analysis. An Early Cretaceous palaeogeographic map is presented, showing Lower Cretaceous successions in the basins and absent intervals in surrounding areas (Figs 1, 7). In several areas, Lower Cretaceous strata were very thin or absent and those areas were likely subject to erosion and/or non-deposition (Jensen *et al.* 1986; Vejbæk 1986; Vejbæk & Andersen 2002; Japsen *et al.* 2003). These areas are evaluated on their location and lithological properties, as they could qualify as source areas for the basins. If these structural highs contain sandstones with diagenetic kaolinite or are rich in feldspars, kaolinite would potentially have washed out into the basin (Exley 1976; Chamley 1989; Lanson *et al.* 2002). The gradual differences between amounts of kaolinite in the two newly studied wells and the North Jens-1 well (Blok *et al.* 2022) are used to determine the main source area.

The aim of this study is to evaluate potential source areas for detrital material and the transport directions into the DCG. Structural highs that have previously been proposed as potential source areas for the DCG are the Baltic Shield (Olivarius *et al.* 2015), the Ringkøbing–Fyn High High (Mørk *et al.* 2003; Olivarius *et al.* 2015) and the Heno Plateau (Weibel *et al.* 2020). The presented study provides a better spatial constraint on the Early Cretaceous palaeogeographic evolution of the DCG and DB.

Basin configuration and lithostratigraphy

The Danish Central Graben (DCG)

The Boje-2C and North Jens-1 wells are located in the DCG, in the western part of the Danish North Sea, which is part of the North Sea rift system that extends from offshore Norway and UK, southwards towards the Dutch offshore area (Fig. 1). Intense Jurassic rifting, with NNW–SSE-orientated faulting, was initiated during the Bajocian and continued into the Volgian (Tithonian) creating a system of half-grabens (Vejbæk 1986; Johannessen & Andsbjerg 1993; Johannessen 2003; Michelsen *et al.* 2003). Syn-rift subsidence first resulted in the deposition of middle Jurassic fluviodeltaic sediments (Andsbjerg & Dybkjær 2003). As the subsidence rates increased during the late Kimmeridgian, and more accommodation space was created, the DCG was filled with the organic-rich marine mudstones of the Lola and Farsund Formations (Ponsaing *et al.* 2020). However, subsidence was less pronounced on the complexly faulted Heno Plateau, especially in the north shallow-marine sandstones might indicate that the water depths were shallower than in the rest

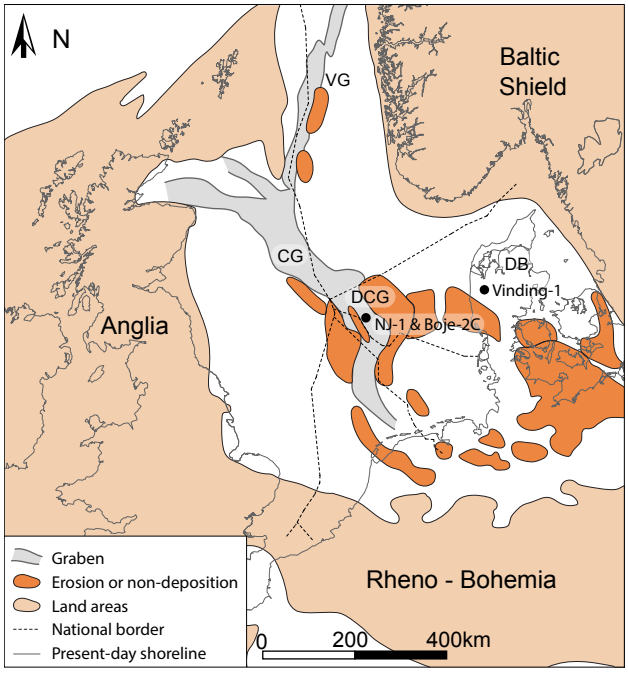


Fig. 1. Early Cretaceous palaeogeographic map based on Copestake *et al.* (2003), Mutterlose and Böckel (1998) and Lauridsen *et al.* (2022). The studied wells marked are areas of erosion or non-deposition during the Early Cretaceous are marked with a dark orange colour. NJ-1 = North Jens-1, VG = Viking Graben, CG = Central Graben, DCG = Danish Central Graben, DB = Danish Basin.

of the basin (Johannessen & Andsbjerg 1993; Johannessen 2003). In the late Volgian – early Ryazanian (late Tithonian – early Berriasian), turbidites of the Poul Formation and organic-rich mudstone of the Bo Member in the Farsund Formation were deposited (Jensen *et al.* 1986; Ineson *et al.* 2003; Ponsaing *et al.* 2020).

Cessation of rifting in the Ryazanian (Berriasian) led to the onset of thermal subsidence and the inherited Jurassic rift topography was filled with the Lower Cretaceous Cromer Knoll Group (Jensen *et al.* 1986; van Buchem *et al.* 2017). It consists of the Vyl, Valhall (including the Leek Member), Tuxen, Sola and Rødby Formations, with its lower boundary commonly referred to as the Base Cretaceous Unconformity (BCU; Fig. 2; Jensen *et al.* 1986; Kyrkjebø *et al.* 2004; van Buchem *et al.* 2017). The argillaceous Valhall Formation of Valanginian – Hauterivian age locally has a base of sands referred to as the Vyl Formation (Jensen *et al.* 1986; Ineson 1993; Vidalie *et al.* 2014). The Valhall Formation is overlain by alternating chalks and marlstones of the Tuxen, Sola and Rødby Formations (Ineson 1993). Deposition was influenced by phases of basin inversion beginning in the Hauterivian and peaking in the Late Cretaceous (Vejbæk 1986; Vejbæk & Andersen 1987, 2002; van Buchem *et al.* 2017). A period of reduced water circulation during the Barremian created anoxic conditions at the sea floor, resulting in preservation of organic matter and deposition of the Munk Marl Bed (Tuxen Formation; Thomsen 1989; Rudra *et al.* 2021). The Sola Formation includes the organic-rich Fischschiefer Member, which was deposited during the well-documented early Aptian Oceanic Anoxic Event 1a (OAE-1a; Arthur *et al.* 1990; Jenkyns 2010; Kuhnt *et al.* 2011; Föllmi 2012). A detailed study of late Hauterivian – early Aptian palaeoclimatic changes in the Boreal Realm, shows a long-term change from humid to more arid conditions for the late Hauterivian – late Barremian interval (Blok *et al.* 2022).

The Cromer Knoll Group has a maximum thickness of approximately 750 m in the DCG, but is absent in other parts of the basin (Vejbæk 1986; van Buchem *et al.* 2017). Compared to the homogeneous chalks of the Upper Cretaceous Chalk Group (Hardman 1982; Surlyk *et al.* 2003), the Lower Cretaceous is more argillaceous and organic-rich (Jensen & Buchardt 1987; Copestake *et al.* 2003). This paper is focussed on the uppermost Valhall Formation, the Tuxen Formation, including the Munk Marl Bed and the lower Sola Formation including the Fischschiefer Member (Fig. 2).

The Danish Basin (DB)

The present-day position of the Vinding-1 well, onshore Denmark, corresponded to a shallow shelf area of the DB during the Early Cretaceous (Fig. 1;

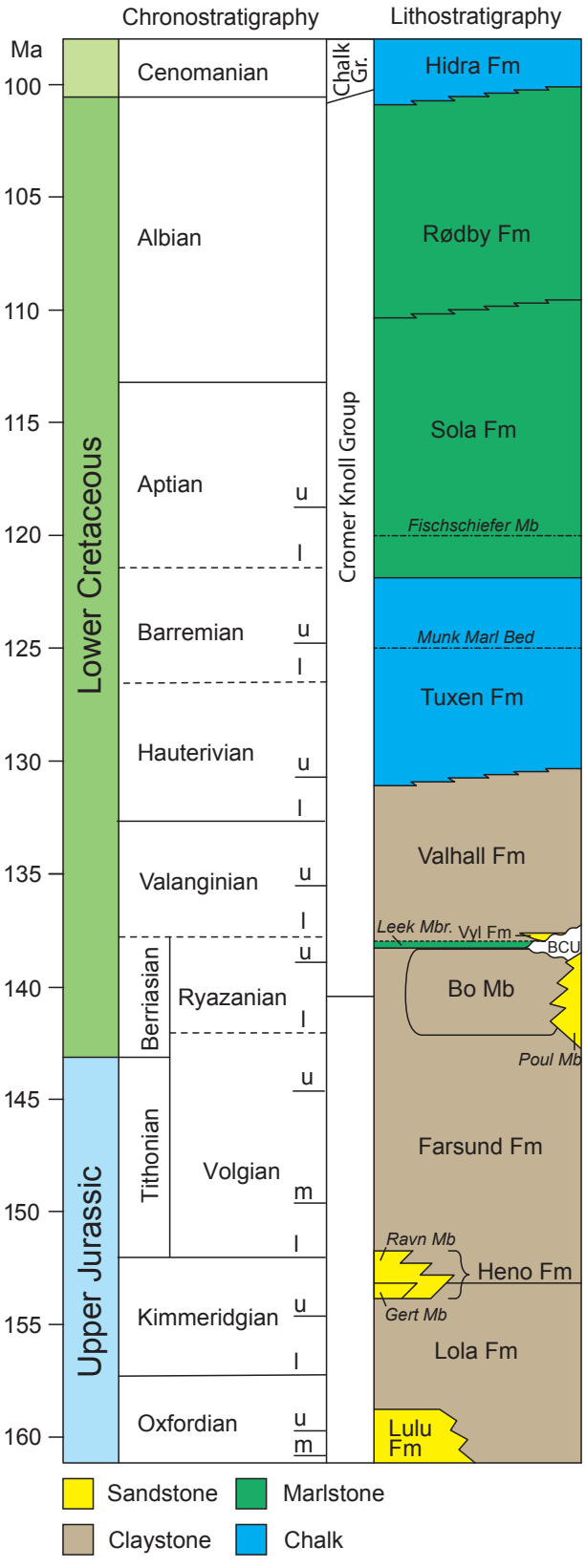


Fig. 2. Upper Jurassic – Lower Cretaceous chronostratigraphy and lithostratigraphy of the Danish Central Graben (modified after Jelby *et al.* (2022). Cretaceous chronostratigraphy is based on Gale *et al.* (2020). BCU = Base Cretaceous Unconformity.

Lauridsen *et al*. 2022). In the Early Cretaceous, the DB was bound to the northeast by the Fennoscandian Border Zone and to the south by the Ringkøbing–Fyn High (Nielsen 2003). Formation of the DB was initiated by crustal extension during the Late Carboniferous – Early Permian, followed by thermal cooling and subsidence that continued into the Late Jurassic, with a short regional uplift-event and associated erosion during the Early – Middle Jurassic (Vejbæk 1989; Nielsen 2003; Petersen *et al*. 2008). The basin continued to expand during the Early Cretaceous and as sea level rose, the upper Hauterivian – upper Barremian interval was dominated by siliciclastic material and became generally more enriched in pelagic carbonates. The Aptian succession varies between marlstone and chalk controlled by sea-level fluctuations (e.g. Ruffell 1991; Copestake *et al*. 2003). In the DB this stratigraphic interval is referred to the Vedsted Formation (Larsen 1966).

Methods and material

Sampling

Ten samples from core 25 of Vinding-1 (approx. 5 m) and 108 samples from cores 1–4 from the *c*. 80 m long Boje-2C core were selected for whole-rock and clay mineral analysis. The biostratigraphy of the Boje-2C core was based on calcareous nannofossils using the Boreal (BC) zonation scheme (Bown *et al*. 1998). A detailed sedimentological description of facies in the Boje-2C core is presented by Jelby *et al*. (2022). The chronostratigraphy and a lithological description of the Vinding-1 well are described by Lauridsen *et al*. (2022).

X-ray Diffraction (XRD)

Two grams of each sample were crushed and homogenised in an agate mortar for whole-rock mineralogy analysis. Approximately one gram of each sample was placed in a steel holder, analysed on the Thermo Scientific ARL Thermo X'tra diffractometer (Institute of Earth Sciences, University of Lausanne, Lausanne) and the mineralogy was quantified with a standard error between 5 and 10 % (Klug & Alexander 1974; Kübler 1983; Adatte *et al*. 1996).

For the clay mineral analysis, two grams of each sample were crushed into 0.2 – 0.5 mm chips, using an agate mortar. The rock chips were treated with 3% H_2O_2, to remove the main part of the organic matter (Righi *et al*. 1995). Separation and analysis of the clay fraction (<2 μm) was based on Kübler (1987) and Adatte *et al*. (1996), including decarbonation with 1.25N HCl and clay settling based on Stoke's law. Quantification of the clay mineralogy was conducted on oriented, air-dried, ethylene-glycolated smear slides which were measured on the Thermo Scientific ARL Thermo X'tra diffractometer, based on the methods of Kübler (1987) and Moore and Reynolds (1989) (Fig. 3). The error is minimised to less than 5%. The kaolinite/(illite + chlorite) ratio is used to indicate the significance of the weathering and is referred to as the weathering index (WI).

Results

The Boje-2C core spans the lower Hauterivian – upper Barremian nannofossil Zones BC9 to BC17 (Figs 4, 5; Gale *et al*. 2020). The whole-rock mineralogy of the Boje-2C well is presented in figure 3, showing that the amount of clay minerals varies between 6–50%, with an average of 24% (supplement 1). The most abundant mineral is calcite (32–89%, average 67%), followed by quartz (2–15%, average 5%) and pyrite (0–5%, average 1%). In some samples, traces of dolomite, gypsum or hematite were observed. Clay mineral analysis of the core shows that the most abundant clay type is kaolinite, varying between 30–73% with an average of 49% (Fig. 5; supplement 1). It is followed by illite, with a range of 9.0–33.6%, averaging 23%. The two least abundant types are illite/smectite (I/S) mixed layers (6–34%) and chlorite (5–21%), averaging 17% and 12%, respectively. Pure smectite is completely absent in the core.

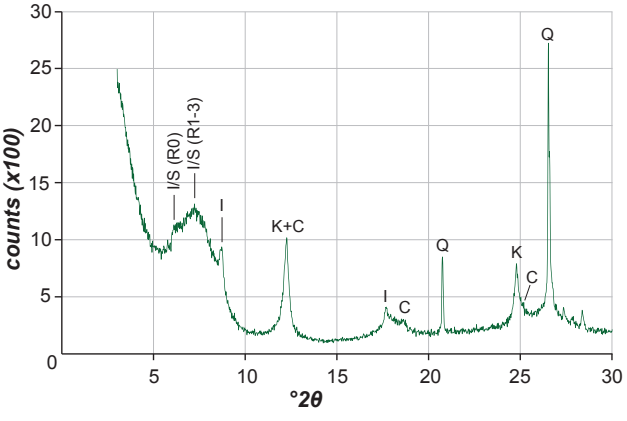


Fig. 3. Clay mineral X-ray Diffractogram (XRD) of sample Boje-2C #119. The diagram shows raw data of the intensity of the different clay mineral peaks. I/S = interstratified illite/smectite, I = illite, K = kaolinite, C = chlorite, Q = quartz. The peaks were quantified and this sample contains 34% kaolinite, 31% interstratified illite/smectite, 27% illite and 8% chlorite (supplement 1).

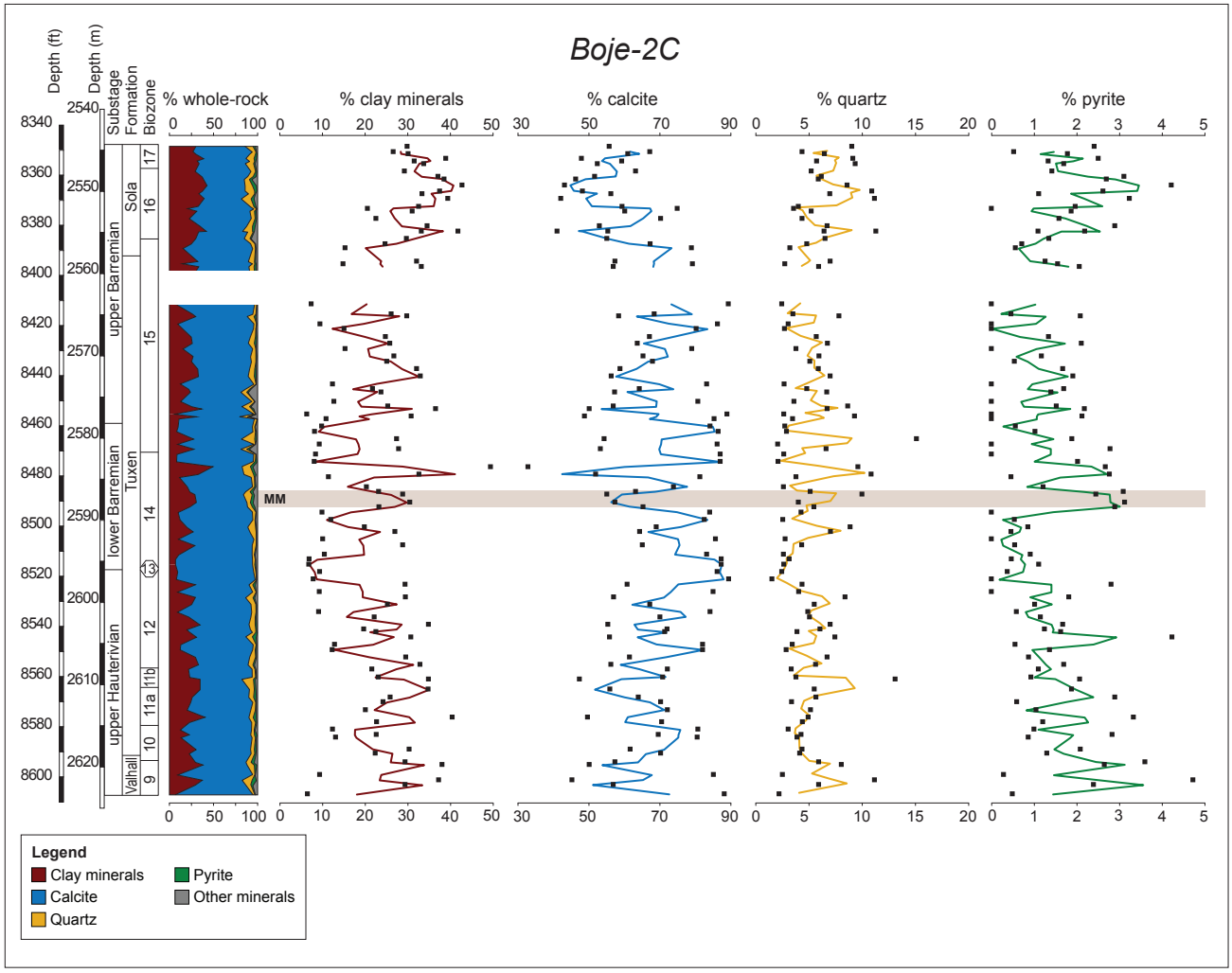


Fig. 4. Whole-rock mineral assemblages of the Boje-2C core, based on XRD analysis. 'Other minerals' include dolomite, gypsum, hematite and undefined minerals (supplement 1). The curves are based on a two-period moving average. MM = Munk Marl Bed.

The whole-rock mineralogy of the Vinding-1 well is dominated by calcite (35–90%), clay minerals (8–43%) and quartz (2–15%) (Fig. 6, supplement 2). In addition to small amounts of K-feldspar (0–4%) and Na-plagioclase (0–3%) traces of gypsum, pyrite, hematite and goethite are present in the core. The clay mineralogy of the upper Hauterivian – lower Aptian of the Vinding-1 well is dominated by kaolinite (20–53%), followed by I/S (9–44%) and illite (23–32%). Chlorite (5–14%) and smectite (0–4%) occur in small amounts in this core (Fig. 6, supplementary).

The trend lines of the kaolinite and WI curves in the Boje-2C well show similar trends, with a slight increase in nannofossil Zones BC9–BC11 (upper Hauterivian), followed by a decrease towards the Munk Marl Bed (BC14; lower Barremian) (Fig. 7). Just above the Munk Marl Bed, an increase in kaolinite in the upper BC14 and BC15 (lower – upper Barremian) is observed. This trend continues into BC16 (upper Barremian) for the WI, but the kaolinite percentage drops slightly in this zone.

Discussion

Significance of clay mineral assemblages

Impact of diagenesis

Evaluation of clay mineral origin and transport is essential in order to use clay mineral assemblages for palaeoclimatic or palaeogeographic reconstruction in the DCG and DB. Clay mineral assemblages could have been influenced by factors of detrital or authigenic nature (Chamley 1989). Two processes contribute to *in situ* clay mineral formation: i) diagenetic precipitation in pore spaces, and ii) recrystallisation due to increased pressure and/or temperature during

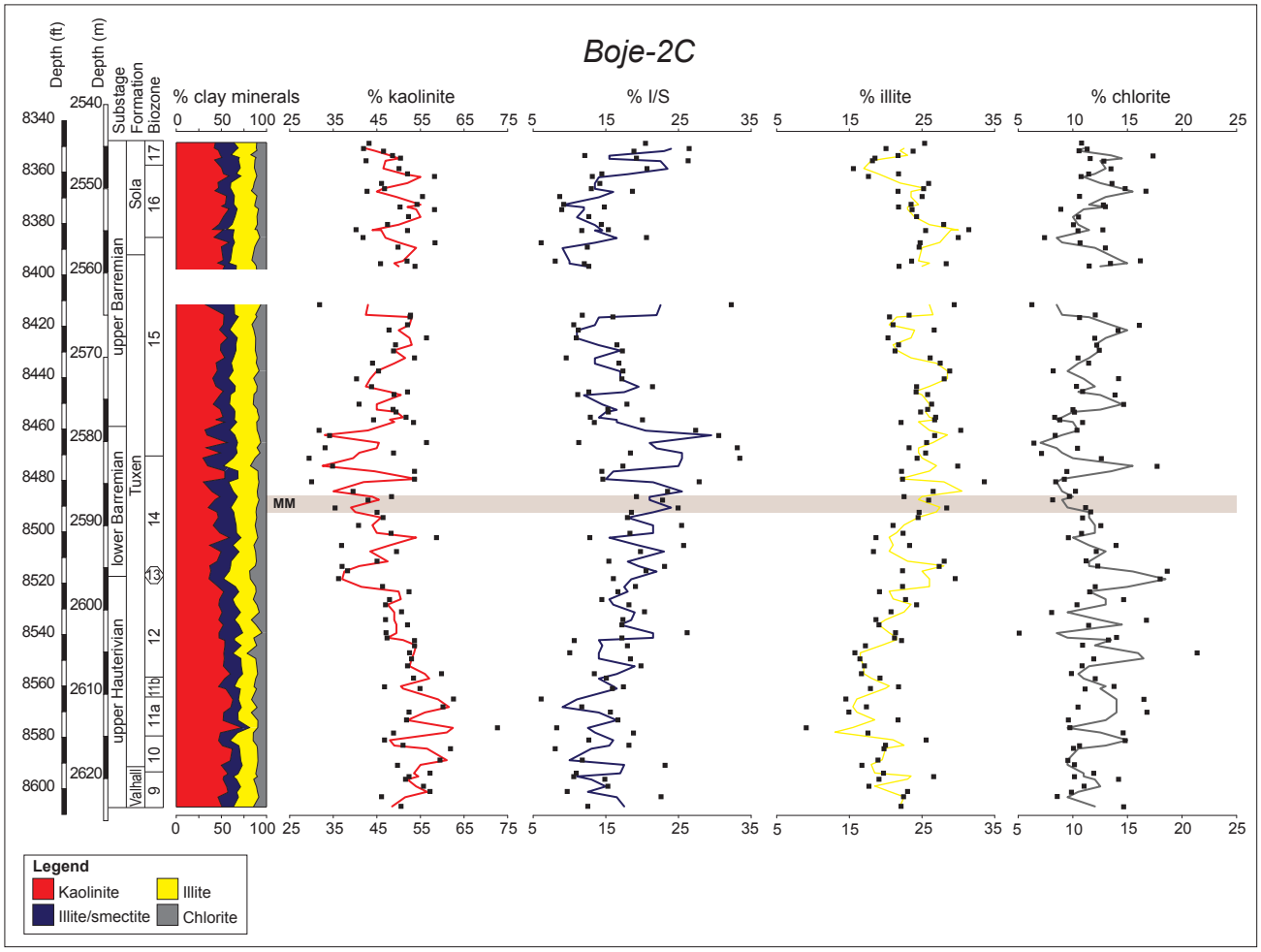


Fig. 5. Clay mineral assemblages of the Boje-2C core, based on XRD analysis. The curves are based on a two-period moving average. MM = Munk Marl Bed.

burial (Singer 1984). Authigenic clay mineral formation would clearly obscure the original detrital signal and therefore needs to be evaluated in the Boje-2C and Vinding-1 cores.

Illite, chlorite and kaolinite are known to form diagenetically in pore spaces due to fluid circulation, but this is more likely to happen in sandstones than in the low porosity and permeability marlstones and chalks of the Lower Cretaceous successions (Shelton 1964; Weaver 1990; Lanson *et al.* 2002; Jakobsen *et al.* 2004; Wilson *et al.* 2014). Scanning Electron Microscopy (SEM) images of selected North Jens-1 core samples have shown that the dominant kaolinite minerals have a detrital origin, based on their anhedral crystal shape (Blok *et al.* 2022). Due to the very similar lithologies in the Boje-2C well (Jelby *et al.* 2022), it is highly unlikely that diagenetic clay mineral precipitation took place in either well. Clay minerals in the Vinding-1 well also appear to have a detrital origin, as SEM images presented by Lauridsen *et al.* (2022) do not show any indication of authigenic clay mineral formation.

Burial diagenesis could result in recrystallisation of clay minerals during burial and pressure and/or temperatures increase (Curtis 1985). Illitisation of smectite could occur at depths greater than 2000 m (Burtner & Warner 1986). The Boje-2C samples were collected from depths of approximately 2540 to 2630 m and therefore subject to burial diagenesis (Fig. 4). At the present day, the Lower Cretaceous succession of the Vinding-1 well is found at a depth of *c.* 1300 m (Lauridsen *et al.* 2022), but burial history curves of nearby cores indicate that the succession has been exposed to a burial depth of approximately 2000 m (Weibel 1999). Smectite is completely absent in the Boje-2C core and only minor amounts were observed in the Vinding-1 core, and it is therefore highly likely that burial diagenesis has transformed smectite into mixed layers of illite/smectite type, similar to observations in the North Jens-1 core (Blok *et al.* 2022). Nevertheless, kaolinite is still present in large amounts, implying that burial diagenesis only had an overall limited effect (Fig. 5).

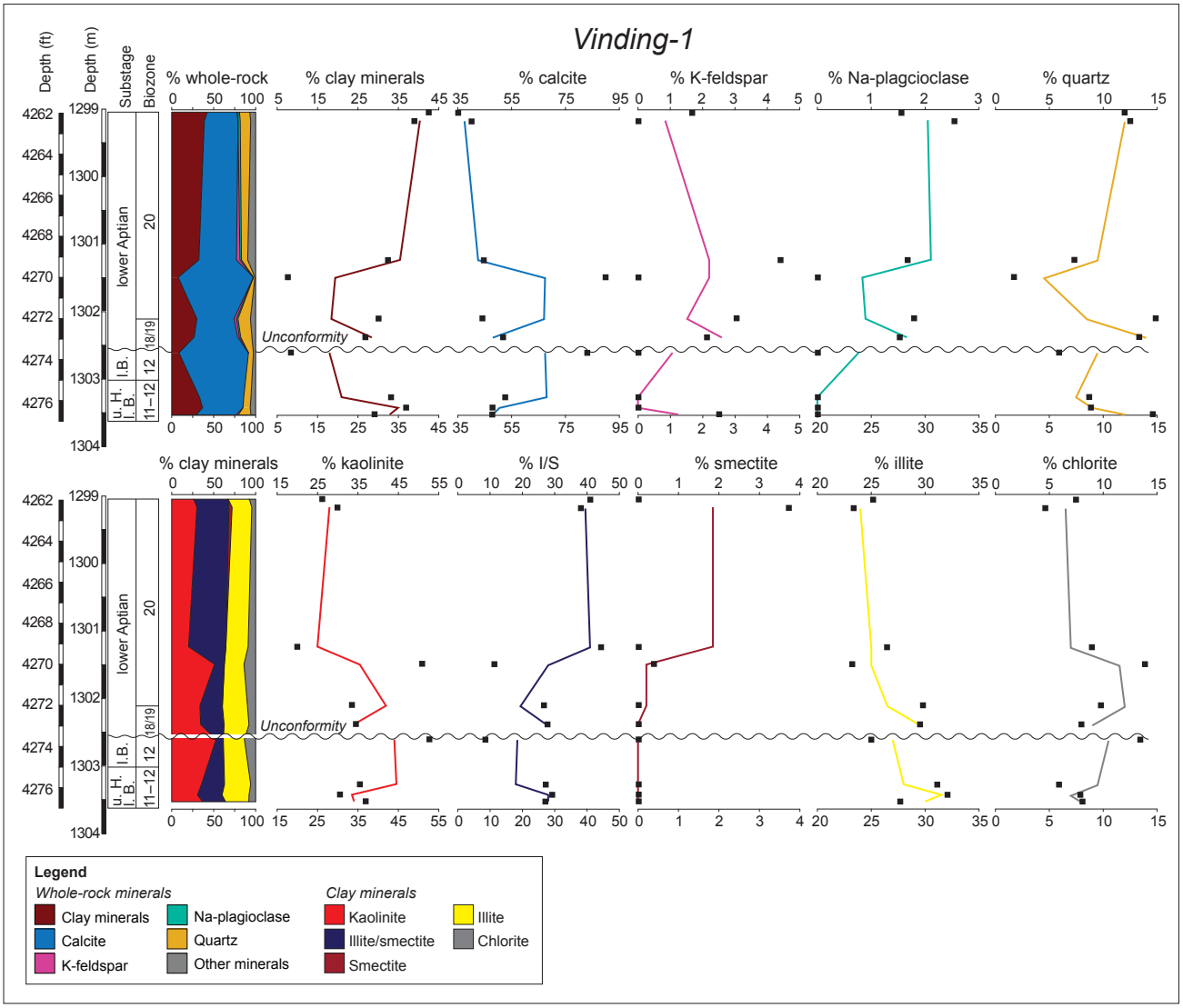


Fig. 6. Whole-rock and clay mineral assemblages of the Vinding-1 cores, based on XRD analysis. The curves are based on a two-period moving average. Chronostratigrahpy and biostratigraphy from Lauridsen *et al.* (2022). 'Other minerals' include gypsum, pyrite hematite, goethite and undefined minerals (supplement 2). u.H. = upper Hauterivian, l. B. = lower Barremian.

Detrital clay minerals

The clay mineral abundancies can be used to reconstruct palaeoclimate and palaeogeography, as authigenic clay mineral formation has been limited to transformation of smectite into I/S. Detrital clay minerals could have three different origins: i) they were formed in palaeosols under specific palaeoclimatic conditions (Chamley 1989; Ruffell *et al.* 2002), ii) they are the product of weathering feldspars in older sandstones, basement or volcanic rocks (Exley 1976; Keller 1978) or, iii) they were eroded from older diagenetically-derived clay minerals that were formed in porous sandstones (Deconinck *et al.* 2019). Detrital clay mineral assemblages can form a combination of the aforementioned formation processes, in which case the rate of erosion could be influenced by various factors. Relative sea-level fall can increase the area subject to erosion, resulting in enhanced erosion of detrital material. Changes in palaeoclimate to more humid conditions will intensify continental runoff and the amount of detrital material transported (Ketzer *et al.* 1999. A combination of these processes commonly affects transport of detrital material (e.g. Hallam *et al.* 1991; Adatte *et al.* 2002; Deconinck *et al.* 2019).

There are no indications of major eustatic sea-level fluctuations or tectonic uplift during the late Hauterivian – early Aptian in the DCG, that could have significantly influenced detrital transport to the basins (Haq 2014; van Buchem *et al.* 2017). Based on changes in clay minerals and nannofossil assemblages a long-term trend towards drier conditions in the late Hauterivian – late Barremian followed by a change

towards more humid conditions in the early Aptian was observed in the Boreal Realm, which probably led to changes in the transport of detrital material (Mutterlose & Bottini 2013; Blok *et al.* 2022).

Distribution of kaolinite

The source area providing detrital material to the DCG during the Early Cretaceous has been proposed to be the Baltic Shield with weathered basement rocks located towards the north (e.g. Christensen *et al.* 2002; Jakobsen *et al.* 2004). The Ringkøbing–Fyn High has been proposed as an alternative source area during the Triassic – earliest Cretaceous, although it is unclear whether similar processes were active during the remaining part of the Early Cretaceous (Nielsen *et al.* 2015; Olivarius *et al.* 2017; Petersen & Jakobsen 2021). Clay mineral assemblages and more specifically, kaolinite abundance is here used to infer the potential source area(s) for the DCG. Kaolinite percentages for the upper Hauterivian – upper Barremian (BC9–BC17) in the North Jens-1 core are relatively high with an average of *c.* 74%, compared to the Vinding-1 (39%) and Boje-2C (49%) wells (Fig. 7; Blok *et al.* 2022). This significant difference of *c.* 25–40%, and the fact that the distance between the Boje-2C and North Jens-1 wells is only *c.* 10 km suggests that there must be an additional influx of kaolinite for the North Jens-1 well, compared to the suggested kaolinite source to the north (Fig. 7). Thus, given that kaolinite minerals settle relatively rapidly due to their large size (Ruffell *et al.* 2002), it appears that the North Jens-1 well was located close to a source providing substantial amounts of kaolinite, whereas the Vinding-1 and Boje-2C wells were located further away or had a different source.

Subaerial exposure or shallow-marine settings are

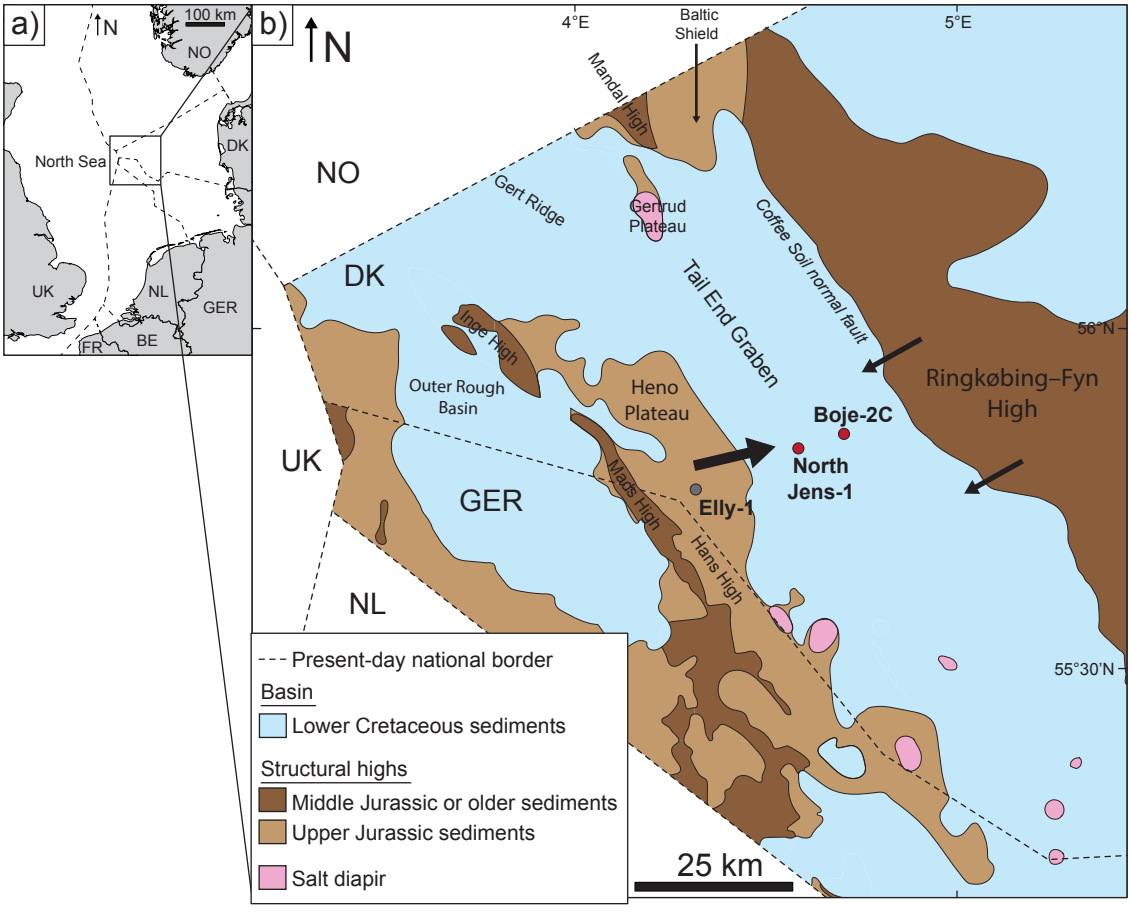


Fig. 7. a) Present-day map of the North Sea, with borders of countries. NO = Norway, DK = Denmark, GER = Germany, NL = Netherlands, BE = Belgium, FR = France, UK = United Kingdom. b) Palaeogeograpic map for the Early Cretaceous of the Danish Central Graben and north-western German North Sea based on Upper Jurassic and Lower Cretaceous isochore maps of the Danish (Vejbæk & Andersen 2002) and German (Arfai *et al.* 2014) sectors. Areas of erosion or non-deposition during the Early Cretaceous are indicated with brown colours. Blue colours indicate where Lower Cretaceous sediments were deposited. The arrows indicate the transport direction of detrital material and a bigger arrow indicates a higher influx, showing the Heno Plateau as the main source area of the DCG.

required to form kaolinite in palaeosols and/or erode it from older rocks before it is transported seawards by fluvial and/or coastal processes. In shallow-marine settings, sediments could be eroded by wave action and transported towards more basinal areas (Zecchin *et al.* 2019). Figure 7 illustrates where the Lower Cretaceous sediments are present in the DCG and German sector of the North Sea and where they are absent. This suggests that those areas were likely subaerially exposed or formed shallow marine areas subject to erosion and/or non-deposition. Potential areas that were most likely characterised by erosion or non-deposition during the Early Cretaceous include the Baltic Shield (Fig. 1; Mørk *et al.*, 2003), the Ringkøbing–Fyn High (Fig. 7; Olivarius *et al.* 2015), and the Heno Plateau (Fig. 7; Pedersen *et al.* 2018; Weibel *et al.* 2020).

Potential clay source areas

Baltic Shield

Weathering of feldspars from basement rock of the Baltic Shield (Fig. 1) could provide material that was transported into the Norwegian, Danish and Northern German basins (Olivarius *et al.* 2015). Kaolinite, of authigenic and detrital nature, was the dominant clay mineral in the Upper Triassic – Lower Jurassic, located west of the Baltic Shield (Mørk *et al.* 2003). It is therefore possible that this area, which is located at least 300 km north-east of the DCG, was a potential source area for the clay minerals preserved in the DCG and distal DB. However, given the tendency for kaolinite to accumulate close to the detrital source and the distance from the Baltic Shield to the DCG and distal parts of the DB, makes it implausible that the Baltic Shield was the main source area. Nevertheless, it is likely that small amounts of kaolinite were weathered from the shield and transported transport into the DB and DCG.

Ringkøbing–Fyn High

A closer potential source is the Ringkøbing–Fyn High, which consists of basement rock, overlain by Palaeozoic and Mesozoic sediments (Olivarius *et al.* 2015). Zircon U-Pb dating shows that the basement of the Ringkøbing–Fyn High and southern Baltic Shield was created during the same orogeny and consist of similar gneissic basement (Olivarius *et al.* 2015). The sediments on top of the basement rock mainly consist of (locally) a thin layer of the Permian evaporites, Triassic sand- and claystones and chalks from the Upper Cretaceous (Olivarius *et al.* 2015). This also indicates that the Jurassic and Lower Cretaceous sediments are absent. Non-deposition of Lower Cretaceous sediments on the Ringkøbing–Fyn High suggests that this area was subaerially exposed during the Early Cretaceous (Fig. 7; van Buchem *et al.* 2017). However, no sedimentary evidence, such as terrestrial deposits, palaeosols, plant remains or coal beds has yet been found. This could imply that the Ringkøbing–Fyn–High was a shallow marine plateau affected by wave action and/or erosion, potentially supplying sediments to the DCG and DB. The Ringkøbing–Fyn High has been proposed as a sediments source in several other studies, *e.g.* for the Lower Triassic Bunter Sandstone Formation (Olivarius *et al.* 2017) or the gravity-flow sandstone deposits of the Farsund Formation (Fig. 2; Nielsen *et al.* 2015). However, these events were related to intense uplift of the high, resulting in enhanced weathering, which has not been recognised during the Early Cretaceous (Vejbæk 1986; van Buchem *et al.* 2017). In addition, the grain size in these gravity-flow sandstones is larger than the fine-grained clay and limestone that is observed in the Vinding-1 (Fig 6; Lauridsen *et al.* 2022), Boje-2C (Fig. 4) and North Jens-1 core (Blok *et al.* 2022). Furthermore, kaolinite is primarily formed by continental chemical weathering processes and not by wave erosion of pre-existing (e.g. Exley 1976; Chamley 1989). Therefore, it seems unlikely the Ringkøbing–Fyn High was the major supplier of detrital material for the DCG or the DB, although minor influxes could have originated from the High.

Heno Plateau

The Heno Plateau is located to the west of the North Jens-1 and Boje-2C wells and the DCG (Fig. 7). The absence of Lower Cretaceous sediments on the Heno Plateau, as indicated by seismic profiles (van Buchem *et al.* 2017), isopach maps (Vejbæk & Andersen 2002) and isochore maps (Ineson *et al.* 2022a), suggest that it is highly likely that the plateau was subaerially exposed or subject to wave erosion. This is observed in the Elly-1 well, where the feldspar-rich sandstones of the Heno Formation (upper Kimmeridgian – lowermost Volgian/Tithonian) were partly eroded and are overlain by Upper Cretaceous chalk (Michelsen *et al.* 2003; van Buchem *et al.* 2017; Pedersen *et al.* 2018). During the Volgian (Tithonian), most highs and basins in the DCG were overlain by offshore mudstones of the Farsund Formation (Fig. 2; Johannessen *et al.* 2010; Ineson *et al.* 2022b). However, the Elly-1 well shows that parts of the Heno Plateau were not covered by the offshore mudstone during the Early Cretaceous, either due to non-deposition or Late Jurassic – Early Cretaceous erosion. Early Cretaceous exposure of the Heno Formation might therefor be limited to a fault block in the southern part of the plateau in the Danish sector, though likely extending into the German sector (Fig. 7).

The Heno Formation is divided into the Gert Mem-

ber, composed of very fine- to fine-grained quartz and feldspar sandstones, formed in the back-barrier and shoreface and the Ravn Member, encompassing shoreface sandstones, with quartz and K-feldspar as the dominant minerals (Michelsen *et al.* 2003; Weibel *et al.* 2020). Partial dissolution of the K-feldspars is common in the Ravn Member, which could be related to early weathering or instability during burial (Johannessen *et al.* 2010; Pedersen *et al.* 2018). Burial diagenesis plays an important role in the dissolution of K-feldspar in various wells in the DCG (e.g. Weibel *et al.* 2020). The Upper Jurassic succession on the Heno Plateau is at present buried at *c.* 3.5–4 km (Pedersen *et al.* 2018; Weibel *et al.* 2020), initiating illitisation of both feldspars and if present, kaolinite (Lanson *et al.* 2002; Mantovani & Becerro 2010). However, at various locations in the DCG, limited traces of illitisation and dissolution traces on feldspar grains, lack of feldspar grains and kaolinite substitute indicate intense pre-burial weathering of the Heno Formation (Weibel *et al.* 2020). It is very likely that, similar conditions were established around the Elly-1 well and that the Upper Jurassic succession was subject to intense weathering, providing substantial amounts of kaolinite. The Heno Formation is sandstone-rich, and the North Jens-1 well is located closest to the plateau (Fig. 7). Kaolinite is one of the largest clay mineral, thus prone to settling first (Ruffell *et al.* 2002), and the Heno Plateau is considered to be the main source area for the North Jens-1 and Boje-2C wells. This implies that transport of detrital material into the DCG was dominated by influx from the west to south west. The DB is unlikely to contain sediments eroded from the Heno Plateau, since the Ringkøbing–Fyn High acts as a barrier between the high and the basin.

Early Cretaceous palaeoclimate

Kaolinite in the DCG has two origins: 1) part was formed in soils due to changes in palaeoclimate and 2) part was weathered or reworked from a kaolinite- or feldspar-rich source. The high influx of kaolinite into the DCG is thus partially related to a kaolinite-rich source close to the North Jens-1 well, which gives the

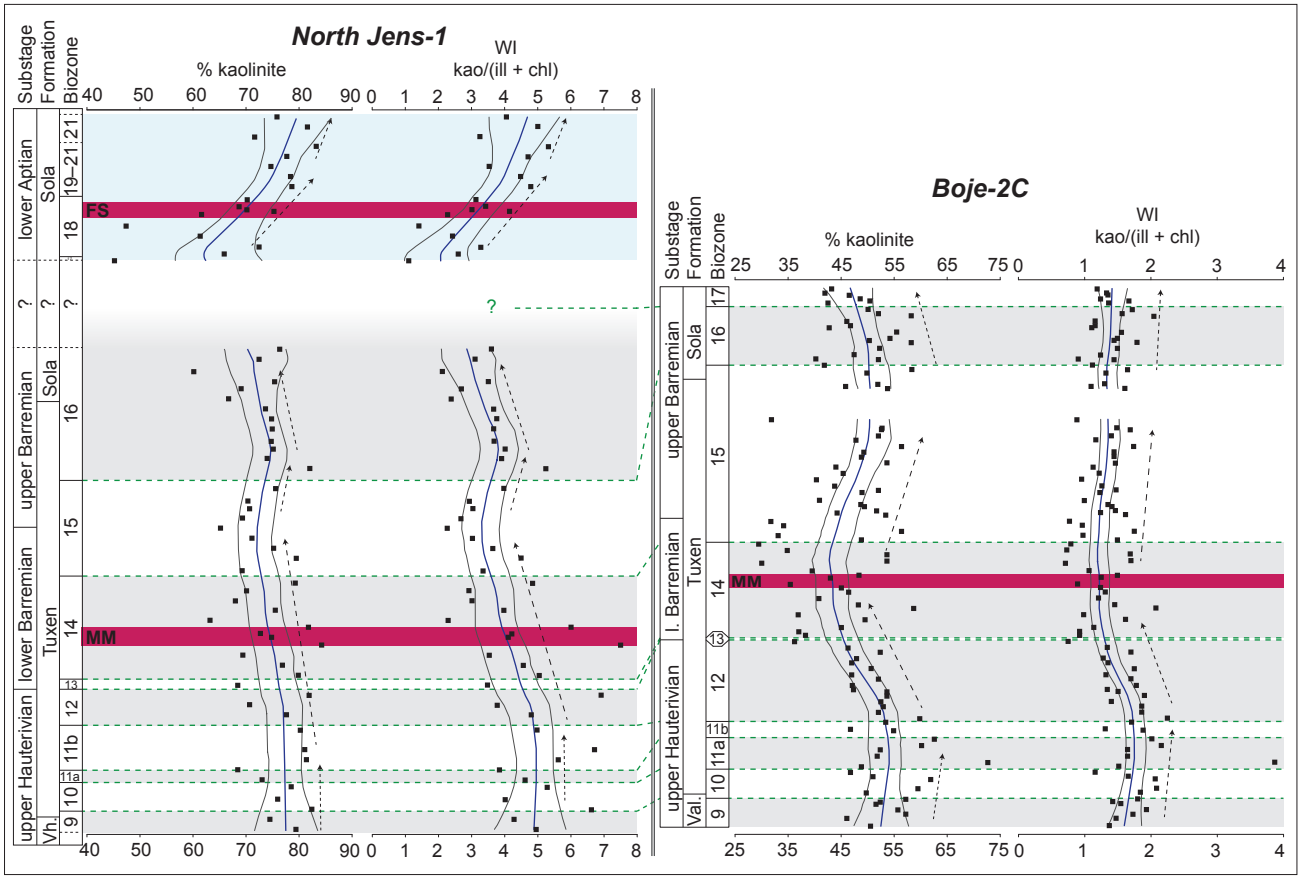


Fig. 8. Comparison of kaolinite percentage and the weathering index (WI) of the North Jens-1 (Blok *et al.* 2022) and Boje-2C wells (this study). The trend lines are based on the LOESS curve (blue line) and a 95% confidence curve (dark grey lines), using the PAST software (Hammer *et al.* 2001). Note that the lower Aptian (NJ-1; blue box) is not absent in the Boje-2C well. FS = Fischschiefer Member, MM = Munk Marl Bed.

clay mineral record a high background signal superimposed on the palaeoclimatic signal.

In the Boreal Realm, the palaeoclimatic changes from the Hauterivian to the late Barremian record a long-term transition to dryer conditions based on the blooming of nannoconids (Malkoč & Mutterlose 2010; Mutterlose & Bottini 2013), decreasing kaolinite contents in England (Ruffell & Batten 1990) and recently published kaolinite data from the DCG (Blok *et al*. 2022). This is also observed in the Tethyan Realm, based on a change towards more oxygenated oceans (Ce anomaly) and decreasing nutrients in the basin (phosphorus accumulation rates; Bodin *et al*. 2006; Bodin *et al*. 2013). In both realms, the latest Barremian – early Aptian was characterised by a trend towards more humid conditions, peaking during Oceanic Anoxic Event 1a, although this change is slightly delayed in the Boreal Realm (e.g. Ruffell & Worden 2000; Bodin *et al*. 2013; Mutterlose & Bottini 2013; Godet *et al*. 2014; Blok *et al*. 2022).

However, the Boje-2C core (this study) has an even higher resolution of clay mineral data for the late Hauterivian – late Barremian, permitting a more precise palaeoclimatic interpretation. The Boje-2C core shows overall decreasing kaolinite values, as in the North Jens-1 core, although the WI is more stable in the Boje-2C core than in the North Jens-1 core. (Fig. 8; Blok *et al*. 2022). The kaolinite values show an increase with time towards nannofossil subzone 11b, a decrease towards the Munk Marl Bed, and a slight increase towards the end of deposition of the Tuxen Formation (zone 15). In the Sola Formation the values decrease slightly upwards towards zone 17. The overall evolution towards drier conditions is interrupted by small fluctuations to more humid conditions as seen by increases in kaolinite. These fluctuations can be observed in the North Jens-1 well, but are better expressed in the Boje-2C well (Fig. 8).

Conclusions

A detailed clay-mineral study, specifically of kaolinite, has led to a better understanding of detrital input and source-to-sink patterns in the Danish Central Graben during the Early Cretaceous.

1. The high kaolinite percentages in Boje-2C and NJ-1 core indicate that the detrital input into the DCG have a dual origin during the Early Cretaceous: i) palaeoclimatic changes and ii) reworking of kaolinite-rich sediments located closest to the North Jens-1 well and providing substantial amounts of kaolinite.
2. A palaeogeographic map has been constructed and indicates areas where the Lower Cretaceous is missing or very thin. Those areas were very likely subaerially exposed and subject to erosion or non-deposition. They are potential source areas for detrital material that was washed into the basin during the Early Cretaceous.
3. Possible highs and their corresponding lithologies that could have acted as source areas were i) the granitic basement in the Baltic Shield and its Upper Triassic to Lower Jurassic succession, ii) the basement rocks and overlying Palaeozoic and Early Mesozoic sediments of the Ringkøbing–Fyn High and iii) the Upper Jurassic sandstones of the Heno Plateau.
4. The Heno Plateau is considered to have been the main source area for the DCG, based on clay mineral assemblages. The North Jens-1 well contains the highest amounts of kaolinite and therefore a kaolinite-rich source close to this well is very likely. The feldspar-rich sandstones of the Heno Formation were subject to weathering before burial. The Baltic Shield and Ringkøbing–Fyn High probably only provided minor amounts of detrital material for the basin.
5. The combination of clay mineral assemblages from the North Jens-1 core and the Boje-2C core give very clear indications of palaeoclimatic conditions during late Hauterivian – early Aptian. A long-term decrease in kaolinite in the late Hauterivian – late Barremian also indicates changes towards drier palaeoclimatic conditions. Small variations in this record imply slight fluctuations between more humid and drier periods.

Acknowledgements

We thank the Danish Offshore Technology Centre (DTU offshore) under the TRD Lower Cretaceous programme for funding this research. The data and permission to publish this work was kindly granted by the Danish Underground Consortium (TotalEnergies E&P Denmark, Noreco & Nordsøfonden). In addition, M.E. Jelby gratefully acknowledges the Carlsberg Foundation for funding an Internationalisation Fellowship during which this work was partly undertaken. We thank Finn Surlyk and Gunver Krarup Pedersen for their valuable and constructive reviews.

References

Adatte, T., Stinnesbeck, W. & Keller, G. 1996: Lithostratigraphic and mineralogic correlations of near K/T boundary clastic sediments in northeastern Mexico: Implications for origin and nature of deposition. In: Ryder, G., *et al.* (eds): The Cretaceous-Tertiary Event and Other Catastrophes in Earth History, 211–226. https://doi.org/10.1130/0-8137-2307-8.211

Adatte, T., Keller, G. & Stinnesbeck, W. 2002: Late Cretaceous to early Paleocene climate and sea-level fluctuations: the Tunisian record. Palaeogeography, Palaeoclimatology, Palaeoecology 178, 165–196. https://doi.org/10.1016/S0031-0182(01)00395-9

Andsbjerg, J. & Dybkjær, K. 2003: Sequence stratigraphy of the Jurassic of the Danish Central Graben. GEUS Bulletin 1, 265-300.

Arfai, J., Jähne, F., Lutz, R., Franke, D., Gaedicke, C. & Kley, J. 2014: Late Palaeozoic to Early Cenozoic geological evolution of the northwestern German North Sea (Entenschnabel): new results and insights. Netherlands Journal of Geosciences 93, 147–174. https://doi.org/10.1017/njg.2014.22

Arthur, M.A., Jenkyns, H.C., Brumsack, H.-J. & Schlanger, S.O. 1990: Stratigraphy, geochemistry and paleoceanography of organic-rich Cretaceous sequences. In: Ginsburg, R.N. & Beaudoin, B. (eds): Cretaceous resources, events and rhythms. 304, 75–119. https://doi.org/10.1007/978-94-015-6861-6_6

Blok, C., Ineson, J., Anderskouv, K., Fantasia, A., Sheldon, E., Thibault, N., Jelby, M.E., Adatte, T. & Bodin, S. 2022: Latitude-dependant climate changes across the Aptian Oceanic Anoxic Event 1a. Palaeogeography, Palaeoclimatology, Palaeoecology 601, 111085. https://doi.org/10.1016/j.palaeo.2022.111085

Bodin, S., Godet, A., Föllmi, K.B., Vermeulen, J., Arnaud, H., Strasser, A., Fiet, N. & Adatte, T. 2006: The Late Hauterivian Faraoni oceanic anoxic event in the western Tethys: Evidence from phosphorus burial rates. Palaeogeography, Palaeoclimatology, Palaeoecology 235, 245–264. https://doi.org/10.1016/j.palaeo.2005.09.030

Bodin, S., Godet, A., Westermann, S. & Föllmi, K.B. 2013: Secular change in northwestern Tethyan water-mass oxygenation during the late Hauterivian-early Aptian. Earth and Planetary Science Letters 374, 121–131. https://doi.org/10.1016/j.epsl.2013.05.030

Bown, P., Rutledge, D., Crux, J. & Gallagher, L. 1998: Lower Cretaceous. In: Bown, P. (ed.): Calcareous nannofossil biostratigraphy, 86–131.

Burtner, R.L. & Warner, M.A. 1986: Relationship between illite/smectite diagenesis and hydrocarbon generation in Lower Cretaceous Mowry and Skull Creek shales of the northern Rocky Mountain area. Clays and Clay Minerals 34, 390–402. https://doi.org/10.1346/ccmn.1986.0340406

Chamley, H. 1989: Clay Sedimentology, 623 pp. Berlin: Springer-Verlag. https://doi.org/10.1007/978-3-642-85916-8

Chenot, E., Deconinck, J.-F., Puceat, E., Pellenard, P., Guiraud, M., Jaubert, M., Jarvis, I., Thibault, N., Cocquerez, T., Bruneau, L., Razmjooei, M.J., Boussaha, M., Richard, J., Sizun, J.-P. & Stemmerik, L. 2018: Continental weathering as a driver of Late Cretaceous cooling: new insights from clay mineralogy of Campanian sediments from the southern Tethyan margin to the Boreal realm. Global and Planetary Change 162, 292–312. https://doi.org/10.1016/j.gloplacha.2018.01.016

Christensen, H., Jakobsen, F., Jørgensen, M. & Stemmerik, L. 2002. Assessment of the Lower Cretaceous reservoir succession in Valdemarand adjacent area. PRIORITY symposium proceedings, Helsingør, Denmark 1, 66.

Copestake, P., Sims, A., Crittenden, S., Hamar, G., Ineson, J., Rose, P., Tringham, M., Evans, D., Graham, C. & Armour, A. 2003: Lower Cretaceous. In: Evans, D., *et al.* (eds): The Millennium Atlas: petroleum geology of the central and northern North Sea, 191–211.

Curtis, C.D. 1985: Clay mineral precipitation and transformation during burial diagenesis. Philosophical Transactions of the Royal Society of London. Series A, Mathematical and Physical Sciences 315, 91–105. https://doi.org/10.1098/rsta.1985.0031

Deconinck, J.F., Hesselbo, S.P. & Pellenard, P. 2019: Climatic and sea-level control of Jurassic (Pliensbachian) clay mineral sedimentation in the Cardigan Bay Basin, Llanbedr (Mochras Farm) borehole, Wales. Sedimentology 66, 2769–2783. https://doi.org/10.1111/sed.12610

Exley, C. 1976: Observations on the formation of kaolinite in the St. Austell Granite, Cornwall. Clay Minerals 11, 51–63. https://doi.org/10.1180/claymin.1976.011.1.06

Föllmi, K.B. 2012: Early Cretaceous life, climate and anoxia. Cretaceous Research 35, 230–257. https://doi.org/10.1016/j.cretres.2011.12.005

Gale, A., Mutterlose, J., Batenburg, S., Gradstein, F., Agterberg, F., Ogg, J. & Petrizzo, M. 2020: The Cretaceous Period. In: Geologic Time Scale 2020, 1023–1086. https://doi.org/10.1016/B978-0-12-824360-2.00027-9

Godet, A., Hfaiedh, R., Arnaud-Vanneau, A., Zghal, I., Arnaud, H. & Ouali, J. 2014: Aptian palaeoclimates and identification of an OAE1a equivalent in shallow marine environments of the southern Tethyan margin: Evidence from Southern Tunisia (Bir Oum Ali section, Northern Chott Chain). Cretaceous Research 48, 110–129. https://doi.org/10.1016/j.cretres.2013.12.006

Hallam, A., Grose, J.A. & Ruffell, A.H. 1991: Palaeoclimatic significance of changes in clay mineralogy across the Jurassic-Cretaceous boundary in England and France. Palaeogeography, Palaeoclimatology, Palaeoecology 81, 173–187. https://doi.org/10.1016/0031-0182(91)90146-I

Hammer, Ø., Harper, D.A.T. & Ryan, P.D. 2001: PAST: Paleontological statistics software package for education and data analysis. Palaeontologia Electronica 4, 1–9.

Haq, B.U. 2014: Cretaceous eustasy revisited. Global and Planetary Change 113, 44–58. https://doi.org/10.1016/j.gloplacha.2013.12.007

Hardman, R. 1982: Chalk reservoirs of the North Sea. Bulletin

of the geological Society of Denmark 30, 119–137. https://doi.org/10.37570/bgsd-1981-30-12

Ineson, J.R. 1993. The Lower Cretaceous chalk play in the Danish Central Trough. Geological Society, London, Petroleum Geology Conference series, 4, 175–183. https://doi.org/10.1144/0040175

Ineson, J.R., Bojesen-Koefoed, J.A., Dybkjær, K. & Nielsen, L.H. 2003: Volgian–Ryazanian 'hot shales' of the Bo Member (Farsund Formation) in the Danish Central Graben, North Sea: stratigraphy, facies and geochemistry. GEUS Bulletin 1, 403–436. https://doi.org/10.34194/geusb.v1.4679

Ineson, J.R., Petersen, H.I., Andersen, C., Bjerager, M., Jakobsen, F.C., Kristensen, L., Mørk, F. & Sheldon, E. 2022a: Early Cretaceous stratigraphic and basinal evolution of the Danish Central Graben: a review. Bulletin of the Geological Society of Denmark 71. https://doi.org/10.37570/bgsd-2022-71-05

Ineson, J.R., Sheldon, E., Dybkjær, K., Andersen, C., Alsen, P. & Jakobsen, F. 2022b: The 'Base Cretaceous Unconformity'in a basin-centre setting, Danish Central Graben, North Sea: A cored record of resedimentation and condensation accompanying transgression and basinal overturn. Marine and Petroleum Geology 137, 105489. https://doi.org/10.1016/j.marpetgeo.2021.105489

Jakobsen, F., Ineson, J.R., Kristensen, L. & Stemmerik, L. 2004: Characterization and zonation of a marly chalk reservoir: the Lower Cretaceous Valdemar Field of the Danish Central Graben. Petroleum Geoscience 10, 21–33. https://doi.org/10.1144/1354-079303-584

Japsen, P., Britze, P. & Andersen, C. 2003: Upper Jurassic–Lower Cretaceous of the Danish Central Graben: structural framework and nomenclature. Geological Survey of Denmark and Greenland (GEUS) Bulletin 1, 231–246. https://doi.org/10.34194/geusb.v1.4653

Jelby, M.E., Ineson, J.R., Thibault, N., Bodin, S., Blok, C.N., Edvardsen, N., Clemmensen, T.S., Buls, T. & Anderskouv, K. 2022: Facies and depositinal processes of Lower Cretaceous carbonates, Danish Central Graben. Bulletin of the Geological Society of Denmark 71, 51–74. https://doi.org/10.37570/bgsd-2022-71-04

Jenkyns, H.C. 2010: Geochemistry of oceanic anoxic events. Geochemistry, Geophysics, Geosystems 11, 1–30. https://doi.org/10.1029/2009GC002788

Jensen, T.F., Holm, L., Frandsen, N. & Michelsen, O. 1986: Jurassic-Lower Cretaceous lithostratigraphic nomenclature for the Danish Central Trough. Danmarks Geologiske Undersøgelse Serie A 12, 1–65. https://doi.org/10.34194/seriea.v12.7031

Jensen, T.F. & Buchardt, B. 1987. Sedimentology and geochemistry of the organic carbon-rich lower cretaceous Sola formation (Barremian-Albian), Danish North Sea. Conference on petroleum geology of North West Europe 3, 431–440.

Jeremiah, J. 2001: A Lower Cretaceous nannofossil zonation for the North Sea Basin. Journal of Micropalaeontology 20, 45–80. https://doi.org/10.1144/jm.20.1.45

Johannessen, P.N. 2003: Sedimentology and sequence stratigraphy of paralic and shallow marine Upper Jurassic sandstones in the northern Danish Central Graben. GEUS Bulletin 1, 367–402. https://doi.org/10.34194/geusb.v1.4678

Johannessen, P. & Andsbjerg, J. 1993. Middle to Late Jurassic basin evolution and sandstone reservoir distribution in the Danish Central Trough. Geological Society, London, Petroleum Geology Conference series, 4, 271–283. https://doi.org/10.1144/0040271

Johannessen, P., Dybkjær, K., Andersen, C., Kristensen, L., Hovikoski, J. & Vosgerau, H. 2010. Upper Jurassic reservoir sandstones in the Danish Central Graben: new insights on distribution and depositional environments. Geological Society, London, Petroleum Geology Conference series, 7, 127–143. https://doi.org/10.1144/0070127

Keller, W. 1978: Kaolinization of feldspar as displayed in scanning electron micrographs. Geology 6, 184–188. https://doi.org/10.1130/0091-7613(1978)6<184:KOFADI>2.0.CO;2

Ketzer, J., Morad, S. & Amorosi, A. 1999: Predictive diagenetic clay mineral distribution in siliciclastic rocks within a sequence stratigraphic framework. Clay mineral cements in sandstones, 43–61. https://doi.org/10.1002/9781444304336.ch2

Klug, H.P. & Alexander, L.E. 1974: X-ray diffraction procedures: for polycrystalline and amorphous materials.

Kübler, B. 1983: Dosage quantitatif des minéraux majeurs des roches sédimentaires par diffraction X. Cahiers de l'Institut de Géologie Series AX 1.1 and 1.2.

Kübler, B. 1987: Cristallinité de l'illite: méthodes normalisées de préparation, méthode normalisée de mesure, méthode automatique normalisée de mesure. Cahiers de l'Institut de Géologie, Université de Neuchâtel, Suisse Série ADX 2 21, 13 pp.

Kuhnt, W., Holbourn, A. & Moullade, M. 2011: Transient global cooling at the onset of early Aptian oceanic anoxic event (OAE) 1a. Geology 39, 323–326. https://doi.org/10.1130/G31554.1

Kyrkjebø, R., Gabrielsen, R. & Faleide, J. 2004: Unconformities related to the Jurassic–Cretaceous synrift–post-rift transition of the northern North Sea. Journal of the Geological Society 161, 1–17. https://doi.org/10.1144/0016-764903-051

Lanson, B., Beaufort, D., Berger, G., Bauer, A., Cassagnabere, A. & Meunier, A. 2002: Authigenic kaolin and illitic minerals during burial diagenesis of sandstones: a review. Clay minerals 37, 1–22. https://doi.org/10.1180/0009855023710014

Larsen, G. 1966: Rhaetic-Jurassic-Lower Cretaceous sediments in the Danish Embayment (a heavy-mineral study). Danmarks Geologiske Undersøgelse II. Række 91, 1–127. https://doi.org/10.34194/raekke2.v91.6882

Lauridsen, B.W., Lode, S., Sheldon, E., Frykman, P., Anderskouv, K. & Ineson, J.R. 2022: Lower Cretaceous (Hauterivian–Aptian) pelagic carbonates in the Danish Basin: new data from the Vinding-1 well, central Jylland, Denmark. Bulletin of the Geological Society of Denmark 71, 7–29. https://doi.org/10.37570/bgsd-2022-71-02

Malko, M. & Mutterlose, J. 2010: The Early Barremian warm pulse and the Late Barremian cooling: A high-resolution

geochemical record of the Boreal realm. Palaios 25, 14–23. https://doi.org/10.2110/palo.2010.p09-029r

Mantovani, M. & Becerro, A.I. 2010: Illitization of kaolinite: The effect of pressure on the reaction rate. Clays and Clay Minerals 58, 766–771. https://doi.org/10.1346/ccmn.2010.0580604

Michelsen, O., Nielsen, L.H., Johannessen, P.N., Andsbjerg, J. & Surlyk, F. 2003: Jurassic lithostratigraphy and stratigraphic development onshore and offshore Denmark. Geological Survey of Denmark and Greenland Bulletin 1, 147–216. https://doi.org/10.34194/geusb.v1.4651

Moore, D.M. & Reynolds, R. C. 1989: X-ray Diffraction and the Identification and Analysis of Clay Minerals, 378 pp. Oxford: Oxford University Press (OUP).

Mørk, M.B.E., Vigran, J.O., Smelror, M., Fjerdingstad, V. & Bøe, R. 2003: Mesozoic mudstone compositions and the role of kaolinite weathering-a view from shallow cores in the Norwegian Sea (Møre to Troms). Norwegian Journal of Geology/ Norsk Geologisk Forening 83, 61–78.

Mutterlose, J. & Böckel, B. 1998: The Barremian–Aptian interval in NW Germany: a review. Cretaceous Research 19, 539–568. https://doi.org/10.1006/cres.1998.0119

Mutterlose, J. & Bottini, C. 2013: Early Cretaceous chalks from the North Sea giving evidence for global change. Nature Communications 4, 1686, 1–6. https://doi.org/10.1038/ncomms2698

Nielsen, L.H. 2003: Late Triassic – Jurassic development of the Danish Basin and the Fennoscandian Border Zone, southern Scandinavia. Geological Survey of Denmark and Greenland Bulletin 1, 459–526. https://doi.org/10.34194/geusb.v1.4681

Nielsen, M.T., Weibel, R. & Friis, H. 2015: Provenance of gravity-flow sandstones from the Upper Jurassic–Lower Cretaceous Farsund Formation, Danish Central Graben, North Sea. Marine and Petroleum Geology 59, 371–389. https://doi.org/10.1016/j.marpetgeo.2014.09.016

Olivarius, M., Friis, H., Kokfelt, T.F. & Wilson, J.R. 2015: Proterozoic basement and Palaeozoic sediments in the Ringkøbing–Fyn High characterized by zircon U–Pb ages and heavy minerals from Danish onshore wells. Bulletin of the Geological Society of Denmark 63, 29–43. https://doi.org/10.37570/bgsd-2015-63-04

Olivarius, M., Weibel, R., Friis, H., Boldreel, L.O., Keulen, N. & Thomsen, T.B. 2017: Provenance of the Lower Triassic Bunter Sandstone Formation: implications for distribution and architecture of aeolian vs. fluvial reservoirs in the North German Basin. Basin Research 29, 113–130. https://doi.org/10.1111/bre.12140

Pedersen, S., Weibel, R., Johannessen, P.N. & Schovsbo, N.H. 2018: Diagenetic impact on reservoir sandstones of the Heno Formation in the Ravn-3 well, Danish Central Graben. GEUS Bulletin 41, 9–12. https://doi.org/10.34194/geusb.v41.4330

Petersen, H. & Jakobsen, F. 2021: Lithostratigraphic definition of the Upper Jurassic–lowermost Cretaceous (upper Volgian–Ryazanian) organic-rich and oil-prone Mandal Formation in the Danish Central Graben, North Sea. Marine and Petroleum Geology 129, 105116. https://doi.org/10.1016/j.marpetgeo.2021.105116

Petersen, H.I., Nielsen, L.H., Bojesen-Koefoed, J.A., Mathiesen, A., Kristensen, L. & Dalhoff, F. 2008: Evaluation of the quality, thermal maturity and distribution of potential source rocks in the Danish part of the Norwegian–Danish Basin. GEUS Bulletin 16, 1–66. https://doi.org/10.34194/geusb.v16.4989

Ponsaing, L., Petersen, H., Bojesen-Koefoed, J., Nytoft, H., Schovsbo, N. & Stemmerik, L. 2020: Source rock quality variations of Upper Jurassic–lowermost Cretaceous marine shales and their relationship to oils in the Valdemar Field, Danish North Sea. Journal of Petroleum Geology 43, 49–74. https://doi.org/10.1111/jpg.12749

Righi, D., Dinel, H., Schulten, H.R. & Schnitzer, M. 1995: Characterization of clay–organic matter complexes resistant to oxidation by peroxide. European Journal of Soil Science 46, 423–429. https://doi.org/10.1111/j.1365-2389.1995.tb01338.x

Rudra, A., Sanei, H., Nytoft, H., Petersen, H., Blok, C., Bodin, S. & Bojesen-Koefoed, J. 2021: Organic matter characterization of the Lower Cretaceous tight reservoirs in the Danish North Sea. International Journal of Coal Geology 238, 103714. https://doi.org/10.1016/j.coal.2021.103714

Ruffell, A. & Batten, D.J. 1990: The Barremian-Aptian arid phase in western Europe. Palaeogeography, Palaeoclimatology, Palaeoecology 80, 197–212. https://doi.org/The Barremian-Aptian arid phase in western Europe.

Ruffell, A. 1991: Sea-level events during the Early Cretaceous in western Europe. Cretaceous Research 12, 527–551. https://doi.org/10.1016/0195-6671(91)90006-X

Ruffell, A. & Worden, R. 2000: Palaeoclimate analysis using spectral gamma-ray data from the Aptian (Cretaceous) of southern England and southern France. Palaeogeography, Palaeoclimatology, Palaeoecology 155, 265–283. https://doi.org/10.1016/S0031-0182(99)00119-4

Ruffell, A., McKinley, J.M. & Worden, R.H. 2002: Comparison of clay mineral stratigraphy to other proxy palaeoclimate indicators in the Mesozoic of NW Europe. Philosophical Transactions of the Royal Society, London, A 360, 675–693. https://doi.org/10.1098/rsta.2001.0961

Shelton, J.W. 1964: Authigenic kaolinite in sandstone. Journal of Sedimentary Research 34, 102–111. https://doi.org/10.1306/74D70FDD-2B21-11D7-8648000102C1865D

Singer, A. 1984: The paleoclimatic interpretation of clay minerals in sediments – a review. Earth-Science Reviews 21, 251–293. https://doi.org/10.1016/0012-8252(84)90055-2

Surlyk, F., Dons, T., Clausen, C.K., Higham, J., Evans, D., Graham, C., Armour, A. & Bathurst, P. 2003: Upper cretaceous. In: Evans, D. *et al.* (eds): The Millennium Atlas: Petroleum Geology of the Central and Northern North Sea, 213–233.

Thomsen, E. 1989: Seasonal variability in the production of Lower Cretaceous calcareous nannoplankton. Geology 17, 715–717. https://doi.org/10.1130/0091-7613(1989)017<0715:SVITPO>2.3.CO;2

van Buchem, F., Smit, F.W.H., Buijs, G., Trudgill, B. & Larsen, P.-H. 2017: Tectonostratigraphic framework and depositional history of the Cretaceous–Danian succession of the Danish

Central Graben (North Sea)–new light on a mature area. Geological Society, London, Petroleum Geology Conference series 8, 9–46. https://doi.org/10.1144/PGC8.24

Vejbæk, O. & Andersen, C. 1987: Cretaceous-early Tertiary inversion tectonism in the Danish Central Trough. Tectonophysics 137, 221–238. https://doi.org/10.1016/0040-1951(87)90321-0

Vejbæk, O. & Andersen, C. 2002: Post mid-Cretaceous inversion tectonics in the Danish Central Graben-regionally synchronous tectonic events? Bulletin of the Geological Society of Denmark 49, 129–144. https://doi.org/10.37570/bgsd-2003-49-11

Vejbæk, O.V. 1986: Seismic stratigraphy and tectonic evolution of the Lower Cretaceous in the Danish Central Trough. Danmarks Geologiske Undersøgelse Serie A11, 46 pp. https://doi.org/10.34194/seriea.v11.7030

Vejbæk, O.V. 1989: Effects of asthenospheric heat flow in basin modelling exemplified with the Danish Basin. Earth and Planetary Science Letters 95, 97–114. https://doi.org/https://doi.org/10.1016/0040-1951(87)90321-0

Vidalie, M., van Buchem, F., Schmidt, I. & Uldall, A. 2014: Seismic stratigraphy of the Lower Cretaceous Valhall Formation (Danish Graben, North Sea). First break 32. https://doi.org/https://doi.org/10.3997/1365-2397.2014008

Weaver, C.E. 1990: Clays, muds, and shales. Elsevier. https://doi.org/10.1016/s0070-4571(08)x7036-0

Weibel, R. 1999: Effects of burial on the clay assemblages in the Triassic Skagerrak Formation, Denmark. Clay Minerals 34, 619–635. https://doi.org/10.1180/000985599546488

Weibel, R., Nielsen, M., Therkelsen, J., Jakobsen, F., Bjerager, M., Mørk, F., Mathiesen, A., Hovikoski, J., Pedersen, S. & Johannessen, P. 2020: Illite distribution and morphology explaining basinal variations in reservoir properties of Upper Jurassic sandstones, Danish North Sea. Marine and Petroleum Geology 116, 104290. https://doi.org/10.1016/j.marpetgeo.2020.104290

Wilson, M., Wilson, L. & Patey, I. 2014: The influence of individual clay minerals on formation damage of reservoir sandstones: a critical review with some new insights. Clay Minerals 49, 147–164. https://doi.org/10.1180/claymin.2014.049.2.02

Zecchin, M., Catuneanu, O. & Caffau, M. 2019: Wave-ravinement surfaces: classification and key characteristics. Earth-science reviews 188, 210-239. https://doi.org/10.1016/j.earscirev.2018.11.011

Supplementary data I: Whole-rock and clay mineralogy of the Boje-2C core.

Supplementary data II: Whole-rock and clay mineralogy of the Vinding-1 core.

Assessment of pore collapse in North Sea Lover Cretaceous carbonates using downhole elastic strain

IDA L. FABRICIUS & LEONARDO T. P. MEIRELES

Geological Society of Denmark
https://2dgf.dk

Received 19 December 2024
Accepted in revised form 1 May 2025
Published online 13 May 2025

© 2025 the authors. Re-use of material is permitted, provided this work is cited. Creative Commons License CC BY: https://creativecommons.org/licenses/by/4.0/

Fabricius, I.L. & Meireles, L.T.P. 2025. Assessment of pore collapse in North Sea Lover Cretaceous carbonates using downhole elastic strain. Bulletin of the Geological Society of Denmark, Vol. 71, pp. 115–125. ISSN 2245-7070. https://doi.org/10.37570/bgsd-2025-71-07

The potential for pore collapse is a concern when producing hydrocarbons from fragile sedimentary rocks, like chalks. The reason is that although pore collapse can be a valuable drive mechanism, it can also cause large scale compaction and surface subsidence. This risk is as a rule evaluated from results of rock mechanical testing of core samples, but because a given reservoir typically comprises layers of different porosity, the stress required for fracturing or pore-collapse is then generalized as a function of porosity. Due to different diagenetic history, different reservoirs can have different degree of cementation (induration) for a given porosity, so each reservoir requires a separate stress-porosity relationship.

Recent studies of chalk indicate that pore collapse happens at a critical elastic strain irrespective of porosity, pore fluid, and induration. This should not be surprising, bearing in mind that the strain of the rock represents an equal strain of the mineral crystals constituting the rock frame, so that onset of pore collapse in chalk is governed by the *in situ* elastic strain of the calcite. Chalk can be rich in minerals like clay or quartz, but when calcite constitutes the frame, it is calcite that is elastically strained. The simple point is that elastic strain of the calcite crystals is the same as the elastic strain of the rock.

A complication with rock mechanical data is that the tested material has been brought to the surface by coring, a process that typically causes tested rocks to contain microcracks (small unloading fractures), so that the tested rocks do not truly represent the rock *in situ*. This issue points to using downhole deformation data, but these are sparse. A possibility is then to use information from geophysical well logs, because *in situ* elastic strain can be calculated from well log data, so that the results from rock mechanical testing can be generalized in a simple way. The method for strain calculation is here applied to data from the Valdemar field, which produces hydrocarbons from the Tuxen and Sola formations, a clay-rich Lower Cretaceous chalk interval in the Central North Sea.

Key words. Aptian, Barremian, Cretaceous, chalk, marlstone, rock physics, pore collapse, small strain

Ida L. Fabricius [ilfa@dtu.dk] and Leonardo T. P. Meireles, Department of Environmental and Resource Engineering, Technical University of Denmark, Denmark. *present address: [LETE@equinor.com]*

Already at a relatively early stage, production of hydrocarbons from highly porous chalk fields of the North Sea led to concerns about their strength in relation to possible pore collapse and reservoir compaction (*e.g.* Andersson *et al*. 1985; Ruddy *et al*. 1989; Hermansen *et al*. 1996). Andersson *et al*. (1985) cited rock mechanical experimental results which indicate that pore collapse can happen at 0.7% elastic strain in a chalk of 40% porosity. They then turned their focus to the quite significant correlation between strength and porosity, so consequently results from rock mechanical tests and seismic data are typically interpreted in terms of stress and porosity (*e.g.* Ruddy *et al*. 1989; Bredesen *et al*. 2021). Strength can be defined as the stress attained before pore collapse, and strength of chalk has been found to not only depend on porosity, but also on induration (cementation), and saturating fluids (*e.g*. Nermoen *et al*. 2018), but this finding may be a complicated way to predict the onset of collapse caused by stress: Because calcite constitutes the supporting frame in chalk, it would be a simple assumption, that for a given stress

geometry, irrespective of porosity and cementation, pore collapse would happen at a critical elastic strain of calcite, and consequently a similar elastic strain of the rock. Recent studies have indeed indicated that elastic strain at pore collapse is remarkably similar for different specimens and saturating fluids when tested under hydrostatic conditions, and also similar when tested under oedometer conditions (Meireles & Fabricius 2022; Proestakis *et al*. 2023; Orlander & Christensen 2024, 2025). The critical strain differs depending on stress geometry and was found to be higher for hydrostatic geometry where pervasive pore collapse takes place than for oedometric geometry where pore collapse takes place in the form of compaction bands (Orlander & Christensen 2024, 2025).

Orlander & Christensen (2025) did uniaxial strain tests on core samples of chalk from the Tuxen Formation, and because a core sample retrieved from burial contains microcracks caused by unloading, it is not simple, from mechanical strain data alone, to ascertain which part of the mechanical deformation is plastic (*i.e.* closure of cracks) and which part is elastic. Elastic waves are purely elastic, so when the tests are monitored by elastic waves, elastic moduli, Biot's coefficient and elastic strain can be calculated throughout the test according to the procedure of Gram *et al*. (2021), and then plastic strain due to closure of microcracks can be quantified. In this way, Orlander & Christensen (2025) found the onset of pore collapse to be at markedly constant uniaxial elastic strain (0.20–0.24%) corresponding to *c.* 0.45% volumetric strain, across samples with different porosity and different induration, and even with different saturating fluid. For this reason, we find it relevant to present a simple method to derive the *in situ* elastic strain of a formation using petrophysical logging data (Fabricius & Omdal 2021).

Theory

Most North Sea chalk fields are presently buried to an effective stress of more than 10 MPa, and the chalk accordingly will expand and contain unloading fractures when retrieved in cores. The mechanism behind the formation of unloading fractures is described by *e.g*. Santamarina (2001). They arise because the stress field during burial has a dominating vertical component, whereas during exhumation the stress field transits via hydrostatic to have dominating lateral components. This causes extensional horizontal microcracks and fractures. Because the stress field during burial is uniaxial, samples for rock mechanical testing are as a rule cut as vertical cylinders, and when loaded with a stress, σ_v under uniaxial strain conditions, a part of the total strain will reflect the closure of microcracks. Under hydrostatic stress, σ_H, total strain will also include closure of microcracks. To overcome the ambiguity caused by microcracks, the elastic strain during a test can be derived by monitoring total strain, ε_t and elastic wave velocities (v_P and v_S). First step is to calculate sample porosity, ϕ, and bulk density, ρ_b:

$$\phi = (\phi_o - \varepsilon_t)/(1- \varepsilon_t), \quad (1)$$

$$\rho_b = \rho_g (1- \phi) + \rho_{pf} \phi, \quad (2)$$

where ϕ_o is initial porosity, ρ_g is grain density, and ρ_{pf} is density of the pore fluid.

Next step is to calculate elastic moduli (*e.g*. Mavko *et al*. 2009):

$$\text{Shear modulus, } G = \rho_b v_S^2, \quad (3)$$

$$\text{P-wave modulus, } M = \rho_b v_P^2, \quad (4)$$

$$\text{Bulk modulus, } K = M - 4G/3. \quad (5)$$

The uniaxial, ε_M, and bulk, ε_K, elastic strain can be calculated:

$$\varepsilon_M = \sigma_v/M, \quad (6)$$

$$\varepsilon_K = \sigma_H/K. \quad (7)$$

The reasoning is now that the elastic strain measured from velocities in the laboratory will correspond to elastic strain derived from well logs *in situ*. This is justified by the finding that elastic waves in chalks are in the low frequency regime (Biot 1956) for frequencies up to 1 MHz (Fabricius *et al*. 2010), *i.e.* well above the logging frequency (20-35 kHz) and laboratory frequency (300 kHz and 600 kHz, for respectively P- and S-waves). We thus infer that there is a robust basis for implementing rock mechanical data to *in situ* conditions, where well logs can give information on ϕ, ρ_b, v_P and v_S, so that elastic moduli can be calculated. Vertical effective *in situ* stress, σ_v', can be estimated from depth, d, density of overburden, ρ_{ob}, the acceleration of gravity, g, and pore pressure, P:

$$\sigma_v' = g\, d\, \rho_{ob} - aP, \quad (8)$$

where a is Biot's coefficient (Biot & Willis 1957):

$$a = 1 - K_{fr}/K_{min}. \quad (9)$$

Bulk modulus of the mineral K_{min} is derived from tabulated data, or via the method presented by

Meireles & Fabricius (2023). When the bulk modulus of the pore fluid, K_{fl} can be assessed, bulk modulus of the mineral frame K_{fr} can be modelled by using Gassman's equation (Gasmann 1951):

$$\frac{K}{K_{min}-K}=\frac{K_{fr}}{K_{min}-K_{fr}}+\frac{K_{fl}}{\phi\left(K_{min}-K_{fl}\right)} \qquad (10)$$

Geological setting

The Valdemar field is located in the Danish sector of the central North Sea. It is over-pressured and unlike most reservoirs in the Danish Central Graben, the Valdemar field mainly hosts hydrocarbons in the Lower Cretaceous Tuxen and Sola formations, although hydrocarbons are also produced from the Upper Cretaceous chalks (Danish Energy Agency 2013). The western part of the Valdemar field is dominated by an elongated N-S structure that presents two structural highs (in this study represented by respectively Valdemar-2H and Bo-2X) separated by a saddle point (Fig. 1). In the eastern part of the field, a separate dome structure hosting hydrocarbons remains undeveloped (represented by Boje-2C). The geological setting and sedimentology of the Valdemar Field have been studied by several authors (*e.g.* Jakobsen *et al*. 2004, 2005; Ineson *et al*. 2022a, 2022b; Jelby *et al*. 2022). The studied formations comprise interbedded chalk, slightly marly chalk, marly chalk, chalky marlstones, marlstones and shale (Fig. 2). Blok *et al*. (2023) studied the clay mineralogy of these formations and found kaolinite to dominate (average content around 50%) followed by illite, mixed layer illite/smectite and chlorite. Pyrite content is low (0-5%) but can play a role in electrical conductivity (Storebø *et al*. 2022). Due to the varied lithology, water saturation varies significantly downhole. In combination with some questionable early downhole formation-tester pressure data, this has caused the belief that the reservoir is compartmentalized stratigraphically (Jakobsen *et al*. 2005; Glad *et al*. 2022), but a more detailed analysis indicates pore pressure equilibrium between Sola and Tuxen formations in a given structure (Fabricius *et al*. 2005).

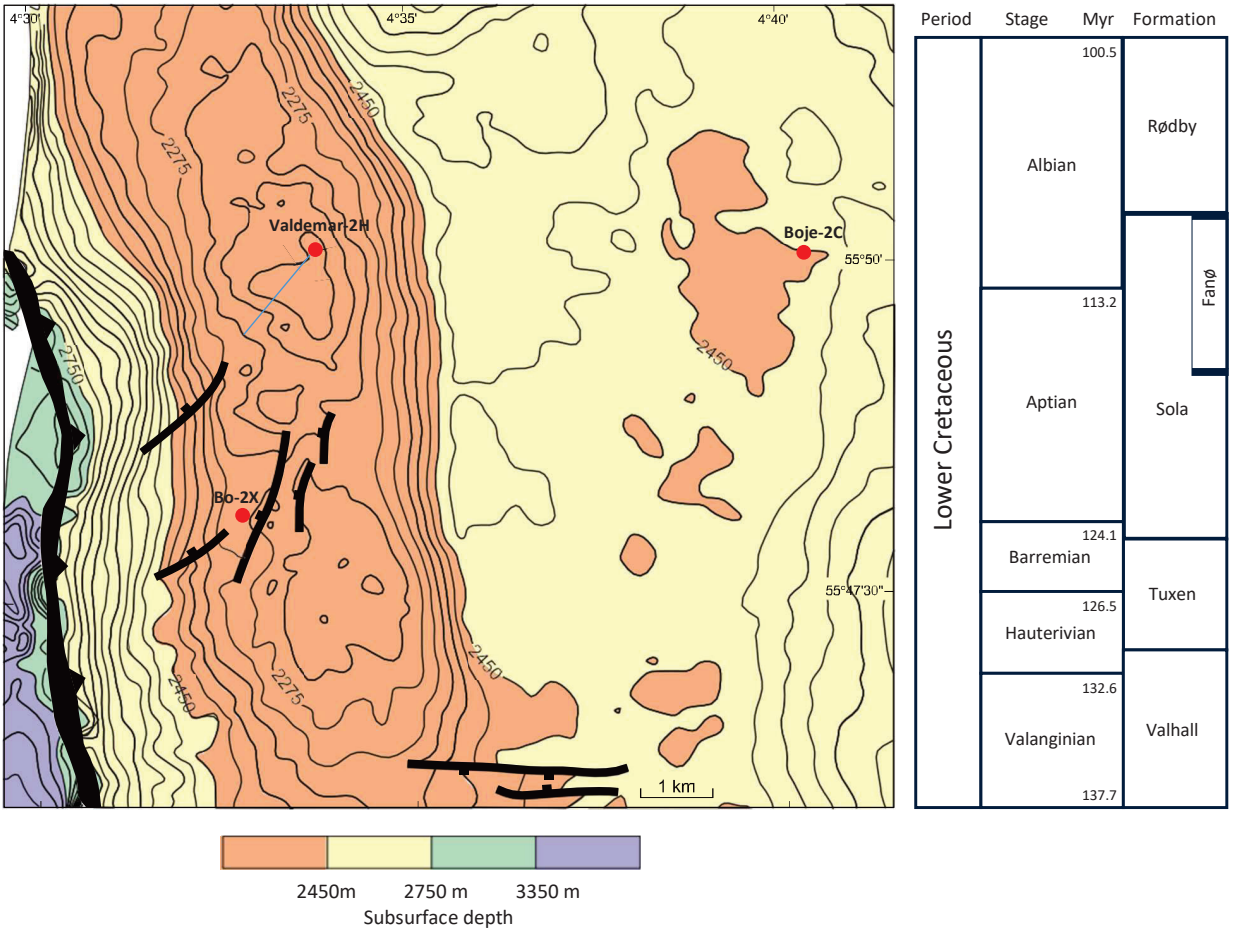
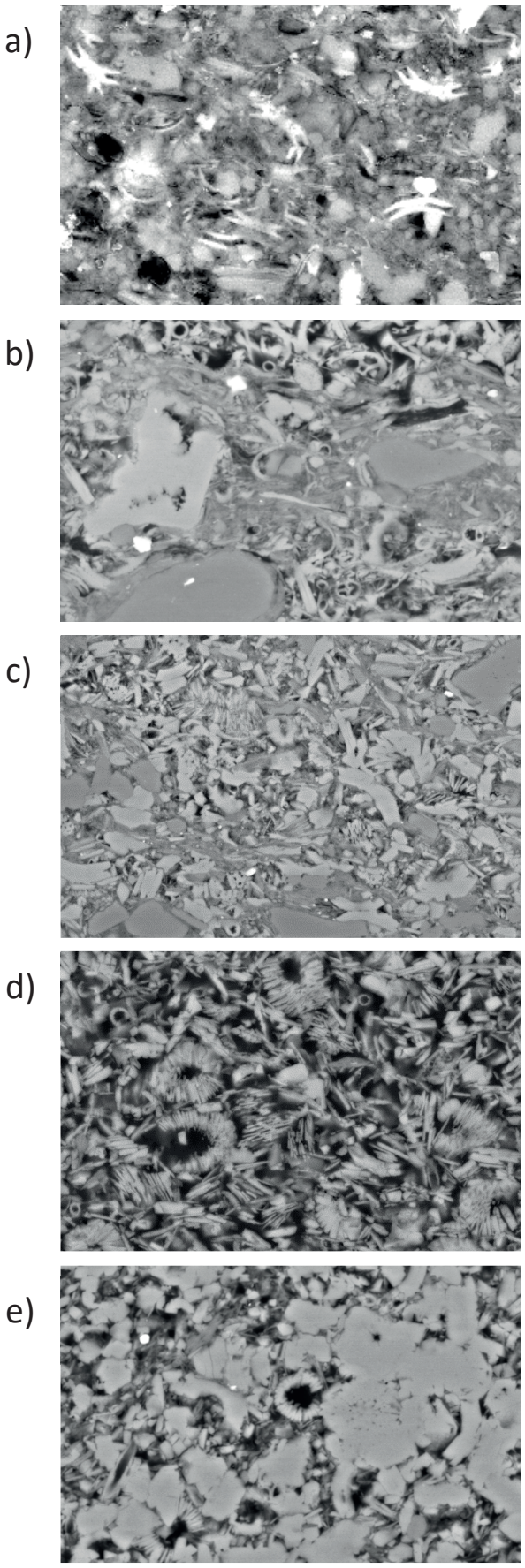


Fig. 1. (a) Structure map of the Lower Cretaceous Tuxen Formation (modified after Jakobsen *et al.* 2004) (b) Stratigraphic column (modified after Jelby *et al*. 2022).



Methodology

Downhole vertical elastic deformation is calculated from well logs covering the Lower Cretaceous Cromer Knoll Group, comprising Valhall, Tuxen, Sola and Rødby formations of wells Bo-2X, Valdemar-2H, and Boje-2C (Fig. 3), bottomhole temperature recorded was respectively; 83ºC, 80ºC, and 95ºC. Pore pressure data were available from the downhole formation tester tool of Bo-2X and Boje-2C. The data indicate an overpressure of 3 MPa in Bo-2X and of 9 MPa in the deeper Boje-2C. No pressure data are available for Valdemar-2H, but because this well is located in the same structure as Bo-2X, a similar overpressure is assumed (Fig. 1).

The caliper log indicates that the holes in Bo-2X and Boje-2C are practically in gauge, while the close to horizontal hole of Valdemar-2H is rough, in the sense that intervals with high natural gamma ray signal tend to have high diameter. The natural gamma ray log fluctuates as a reflection of varying content of radioactive clays, but in general, calcite is the loadbearing phase (Meireles & Fabricius 2023). The natural gamma ray log was used for estimating solid volume fraction of calcite, V_c, and of noncarbonates, V_{ir}.

All wells have deep (R_t) as well as medium (R_m) resistivity information. Boje-2C was drilled with oil-based mud, and mud filtrate invasion causes no discernable difference between the deep and medium resistivity logs. Bo-2X and Valdemar-2H were drilled with water-based mud, and whereas only a small split between the two resistivity-curves is seen for well Bo-2X, a significant split between the two curves is seen in Valdemar 2H. This can reflect mud filtrate invasion or be caused by the rough hole. The neutron porosity log was compared to the density log on an equivalent limestone porosity scale. The two logs indicate no marked effect of hydrocarbons. They are close where the natural gamma radiation is low and deviate where natural gamma radiation is high, so that a high clay content is indicated by a high neutron porosity. The bulk density log and medium resistivity logs were used for iterative calculation of near wellbore water saturation and porosity (S_{xo} and ϕ) by using grain density, ρ_g, derived from core data:

Fig. 2. Backscatter electron micrographs. **a**) Upper Sola Formation, Valdemar-1P, 7295 ft ss. Mixed sediment of clay, coccoliths and silt. **b**) Lower Sola Formation, Boje-2C, 8220 ft ss. Laminated carbonate ooze and clay with silt and shell fragments. **c**) Upper Tuxen Formation, Boje-2C, 8256 ft ss. Laminated carbonate ooze, clay and silt. **d**) Middle Tuen Formation, Valdemar-2H, 7568 ft ss. Massive carbonate ooze with nannoconids. **e**) Lower Tuxen Formation, Boje-2C, 8442 ft ss. Clay bearing chalk with recrystallized calcite.

$$\phi = (\rho_g - \rho_b)/(\rho_g - \rho_{pf}), \quad (11)$$

$$S_{xo} = (R_w/(\phi^{\,m} R_m))^{1/n}, \quad (12)$$

$$\rho_{pf} = \rho_w S_{xo} + (1 - S_{xo})\rho_{hc}. \quad (13)$$

Based on service company special core analysis data involving measurements of electrical conductivity of chalk samples saturated with systematically varying salinity of saturating brine and hydrocarbon content, the porosity exponent, m, was set to 2.02 for Bo-2X and Valdemar-2H, and to 2.00 for Boje-2C, similarly

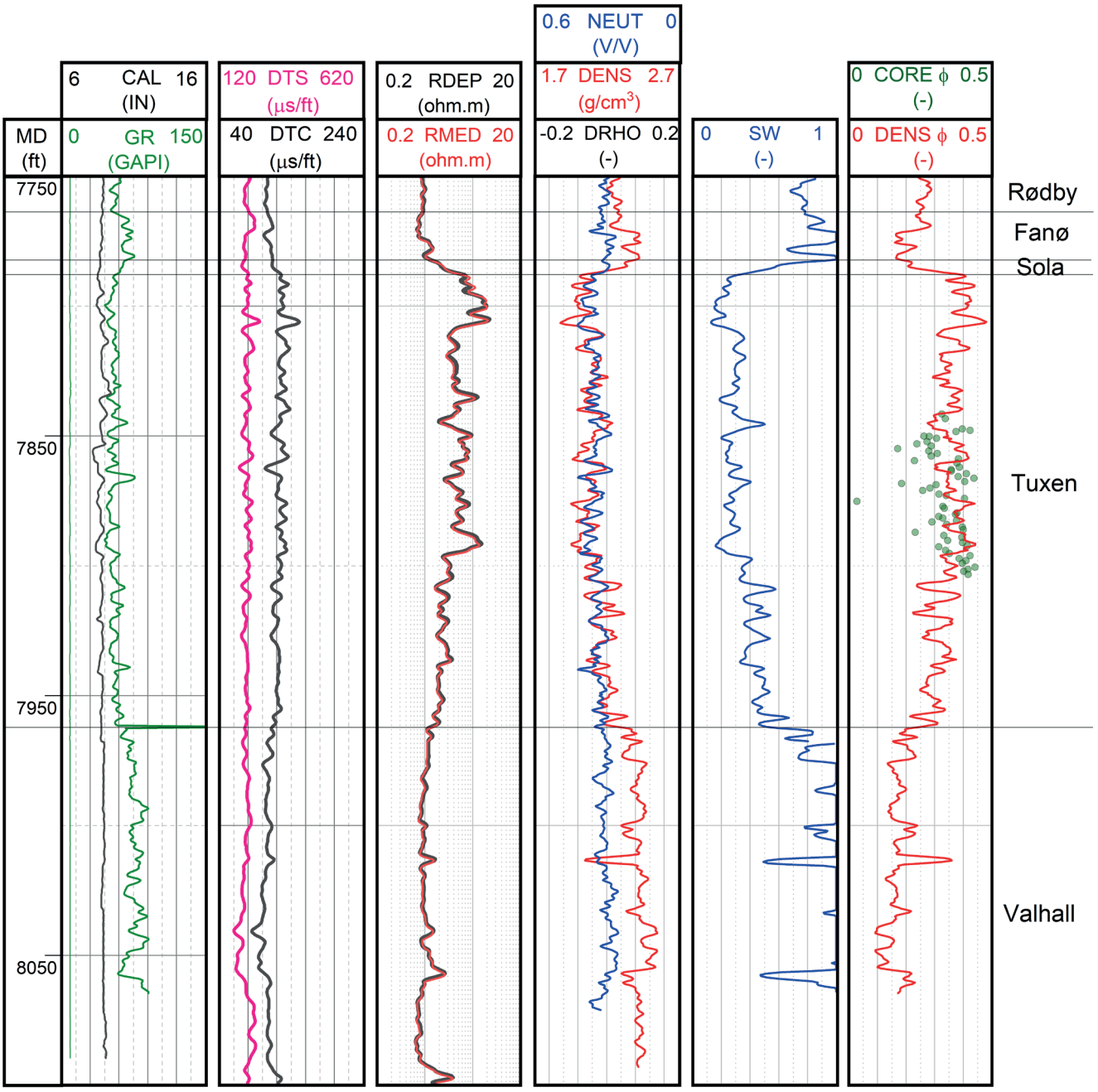


Fig. 3. Petrophysical downhole logs. **a**) Bo-2X (2307 m – 2407 m sub sea level). **b**) Valdemar-2H (horizontal: 2179–2273 m sub sea level). **c**) Boje-2C (2456–2578 m sub sea level). CAL: Borehole diameter (inches) measured by caliper; GR: Natural gamma ray radiation intensity measured in API units; DTS: Travel time (slowness) of elastic shear waves measured in microseconds per foot; DTC: Travel time (slowness) of elastic compressional waves measured in microseconds per foot; RDEP: Deep electrical resistivity measured in Ωm; RMED: Medium electrical resistivity measured in Ωm; NEUT: Neutron porosity calibrated in limestone, volume fraction V/V; DENS: Bulk density measured by gamma ray attenuation; DRHO: tool-indicated uncertainty on density reading; SW: modelled water saturation; Porosity, ϕ, from core data (CORE) and as calculated from density log (DENS).

the saturation exponent, n, was set to 2.11 for Bo-2X and Valdemar-2H, and to 2.00 for Boje-2C. Resistivity of pore water, R_w was estimated from temperature and pore water salinity (30.000 ppm for Bo-2X and Valdemar-2H and 100.000 ppm for Boje-2C). Water density, ρ_w, and bulk modulus, K_w, were estimated from salinity, temperature and pressure (Batzle & Wang 1992, as cited in Mavko *et al*. 2009). Hydrocarbon density, ρ_{hc}, and bulk modulus, K_{hc}, were estimated from production data, pressure and temperature. The water saturation, S_w, was then calculated from:

$$S_w = (R_w/(\phi^m R_t))^{1/n}. \quad (14)$$

The water saturation was found to be relatively low

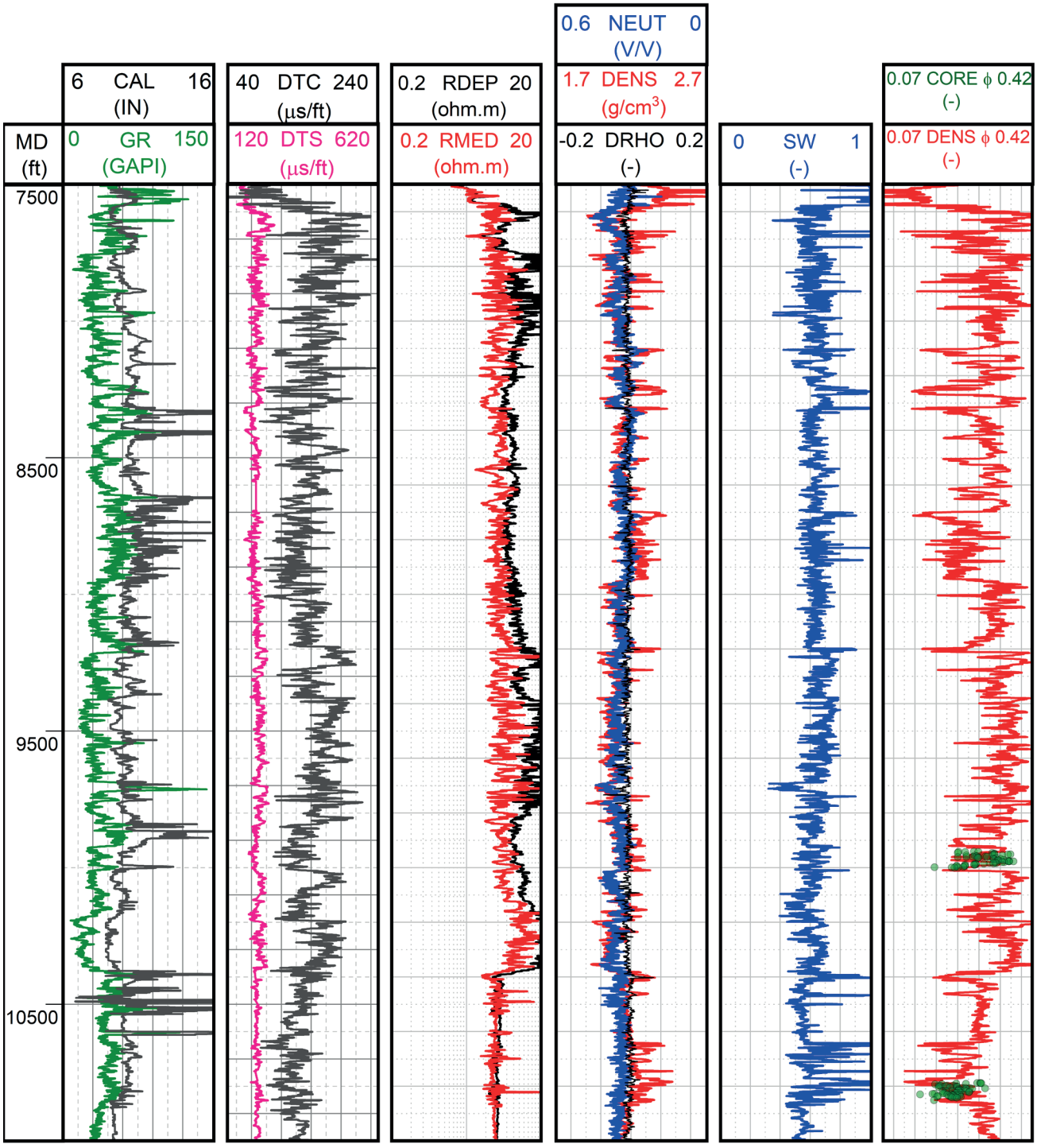


Fig. 3b. Valdemar-2H.

(S_w = 0.25) in the upper 100 ft of the Tuxen Formation of Bo-2X but increases to S_w = 0.6 near the transition to Valhall Formation. Bearing in mind the high and highly variable specific surface of these clay-rich chalks, these saturations would both correspond to irreducible water saturation (Fabricius *et al*. 2005). The high water saturation of Valdemar-2H is probably the effect of moderate clay content and can well be irreducible. In the Tuxen Formation of Boje-2C in the eastern structure, S_w increases depth-wise from 0.4 to 1.0, probably reflecting a transition to the water zone.

In situ P-wave modulus, *M*, and bulk modulus, *K*, were directly calculated from logging data (equations 3-5), whereas bulk modulus of the pore fluid, K_{fl}, and bulk modulus of the mineral phase, K_{min}, depend on component values. Both can be estimated as softest and stiffest mixtures, according to Reuss and Voigt bounds (Mavko *et al*. 2009):

$$1/K_{fl} = S_w/K_w + (1-S_w)/K_{hc}, \text{ or} \quad (15)$$

$$K_{fl} = S_w K_w + (1-S_w) K_{hc}, \text{ and} \quad (16)$$

$$1/K_{min} = V_c/K_c + (V_{ir})/K_{ir}, \text{ or} \quad (17)$$

$$K_{min} = V_c K_c + (V_{ir}) K_{ir}. \quad (18)$$

This allows a softest and stiffest estimate of K_{fr}. The bulk modulus of calcite, K_c, was set to 71 GPa, in accordance with citations in Mavko *et al*. (2009). Bulk modulus of the non-carbonate fraction, K_{ir}, was mod-

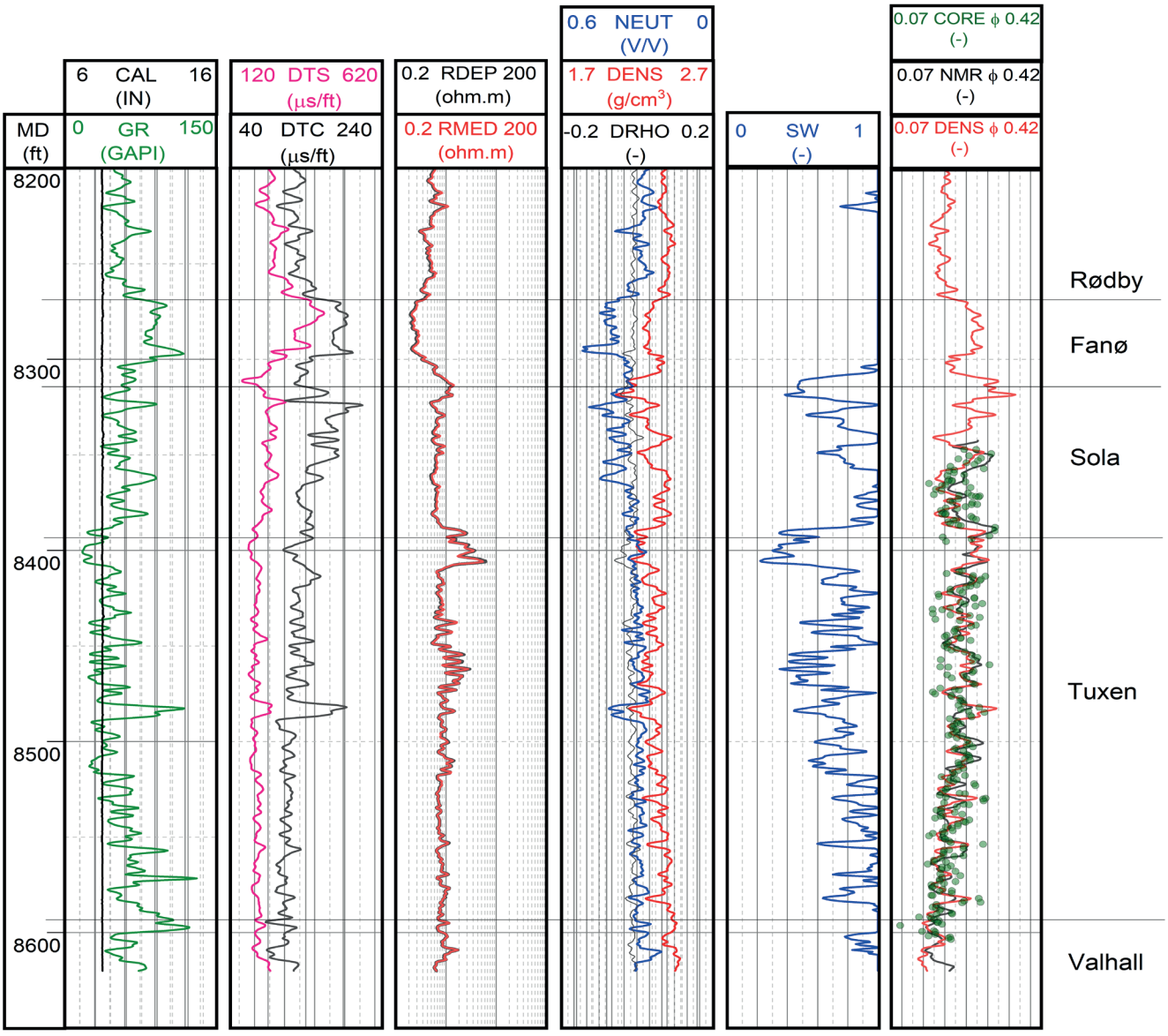
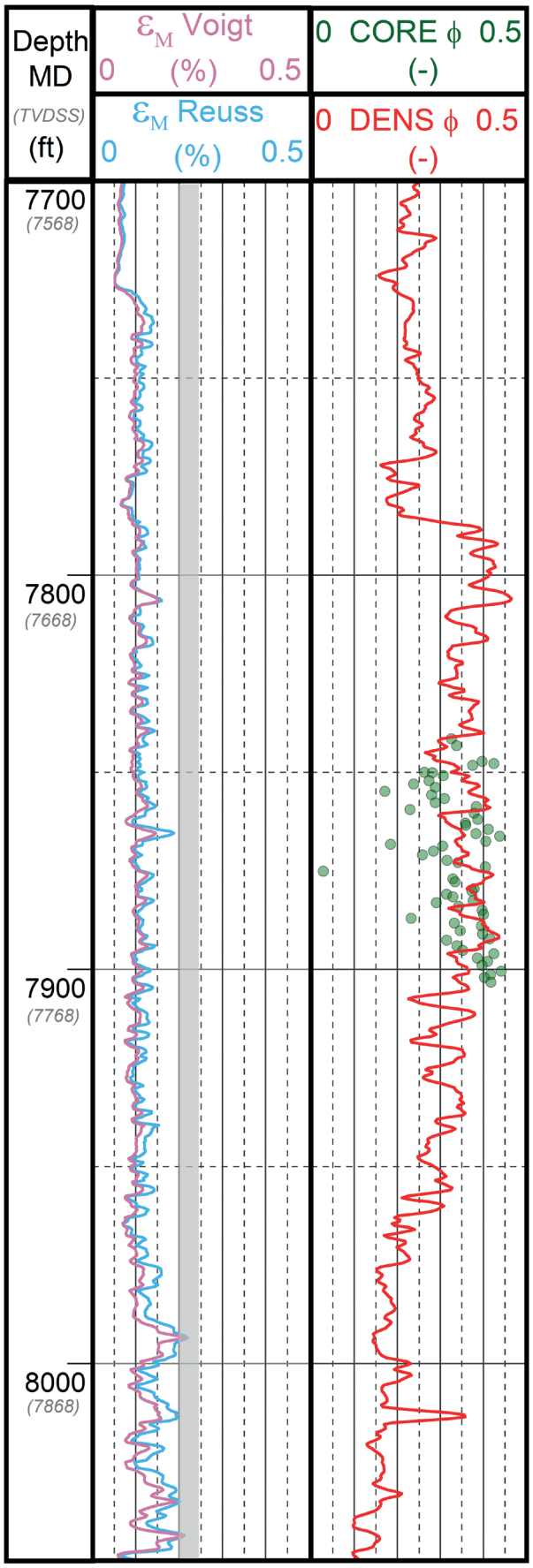


Fig. 3c. Boje-2C.



elled according to the method of Meireles & Fabricius (2023). Gassmann's equation (10) was used for the estimate of bulk modulus of the frame, K_{fr}, and Biot's coefficient, a was calculated from equation (9).

In situ vertical effective stress, σ_v', was calculated from equation (8). Data on vertical depth below sea level, d, were available for all wells (Figure 4) and the acceleration of gravity was set to 9.81 m/s^2. The average density of the overburden was set to 2.00 g/cm^3. The vertical *in situ* elastic strain can now be estimated from:

$$\varepsilon_M = \sigma'/M. \quad (19)$$

Results and discussion

Resulting porosity and elastic strain curves (Fig. 4) indicate that *in situ* elastic strain falls in the range 0.05% to 0.25%, which is relatively high as compared to typical Upper Cretaceous Chalk (Fabricius 2020). The calculated strain reflects a sediment with contact cementation but little pore filling cementation as a reflection of the absence of observed stylolites (Glad *et al*. 2022). The stiffest and softest choice of mixing of minerals and of pore fluids (Voigt and Reuss) do not give significantly different results. It should be noted though, that the difference between the Voigt and Reuss bounds is largest when near equal amounts of two components are mixed (non-carbonate and calcite, or oil and water; refer to equations 15–18).

For Bo-2X, elastic *in situ* strain was found to be relatively constant around 0.1% in the Tuxen Formation, whereas it alternates between 0.1% and 0.2% in the underlying Valhall Formation. The higher strain represents intervals with relatively high natural GR radiation reflecting high content of clay, where integrated contact area between calcite crystals is smaller and stress accordingly higher. Similarly, for Valdemar-2H, elastic *in situ* strain is rather constant and close to 0.1% as a reflection of the well being drilled horizontally in an interval with moderate clay content. In Boje-2C with higher overpressure (9 MPa *vs*. 3 MPa) and consequent lower effective stress in spite of deeper level, the situation is different: In the modestly clay-bearing Rødby and Sola formations and the underlying relatively clay poor Tuxen Formation, *in situ* strain is generally below 0.1% in the

Fig. 4. Modelled elastic strain logs, where critical strain is marked by grey box. **a**) Bo-2X (2307–2407 m subsea level). **b**) Valdemar-2H (horizontal: 2179–2273 m sub sea level). **c**) Boje-2C (2456–2578 m sub sea level). The *in situ* vertical uniaxial strain, ε_M, was modelled from *in situ* vertical effective stress and stiffness of rock and fluid components mixed in stiffest (Voigt) and softest (Reuss) way. Porosity, ϕ, from core data (CORE) and as calculated from density log (DENS).

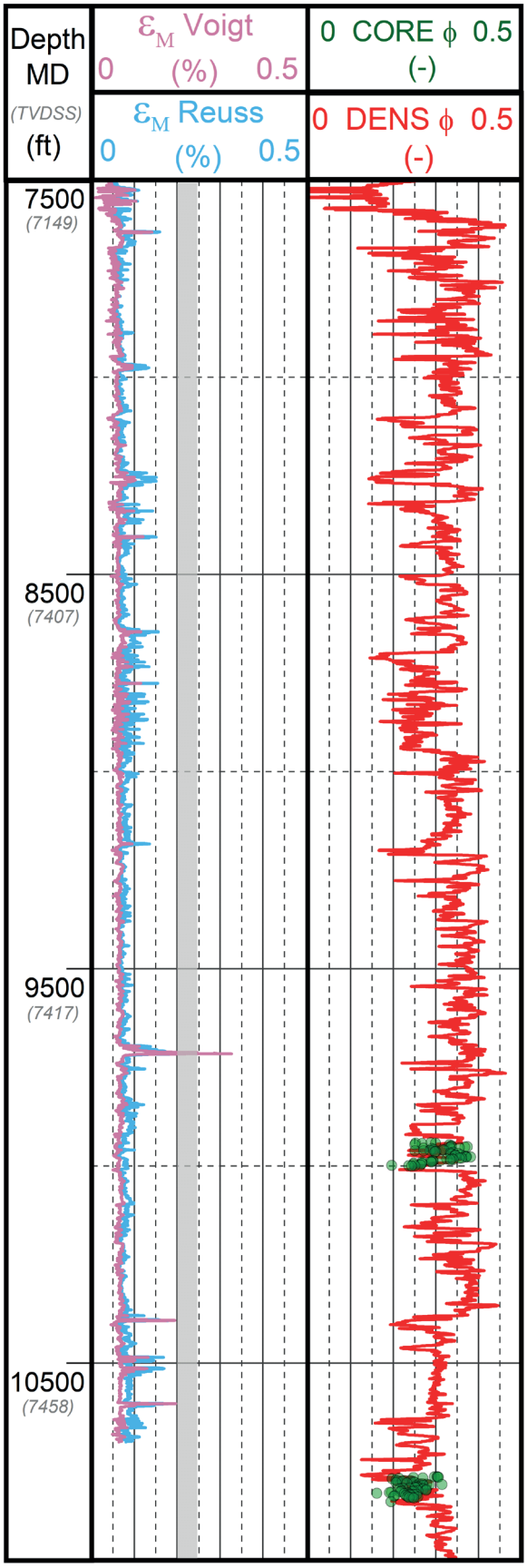


Fig. 4b. Valdemar-2H.

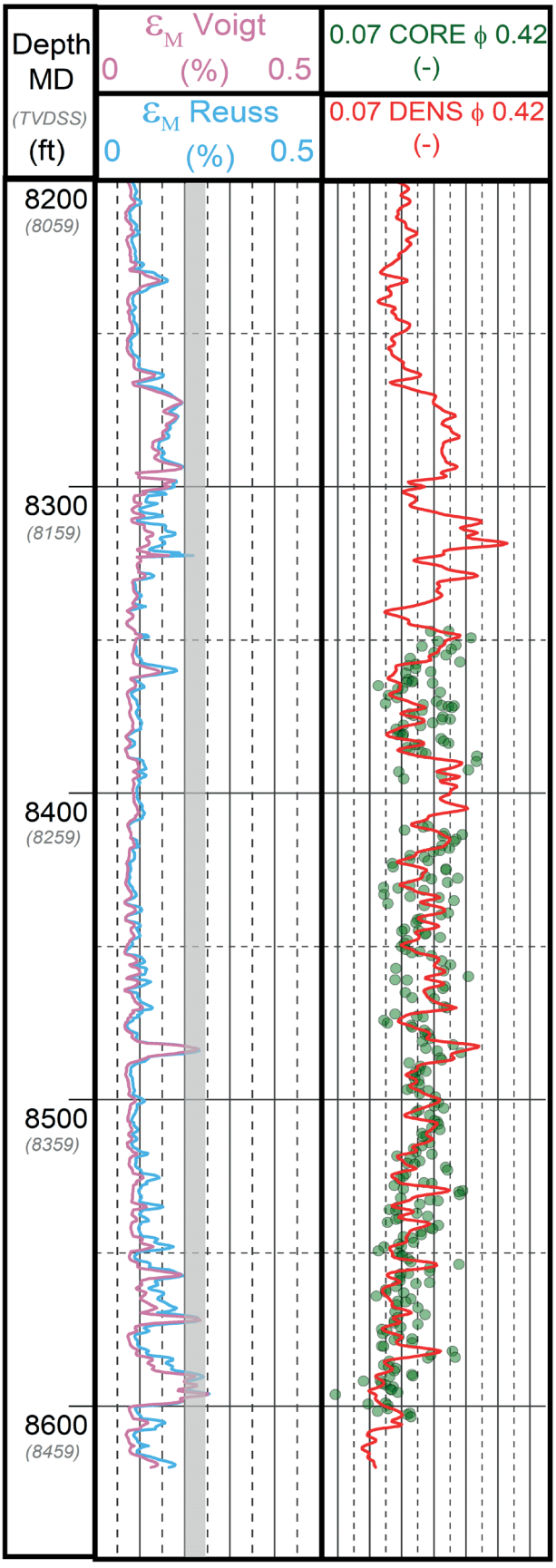


Fig. 4c. Boje-2C.

upper part but increases with depth as clay content and water saturation increases, and in single beds is estimated to exceed 0.3%. In the clay-rich Fanø Member in situ strain is modelled to approach 0.3%. In situ strain higher than critical strain according to Orlander & Christensen (2025; 0.20–0.24%) is thus generally found outside potential reservoir intervals.

The analyzed data are recorded pre-production, so falling pore pressure due to production could change this picture. For example, in wells from Ekofisk field, 20 years of production led to an increase in modelled *in situ* strain from 0.2% to 0.4% (Fabricius & Omdal 2021).

For Boje-2C the present vertical stress is around 50 MPa, and the pore pressure 34 MPa including 9 MPa over-pressure. For an interval with M = 12.5 GPa, this corresponds to an in situ strain of 0.13%, and if all over-pressure were released, to an in situ strain of 0.2%, close to the critical interval for pore collapse. For the two western wells in the Valdemar field, present vertical stress is around 45 MPa, and pore pressure is 26 MPa including 3 MPa overpressure. For an interval with M = 12.5 GPa, this corresponds to an in situ strain of 0.13%, and if all overpressure were released, to an in situ strain of 0.15%, apparently safely below the critical strain for pore collapse. For the Valdemar field the presented method thus allows us to identify pore-collapse-susceptible zones that could fail during depletion of the reservoir. This could inspire improving completion design, planned trajectory of infill wells, as well as abandonment practices. It should be borne in mind that the present approach assumes a stress field corresponding to uniaxial strain, so results should not be seen as more than an indication. More reliable results would require geomechanical modelling based on more detailed stress field information.

Conclusion

We have presented a method that allows us to model *in situ* elastic vertical strain from geophysical bore hole data. This is highly relevant for predicting potential for pore collapse in fragile reservoirs as chalk. The results are compared with experimental data which indicate that for a given stress-geometry, the onset of pore collapse in a given sedimentary rock is governed by a single critical elastic strain, irrespective of porosity and saturating pore fluid.

The analysed data represent the Lower Cretaceous chalk of Valdemar field and were recorded prior to production. At that stage the *in situ* strain was relatively low, and even if all over-pressure were relieved, no critical strain is to be anticipated in Bo-2X and Valdemar-2H. By contrast, if Boje-2C, where pore overpressure is higher, were put in production and all over-pressure released, reservoir intervals that presently have an *in situ* strain above 0.13%, would come near the critical strain of 0.2%.

Acknowledgements

We gratefully acknowledge the Danish Underground Consortium (TotalEnergies E&P Denmark, Noreco and Nordsøfonden) for granting permission to publish this work. The study was funded by the Danish Offshore Technology Centre (DTU Offshore). Morten Leth Hjuler is thanked for recording backscatter electron micrographs. Helle Foged Christensen and an anonymous referee are thanked for critical reviews of an earlier version of this paper.

References

Anderson, R.A., Edwards, D.P. & Ormerod, L. 1985: Log interpretation techniques to evaluate formation collapse in the North Sea chalk. Paper for Symposium of North Sea Chalk, sponsored by the Norwegian government, Stavanger, Norway, 21–22 May 1985, 1–20.

Batzle, M. & Wang, Z. 1992: Seismic properties of pore fluids. Geophysics 57, 1396–1524. https://doi.org/10.1190/1.1443207.

Biot, M.A. 1956: Theory of propagation of elastic waves in a fluid-saturated porous solid. I. Low-frequency range. The Journal of the Acoustical Society of America 28, 168–178. https://doi.org/10.1121/1.1908239

Biot, M.A. & Willis, D.G. 1957: The elastic coefficient of the theory of consolidation. Journal of Applied Mechanics 24, 594–601. https://doi.org/10.1115/1.4011606

Blok, C.N., Adatte, T., Ineson, J.R., Sheldon, E., Jelby, M.E., Smit, F.W.H., Lauridsen, B.W., Anderskouv, K. & Bodin, S. 2023: Clay mineral assemblages as a tool in source-to-sink studies: an example from the Lower Cretaceous of the North Sea Basin. Bulletin of the Geological Society of Denmark 71, 99–113. https://doi.org/10.37570/bgsd-2023-71-06

Bredesen, K., Lorentzen, M., Nielsen, L. & Mosegaard, K. 2021: Quantitative seismic interpretation of the Lower Cretaceous reservoirs in the Valdemar Field, Danish North Sea. Petroleum Geoscience 27, 1–17. https://doi.org/10.1144/petgeo2021-016

Danish Energy Agency 2013: Oil and gas production in Denmark 2013 and subsoil use, 105 pp. Copenhagen: Energistyrelsen.

Fabricius, I.L., Olsen, C. & Prasad, M. 2005: Log interpretation of marly chalk, the Lower Cretaceous Valdemar Field, Danish North Sea. Application of iso-frame and pseudo water film concepts. The Leading Edge 24, 449–560. https://doi.org/10.1190/1.1926807

Fabricius I.L., Bächle, G.T. & Eberli, G.P. 2010: Elastic moduli of dry and water-saturated carbonates – effect of depositional texture, porosity, and permeability. Geophysics 75, 65–78. https://doi.org/10.1190/1.3374690

Fabricius I.L. 2020: Porosity in chalk – roles of elastic strain

and plastic strain. Sedimentology 67, 3451–3470. https://doi.org/10.1111/sed.12750

Fabricius, I.L. & Omdal, E. 2021: Elastic strain of chalk due to oil production. Biot-Bažant Conference, June 1–3, 2021, Northwestern University, Evanston, IL.

Gassman, F. 1951: Über die Elastizität poröser Medien. Vierteljahrsschrift der Naturforschenden Gesellschaft in Zürich 96, 1–23.

Glad, A.C., Amour, F., Welch, M.J., Clausen, O.R., Anderskouv, K. Ineson, J.R., Sheldon, E. & Nick, H.M. 2022: Natural fractures and discontinuities in a Lower Cretaceous chalk-marlstone reservoir, Valdemar Field, Danish North Sea. Marine and Petroleum Geology 136, 1–15. https://doi.org/10.1016/j.marpetgeo.2021.105445

Gram, T.B., Ditlevsen, F.P., Mosegaard, K. & Fabricius, I.L. 2021: Water-flooding and consolidation of reservoir chalk – effect on porosity and Biot's coefficient. Geophysical Prospecting 69, 495–513. https://doi.org/10.1111/1365-2478.13047

Hermansen, H., Thomas, L.K., Sylte, J.E. & Aasbøe, B.T. 1997: Twentyfive years of Ekofisk reservoir management. Presented at the Annual Technical Conference and Exhibition, San Antonio, Texas, 5–8 October. SPE-38927. https://doi.org/10.2118/38927-ms

Ineson, J.R., Petersen, H.I., Andersen, C., Bjerager, M., Jakobsen, F.C., Kristensen, L., Mørk, F. & Sheldon, E. 2022a: Early Cretaceous stratigraphic and basinal evolution of the Danish Central Graben: a review: Bulletin of the Geological Society of Denmark 71, 75–98. https://doi.org/10.37570/bgsd-2022-71-05

Ineson, J.R., Lauridsen, B.W., Lode, S., Sheldon, E., Sørensen, H.O., Wisshak, M. & Anderskouv, K. 2022b: A condensed chalk–marl succession on an Early Cretaceous intrabasinal structural high, Danish Central Graben: Implications for the sequence stratigraphic interpretation of the Munk Marl Bed. Sedimentary Geology 440, 106234, 1–24. https://doi.org/10.1016/j.sedgeo.2022.106234

Jakobsen, F., Ineson, J.R. Kristensen, L. & Stemmerik, L. 2004: Characterization and zonation of a marly chalk reservoir: the Lower Cretaceous Valdemar Field of the Danish Central Graben. Petroleum Geoscience 10, 21–33. https://doi.org/10.1144/1354-079303-584

Jakobsen, F., Ineson, J.R., Kristensen, L., Nytoft, H.P. & Stemmerik, L. 2005: The Valdemar Field, Danish Central Graben: field compartmentalization and regional prospectivity of the Lower Cretaceous chalk play. In: Doré, A.G. & Vinning, B.A. (eds): Petroleum Geology: North-West Europe and Global Perspectives – Proceedings of the 6th Petroleum Geology Conference, 177–186. https://doi.org/10.1144/0060177

Jelby, M.E., Ineson, J.R., Thibault, N., Bodin, S., Blok, C.N., Edvardsen, N., Clemmensen, T.S., Buls, T. & Anderskouv, K. 2022: Facies and depositional processes of Lower Cretaceous carbonates, Danish Central Graben. Bulletin of the Geological Society of Denmark 71, 51–74. https://doi.org/10.37570/bgsd-2022-71-04

Mavko, G., Mukerji, T., and Dvorkin, J., 2009: Rock physics handbook: Tools for seismic analysis in porous media. Cambridge University Press. https://doi.org/10.1017/cbo9780511626753

Meireles, L.T.P. & Fabricius, I.L. 2022: Strain modeling in a marly chalk reservoir. In: Delgado-Martin, J., Muñoz-Ibañez, A. & Falcon-Suarez, I.H. (eds): 6th International Workshop on Rock Physics, A Coruña, Spain 13 –17 June 2022: Book of Abstracts, 53–54. https://doi.org/10.17979/spudc.000005

Meireles, L.T.P. & Fabricius, I.L. 2023: Deriving mineral moduli of the noncarbonate fraction in a marly chalk reservoir using petrophysical logging data and an isoframe model. Geophysics 88, D411-D425. https://doi.org/10.1190/geo2022-0493.1

Nermoen, A., Korsnes, R.I., Storm, E., Stodle, T., Madland, M.V. & Fabricius, I.L. 2018: Incorporating electrostatic effects into the effective stress relation – insights from chalk experiments. Geophysics 83, MR123-MR135. https://doi.org/10.1190/geo2016-0607.1

Orlander, T. & Christensen, H.F. 2024: Compaction phases and pore collapse in Lower Cretaceous chalk – insight from Biot's coefficient. Rock Mechanics and Rock Engineering. https://doi.org/10.1007/s00603-024-03963-x

Orlander, T. & Christensen, H.F. 2025: Elastic and plastic deformation of Lower Cretaceous North Sea Chalk during stress and time-dependent uniaxial strain compaction. Submitted to Rock Mechanics and Rock Engineering. https://doi.10.1007/s00603-025-04691-6

Proestakis, E., Christensen, H.F., Meireles, L.T.P., Storebø, E.M., Shamsolhodaei, A. & Orlander, T. 2023: Detection and picking of shear wave arrival for stiffness evaluation of highly porous chalk. Geophysical Prospecting 72, 733–751. https://doi.org/10.1111/1365-2478.13435

Ruddy, I., Andersen, M.A., Pattillo, P.D., Bishlawi, M. & Foged, N. 1998: Rock compressibility, compaction, and subsidence in a high-porosity chalk reservoir: A case study of Valhall Field. Journal of Petroleum Technology 41, 741–746, (SPE-18278-PA). https://doi.org/10.2118/18278-pa

Santamarina, J.C. 2001: Soil behavior at the microscale: Particle forces. Proc. Symp. Soil Behavior and Soft Ground Construction, in honor of Charles C. Ladd – October 2001, MIT, 31 pp. https://doi.org/10.1061/40659(2003)2

Storebø, E.M., Hjuler, M.L., Meireles, L.T.P. & Fabricius, I L. 2022: Effect of pyrite in water saturation evaluation of clay-rich carbonate. Petrophysics 63, 172–198. https://doi.org/10.30632/pjv63n2-2022a3

Microscopic character of the Lower Cretaceous Tuxen and Sola formations in the Boje-2C well, Danish Central Graben

IDA L. FABRICIUS, MORTEN L. HJULER, MADS E. JELBY & KRESTEN ANDERSKOUV

Geological Society of Denmark
https://2dgf.dk

Received 20 December 2024
Accepted in revised form 12 June 2025
Published online 20 October 2025

© 2025 the authors. Re-use of material is permitted, provided this work is cited. Creative Commons License CC BY: https://creativecommons.org/licenses/by/4.0/

Fabricius, I.L., Hjuler, M.L., Jelby, M.E. & Anderskouv, K. 2025. Microscopic character of the Lower Cretaceous Tuxen and Sola formations in the Boje-2C well, Danish Central Graben. Bulletin of the Geological Society of Denmark, Vol. 71, pp. 127–162. ISSN 2245-7070. https://doi.org/10.37570/bgsd-2025-71-08

The Lower Cretaceous Tuxen and Sola formations in the Danish Central Graben (North Sea) constitute pelagic chalks and marlstones, which locally are hydrocarbon-bearing. Based on previous identification of 21 sedimentary facies in the cored Boje-2C well of the Boje Field, 66 samples were analysed through backscattered electron microscopy to delineate how the microscopic character reflects the macroscopic sedimentary facies and to identify indications of diagenesis. For most samples, microscopic characters can clearly be related to the previously identified sedimentary facies. Bioturbation and shear deformation, however, were not consistently reflected in the microscopic character. In all samples, the microtexture is characterised by massive or laminated calcareous mudstone with varying content of mainly kaolinitic clay and only sparse remains of microfossils or shell fragments, whereas particles of quartz silt and kaolinitic claystone silt are common. Porosity is mainly interparticular, typically reaching 25% in the Sola and upper Tuxen formations, and declining with depth to ca. 17% in the lower Tuxen and upper Valhall formations. Diagenesis is reflected in the occurrence of calcite cementation, pyrite and calcite-rimmed dolomite, and some pores may represent moulds after silicious microfossil fragments, which probably sourced the locally observed silicification of the sediment. Further, in clay-poor intervals below the oil zone, a significant diagenetic feature constitutes biogenic calcite mud particles that become increasingly recrystallized and euhedral with depth. It is therefore possible that burial-related crystal ripening was delayed in the oil zone represented by the upper part of the core. In the underlying transition zone, which in the Boje-2C well comprises most of the Tuxen Formation, the degree of recrystallization increases with depth as water saturation increases. Pressure dissolution features were noted in clay-rich intervals, but proper stylolites were not encountered, reflecting the generally high clay content of these marly chalks.

Keywords. Aptian, Barremian, chalk, diagenesis, marlstone, SEM

Ida L. Fabricius [ilfa@dtu.dk] and Morten L. Hjuler, Department of Environmental and Resource Engineering, Technical University of Denmark, Denmark. Mads E. Jelby [jelby@geo.au.dk], Department of Geoscience, Aarhus University, Aarhus, Denmark. Kresten Anderskouv [ka@ign.ku.dk], Department of Geosciences and Natural Resource Management, University of Copenhagen, Denmark

Inferences of the depositional history of pelagic carbonates are largely based on macroscopic features, whereas rock properties are mainly controlled by features that can only be observed microscopically. The relation between microscopic features and depositional (macroscopic) facies in the Lower Cretaceous chalk and marlstone of the Tuxen and Sola formations in the Danish Central Graben (DCG), North Sea, has not been presented in detail. Herein, a systematic analysis of the microscopic character of macroscopically identified pelagic carbonate facies is presented as a case study, utilizing the cored section of the Boje-2C well in the central part of the DCG.

The Lower Cretaceous succession in the DCG is largely encompassed by the Cromer Knoll Group, an up to one kilometre thick succession of siliciclastic mudstone, marlstone and chalk of predominantly hemipelagic and pelagic origin (Figs 1A, 2; Copestake *et al.* 2003; Mutterlose & Bottini 2013; van Buchem *et al.* 2018). Initial exploration-related drilling campaigns in the DCG (e.g. Damtoft *et al.* 1992) led to the recognition of the Lower Cretaceous chalk

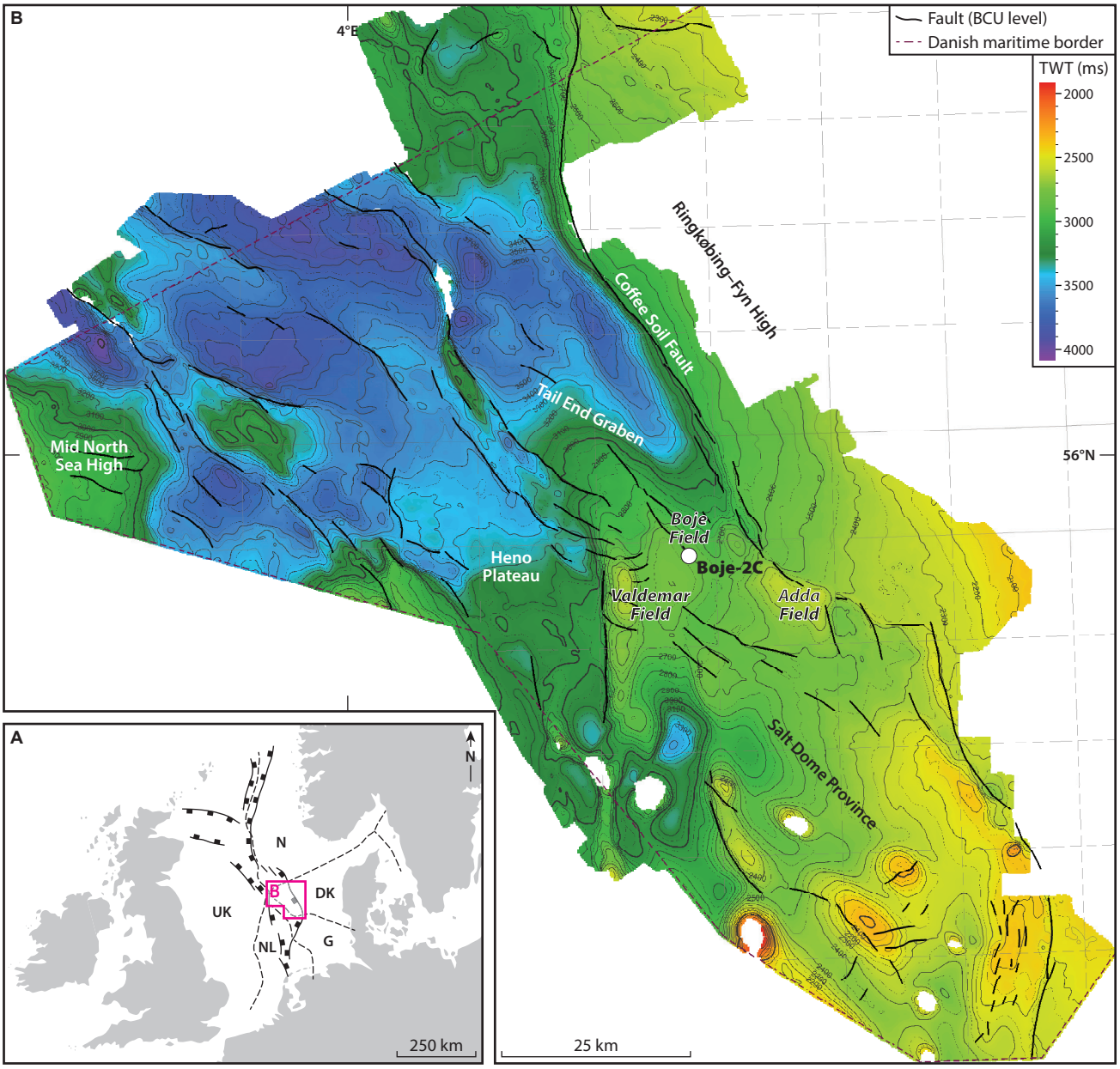


Fig. 1. A. Simplified structural configuration of the larger North Sea Basin (modified from Japsen *et al.* 2003; Møller & Rasmussen 2003), indicating the Danish (DK), German (G), Norwegian (N), Dutch (NL) and United Kingdom (UK) sectors of the Central Graben. **B**. Time-structure map (two-way travel time (TWT)) of the Base Cretaceous Unconformity (BCU), indicating the position of the Boje-2C well in the Boje Field located between the Valdemar Field and Adda Field (modified from Jelby *et al.* 2024, based on Ineson *et al.* 2022b).

succession as a potential reservoir, and with the Tuxen and overlying Sola formations (Hauterivian–Albian) being oil-bearing, the Valdemar Field and adjacent Adda Field were declared commercial (Fig. 1B; Ineson 1993). Consequently, these formations have been repeatedly drilled, geophysically logged, cored, and described with different focus, notably including: reservoir properties (Jakobsen *et al.* 2004, 2005; Fabricius *et al.* 2005; Storebø *et al.* 2022a, b; Meireles & Fabricius 2023); mineralogy, palaeoenvironment and palaeoclimate (Blok *et al.* 2022, 2023); fractures (Glad *et al.* 2022); as well as sedimentology and facies architecture (Michelsen *et al.* 1987; Ineson 1993; Ineson *et al.* 2022a; Jelby *et al.* 2022, 2024).

The oil-bearing well Boje-2C was drilled in 2013 in the Boje Field situated between the Adda and Valdemar fields (Fig. 1B). Interpretation of log and core data from the Tuxen and Sola formations indicates porosity in the range of 20–30% and permeability in the range of 0.01–1 mD (Storebø *et al.* 2022a, b). The specific surface area with reference to bulk volume varies from 10 to 40 m^2/cm^3, thus, although water saturation varies

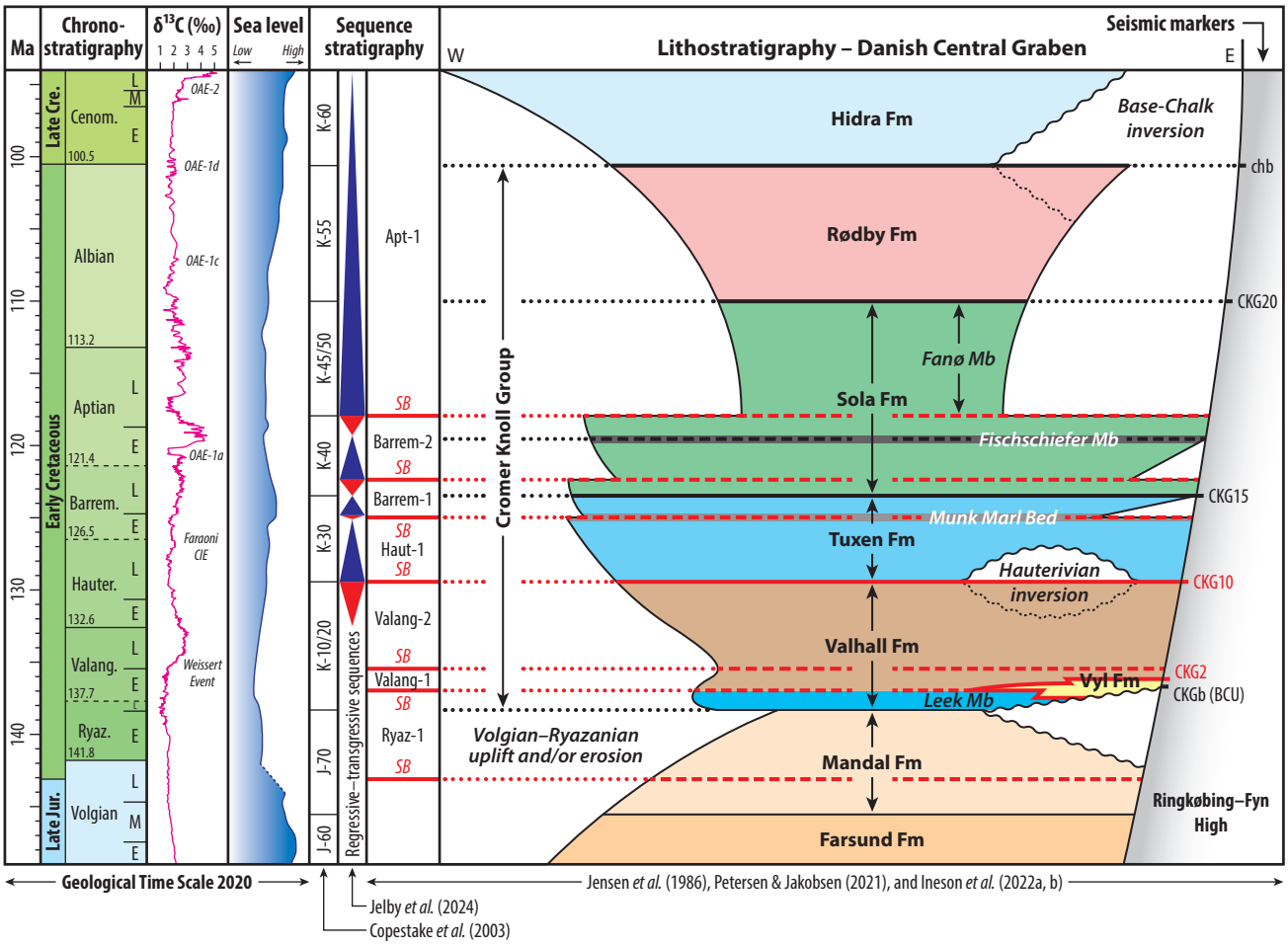


Fig. 2. Stratigraphic summary chart of the Danish Central Graben, showing the gross relative lateral distribution, sequence stratigraphic models of previous key studies, and key seismic horizons of the Lower Cretaceous Cromer Knoll Group in a W–E-oriented cross-section, compiled from Jensen *et al.* (1986), Petersen & Jakobsen (2021), Ineson *et al.* (2022a, b), and Jelby *et al.* (2024). Numerical ages, chronostratigraphy, stable carbon-isotope ($\delta^{13}C$) stratigraphy and events, as well as sea-level curve are compiled from Gale *et al.* (2020) and Hesselbo *et al.* (2020). BCU, Base Cretaceous Unconformity; SB, sequence boundary.

through the section, water is interpreted to be irreducible down to the upper part of the Tuxen Formation. Accordingly, no indication of compartmentalization has been reported (Storebø *et al.* 2022a, b).

Palaeoenvironmental studies indicate that deposition took place at ~46°N in a sub-photic, epicontinental ramp setting as part of the larger Euro-Boreal Realm (Blok *et al.* 2022; Jelby *et al.* 2024). Blok *et al.* (2022, 2023) found that the main mineralogical component of the succession is calcite with co-varying constituents of quartz and kaolinite clay indicating a detrital source from exposed continental rock, possibly in the form of nearby islands. The relative proportion of calcite and siliciclastic material varies stratigraphically, reflecting variation in pelagic carbonate production and continental runoff. Minor mineralogical constituents include illite, smectite-illite, and chlorite, while pyrite, dolomite, siderite and goethite occur locally (Blok *et al.* 2022, 2023).

With respect to post-depositional deformation, thin inclined deformation (compaction) bands and shear fractures have been noted in both the Boje-2C and other cores from the Valdemar Field (Glad *et al.* 2022; Jelby *et al.* 2022). Flaser lamination (*sensu lato* solution seams; Garrison & Kennedy 1977) have also been noted in chalk-dominated divisions, but no proper stylolites were reported.

Jelby *et al.* (2022) provided a detailed sedimentological description of several cored wells, including Boje-2C (Fig. 3). In addition to a minor occurrence of volcanic tuff, the authors identified five chalk–marlstone lithologies and seven different sedimentary structures or fabrics. In the Boje-2C core, the combination of the lithologies and sedimentary structures represents 21 facies, of which 18 are described herein with focus on their corresponding microscopic character (Tables 1, 2).

Thus, the primary aim of the present study is to

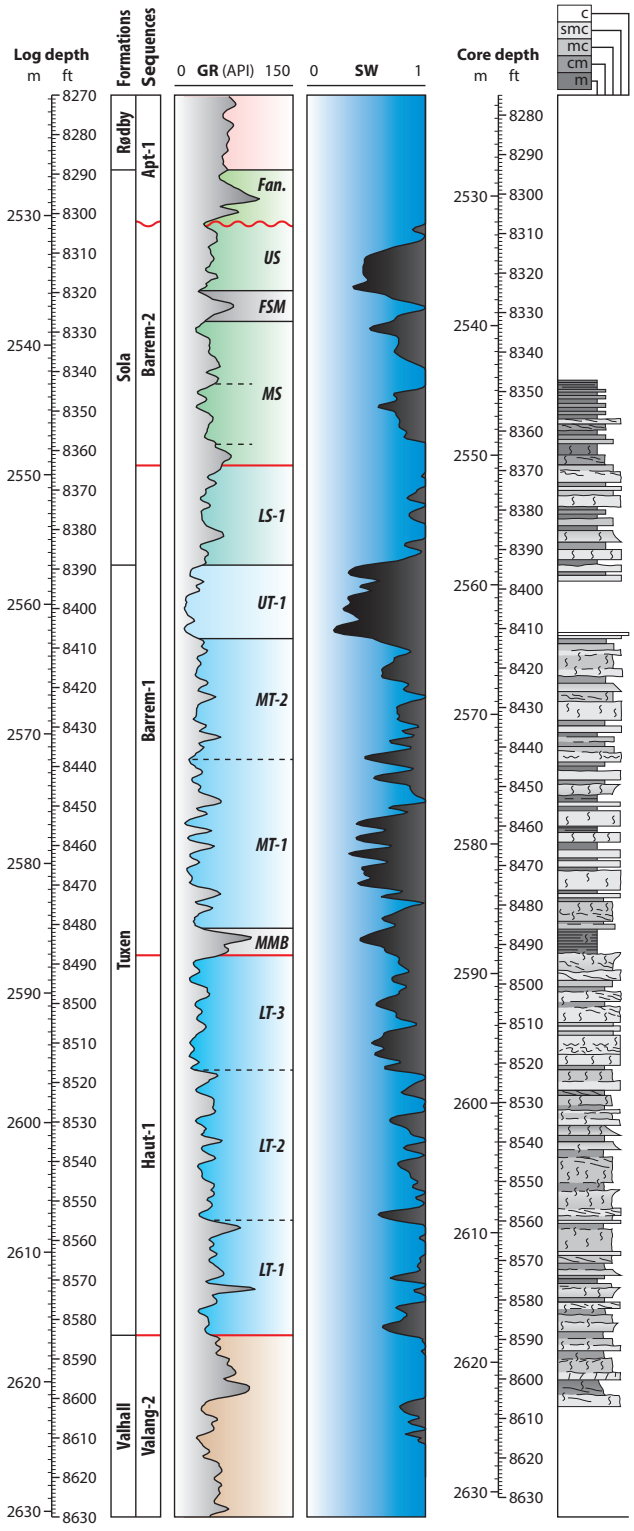


Fig. 3. Sedimentological and gamma-ray (GR) logs, water saturation (SW) log (Meireles & Fabricius 2023), reservoir zones (Jakobsen *et al.* 2004) and depositional sequences (Ineson *et al.* 2022a, b) in the Boje-2C well (modified from Jelby *et al.* 2022, 2024). The core:log depths are shifted with ~5 ft. Red straight and wavy lines are conformable and unconformable sequence boundaries, respectively. Reservoir -zone abbreviations refer to: LT 1–3, Lower Tuxen 1–3; MMB, Munk Marl Bed; MT 1–2, Middle Tuxen 1–2; UT-1, Upper Tuxen-1; LS-1, Lower Sola-1; MS, Middle Sola; FSM, Fischschiefer Member; US, Upper Sola; Fan., Fanø Member. Lithological abbreviations refer to: c, chalk; smc, slightly marly chalk; mc, marly chalk; cm, chalky marlstone; m, marlstone.

document the microscopic character of facies in the Tuxen and Sola formations in the Boje-2C core. Subordinately, the sedimentary and diagenetic processes that have resulted in the observed microscopic character are discussed, with special emphasis on potential links between macro- and microscopic features and the cause for depth-dependant variation.

Regional setting and stratigraphy

In the Early Cretaceous, the North Sea Basin (Fig. 1A) formed part of a regionally extensive, but enclosed, epicontinental sea with a general low-gradient ramp physiography dissected centrally by a N–S-trending deeper-water graben system, including the DCG. The basin had relatively narrow connections to the open ocean to the north, and progressively to the south during post-Barremian times. Prior to the Aptian, however, the southern margin of the basin was closed off from Tethyan influence (Tyson & Funnell 1987; Mutterlose 1992; Ineson 1993). The DCG consists of a complex series of NNW–SSE-trending half-grabens bounded by the Coffee Soil Fault and Ringkøbing–Fyn High to the east and by the Mid North Sea High to the west (Fig. 1B; e.g. Japsen *et al.* 2003). Formation of the DCG commenced during repeated regional rifting and corresponding fault-controlled subsidence, which was initiated in the Callovian and continued into the Ryazanian (Møller & Rasmussen 2003). In the Early Cretaceous, the active rift phase was replaced by regional thermal subsidence centred on the axial graben system of the DCG, although differential subsidence of Late Jurassic half-grabens persisted from the Ryazanian to the mid-Hauterivian but decreased into the late Hauterivian (Vejbæk 1986; Vejbæk & Andersen 1987).

The Tuxen Formation (lower Hauterivian – upper Barremian) is ~20–80 m (65–260 ft) thick in the DCG (Jensen *et al.* 1986). The formation predominantly consists of white to off-white intensely bioturbated and commonly argillaceous nannofossil chalk interbedded with bioturbated to laminated grey to green-grey marlstone (Fig. 3) of inferred pelagic and hemipelagic origin (Ineson 1993; Jelby *et al.* 2022).

The formation is characterised by two discrete chalk-dominated units separated by an up to 2 m (7 ft) thick unit of dark-grey to black, laminated, organic-rich marlstone of early Barremian age, named the 'Munk

Table 1. List of studied samples. Depth has reference to core and indicates lowermost part of sample

Stratigraphy	Sample ID	Facies
Middle Sola Formation	Bj-2G8348'4" *	5 c
	Bj-2G8350'5" *	4 y
	Bj-2G8352'1" *	4 c
	Bj-2G8369'1"	4 b
Lower Sola Formation	Bj-2G8369'11"	3 b
	Bj-2G8377'2" *	2 z
	Bj-2G8379'11"	2 a
	Bj-2G8381'11" *	5 a
	Bj-2G8385'11" *	5 y
	Bj-2G8388'4" *	5 b
	Bj-2G8390'1" *	2 b
	Bj-2G8393'11" *	5 c
Upper Tuxen Formation	Bj-2G8411'2"	1 a
Middle Tuxen Formation	Bj-2G8413'1"	2 y
	Bj-2G8416'0"	5 b
	Bj-2G8424'11"	3 b
	Bj-2G8430'11"	2 b
	Bj-2G8433'1"	2 b
	Bj-2G8444'11"	2 x
	Bj-2G8446'3" *	5 c
	Bj-2G8450'11" *	3 b
	Bj-2G8451'11" *	3 b
	Bj-2G8456'11" *	2 a
	Bj-2G8459'10" *	2 b
	Bj-2G8469'5" *	2 a
	Bj-2G8472'0"	2 b
	Bj-2G8475'11"	4 a
	Bj-2G8478'3"	1 a
	Bj-2G8480'3" *	3 b
	Bj-2G8485'0" *	3 b
Munk Marl Bed	Bj-2G8486'0" *	5 c
	Bj-2G8487'1" *	5 c
	Bj-2G8488'4" *	5 c
	Bj-2G8488'11" *	5 c
	Bj-2G8490'3"	5 c
	Bj-2G8491'1"	5 c
Lower Tuxen Formation	Bj-2G8491'11"	4 b
	Bj-2G8492'11"	2 b
	Bj-2G8494'1"	2 z
	Bj-2G8495'1"	3 z
	Bj-2G8505'0" *	2 b
	Bj-2G8511'1"	2 b
	Bj-2G8512'9"	2 b
	Bj-2G8515'2"	2 y
	Bj-2G8520'0" *	2 a
	Bj-2G8526'11" *	3 y
	Bj-2G8532'4"	4 a
	Bj-2G8536'0"	3 a
	Bj-2G8539'5" *	4 a
	Bj-2G8541'11" *	2 z
	Bj-2G8550'5" *	2 b
	Bj-2G8557'11"	2 y
	Bj-2G8559'1"	3 b
	Bj-2G8560'0" *	2 b
	Bj-2G8566'1" *	3 b
	Bj-2G8568'8" *	3 b
	Bj-2G8574'1" *	2 b
	Bj-2G8574'10" *	2 a
	Bj-2G8576'1"	3 a
	Bj-2G8579'0" *	3 a
	Bj-2G8581'1"	2 y
	Bj-2G8582'0" *	2 y
	Bj-2G8582'4"	4 a
	Bj-2G8586'0"	2 a
Valhall Formation	Bj-2G8604'2" *	4 b
	Bj-2G8607'0"	2 a

*Samples where mineralogy is confirmed by Energy Dispersive Spectrometry.

Marl Bed' (Jensen *et al.* 1986). The carbonate content of the formation overall increases upwards with the cleanest chalk and best reservoir quality observed in the top of the succession, as indicated by a low, blocky gamma-ray response (Fig. 3; Kühnau & Michelsen 1994; Jakobsen *et al.* 2004; Jelby *et al.* 2022, 2024).

The Sola Formation (upper Barremian – Albian) is ~20–40 m (65–130 ft) thick in the DCG (Jensen *et al.* 1986). The formation generally displays a heterogeneous, and compared to the Tuxen Formation, more marly facies development of mainly grey-green to buff marlstone and claystone, dark-grey to black laminated marlstone and claystone (Fig. 3), as well as pale chalk and argillaceous chalk, and local siltstone and sandstone (Jensen & Buchardt 1987; Ineson 1993; Jelby *et al.* 2022). Alternating pelagic and hemipelagic processes thus dominated deposition, with fluctuation of bottom-water oxygen levels and terrestrially derived sediment input (Jensen & Buchardt 1987; Jelby *et al.* 2022, 2024).

Material and methods

A total of 66 samples from the uppermost Valhall, Tuxen and Sola formations in the Boje-2C core were analysed for their microscopic character (Table 1). The samples were cleaned for pore water-derived salt and for hydrocarbons by reflux with methanol and toluene in a Soxhlet setup; impregnated with epoxy resin; and vertically oriented polished sections were subsequently prepared. Each section was coated with a 7–30 nm thick carbon film to avoid charging issues, and backscattered electron (BSE) images were recorded by an FEI Quanta 200 scanning electron microscope (SEM) equipped with an energy-dispersive X-ray spectrometer (EDS) (X-max 150, Oxford Instruments) at DTU Sustain, Technical University of Denmark. For each sample, several BSE images were taken, herein represented by one image of the texture and one image of the pore structure for each sample (Figs 4–15; A1–A5). Further, identification of the mineralogical content of each sample was aided by extensive EDS analyses of 36 samples (Table 1). The facies are annotated according to Jelby *et al.* (2022). Due to the original well and core depths being reported in imperial units, both these and converted metric units are used throughout this paper.

Microscopic character of facies

Facies 1a. *Homogeneously bioturbated chalk*

This facies is represented by two samples from the Tuxen Formation (Fig. 4; Table 2). Both samples display massive carbonate mudstone with contact ce-

Table 2. Combinations of lithology and fabric in cores from well Boje-2C (Jelby *et al.* 2022)

		Lithology				
		1 Chalk	2 Slightly marly chalk	3 Marly chalk	4 Chalky marlstone	5 Marlstone
Fabric						
a	Homogenous bioturbation	Tuxen (2)	Sola (1) Tuxen (5) Valhall (1)	Tuxen (3)	Tuxen (4)	Sola (1)
b	Mottled bioturbation		Sola (1) Tuxen (11)	Sola (1) Tuxen (8)	Sola (1) Tuxen (1) Valhall (1)	Sola (1) Tuxen (1)
c	Parallel lamination				Sola (1)	Sola (2) Tuxen (1) Munk Marl (6)
x	Flaser lamination		Tuxen (1)			
y	Shear deformation structures		Tuxen (5)	Tuxen (1)	Sola (1)	Sola (1)
z	Silicified fabric		Sola (1) Tuxen (2)	Tuxen (1)		

Formation name indicates where each combination is found and number of samples is given in parantheses. In addition to the Sola and Tuxen formations, also the deeper Valhall Formation is represented.

mentation among the recrystallized particles. The pore space is predominantly inter-particulate with maximal pore diameter less than five microns. The upper sample appears relatively less cemented and contains identifiable nannoconids and sparse diagenetically altered microfossils, one with pore-filling pyrite.

Facies 2a. *Homogeneously bioturbated slightly marly chalk*

This facies is represented by one sample from the Valhall Formation, five samples from the Tuxen Formation, and one sample from the Sola Formation (Figs 5, A1(A–J); Table 2). The samples represent massive clay-bearing carbonate mudstone, consistent with homogenization by bioturbation. The concentration of pyrite crystals in one sample (Fig. A1(A)) probably reflects the location of a trace fossil, because these structures macroscopically are frequently seen to be rich in pyrite. Nannofossils (nannoconids) are seen to contain intrafossil porosity, but pore space is dominated by interparticle porosity with maximal pore diameter less than two microns. Angular pores in the mud matrix of samples represented in Figs A1(A) and A1(C) may be moulds. Calcite particles in samples represented in Figs 5 and A1(E–J) are contact-cemented, and especially the sample from the Valhall Formation (Fig. A1(I, J)) appears significantly recrystallized, causing the rare microfossils to appear as calcite aggregates.

Facies 3a. *Homogeneously bioturbated marly chalk*

This facies is represented by three samples from the Tuxen Formation (Figs 6, A1(K, L); Table 2). The microtexture is seen as a massive silicate-rich carbonate mudstone, where silicates dominate as supporting constituent. Uneven distribution of silicate particles gives rise to mottling on microscale and interparticle porosity with occasional pore diameter of more than two microns. Angular pores may be moulds. A calcitic aggregate represented in Fig. 6A may represent a recrystallized microfossil. This sample also contains disseminated crystals of pyrite (white).

Facies 4a. *Homogeneously bioturbated chalky marlstone*

This facies is represented by four samples from the Tuxen Formation (Figs 7A–D, A1(M–P); Table 2). The microtexture of these samples is a massive, clay-supported carbonate-rich mudstone, probably homogenized by bioturbation. Quartz and kaolinitic claystone clasts of silt size are noted in all samples. Pyrite aggregates, probably representing altered microfossils are relatively common in the sample represented in Fig. A1(O), which also contains shell fragments. Visible porosity is mainly intrafossil porosity, invisible interparticle porosity could reside in the pervasive clay matrix. Single crystals of calcite-rimmed dolomite are noted in Fig. 7A, C.

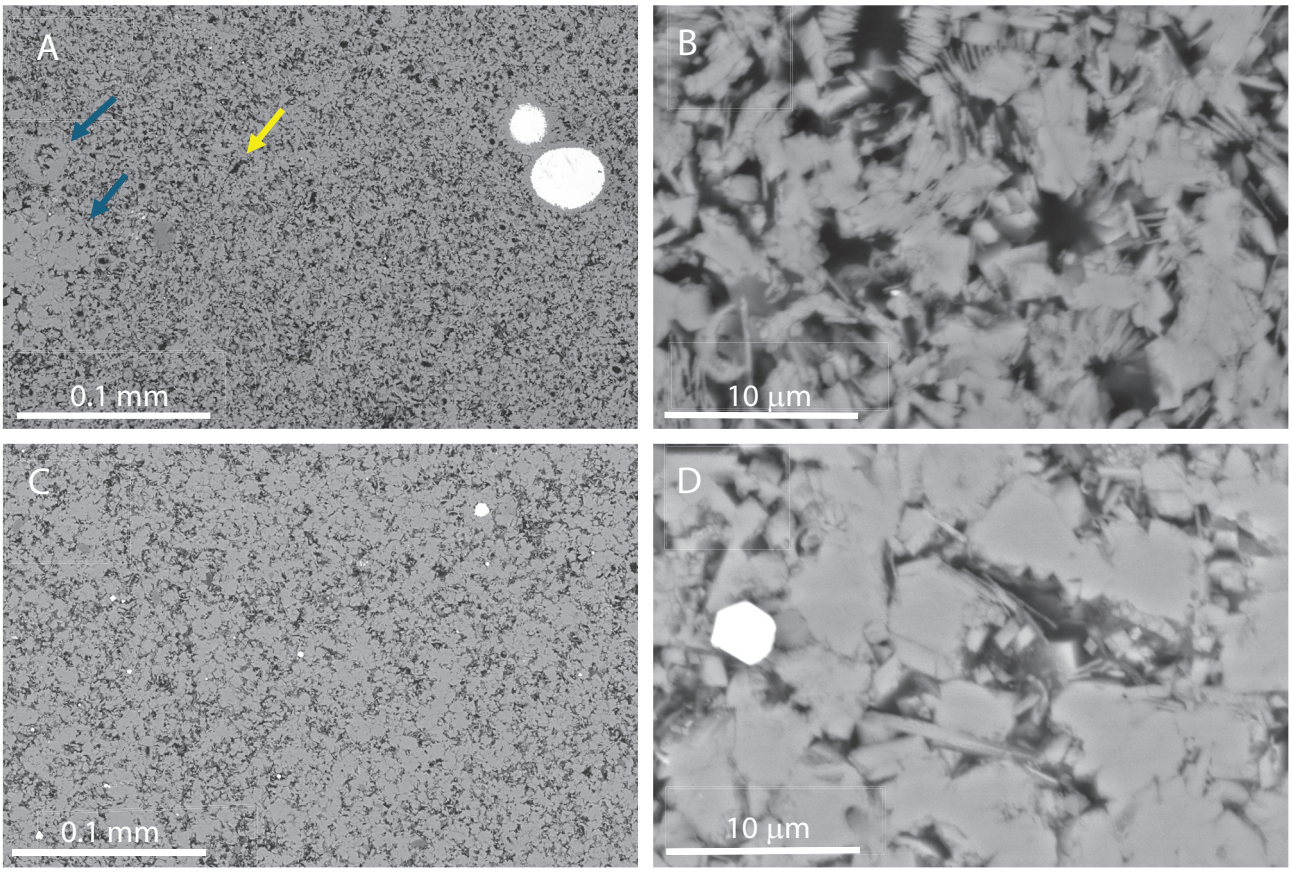


Fig. 4. Backscattered electron micrographs, illustrating texture (left) and pore geometry (right) of Facies 1a (homogeneously bioturbated chalk). (**A, B**) Sample from 8411'2'', Upper Tuxen Formation, oil zone (ref. Fig. 3). The mudstone texture illustrates partial recrystallization of carbonate mud and calcite cementation of calcareous microfossils (blue arrows). Some calcareous nannofossils have preserved intrafossil porosity (yellow arrow). A microfossil is cemented by pyrite (white). The closeup reveals the partial recrystallization of nannoconids, leaving partly degraded intrafossil porosity and high-specific surface crystallites of nannoconid skeletons with interparticle porosity. (**C, D**) Sample from 8478'3'', Middle Tuxen Formation, transition zone (ref. Fig. 3). Calcareous mudstone, where the presence of free water and sparsity of clay minerals may have facilitated the pronounced recrystallization of the carbonate mud. The white polygonal shape represents a pyrite crystal.

Facies 5a. *Homogeneously bioturbated marlstone*

This facies is represented by one sample from the Sola Formation (Fig. 7(E, F); Table 2). The sample represents a laminated, calcareous, clay-supported mudstone. Possible mouldic porosity, intrafossil porosity and interparticle porosity are seen. A plagioclase feldspar clast of 10 micron size is noted.

Facies 2b. *Biomottled slightly marly chalk*

This facies is represented by 11 samples from the Tuxen Formation and one sample from the Sola Formation (Figs 8, A2(A–T); Table 2). In most of these samples the microtexture is seen as massive clay-bearing carbonate mudstone, but in a few samples (Figs 8A, A2(E-P)) uneven distribution of calcitic and silicate particles results in visible mottling. Quartz silt particles are noted in several samples (Figs A2(G, J, L, R, T). Microfossils occur sparsely (Figs 8A, A2(C, G, M)) and are filled with calcite and minor pyrite cement. Nannofossils (nannoconids) are seen to contain intrafossil porosity, but pore space is dominated by interparticle porosity with maximal pore diameter less than two microns. Angular pores in the mud matrix of some samples (Figs 8A, A2(K, Q)) may be moulds. Calcite particles in all samples are contact-cemented. Pore-filling cement is noted in the deepest and stratigraphically lowest samples. Single crystals of calcite-rimmed dolomite are noted in sample represented in Fig. 8A, B.

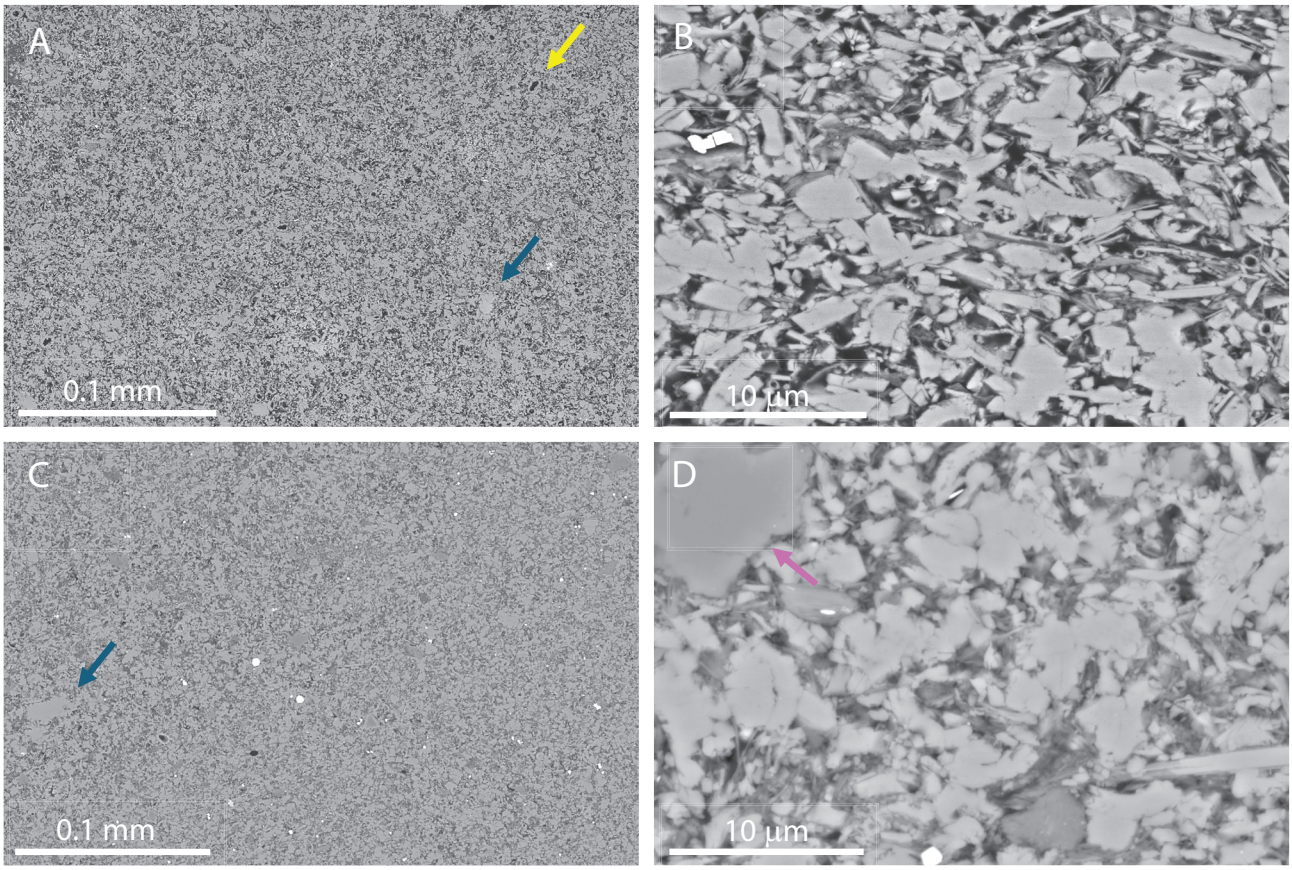


Fig. 5. Backscattered electron micrographs, illustrating texture (left) and pore geometry (right) of Facies 2a (homogeneously bioturbated slightly marly chalk). (**A, B**) Sample from 8456'11'', Middle Tuxen Formation, upper part of transition zone (ref. Fig. 3). The sample has a massive mudstone texture with single calcareous nannofossils, some with preserved intrafossil porosity (yellow arrow), and some cemented by calcite (blue arrow). The closeup reveals local lamination of clay particles (medium grey) and partly recrystallized calcareous nannofossils (light grey) leaving a homogeneous pore space with high specific surface of the interparticle porosity. (**C**, **D**) Sample from 8586', Lower Tuxen Formation, lower part of transition zone (ref. Fig. 3). The sample has massive mudstone texture with single calcareous microfossils cemented by calcite (blue arrow) and submicron-sized pyrite crystals (white). The closeup highlights quartz silt (pink arrow) and clay particles mixed with recrystallized calcite particles of altered biogenic shape. Interparticle porosity is only partly visible at the chosen magnification

Facies 3b. *Biomottled marly chalk*

This facies is represented by eight samples from the Tuxen Formation and one sample from the Sola Formation (Figs 9, A2(U–HH); Table 2). In most of these samples the microtexture is a mottled, clay-bearing carbonate mudstone, where mottling is caused by an uneven distribution of calcitic and silicate particles. Samples generally appear massive. Silt particles of quartz and kaolinitic claystone are noted in samples represented in Figs 9A and A2(BB, DD). Microfossils occur sparsely (Fig. A2(Y, AA, CC)), whereas shell fragments are seen in Figs 9A and A2(CC). Microfossils are filled with calcite or pyrite cement. Nannofossils (nannoconids) are seen to contain intrafossil porosity (Figs 9D and A2(V, X, Z)) but pore space is dominated by interparticle porosity with maximal pore diameter less than two microns. Angular pores in the mud matrix of samples represented in Figs 9A and A2(U, Y, CC) may be moulds. Calcite particles in deeper samples are contact-cemented (Figs 9D, A2(BB, FF, HH)). In these deeper samples, clay minerals seem to form discrete aggregates, whereas clay minerals in upper samples (Figs 9B and A2(V, X, Z)) form a pore-filling network among calcite particles.

Facies 4b. *Biomottled chalky marlstone*

This facies is represented by one sample from the Valhall Formation, one sample from the Tuxen Formation, and one sample from the Sola Formation (Figs 10, A2(II, JJ); Table 2). The microtexture of these samples is a laminated, clay-supported, carbonate-rich mudstone. Rounded pores may represent moul-

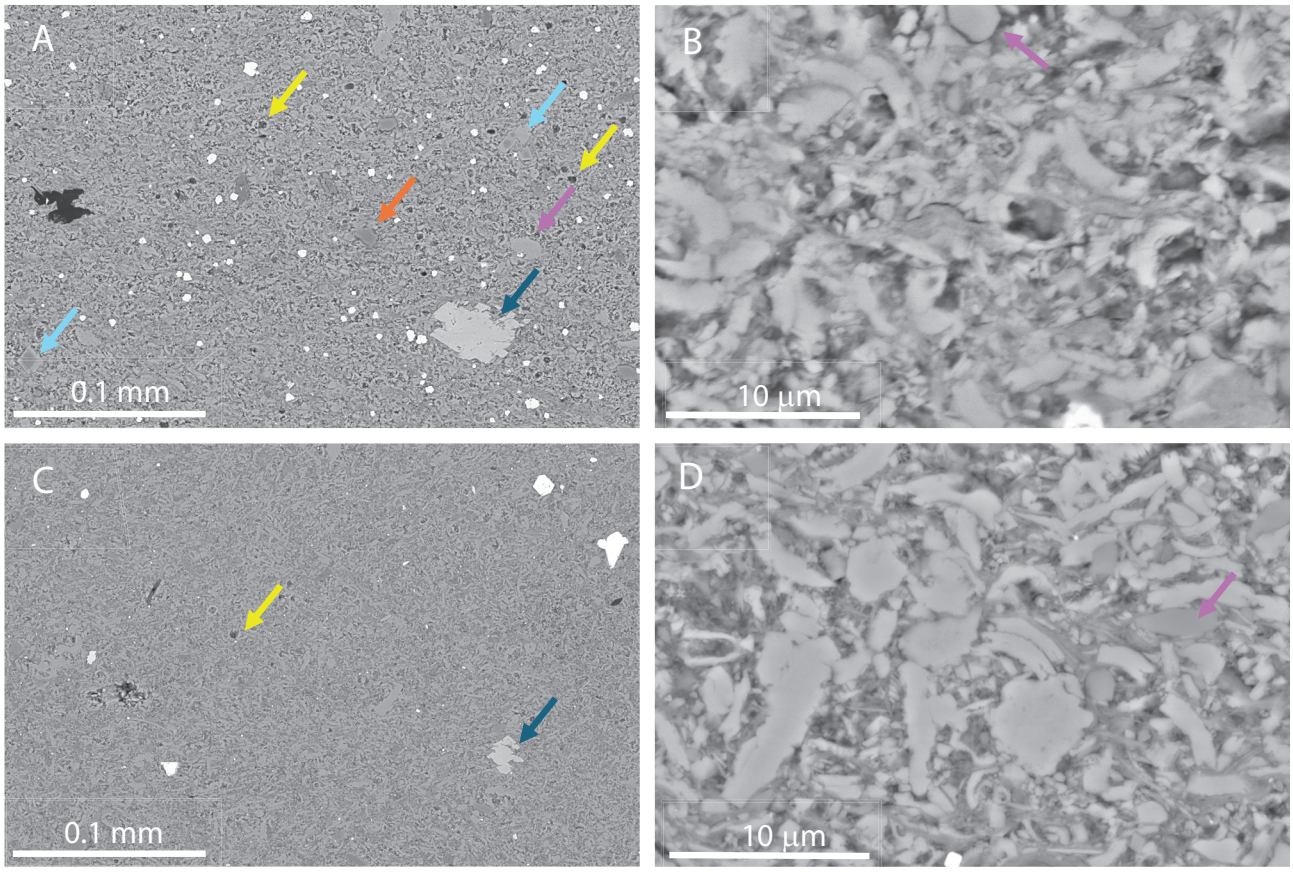


Fig. 6. Backscattered electron micrographs, illustrating texture (left) and pore geometry (right) of Facies 3a (homogeneously bioturbated marly chalk). (**A, B**) Sample from 8536′, Lower Tuxen Formation. (**C**, **D**) Sample from 8579′, Lower Tuxen Formation. Both samples are from lower part of the transition zone (ref. Fig. 3). The samples have massive mudstone texture with single calcitic aggregates probably representing recrystallized microfossils (blue arrows) and single calcareous nannofossils, some with preserved intrafossil porosity (yellow arrows). Silt particles include quartz (pink arrow) and in sample from 8536′ (**A**) also kaolinitic claystone clasts (orange arrow). This sample (**A**) contains calcite-coated dolomite crystals (light blue arrows) and submicron-sized pyrite crystals (white). The sample from 8579′ (**C**) contains micron-sized pyrite crystals. The closeups highlight dense mixtures of quartz silt (pink arrows), clay particles and recrystallized calcite particles of altered biogenic shape. Interparticle porosity is only partly visible at the chosen magnification.

dic porosity, and only little interparticle porosity is visible. The sample represented in Fig. 10A, B contains disseminated micron-sized pyrite crystals. In sample represented in Fig. 10C, D, pyrite is localized in larger aggregates/crystals.

Facies 5b. *Biomottled marlstone*

This facies is represented by one sample from the Tuxen Formation and one sample from the Sola Formation (Fig. 11; Table 2). The samples represent a massive, clay-rich, calcareous mudstone texture in which calcite- and silicate particles are unevenly distributed, giving rise to a mottled appearance. Intrafossil, possible mouldic and interparticle porosity are seen in areas rich in calcite. The sample represented in Fig. 11A, B contains scattered pyrite crystals up to five microns in size.

Facies 4c. *Parallel-laminated chalky marlstone*

This facies is represented by one sample from the Sola Formation (Fig. 12A, B; Table 2). The microtexture is a laminated, calcareous, clay-supported mudstone. Interparticle porosity is visible in laminae rich in calcitic particles, intrafossil porosity and micron-size questionable moulds are relatively common. Micron-sized pyrite occurs as single crystals and loose aggregates. Quartz silt particles of 10 micron size are noted.

Facies 5c. *Parallel-laminated marlstone*

This facies is represented by seven samples from the Tuxen Formation, of which six samples are from the Munk Marl Bed and two samples from the Sola For-

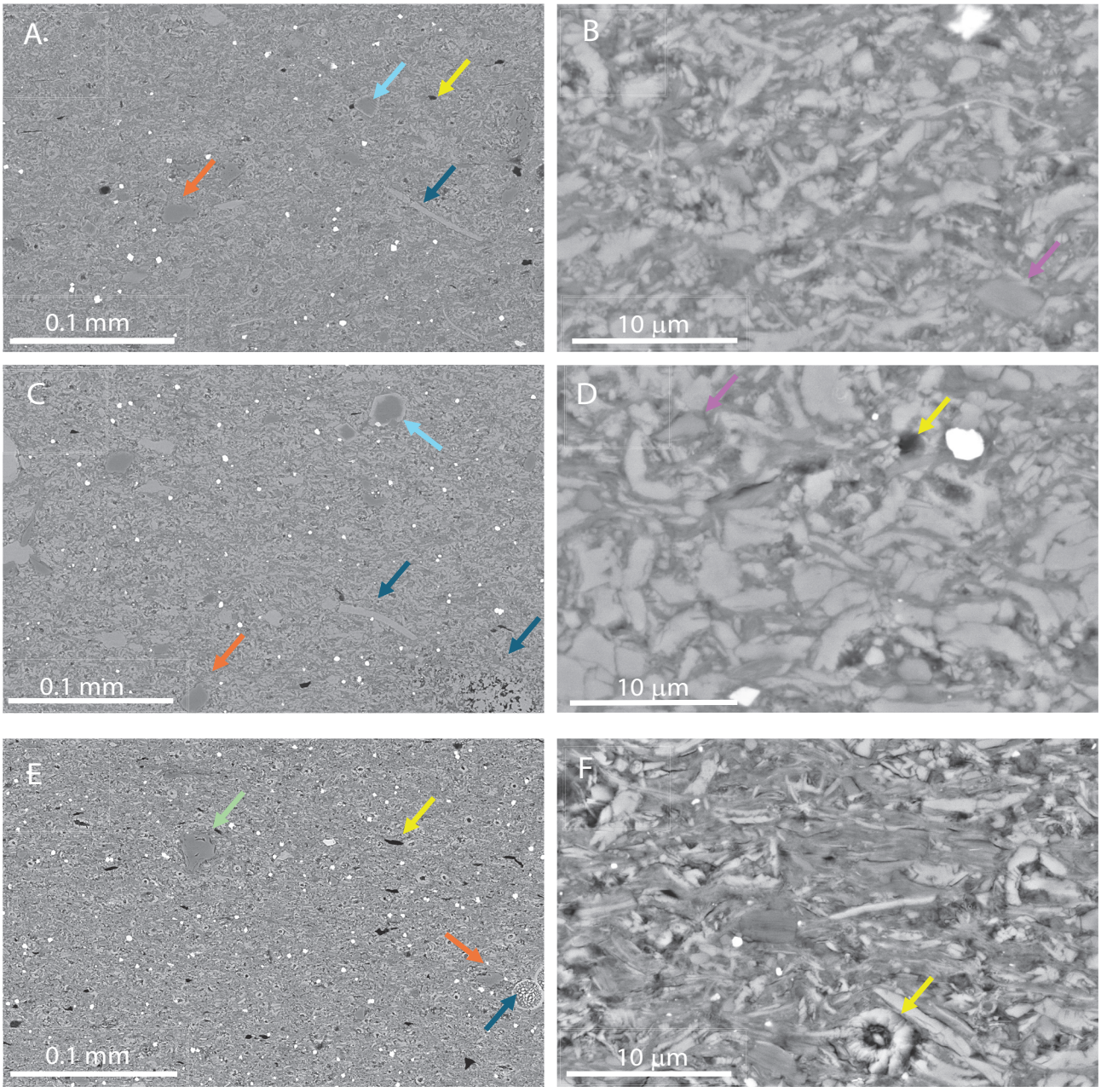


Fig. 7. Backscattered electron micrographs, illustrating texture (left) and pore geometry (right) of Facies 4a (homogeneously bioturbated chalky marlstone; **A–D**) and Facies 5a (homogeneously bioturbated marlstone; **E–F**). (**A**, **B**) Sample from 8532'4'', Lower Tuxen Formation. (**C**, **D**) Sample from 8582'4'', Lower Tuxen Formation. Both samples are from lower part of the transition zone (ref. Fig. 3). The samples have massive mudstone texture with single calcareous fossil clasts and partly recrystallized calcareous microfossils (blue arrows). Silt particles include quartz (pink arrows) and kaolinitic claystone clasts (orange arrows). Both samples contain calcite-coated dolomite crystals (light blue arrows) and submicron-sized pyrite crystals (white). The closeups highlight dense mixtures of quartz silt (pink arrows), clay particles and partly recrystallized biogenic calcite particles. Up to micron-sized porosity may in some cases represent moulds, in other cases shelter porosity (yellow arrow). Interparticle porosity is not visible at the chosen magnification. (**E**, **F**) Sample from 8381'11'', Lower Sola Formation. The sample is from the oil zone (ref. Fig. 3). The sample has mudstone texture with slight lamination indicated by orientation of fossil clasts and voids. A calcareous microfossil has intrafossil porosity (blue arrow). Silt particles include feldspar (green arrow) and kaolinitic claystone clasts (orange arrow). Submicron-sized pyrite crystals are widespread (white). The closeup highlights the dense mixture of clay particles and nannofossil debris. Up to micron-sized pin point porosity may in some cases represent moulds, in other cases intrafossil porosity (yellow arrow).

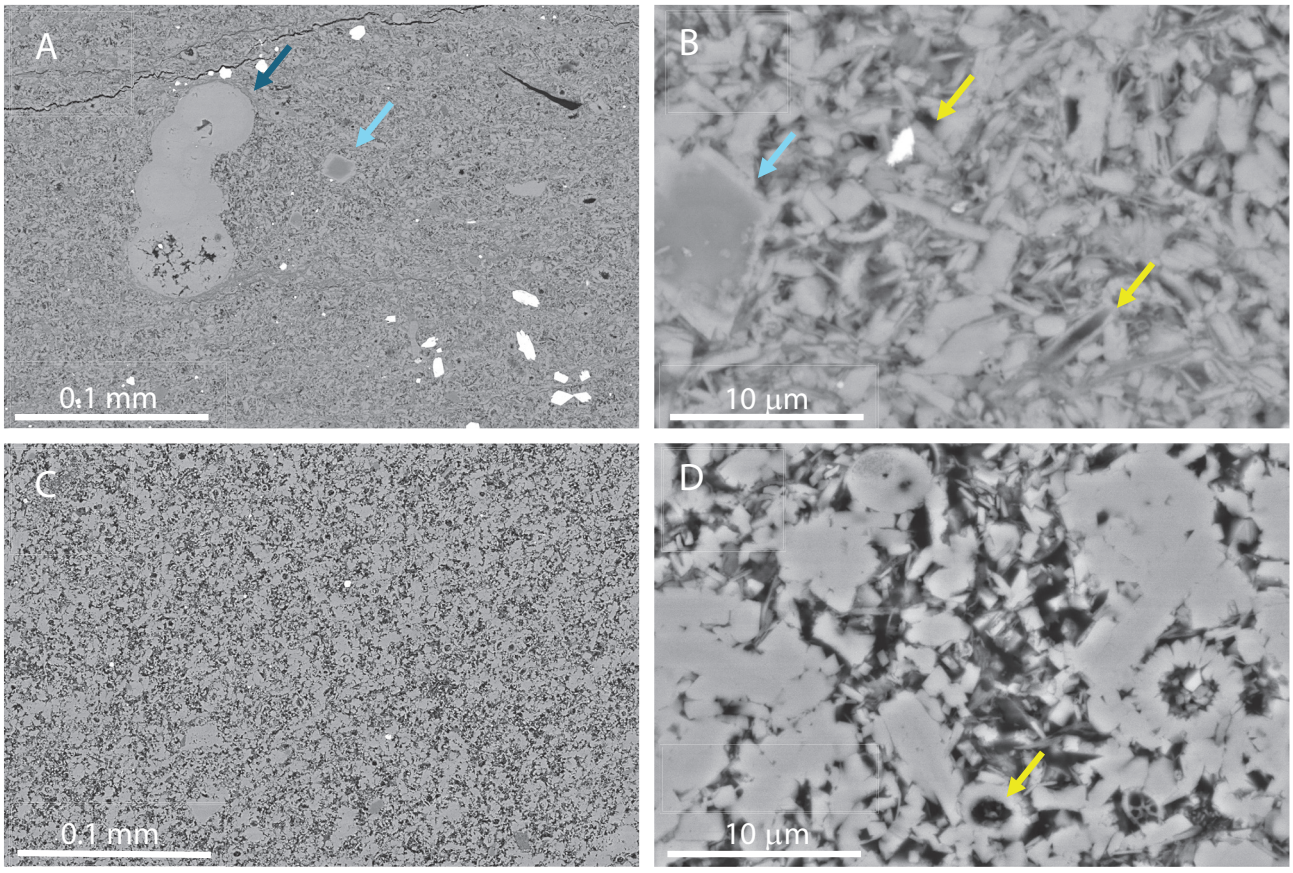


Fig. 8. Backscattered electron micrographs, illustrating texture (left) and pore geometry (right) of Facies 2b (biomottled slightly marly chalk). (**A, B**) Sample from 8430'11'', Middle Tuxen Formation, the oil zone (ref. Fig. 3). The sample has mudstone texture with a foraminifer almost completely cemented by ferroan calcite (blue arrow). Mottling is revealed by uneven distribution of visible interparticle porosity at low magnification. The sample contains calcite-coated dolomite crystals (light blue arrows) and micron-sized pyrite crystals (white). The closeup highlights partly recrystallized nannofossil debris, local lamination in clay content, interparticle porosity and intrafossil porosity (yellow arrows). (**C**, **D**) Sample from 8574'1'', Lower Tuxen Formation, lower part of transition zone (ref. Fig. 3). Calcareous mudstone, where the presence of free water and sparsity of clay minerals have probably facilitated the pronounced recrystallization of the carbonate mud. The closeup reveals recrystallized nannofossils where intrafossil porosity is preserved (yellow arrow). The relatively regular neomorphic calcite and remains of fossils give rise to a moderate specific surface of the interparticle porosity.

mation (Figs 12C–F, A3; Table 2). All samples have laminated, calcite-bearing, silicate mudstone texture. Silt size particles are noticed in samples represented in Fig. A3(J, L). Porosity is visible in most samples but could reflect sample desiccation prior to impregnation with epoxy resin. In most of the samples from the Munk Marl Bed, lamination seems to have been disturbed by shear deformation (Fig. A3(G, K, M)). All samples contain pyrite as micron-sized crystals or in a single sample (Fig. A3(H)) as framboids.

Facies 2x. *Flaser-laminated slightly marly chalk*

This facies is represented by one sample from the Tuxen Formation (Fig. 13; Table 2). The sample is a carbonate-rich, silicate-supported mudstone. The macroscopically described flaser lamination (Jelby *et al.* 2022) is microscopically reflected in uneven laminae of calcite particles and silicates in possible deformation (compaction) bands. The pore space is dominated by interparticle porosity with maximal pore diameter less than two microns. Angular pores in mud matrix may be moulds.

Facies 2y. *Shear-deformed slightly marly chalk*

This facies is represented by five samples from the Tuxen Formation (Figs 14A, B, A4); Table 2). All samples have massive clay-bearing carbonate mudstone texture. Quartz silt is noted (Fig. A4(B, H)). Pore space is dominated by interparticle porosity with maximal pore diameter less than two microns. Calcite particles in all samples are contact-cemented. Single crystals of calcite-rimmed dolomite are pres-

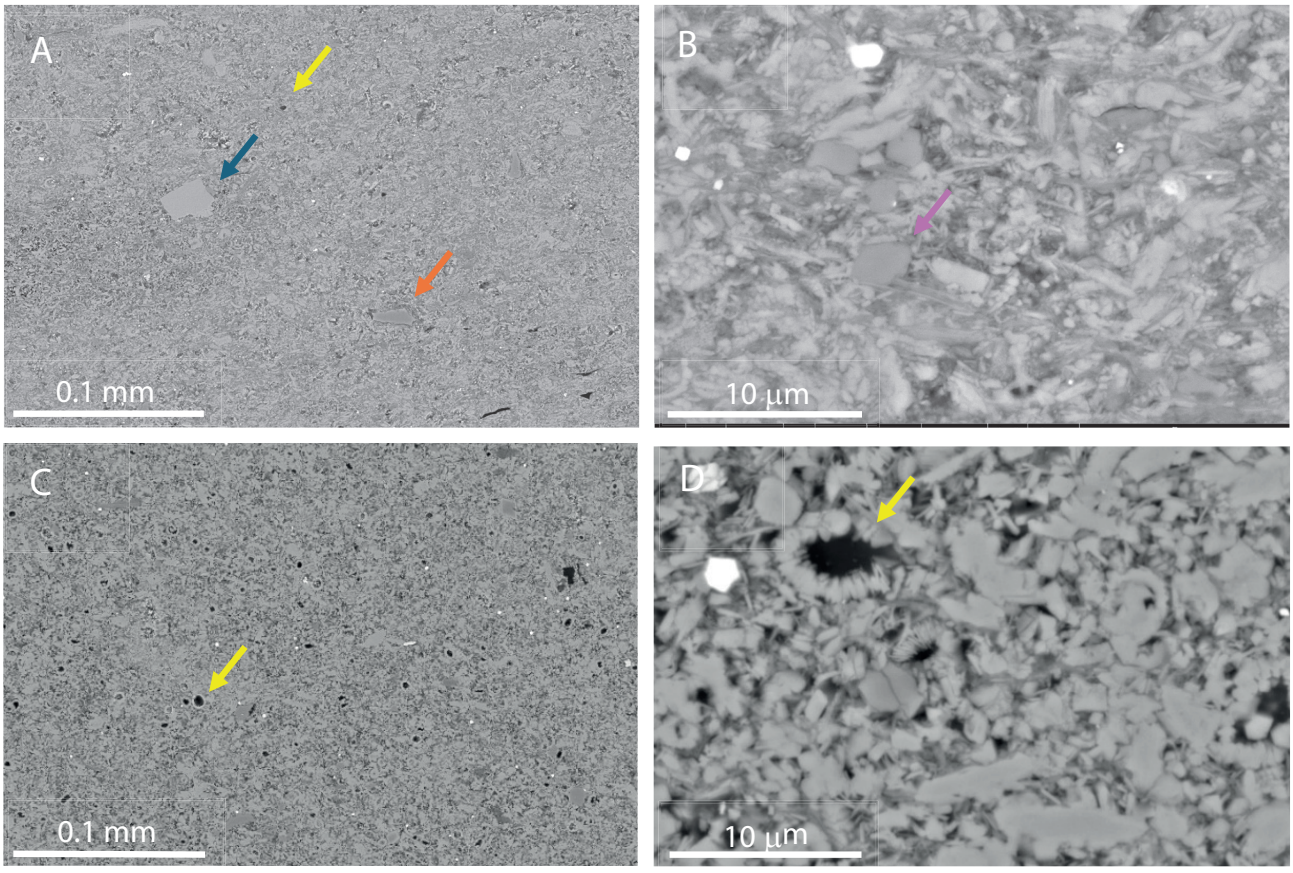


Fig. 9. Backscattered electron micrographs, illustrating texture (left) and pore geometry (right) of Facies 3b (biomottled marly chalk). (**A, B**) Sample from 8369'11'', Lower Sola Formation, the oil zone (ref. Fig. 3). The sample has mudstone texture, where mottling is revealed by uneven distribution of visible interparticle porosity at low magnification. A single fossil fragment is seen (blue arrow), as well as a claystone clast (orange arrow). Possibly mouldic porosity is seen (yellow arrow). Closeup reveals mixture of nannofossil debris, quartz silt (pink arrow) and clay, as well as single submicron-sized pyrite crystals (white). Interparticle porosity is partly visible at the chosen magnification. (**C**, **D**) Sample from 8568'8'', Lower Tuxen Formation, lower part of the transition zone (ref. Fig. 3). The sample has mudstone texture with a less pronounced mottling of interparticle porosity at low magnification than the oil zone sample. Closeup reveals partly recrystallized nannofossil debris as well as single submicron-sized pyrite crystals (white). Interparticle porosity is well visible and has moderate specific surface. Intrafossil porosity in nannoconids is visible at both magnifications (yellow arrows).

ent (Fig. A4(G, H)). The shear deformation structures observed macroscopically are not visible in these electron microscope images.

Facies 3y. *Shear-deformed marly chalk*

This facies is represented by one sample from the Tuxen Formation (Fig. 14C, D; Table 2). The sample has a massive, clay-bearing carbonate mudstone texture. Calcite particles are contact-cemented and pore-filling cement is found as disseminated less than 10 micron-sized aggregates. Nannofossils (nannoconids) are seen to contain intrafossil porosity, but pore space is dominated by interparticle porosity with maximal pore diameter less than two microns. The macroscopically observed shear deformation structures are not visible in this electron microscope image.

Facies 4y. *Shear-deformed chalky marlstone*

This facies is represented by one sample from the Sola Formation (Fig. 14E, F; Table 2). This sample represents a massive, clay-bearing, calcareous mudstone with well-preserved remains of nannofossils. Intrafossil porosity and more dominating interparticle porosity are clearly visible. Macroscopically observed shear deformation structures are not obvious from these electron microscope images.

Facies 5y. *Shear-deformed marlstone*

This facies is represented by one sample from the Sola Formation (Fig. 14G, H; Table 2). It has a massive, clay-supported, calcite-rich mudstone texture. Visible porosity is mainly intrafossil porosity in nan-

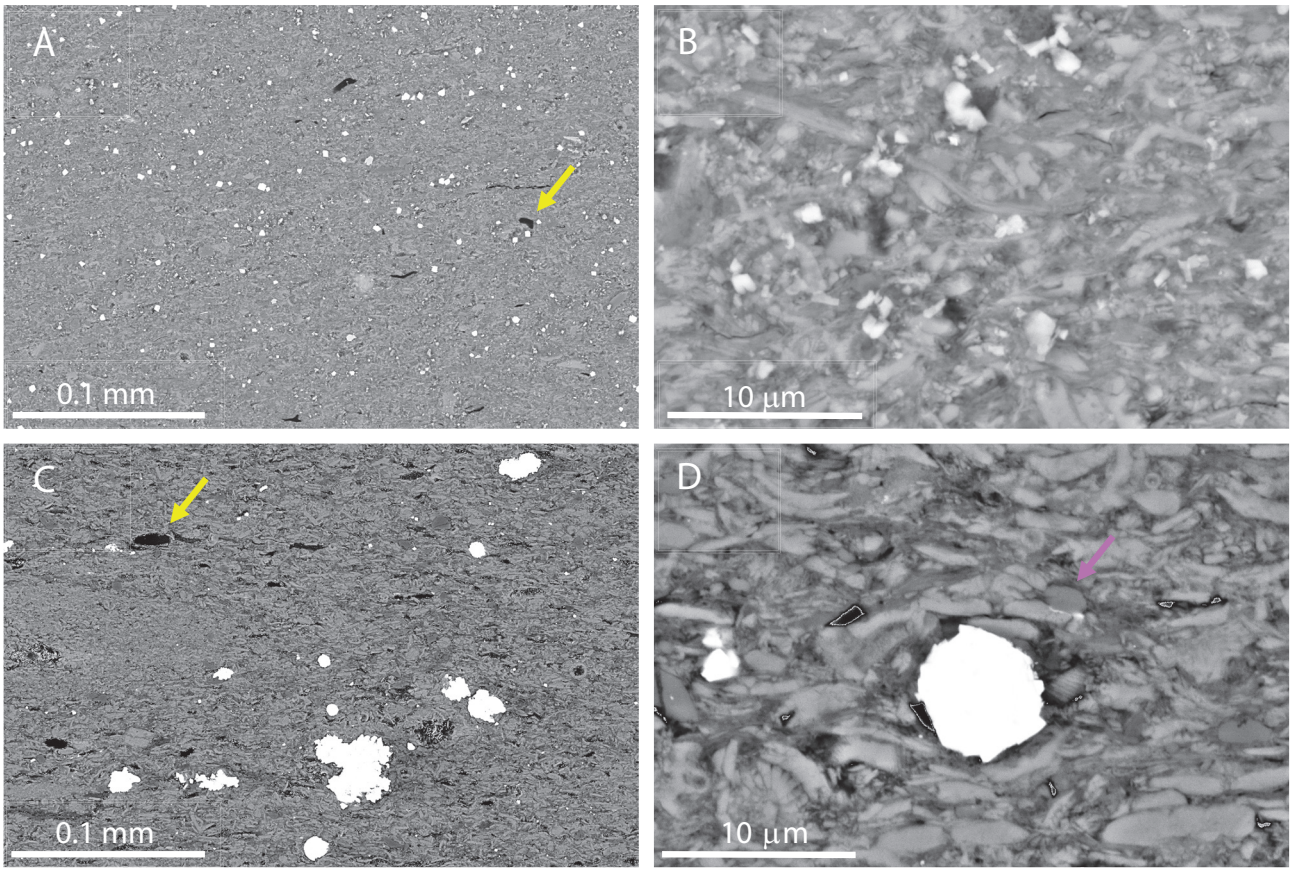


Fig. 10. Backscattered electron micrographs, illustrating texture (left) and pore geometry (right) of Facies 4b (biomottled chalky marlstone). (**A, B**) Sample from 8369'1'', Middle Sola Formation, the oil zone (ref. Fig. 3). The sample has mudstone texture with faint lamination as indicated by nannofossil fragments and possible moulds (yellow arrow). The closeup reveals a dense mixture of nannofossil debris and clay with scattered submicron size pyrite crystals (white). Interparticle porosity is locally visible. (**C**, **D**) Sample from 8491'1'', Lower Tuxen Formation, upper part of the transition zone (ref. Fig. 3). The sample has mudstone texture with pronounced mottling as revealed by the distribution of interparticle porosity. It also has some horizontal lamination as indicated by orientation of voids, possibly representing moulds (yellow arrow). Pyrite crystals of up to 40 micron size (white) are seen. The closeup reveals a laminated mixture of nannofossil debris, clay and quartz silt (pink arrow) with some visible interparticle porosity.

noconids. Micron-sized pyrite crystals are disseminated in the sample. Macroscopic shear deformation structures are not observed at electron microscope scale.

Facies 2z. *Silicified slightly marly chalk*

This facies is represented by two samples from the Tuxen Formation and one sample from the Sola Formation (Figs 15A, B, A5; Table 2). The microtexture of the two deeper samples (Fig. A5) is seen as massive clay-bearing carbonate mudstone, whereas the upper sample is seen as an unevenly silica-cemented, clay-bearing carbonate mudstone (Fig. 15A, B). Calcite-cemented microfossils occur sparsely (Fig. A5(C)). Pore space is dominated by interparticle porosity with maximal pore diameter less than two microns but appears heterogeneously distributed in the silica-cemented sample (Fig. 15A, B). Calcite particles in samples from the Tuxen Formation are contact-cemented (Fig. A5(B, D)). Possible incipient silica cement is noted in pore space of these samples.

Facies 3z. *Silicified marly chalk*

This facies is represented by one sample from the Tuxen Formation (Fig. 15C, D; Table 2). It has a massive, silicate-bearing carbonate mudstone texture. Calcite particles are contact-cemented and pore-filling silica cement is disseminated leaving local interparticle porosity open. Micron-sized pyrite crystals are disseminated in the sample.

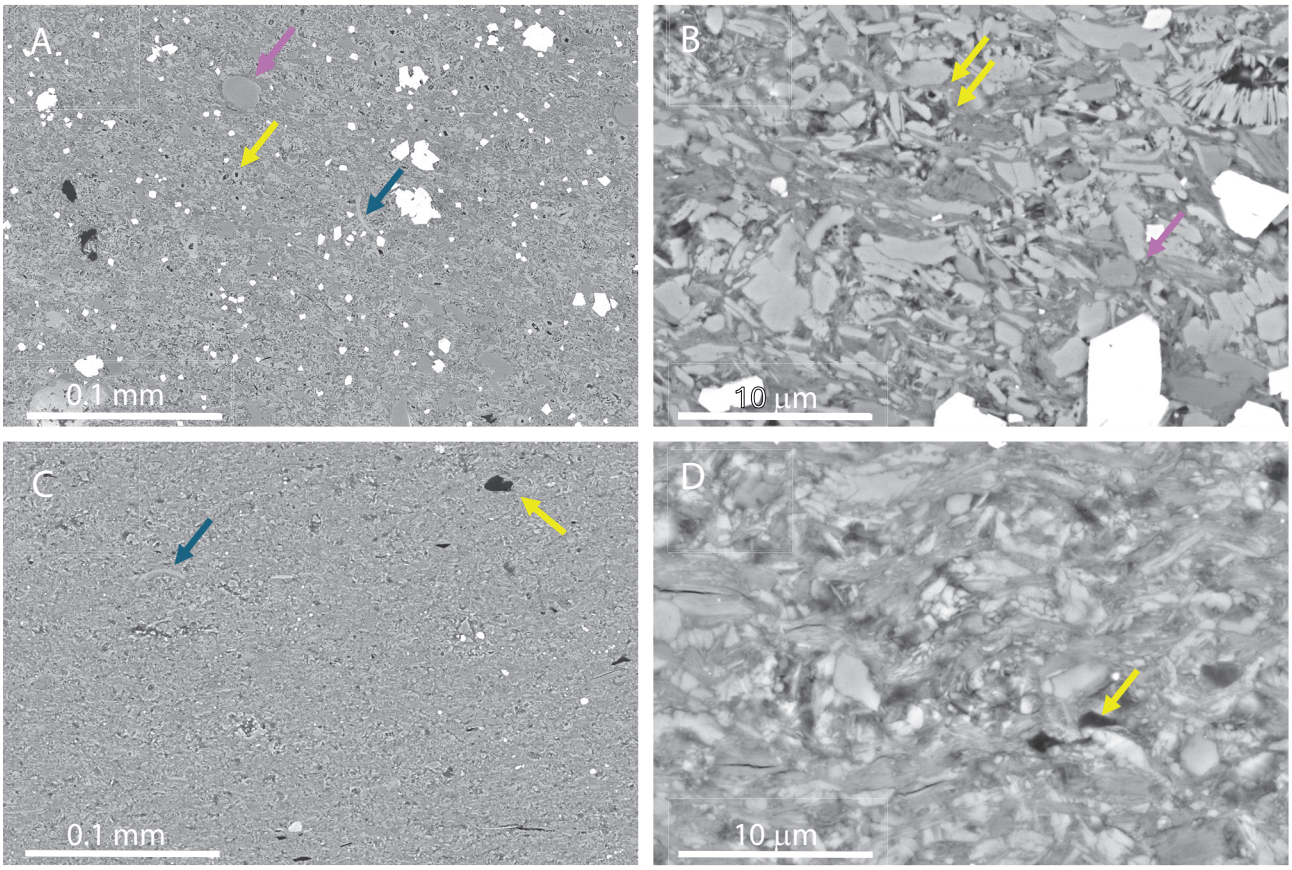
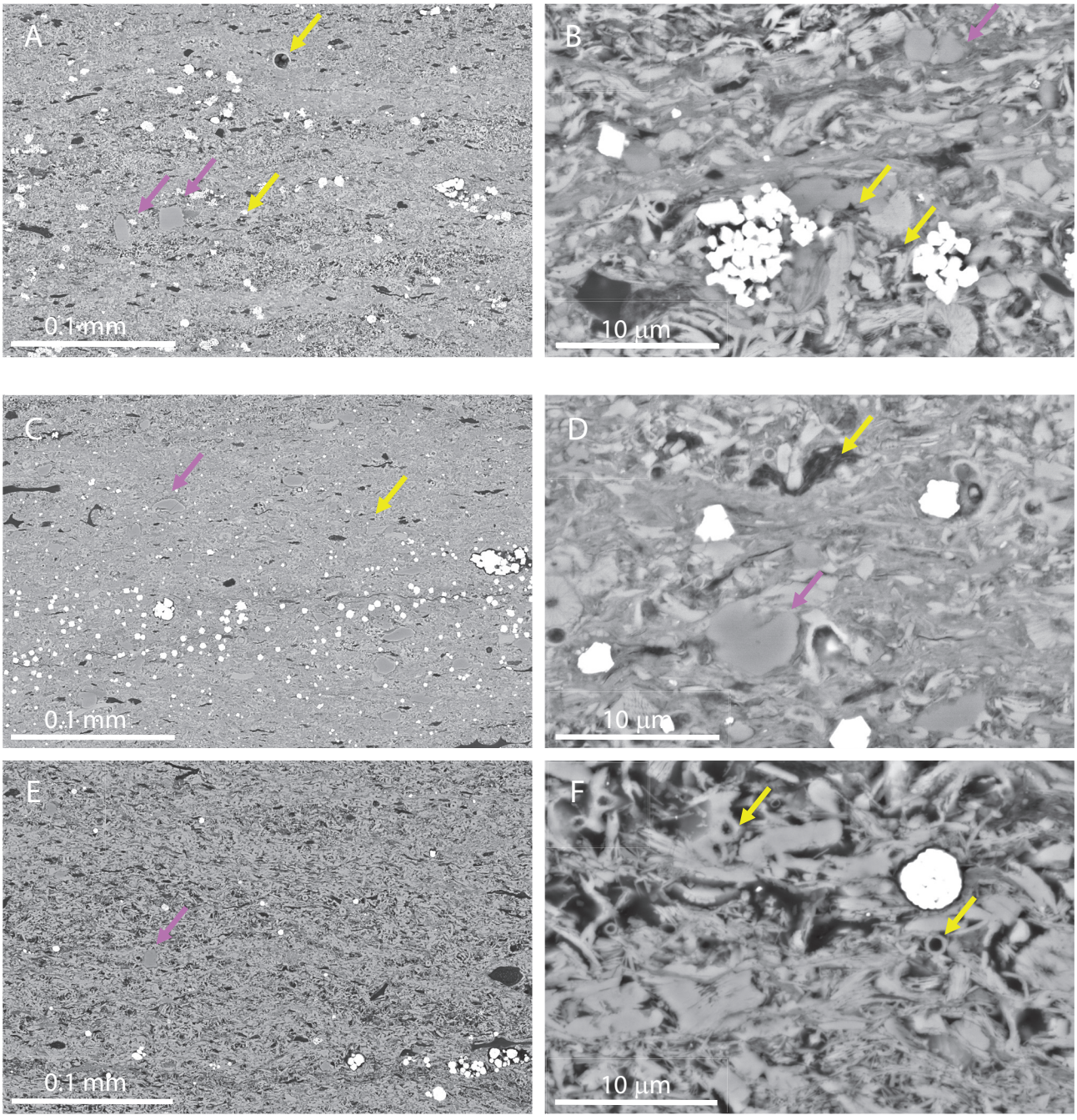


Fig. 11. Backscattered electron micrographs, illustrating texture (left) and pore geometry (right) of Facies 5b (biomottled marlstone). (**A, B**) Sample from 8388'4'', Lower Sola Formation, oil zone (ref. Fig. 3). The sample has massive mudstone texture with single microfossil clasts (blue arrow) and grains of quartz silt (pink arrow), as well as scattered up to 10 micron-sized pyrite crystals (white). Intra-nannofossil porosity is widespread (yellow arrow). The closeup reveals a dense mixture of partly recrystallized nannofossil debris and clay with quartz silt and scattered pyrite crystals (white). Interparticle porosity is locally visible (yellow arrow). (**C, D**) Sample from 8416', Middle Tuxen Formation, upper part of transition zone (ref. Fig. 3). The sample has massive mudstone texture with single microfossil clasts (blue arrow) and scattered less than micron size pyrite crystals (white). Possible mouldic porosity is locally visible (yellow arrow). The closeup reveals a dense mixture of clay and micron size calcitic debris. Interparticle porosity is locally visible (yellow arrow).

Fig. 12. Backscattered electron micrographs, illustrating texture (left) and pore geometry (right) of Facies 4c (parallel-laminated chalky marlstone; **A, B**) and Facies 5c (parallel-laminated marlstone; **C–F**). (**A**, **B**) Sample from 8352'1'', Middle Sola Formation, oil zone (ref. Fig. 3). The sample has mudstone texture with lamination caused by variation in clay content. It contains quartz silt (pink arrow) and nannofossils. Submicron size pyrite crystals (white) occur in both clay-rich and clay-poor intervals. Mouldic porosity is widespread together with rarer intrafossil porosity (yellow arrow). The closeup reveals nannofossil debris in layers with dense packing with clay and quartz silt (pink arrow) alternating with layers with interparticle porosity (yellow arrow). Submicron size pyrite in framboidal aggregate is seen (white). (**C**, **D**) Sample from 8348'4'', Middle Sola Formation, oil zone (ref. Fig. 3). The sample has mudstone texture with lamination caused by variation in clay content. It contains quartz silt (pink arrow). Submicron-sized pyrite crystals (white) occur primarily in clay-poor intervals. Mouldic porosity is widespread together with rarer intrafossil or shelter porosity (yellow arrow). The closeup reveals nannofossil debris in layers with dense packing with clay and quartz silt (pink arrow) alternating with layers with interparticle porosity (yellow arrow). Submicron size pyrite is seen (white). (**E**, **F**) Sample from 8488'11'', Munk Marl Bed in the transition zone (ref. Fig. 3). The sample has mudstone texture with lamination caused by variation in clay content. It contains quartz silt (pink arrow). Submicron size pyrite crystals (white) occur locally. Mouldic and interparticle porosity are widespread. The closeup reveals nannofossil debris in layers with loose packing with clay alternating with layers with interparticle porosity and local intra nannofossil porosity (yellow arrows). Micron size pyrite is seen (white).



Discussion: Origin of microscopic features

Microscopic depositional features versus macroscopic facies

Microscopic features deemed to represent sedimentary processes or diagenesis are listed in Table 3. With respect to depositional features, all studied samples have carbonate mudstone texture, where the supporting mineral is calcite in most samples. Clay-supported texture is rare and mainly confined to chalky marlstone and marlstone (Fig. 7). Biogenic calcareous components represent pelagic organisms (mainly nannofossils such as nannoconids; e.g. Fig. 14) and debris. Pelagic foraminifers are sparsely represented (Figs 4, 8), and benthic biofragments are virtually absent. The scarcity of benthos in the Lower Cretaceous chalks was noted by Jelby *et al.* (2022) and Lauridsen *et al.* (2022); the latter authors suggested that sea-floors consisting of pelagic carbonate ooze had not existed in the study area before the Early Cretaceous and that benthic organisms had yet to

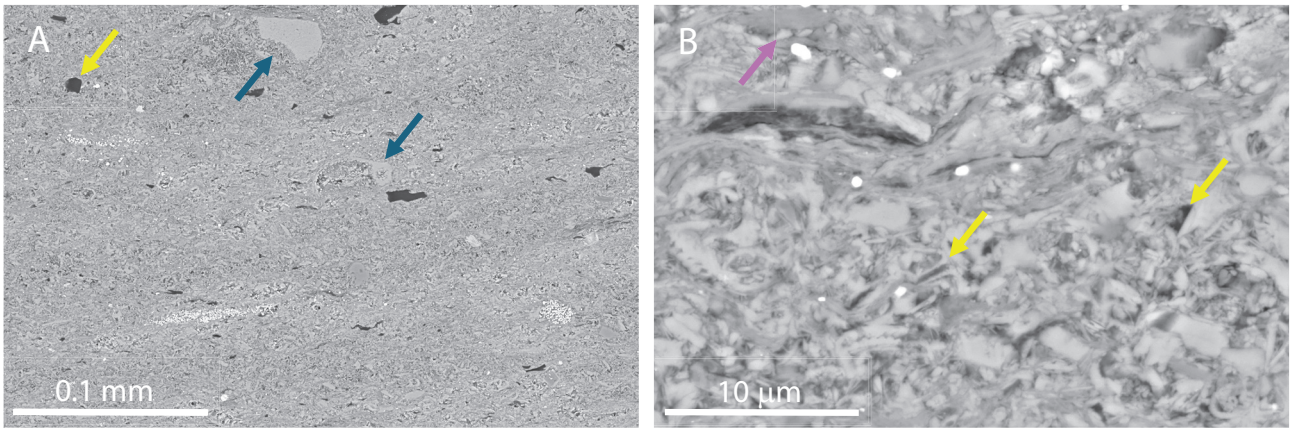


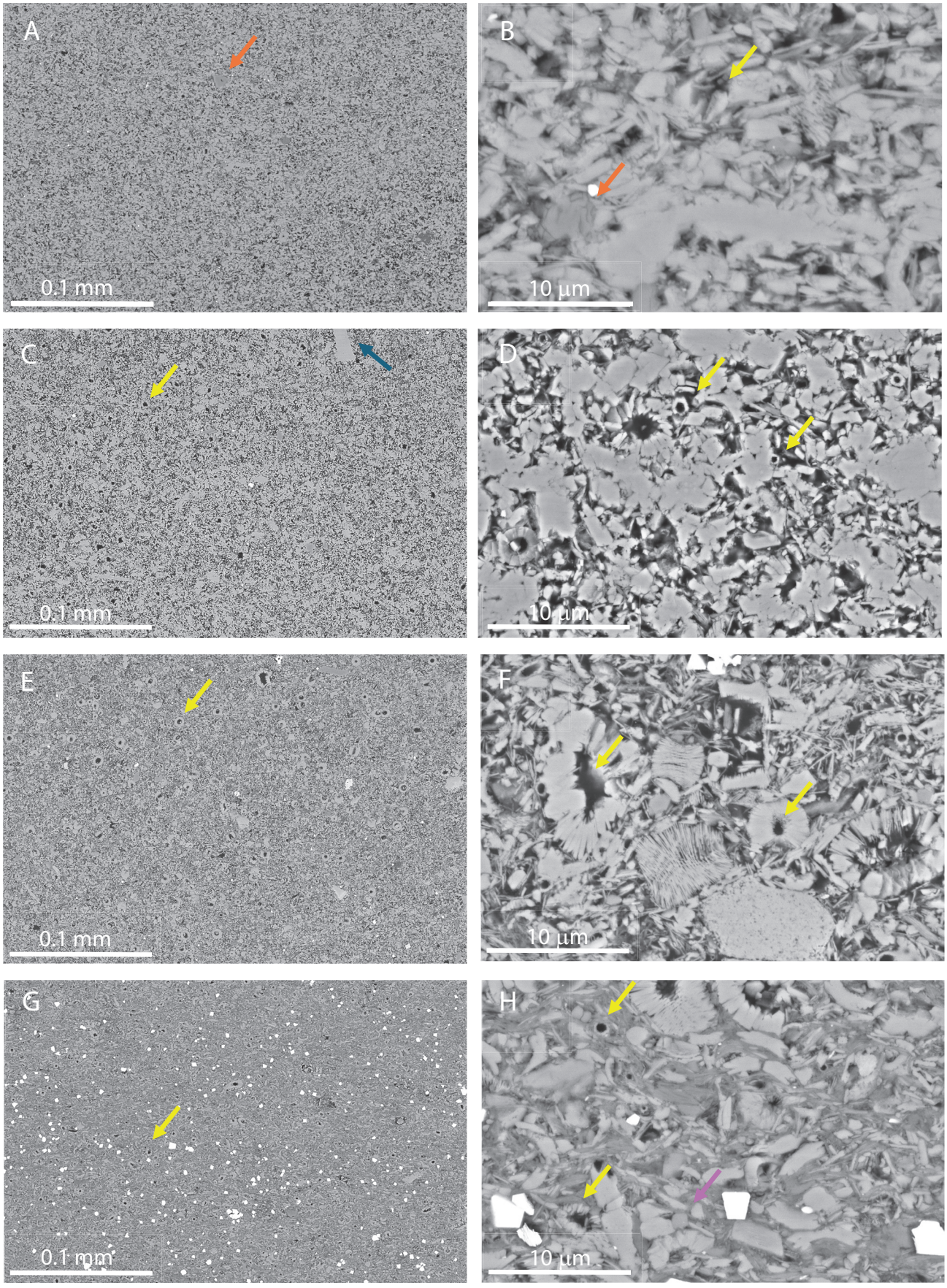
Fig. 13. Backscattered electron micrographs illustrating texture (left) and pore geometry (right) of Facies 2x (flaser-laminated slightly marly chalk). (**A, B**) 8444'11'', Middle Tuxen Formation. The sample is from upper part of the transition zone (ref. Fig. 3) and has mudstone texture. It has contorted lamination representing varying clay content. Fossil debris (blue arrows) and mouldic porosity (yellow arrow) occur locally. Clusters of submicron size pyrite (white) are seen. The closeup reveals nannofossil debris locally packed with clay and quartz silt (pink arrow) and locally bearing interparticle porosity and even intra-nannofossil porosity (yellow arrows).

adapt to the substrate. This model, however, does not explain the scarcity of planktonic microfossils. Biogenic debris is mainly composed of calcite. Silt particles of quartz (Fig. 5) and kaolinitic claystone occur throughout the slightly marly chalk to marlstone lithologies (Fig. 7; Table 3), and a single silt-sized clast of plagioclase feldspar was noted in a marlstone from the lower Sola Formation (8381'11'') (Fig. 7). The clay component is predominately detrital and is primarily kaolinite. The relatively frequent occurrence of kaolinitic claystone clasts points to a nearby source of detrital sediments in accordance with Blok *et al.* (2022, 2023). The dominance of kaolinite and quartz silt together with clay-sized kaolinite point to a weathered granitic source and possible transport by mass flow. The Munk Marl Bed has been reported to have a high concentration of organic matter (Jensen & Buchardt 1987), but this was not unequivocally identified from the SEM sample inspection. Organic particles may be difficult to distinguish from impregnated pores, and resultingly they may have been overlooked.

The macroscopically homogeneous bioturbation appears massive in thin section, although biomottling and trace fossils mainly are discernible in the more clay-rich marlstone lithologies (marly chalk, chalky marlstone and marlstone) (Figs 9, 11). The fact that biomottling is identifiable in the BSE micrographs indicates that the uneven distribution of non-carbonate particles, and thus bioturbation, also occurs at the microscopic scale (Fig. 6).

The macroscopically parallel-laminated Facies 4c and 5c, also microscopically appear laminated and represent the clay-rich chalky marlstone and marlstone lithologies. Shear-deformation has previously been argued as having a significant influence on microfabric based on analyses of porosity patterns in the Upper Cretaceous Chalk Group (Anderskouv & Surlyk 2012), and indeed localized pore collapse caused by stress with a shear component has been

Fig. 14. Backscattered electron micrographs illustrating texture (left) and pore geometry (right) of Facies 2y (shear-deformed slightly marly chalk; **A, B**), Facies 3y (shear-deformed marly chalk; **C**, **D**), Facies 4y (shear-deformed chalky marlstone; **E**, **F**) and Facies 5y (shear-deformed marlstone; **G**, **H**). (**A, B**) Sample from 8413'1'', Middle Tuxen Formation, upper part of transition zone (ref. Fig. 3). The sample has massive mudstone texture with single kaolinitic claystone clasts (orange arrow). The closeup reveals densely packed partly recrystallized nannofossil debris and widespread interparticle porosity (yellow arrow). (**C**, **D**) Sample from 8526'11'', Lower Tuxen Formation. The sample is from the transition zone (ref. Fig. 3) and has massive mudstone texture with single fossil fragments (blue arrow). Intra-microfossil porosity is widespread (yellow arrow). The closeup reveals recrystallized but still visibly biogenic nannofossils with some preserved intrafossil porosity and widespread interparticle porosity (yellow arrows). (**E**, **F**) Sample from 8350'5'', Middle Sola Formation, oil zone (ref. Fig. 3). The sample has massive mudstone texture. Intrafossil porosity is widespread (yellow arrow). The closeup reveals nannofossil debris (including nannoconids) with minor clay. Intrafossil (yellow arrows) and interparticle porosity are widespread. (**G**, **H**) Sample from 8385'11'', Lower Sola Formation, oil zone (ref. Fig. 3). The sample has massive mudstone texture. Intrafossil porosity is widespread (yellow arrow) as are submicron-sized pyrite crystals (white). The closeup reveals partly recrystallized nannofossil debris (including nannoconids) packed with clay and quartz silt (pink arrow). Micron size pyrite crystals (white) are seen. Intrafossil porosity (yellow arrows) and local interparticle porosity are noted.


A
0.1 mm
B
10 µm
C
0.1 mm
D
10 µm
E
0.1 mm
F
10 µm
G
0.1 mm
H
10 µm

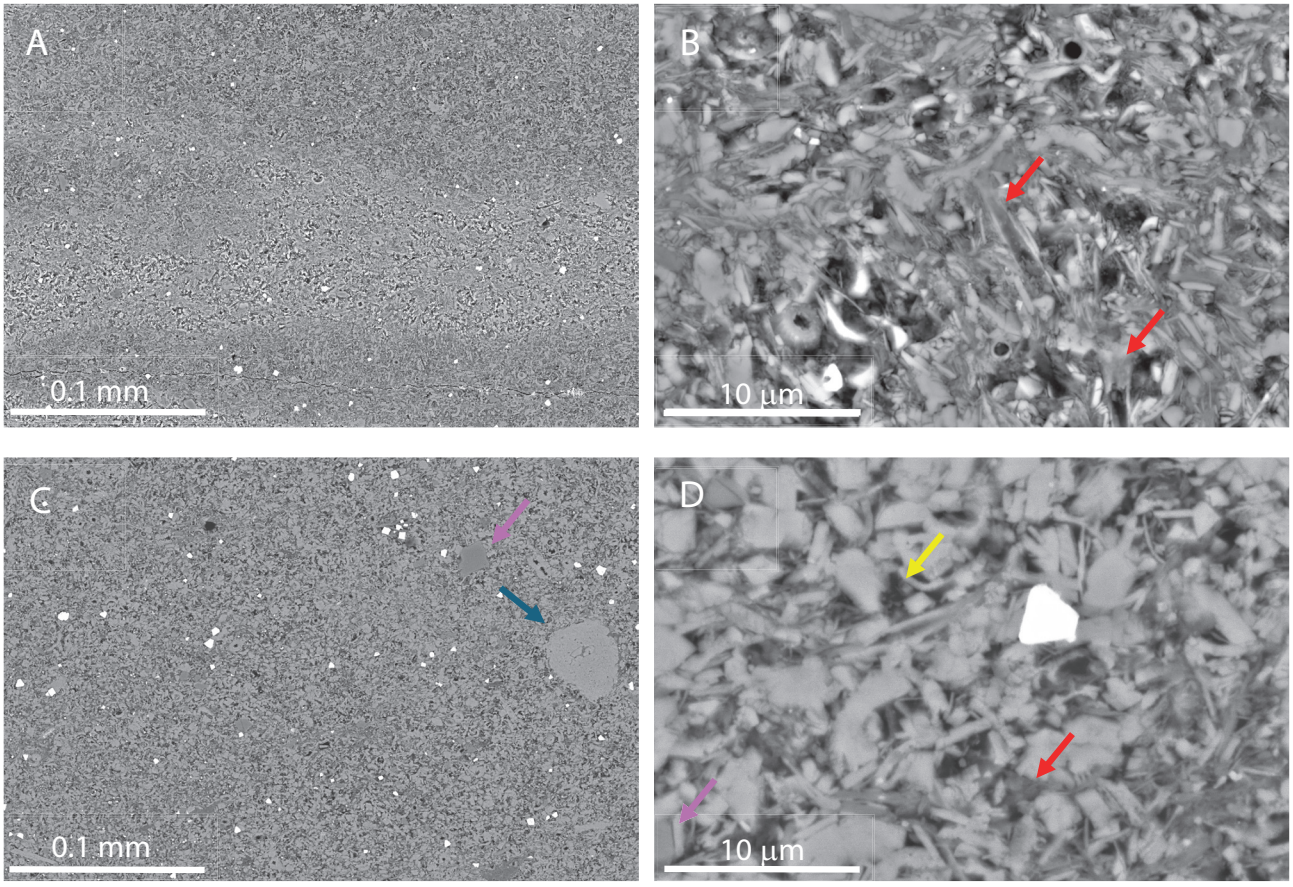


Fig. 15. Backscattered electron micrographs, illustrating texture (left) and pore geometry (right) of Facies 2z (silicified slightly marly chalk; **A, B**) and Facies 3z (silicified marly chalk; **C**, **D**). (**A**, **B**) Sample from 8377'2", Lower Sola Formation, oil zone (ref. Fig. 3). The sample has massive mudstone texture and is unevenly cemented by silica (red arrow). (**C**, **D**) Sample from 8495'1", Lower Tuxen Formation. The sample is from the transition zone (ref. Fig. 3) and has massive mudstone texture with single bioclasts (blue arrow) and quartz silt (pink arrow). Submicron size pyrite crystals (white) are widespread. The closeup reveals moderately recrystallized nannofossil debris, loosely packed with clay and quartz silt (pink arrow). Local possible silica cement is indicated with red arrow. The sample holds widespread interparticle porosity (yellow arrow).

found to result in deformation bands (Wennberg *et al.* 2013; Fabricius 2020). Macroscopically observed deformation bands (Jelby *et al.* 2022) were not observed microscopically, perhaps due to not being sampled (Figs 14, A4).

Shallow burial diagenesis

Pyrite is abundant, generally as dispersed submicron-sized crystals, especially in the more clay-rich facies (Fig. 6). In some cases, the pyrite is localized in layers or clusters, probably reflecting trace fossils (Fig. A1(A)), and in one instance as framboids (in the Munk Marl Bed; Fig. A3(H)). Pyrite in pelagic carbonate ooze has been shown to form at shallow depth when organic matter is consumed by sulphate-reducing bacteria and substituted by pyrite. Musgrave *et al.* (1993) demonstrated how this process can lead to dissolution of magnetite, because Fe is needed for the precipitation of pyrite.

Dolomite is locally present as single crystals (Figs 6–8). The diagenetic formation of this mineral requires a source of magnesium. A typical source would be biogenic, e.g. high-magnesium calcite dissolved during early recrystallization at shallow burial (e.g. Eberli *et al.* 1997). All observed dolomite crystals are overgrown by calcite.

The clay-poor intervals contain minute unidentifiable calcitic particles, which for simplicity is described as nannofossil debris (Figs 4, 5), although an abiogenic diagenetic origin cannot be fully precluded (Tagliavento *et al.* 2021).

Burial diagenesis – impact of oil saturation

Nannofossils are in different degrees of recrystallization, reflecting oil saturation and clay content. The best preserved nannofossils are found in the oil zone,

Table 3. Overview of microscopic observations

Stratigraphy	Lithology and facies	Depositional features	Diagenetic features
Middle Sola Formation	4b, 4y	Massive mudstone texture Well-preserved nannofossil debris	Submicron-sized pyrite
Middle Sola Formation	4c, 5c	Laminated mudstone texture. Variation in clay content. Well-preserved nannofossil debris. Quartz silt	Pyrite crystals location follows lamination Some framboids Rare other sulphides
Lower Sola Formation	2a (clay-rich), 5a, 2b, 3b, 5b, 5y, 2z	Massive mudstone texture. Well-preserved nannofossil debris. Quartz, feldspar and kaolinitic claystone silt. Bioclasts	Submicron-sized and 10 micron sized pyrite Calcite-rimmed dolomite crystals with TiO_2
Lower Sola Formation	5c	Laminated mudstone texture. Variation in clay content. Well-preserved nannofossil debris Kaolinitic claystone silt	
Upper Tuxen Formation	1a	Massive mudstone texture Nannoconid fragments	Partial recrystallization of calcareous nannofossil debris Recrystallized calcitic microfossil Pyrite-cemented microfossils
Middle Tuxen Formation	1a, 2a (clay-poor), 2b (clay-poor)	Massive mudstone texture	Heavily recrystallized (few biogenic features) pyrite
Middle Tuxen Formation	2a (clay-rich), 4a, 2b (clay-rich), 3b, 5b, 2x, 2y	Massive mudstone texture Sparse microfossils and microfossil debris Quartz and kaolinitic claystone silt	Partially recrystallized nannofossil debris Calcite-rimmed dolomite crystals Microfossil cemented by Fe-bearing calcite, TiO_2 Few submicron-sized pyrite crystals
Middle Tuxen Formation	5c	Laminated mudstone texture Variation in clay content Well-preserved nannofossil debris	
Munk Marl Bed	5c	Laminated mudstone texture. Variation in clay content. Well-preserved nannofossil debris. Quartz and kaolinitic claystone silt	Micron-sized pyrite crystals Locally pyrite framboids
Lower Tuxen Formation	2a (clay-poor), 2b (clay-poor), 3b (clay-poor), 2y, 3y, 2z, 3z	Massive mudstone texture Quartz and kaolinitic claystone silt	Heavily recrystallized (single biogenic features) Calcite-rimmed dolomite crystals
Lower Tuxen Formation	2a (clay-rich) 3a, 4a 2b (clay-rich), 3b (clay-rich)	Massive mudstone texture Quartz silt, kaolinitic claystone silt	Partially recrystallized nannofossil debris Calcite-rimmed dolomite crystals Single pyrite clusters and crystals
Valhall Formation	2a (clay-poor)	Massive mudstone texture	Heavily recrystallized carbonate mud Completely recrystallized microfossils
Valhall Formation	4b	Massive mudstone texture Quartz silt	Partially recrystallized nannofossil debris Single pyrite clusters and crystals Diagenetic kaolinite in intrafossil porosity

which in the Boje-2C well comprises the clay-rich Sola Formation and upper Tuxen Formation (Figs 3, 7E, F, 9A, B, 10A, B, 11A, B, 12A–D, 14E, F, A1(A, B), A2(A–F)). Well-preserved nannofossils are also found in the clay-rich Munk Marl Bed (Fig. A3(F)). The clay-poor lithologies of chalk and slightly marly chalk are mainly present in the Tuxen Formation (Figs 4, 5, 8), although one sample from the generally clay-rich Valhall Formation displays the same lithology (Fig. A2(I, J)). The BSE images indicate how the degree of recrystallization gradually increases with depth, while porosity gradually decreases from around 25% to around 17% (Storebø *et al.* 2022a). The recrystallisation is accompanied by pore-filling ce-

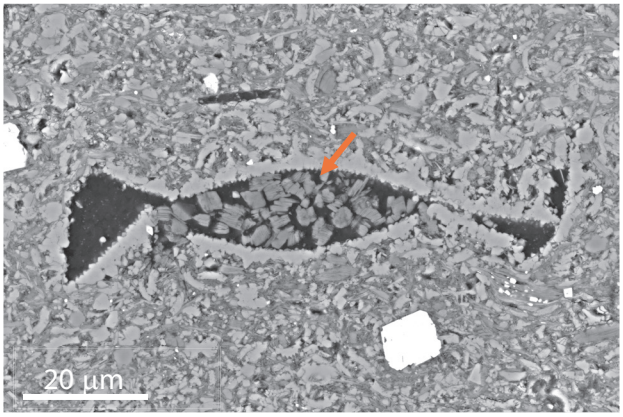


Fig. 16. Backscattered electron micrograph. Diagenetic kaolinite (orange arrow) precipitated in cavity of collapsed microfossil in sample from 8604'2", Valhall Formation, Facies 4b.

mentation, as indicated by the porosity gradient. The calcite is possibly partly sourced from the water zone which was not cored in the Boje-2C well, although pressure dissolution at flaser structures (*sensu lato* solution seams; Garrison & Kennedy 1977; Jelby *et al.* 2022) should also play a role. The difference in calcite cementation between the oil zone and transition zone likely reflects the water saturation at the time of cementation, during which pore space in the upper levels was filled with hydrocarbons and lined with a thin water-film on particle surfaces, while free water dominated the pore space at the deepest levels. Calcite redistribution in the hydrocarbon-bearing interval would then have to have taken place through diffusion in the water film covering the calcite (e.g. Fabricius & Borre 2007).

Burial diagenesis – impact of pressure

During description of the cores from Boje-2C an absence of stylolites was noted (Jelby *et al.* 2022; Glad *et al.* 2022), but flaser structures were observed (*sensu lato* solution seams; Garrison & Kennedy 1977; Jelby *et al.* 2022). Although distinct pressure dissolution features at clay-calcite contacts are not obvious in SEM images (Fig. 13), pressure dissolution may well play a role during the burial diagenesis. In deep sea calcareous sediments, pressure dissolution has been found to take place when the calcite crystals are elastically strained to ~0.003 (Fabricius 2020). (The in situ elastic strain can be calculated from burial depth, bulk density and elastic wave velocity). In deep-sea calcareous pelagic sediments, this strain is reached twice during burial: The first time occurs at the transition from carbonate ooze to chalk, where pressure dissolution causes contact cementation and a drop in strain due to increased particle contact area. In the contact-cemented, carbonate-rich intervals of Boje-2C elastic strain is accordingly around 0.001 (Fabricius & Meireles 2025). The second time pressure dissolution sets in, happens after dispersed clay has recrystallized into clay-rich laminae (Lind 1993; Fabricius & Borre 2007). The dissolved carbonate precipitates as pore-filling cement and no contact cement binds clay and calcite, so strain remains high at this interface and pressure dissolution can continue. In pelagic chalks with low clay content, proper stylolites form (Lind 1993), whereas in more clay-rich pelagic carbonates, a higher density of clay-rich laminae arises and flaser structures develop (Sigurdsson *et al.* 1997; Fabricius 2000). The presence of flaser structures in Boje-2C thus shows that although Boje-2C is overpressured, the pore pressure is not high enough to prevent pressure dissolution.

Silicification and diagenetic kaolinite

Macroscopically evident silicification is not readily identified in the BSE images, probably because silicification is not always pervasive (Fig. 15A) and in some cases only with difficulty noted as aggregates of micro-silica (Fig. 15B).

In a single case, silicification appears as pore-filling cement (Fig. 15), where the silica may have been sourced from siliceous fossils dissolved where the prevalent possible moulds are seen (Figs 10–13). The amorphous appearance of the silica indicates that it may have precipitated as opal-CT, which has later recrystallized to quartz.

Single particles of kaolinite are observed widely in clay-bearing samples and may generally be assumed to be detrital, but some of the particles may have a diagenetic origin, as exemplified by a single case where diagenetic kaolinite was noticed in the intrafossil porosity of a collapsed microfossil (Fig. 16).

Conclusions

A total of 66 samples were analysed in the Lower Cretaceous Tuxen and Sola formations in the cored section of the Boje-2C well (Boje Field, Danish Central Graben, North Sea) through backscatter electron microscopy to delineate how the microscopic character reflects previously recorded macroscopic sedimentary facies and to identify indications of diagenesis. The samples are dominated by calcareous nannofossils, microscopic calcite particles, varying concentrations of presumably detrital clay minerals, minor detrital quartz and kaolinitic claystone (silt) and diagenetic components (calcite cement, silica, pyrite, dolomite). Some of the microscopic calcite particles are clearly derived from nannoconids.

Microfossils are remarkably sparse and particles attributable to benthic fossils are virtually absent.

Porosity is dominantly inter-particular with subordinate intra-particle porosity mainly occurring within nannoconids and less frequently moulds.

In clay-rich samples, kaolinite clay is typically the supporting mineral and calcite particles are separate, embedded in clay. In more calcite-rich samples, calcite particles are in full contact (cemented) and with depth tend to increase in angularity of shape. Pore-filling cementation is found in the deepest samples. The depth-dependant differences in calcite cementation are attributed to the early emplacement of hydrocarbons, which left free water in deeper levels, where cementation took place, while water occurred as film on particles in upper levels where cementation is less prevalent.

Some macroscopic features, such as biomottling and parallel lamination, are clearly reflected in the microscopic texture, whereas shear deformation is indistinguishable from homogeneous bioturbation. By contrast, macroscopically parallel-laminated marlstone of the Munk Marl Bed locally appears microscopically shear-deformed.

Acknowledgements

We gratefully acknowledge the Danish Underground Consortium (TotalEnergies E&P Denmark, BlueNord and Nordsøfonden) for granting permission to publish this work. The study was funded by the Danish Offshore Technology Centre (DTU Offshore). MEJ also acknowledges the Carlsberg Foundation for granting an Internationalisation Fellowship (CF22-0122) and Reintegration Fellowship (CF24-1960), during which this work was partly undertaken. Rikke Weibel and an anonymous reviewer are thanked for constructive comments which helped improve the outcome of this paper. Backscatter micrographs not included in the present paper are available from ILF and KA.

References

Anderskouv, K. & Surlyk, F. 2012: The influence of depositional processes on the porosity of chalk. Journal of the Geological Society 169, 311–325. https://doi.org/10.1144/0016-76492011-079

Blok, C.N., Ineson, J., Anderskouv, K., Fantasia, A., Sheldon, E., Thibault, N., Jelby, M.E., Adatte, T. & Bodin, S. 2022: Latitude dependant climate changes across the Aptian Oceanic Anoxic Event 1a. Palaeogeography, Palaeoclimatology, Palaeoecology 601, 111085. https://doi.org/10.1016/j.palaeo.2022.111085

Blok, C.N., Adatte, T., Ineson, J.R., Sheldon, E., Jelby, M.E., Smit, F.W.H., Lauridsen, B.W., Anderskouv, K. & Bodin, S. 2023.: Clay mineral assemblages as a tool in source-to-sink studies: an example from the Lower Cretaceous of the North Sea Basin. Bulletin of the Geological Society of Denmark, 71, 99–113. https://doi.org/10.37570/bgsd-2023-71-06

Copestake, P., Sims, A.P., Crittenden, S., Hamar, G.P., Ineson, J.R., Rose, P.T. & Tringham, M.E. 2003: Lower Cretaceous. In: Evans, D. et al. (eds): The Millennium Atlas: petroleum geology of the central and northern North Sea. The Geological Society, London, 191–211.

Damtoft, K., Nielsen, L.H., Johannessen, P.N., Thomsen, E. & Andersen, P.R. 1992: Hydrocarbon plays of the Danish Central Trough. In: Spencer, A.M. (ed.): Generation, accumulation and production of Europe's hydrocarbons II, 35–58. Special Publication of the European Association of Petroleum Geoscientists, Springer-Verlag, Berlin. https://doi.org/10.1144/0061331

Eberli, G.P., Swart, P.K., McNeill, D.F., Kenter, J.A.M., Anselmetti, F.S., Melim, L.A. & Ginsburg, R.N. 1997: A synopsis of the Bahamas Drilling Project: results from two deep core borings drilled on the Great Bahama Bank. In: Eberli, G.P., Swart, P.K., Malone, M.J. et al. (eds): Proceedings of the Ocean Drilling Program, Initial Reports 166, 23–41. College Station, TX. https://doi:10.2973/odp.proc.ir.166.103.1997

Fabricius, I.L. 2000: Interpretation of burial history and rebound from loading experiments and the occurence of microstylolites in the mixed sediments of the Caribbean Sites 999 and 1001. In: Leckie, R.M., Sigurdsson, H., Acton, G.D. & Draper, G. (eds): Proceedings of the Ocean Drilling Program, Scientific Results 165, 177–190. College Station, TX. https://doi:10.2973/odp.proc.sr.165.006.2000

Fabricius I.L. 2020: Porosity in chalk – roles of elastic strain and plastic strain. Sedimentology 67, 3451–3470. https://doi:10.1111/sed.12750.

Fabricius, I.L. & Borre, M.K. 2007: Stylolites, porosity, depositional texture, and silicates in chalk facies sediments. Ontong Java Plateau – Gorm and Tyra fields, North Sea. Sedimentology 54, 183–205. https://doi.org/10.1111/j.1365-3091.2006.00828.x

Fabricius, I.L., Olsen, C. & Prasad, M. 2005: Log interpretation of marly chalk, the Lower Cretaceous Valdemar Field, Danish North Sea: application of iso-frame and pseudo water film concepts. The Leading Edge 24, 496–505. https://doi.org/10.1190/1.1926807

Fabricius, I.L. & Meireles, L.T.P. 2025. Assessment of pore collapse in North Sea Lower Cretaceous carbonates using downhole elastic strain. Bulletin of the Geological Society of Denmark, 71, 115–125. https://doi.org/10.37570/bgsd-2025-71-07

Gale, A.S., Mutterlose, J., Batenburg, S., Gradstein, F.M., Agterberg, F.P., Ogg, J.G. & Petrizzo, M.R. 2020: The Cretaceous Period. In: Gradstein, F.M., Ogg, J.G., Schmitz, M.D. and Ogg, G.M. (eds): Geological Time Scale 2020, 1023–1086. Boston: Elsevier. https://doi.org/10.1016/b978-0-12-824360-2.00027-9

Garrison, R.E. & Kennedy, W.J. 1977: Origin of solution seams and flaser structure in Upper Cretaceous chalks of southern England. Sedimentary Geology 19, 107–137. https://doi.org/10.1016/0037-0738(77)90027-6

Glad, A.C., Amour, F., Welch, M.J., Clausen, O.R., Anderskouv, K., Ineson, J.R., Sheldon, E. & Nick, H.M. 2022: Natural fractures and discontinuities in a Lower Cretaceous chalk-marlstone reservoir, Valdemar Field, Danish North Sea. Marine and Petroleum Geology 136, 105445. https://doi.

org/10.1016/j.marpetgeo.2021.105445
Hesselbo, S.P., Ogg, J.G., Ruhl, M., Hinnov, L.A. & Huang, C.J. 2020: The Jurassic Period. In: Gradstein, F.M., Ogg, J.G., Schmitz, M.D. and Ogg, G.M. (eds): Geological Time Scale 2020, 955–1021. Boston: Elsevier. https://doi.org/10.1016/b978-0-12-824360-2.00026-7
Ineson, J.R. 1993: The Lower Cretaceous chalk play in the Danish Central Trough. In: Parker, J.R. (ed.): Petroleum Geology of Northwest Europe: Proceedings of the 4th Conference, 175–183. Geological Society, London. https://doi.org/10.1144/0040175
Ineson, J.R., Lauridsen, B.W., Lode, S., Sheldon, E., Sørensen, H.O., Wisshak, M. & Anderskouv, K. 2022a: A condensed chalk–marl succession on an Early Cretaceous intrabasinal structural high, Danish Central Graben: Implications for the sequence stratigraphic interpretation of the Munk Marl Bed. Sedimentary Geology, 440, 106234. https://doi.org/10.1016/j.sedgeo.2022.106234
Ineson, J.R., Petersen, H.I., Andersen, C., Bjerager, M., Jakobsen, F.C., Kristensen, L., Mørk, F. & Sheldon, E. 2022b: Early Cretaceous stratigraphic and basinal evolution of the Danish Central Graben: a review. Bulletin of the Geological Society of Denmark, 71, 75–98. https://doi.org/10.37570/bgsd-2022-71-05
Jakobsen, F., Ineson, J.R., Kristensen, L. & Stemmerik, L. 2004: Characterization and zonation of a marly chalk reservoir: the Lower Cretaceous Valdemar Field of the Danish Central Graben. Petroleum Geoscience 10, 21–33. https://doi.org/10.1144/1354-079303-584
Jakobsen, F., Ineson, J.R., Kristensen, L., Nytoft, H.P. & Stemmerik, L. 2005: The Valdemar Field, Danish Central Graben: field compartmentalization and regional prospectivity of the Lower Cretaceous chalk play. In: Doré, A.G. & Vining, B.A. (eds): Petroleum Geology: North-West Europe and Global Perspectives—Proceedings of the 6th Petroleum Geology Conference, 177–186. Geological Society, London. https://doi.org/10.1144/0060177
Japsen, P., Britze, P. & Andersen, C. 2003: Upper Jurassic – Lower Cretaceous of the Danish Central Graben: structural framework and nomenclature. Geological Survey of Denmark and Greenland Bulletin 1, 233–246. https://doi.org/10.34194/geusb.v1.4653
Jelby, M.E., Ineson, J.R., Thibault, N., Bodin, S., Blok, C.N., Edvardsen, N., Clemmensen, T.S., Buls, T. & Anderskouv, K. 2022: Facies and depositional processes of Lower Cretaceous carbonates, Danish Central Graben. Bulletin of the Geological Society of Denmark 71, 51–74. https://doi.org/10.37570/bgsd-2022-71-04
Jelby, M.E., Ineson, J.R., Sheldon, E. & Anderskouv, K. 2024: Old chalk, new tricks: revisiting the Lower Cretaceous carbonates of the Danish Central Graben. In: Hart, M.B., Batenburg, S.J., Huber, B.T., Price, G.D., Thibault, N., Wagreich, M. & Walaszczyk, I. (eds): Cretaceous Project 200 Volume 2: Regional Studies. Geological Society, London, Special Publications 545. https://doi.org/10.1144/sp545-2023–134
Jensen, T.F. & Buchardt, B. 1987: Sedimentology and geochemistry of the organic carbon-rich Lower Cretaceous Sola Formation (Baremian–Albian), Danish North Sea. In: Brooks, J. & Glennie, K. (eds): Petroleum Geology of North-West Europe, 431–440. Graham & Trotman.
Jensen, T.F., Holm, L., Frandsen, N. & Michelsen, O. 1986: Jurassic - Lower Cretaceous lithostratigraphic nomenclature for the Danish Central Trough. Danmarks Geologiske Undersøgelse, Serie A, 12, 64 pp. https://doi.org/10.34194/seriea.v12.7031
Kühnau, L. & Michelsen, O. 1994: Detailed log-stratigraphic study of the Lower Cretaceous in the Danish Central Trough, North Sea. Marine and Petroleum Geology 11, 467–477. https://doi.org/10.1016/0264-8172(94)90080-9Get rights and content
Lauridsen, B.W., Lode, S., Sheldon, E., Frykman, P., Anderskouv, K. & Ineson, J. 2022: Lower Cretaceous (Hauterivian–Aptian) pelagic carbonates in the Danish Basin: new data from the Vinding-1 well, central Jylland, Denmark. Bulletin of the Geological Society of Denmark, 71, 7–29. https://doi.org/10.37570/bgsd-2022-71-02
Lind, I.L. 1993: Stylolites in chalk from Leg 130, Ontong Java Plateau. Proceedings of the Ocean Drilling Program, Scientific Results 130, 445–451. College Station, TX. https://doi.org/10.2973/odp.proc.sr.130.006.1993
Meireles, L.T.P. &. Fabricius, I.L. 2023: Deriving mineral moduli of the noncarbonate fraction in a marly chalk reservoir using petrophysical logging data and an isoframe model. Geophysics 88, D411–D425. https://doi.org/10.1190/geo2022-0493.1
Michelsen, O., Frandsen, N., Holm, L., Jensen, T.F., Møller, J.J. & Vejbæk, O.V. 1987: Jurassic - Lower Cretaceous of the Danish Central Trough; – depositional environments, tectonism, and reservoirs. Danmarks Geologiske Undersøgelse, Serie A, 16, 44 pp. https://doi.org/10.34194/seriea.v16.7035
Møller, J.J. & Rasmussen, E.S. 2003: Middle Jurassic – Early Cretaceous rifting of the Danish Central Graben. Geological Survey of Denmark and Greenland Bulletin 1, 247–264. https://doi.org/10.34194/geusb.v1.4654
Musgrave, R.J., Delaney, M.L., Stax, R. & Tarduno, J.A. 1993: Magnetic diagenesis, organic input, interstitial water chemistry, and palaeomagnetic record of the carbonate sequence of the Ontong Java Plateau. Proceedings of the Ocean Drilling Program, Scientific Results 130, 527–546.
Mutterlose, J. 1992: Migration and evolution patterns of floras and faunas in marine Early Cretaceous sediments of NW Europe. Palaeogeography, Palaeoclimatology, Palaeoecology 94, 261–282. https://doi.org/10.1016/0031-0182(92)90123-M
Mutterlose, J. & Bottini, C. 2013: Early Cretaceous chalks from the North Sea giving evidence for global change. Nature Communications 4, 1686.
Petersen, H.I. & Jakobsen, F.C. 2021: Lithostratigraphic definition of the Upper Jurassic – lowermost Cretaceous (upper Volgian–Ryazanian) organic-rich and oil-prone Mandal Formation in the Danish Central Graben, North Sea. Marine and Petroleum Geology, 129, 105116. https://doi.org/10.1016/j.marpetgeo.2021.105116
Sigurdsson, H., Leckie, R.M., Acton, G.D. et al. 1997: Proceedings of the Ocean Deep Drilling Project, Initial Reports 165: College Station, TX (Ocean Drilling Program). https://doi:10.2973/odp.proc.ir.165.1997
Storebø, E.M., Meireles, L.T.P. & Fabricius, I.L. 2022a: Permeability modelling in clay-rich carbonate. Petrophysics 63, 148–171. https://doi: 10.30632/PJV63N2-2022a2

Storebø, E.M., Hjuler, M.L., Meireles, L.T.P. & Fabricius, I.L. 2022b: Effect of pyrite in water saturation evaluation of clay-rich carbonate. Petrophysics 63, 172–198. https://doi: 10.30632/PJV63N2-2022a3

Tagliavento, M., John, C.M., Anderskouv, K. & Stemmerik, L. 2021: Towards a new understanding of the genesis of chalk: Diagenetic origin of micarbs confirmed by clumped isotope analysis. Sedimentology 68, 513–530. https://doi.org/10.1111/sed.12802

Tyson, R.V. & Funnell, B.M. 1987: European Cretaceous shorelines, stage by stage. Palaeogeography, Palaeoclimatology, Palaeoecology 59, 69–91. https://doi.org/10.1016/0031-0182(87)90075-7

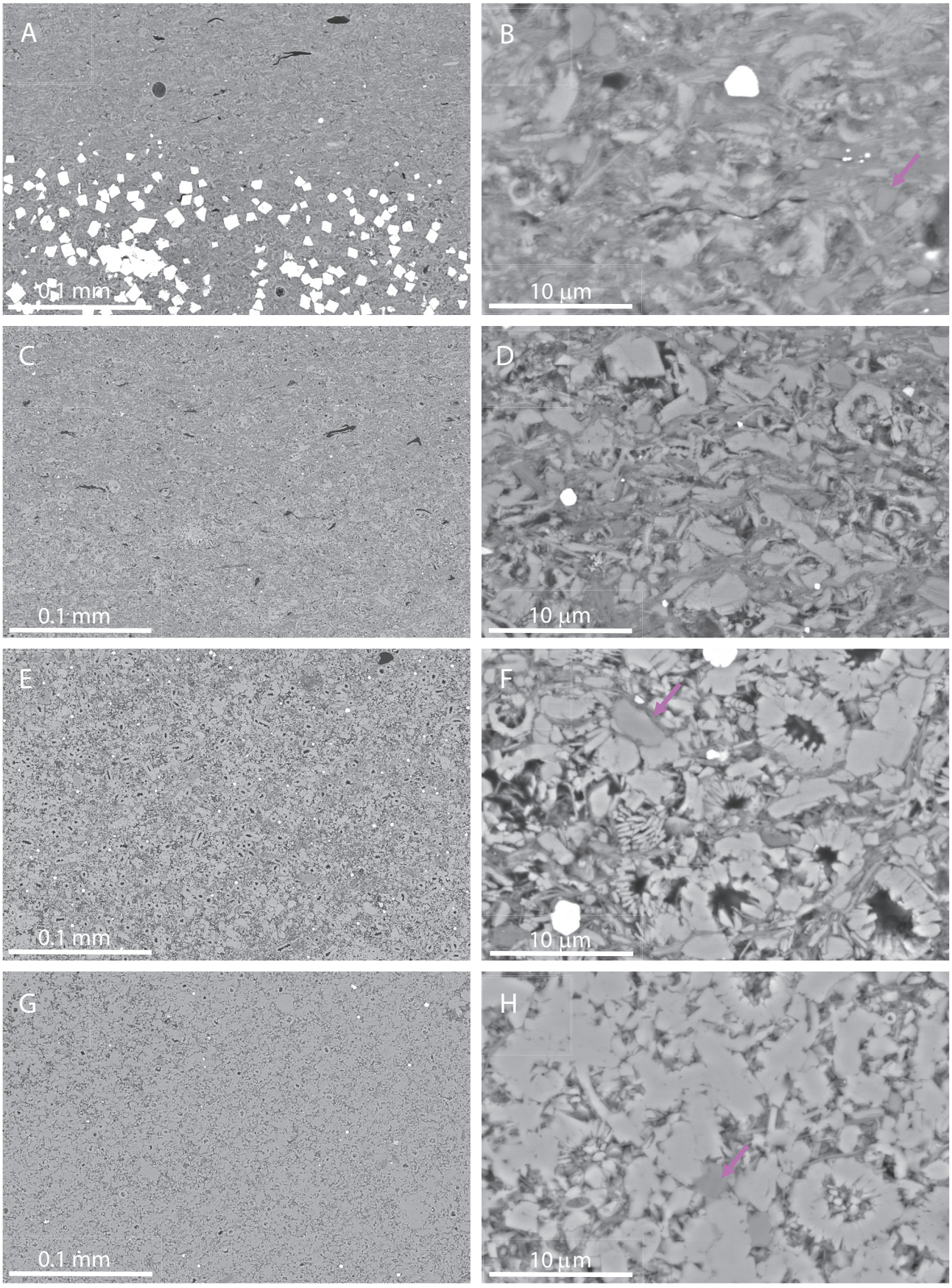
van Buchem, F.S.P., Smit, F.W.H., Buijs, G.J.A., Trudgill, B. & Larsen, P.-H. 2018: Tectonostratigraphic framework and depositional history of the Cretaceous–Danian succession of the Danish Central Graben (North Sea) – new light on a mature area. In: Bowman, M. & Levell, B. (eds): Petroleum Geology of NW Europe: 50 Years of Learning – Proceedings of the 8th Petroleum Geology Conference. Geological Society, London. https://doi.org/10.1144/PGC8.24.

Vejbæk, O.V. 1986: Seismic stratigraphy and tectonic evolution of the Lower Cretaceous in the Danish Central Trough. Danmarks Geologiske Undersøgelse, Serie A, 11, 57 pp. https://doi.org/10.34194/seriea.v11.7030

Vejbæk, O.V. & Andersen, C. 1987: Cretaceous–Early Tertiary inversion tectonism in the Danish Central Trough. Tectonophysics 137, 221–238. https://doi.org/10.1016/0040-1951(87)90321-0

Wennberg, O.P., Casini, G., Jahanpanah, A., Lapponi, F., Ineson, J., Wall, B.G. & Gillespie, P. 2013: Deformation bands in chalk, examples from the Shetland Group of the Oseberg Field, North Sea, Norway. Journal of Structural Geology 56, 103–117. https://doi.org/10.1016/j.jsg.2013.09.005

Appendix


A
0.1 mm
B
10 µm
C
0.1 mm
D
10 µm
E
0.1 mm
F
10 µm
G
0.1 mm
H
10 µm

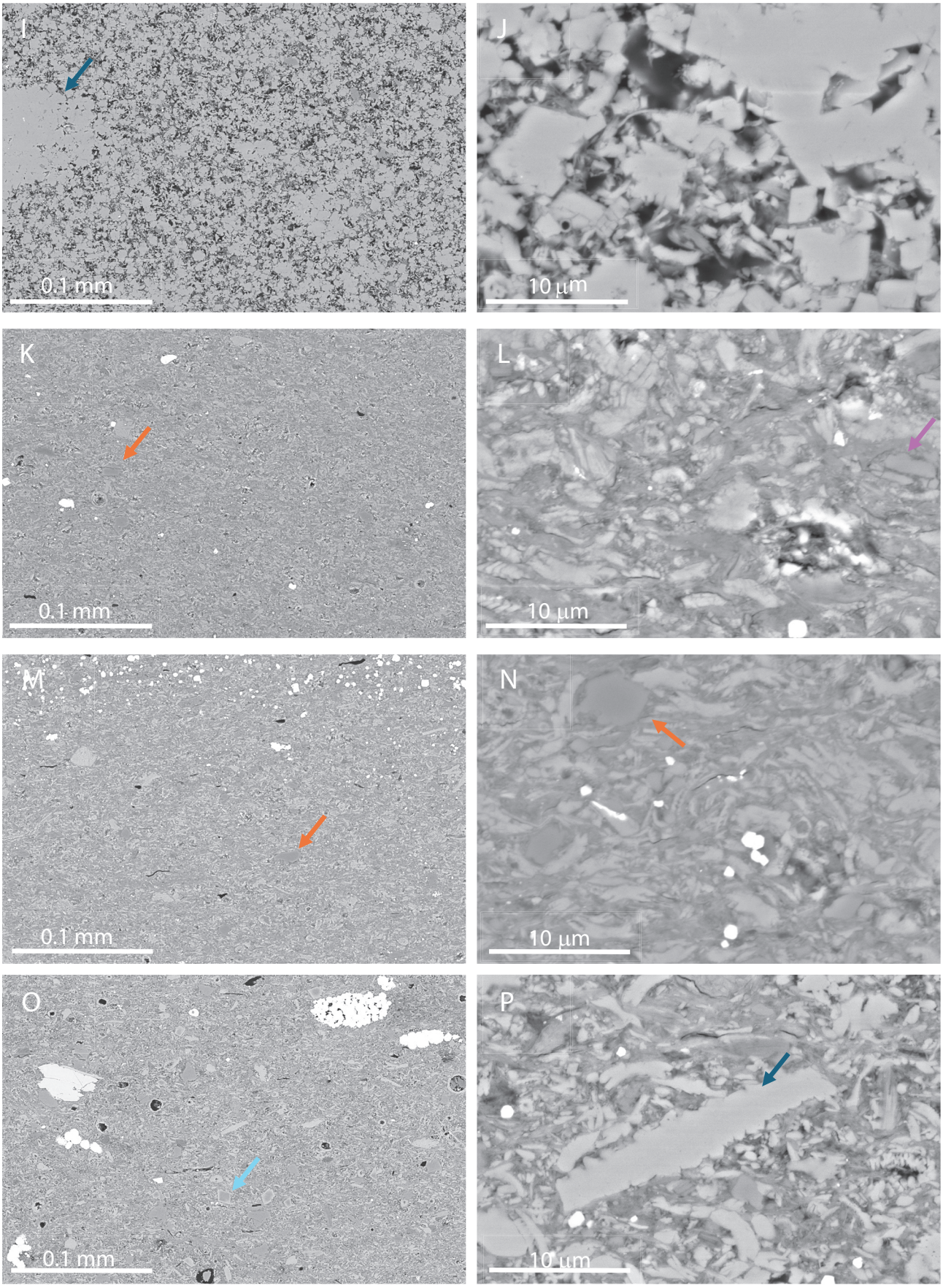
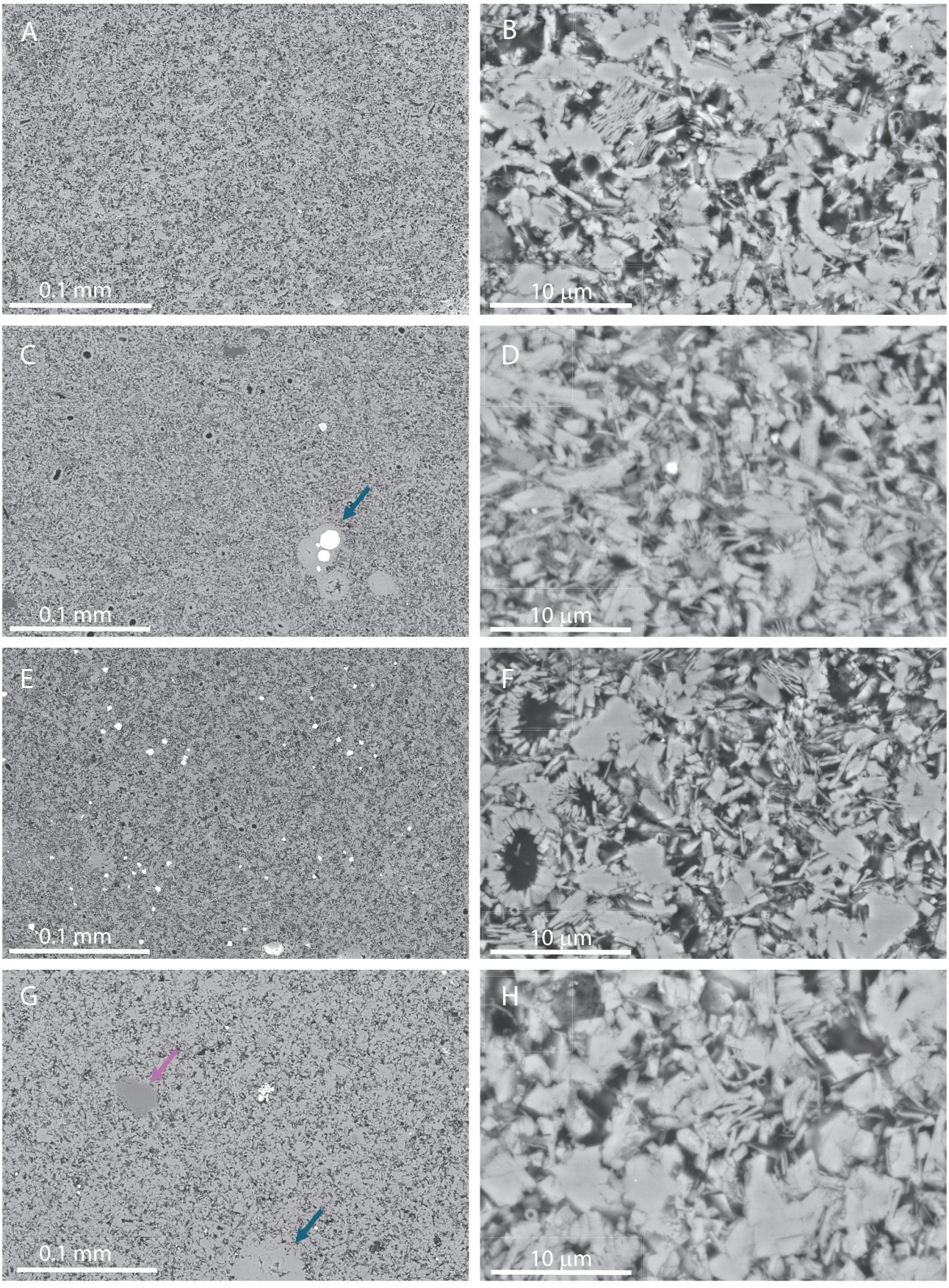
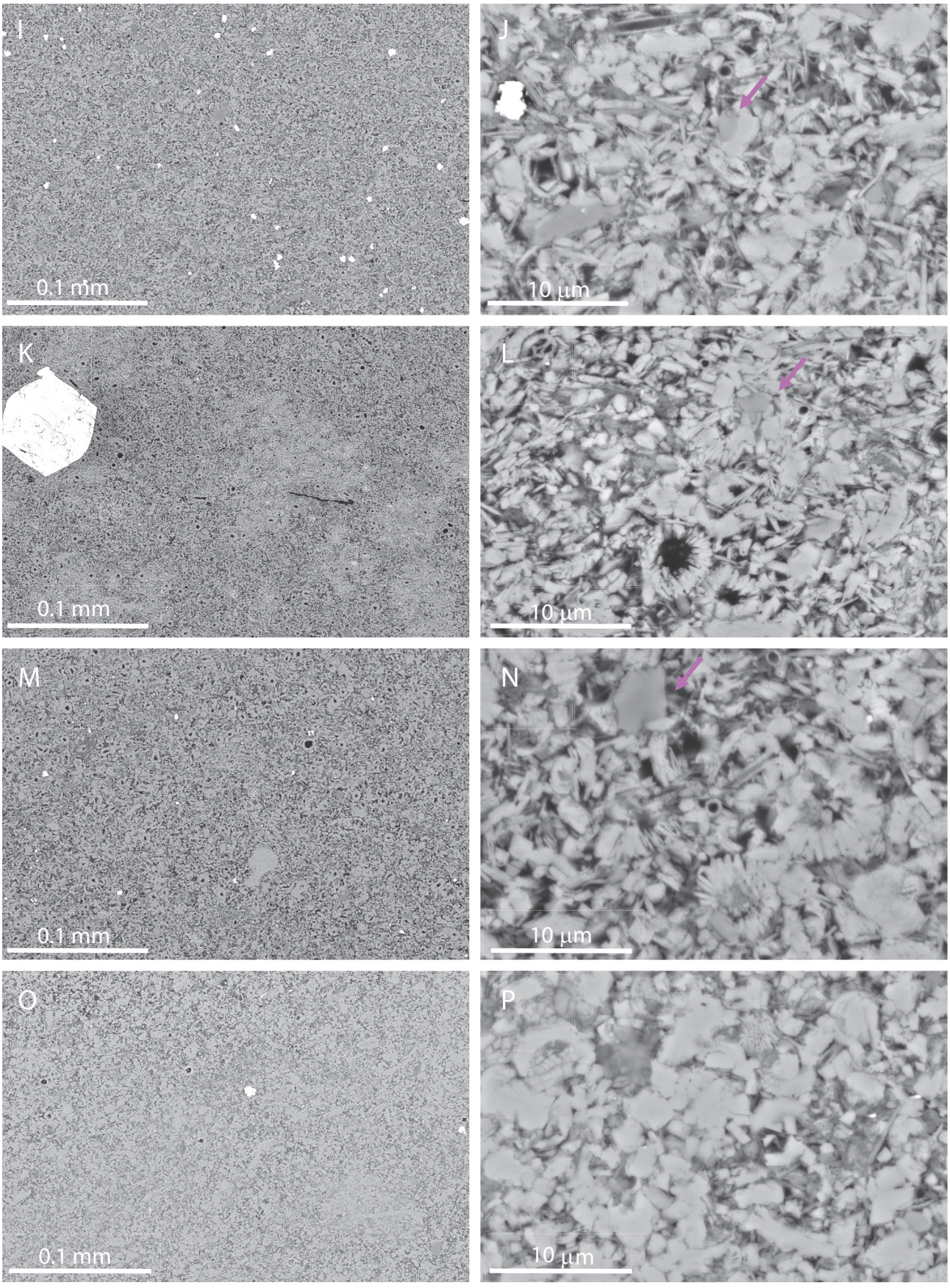
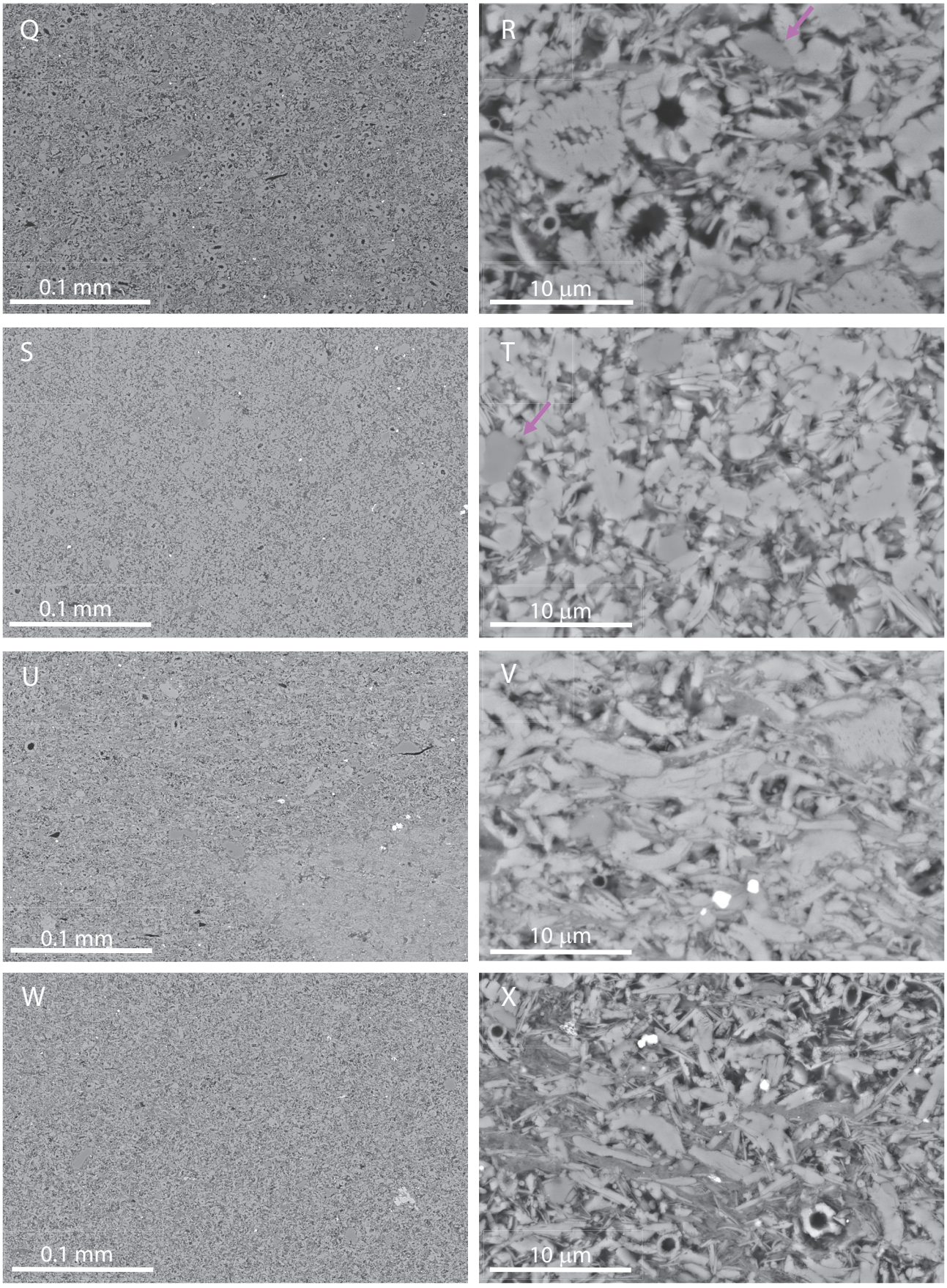
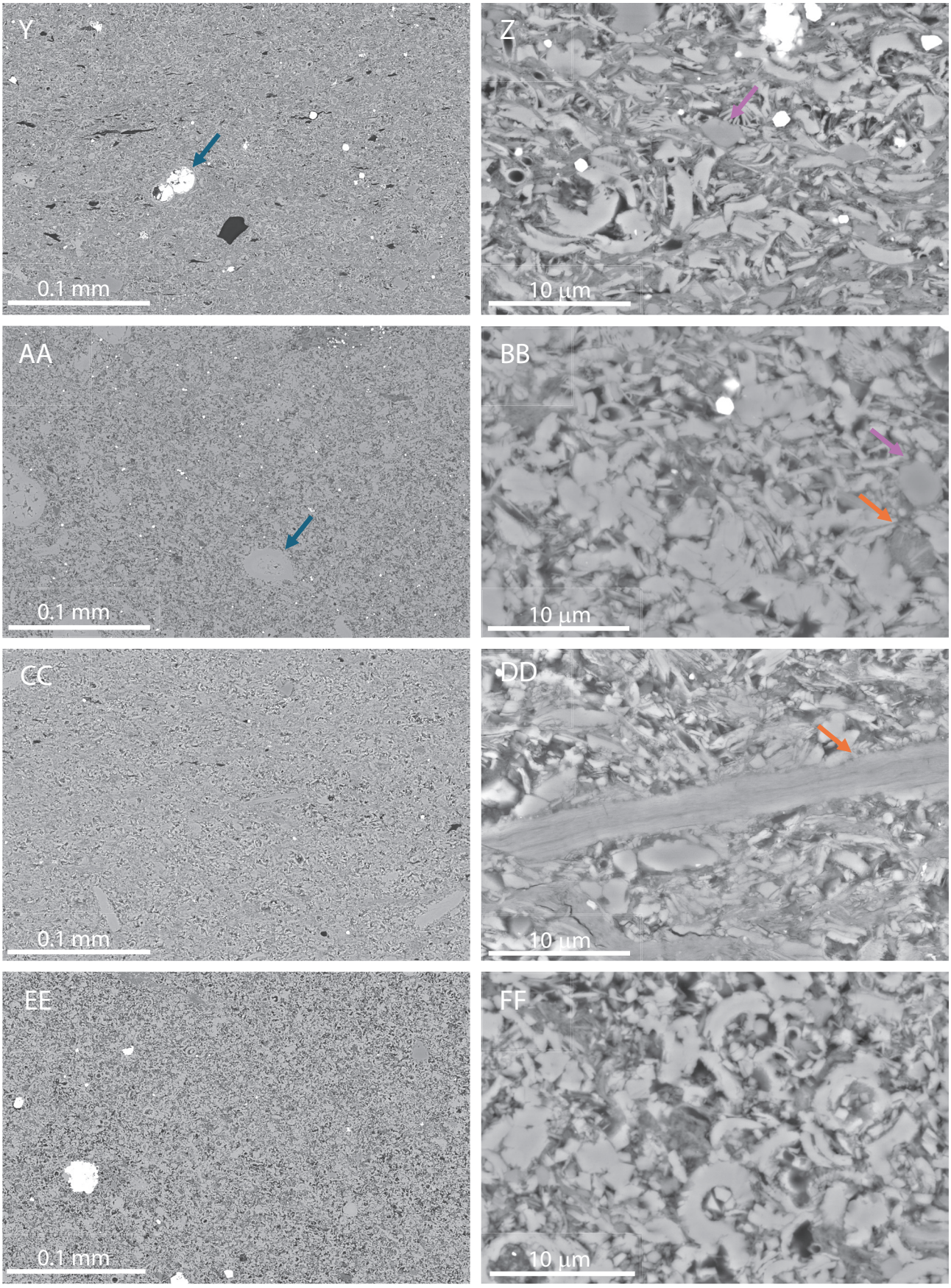

I
0.1 mm
J
10 µm
K
0.1 mm
L
10 µm
M
0.1 mm
N
10 µm
O
0.1 mm
P
10 µm

Fig. A1. Backscattered electron micrographs, illustrating texture (left) and pore geometry (right) of Facies 2a (homogeneously bioturbated slightly marly chalk; **A–J**), Facies 3a (homogeneously bioturbated marly chalk; **K**, **L**) and Facies 4a (homogeneously bioturbated chalky marlstone; **M–P**). (**A**, **B**) Sample from 8379'11'', Lower Sola Formation. (**C**, **D**) Sample from 8469'5'', Middle Tuxen Formation. (**E**, **F**) Sample from 8520', Lower Tuxen Formation. (**G**, **H**) Sample from 8574'10'', Lower Tuxen Formation. (**I**, **J**) Sample from 8607' Valhall Formation. (**K**, **L**) Sample from 8576'1'', Lower Tuxen Formation. (**M**, **N**) Sample from 8475'11'', Middle Tuxen Formation. (**O**, **P**) Sample from 8539'5'', Lower Tuxen Formation. Arrow colours signify: pink: quartz silt, blue: calcite-cemented microfossils, orange: kaolinitic claystone clast, light blue: calcite-rimmed dolomite crystal.


A
0.1 mm
B
10 µm
C
0.1 mm
D
10 µm
E
0.1 mm
F
10 µm
G
0.1 mm
H
10 µm


I
0.1 mm
J
10 µm
K
0.1 mm
L
10 µm
M
0.1 mm
N
10 µm
O
0.1 mm
P
10 µm


Q
0.1 mm
R
10 µm
S
0.1 mm
T
10 µm
U
0.1 mm
V
10 µm
W
0.1 mm
X
10 µm


Y
0.1 mm
Z
10 µm
AA
0.1 mm
BB
10 µm
CC
0.1 mm
DD
10 µm
EE
0.1 mm
FF
10 µm

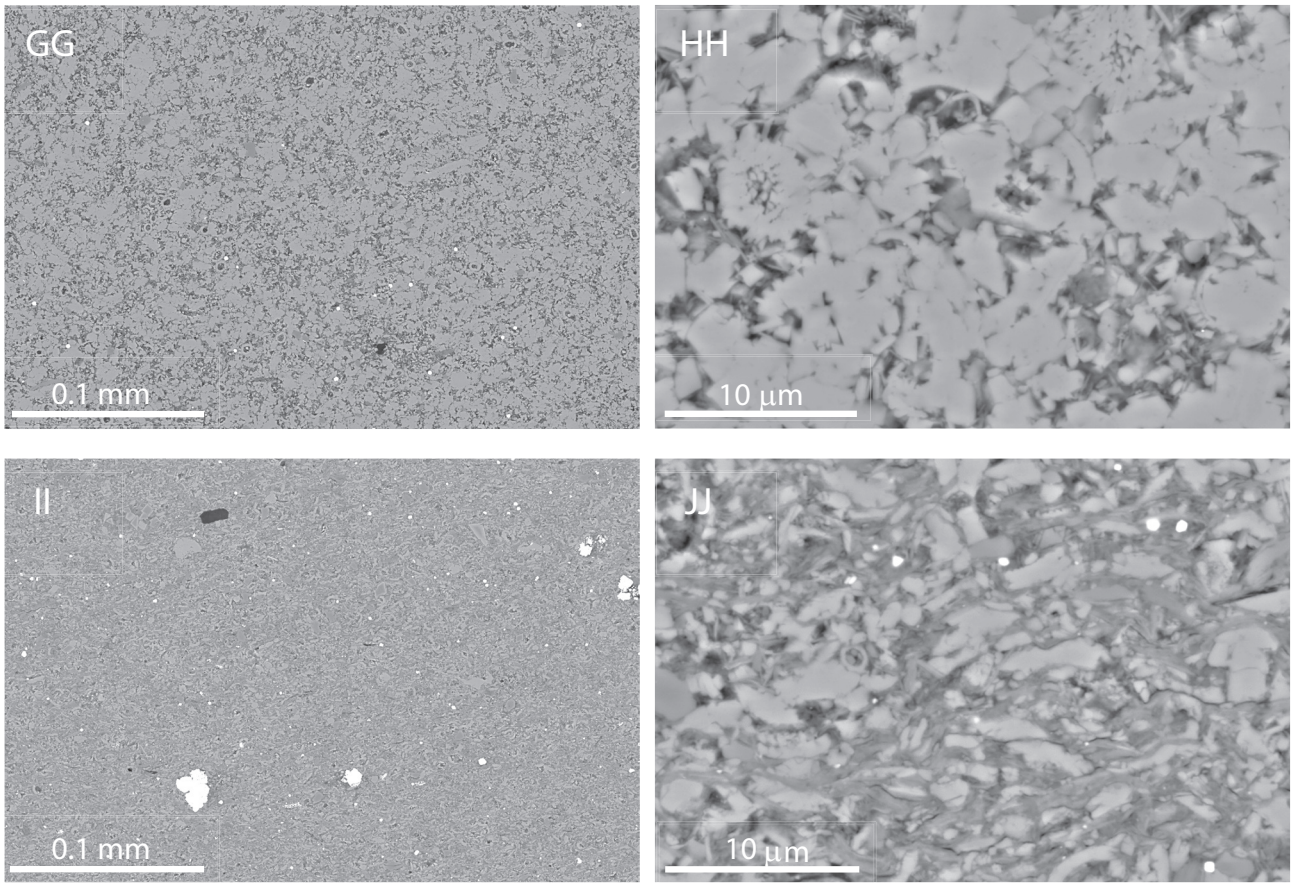
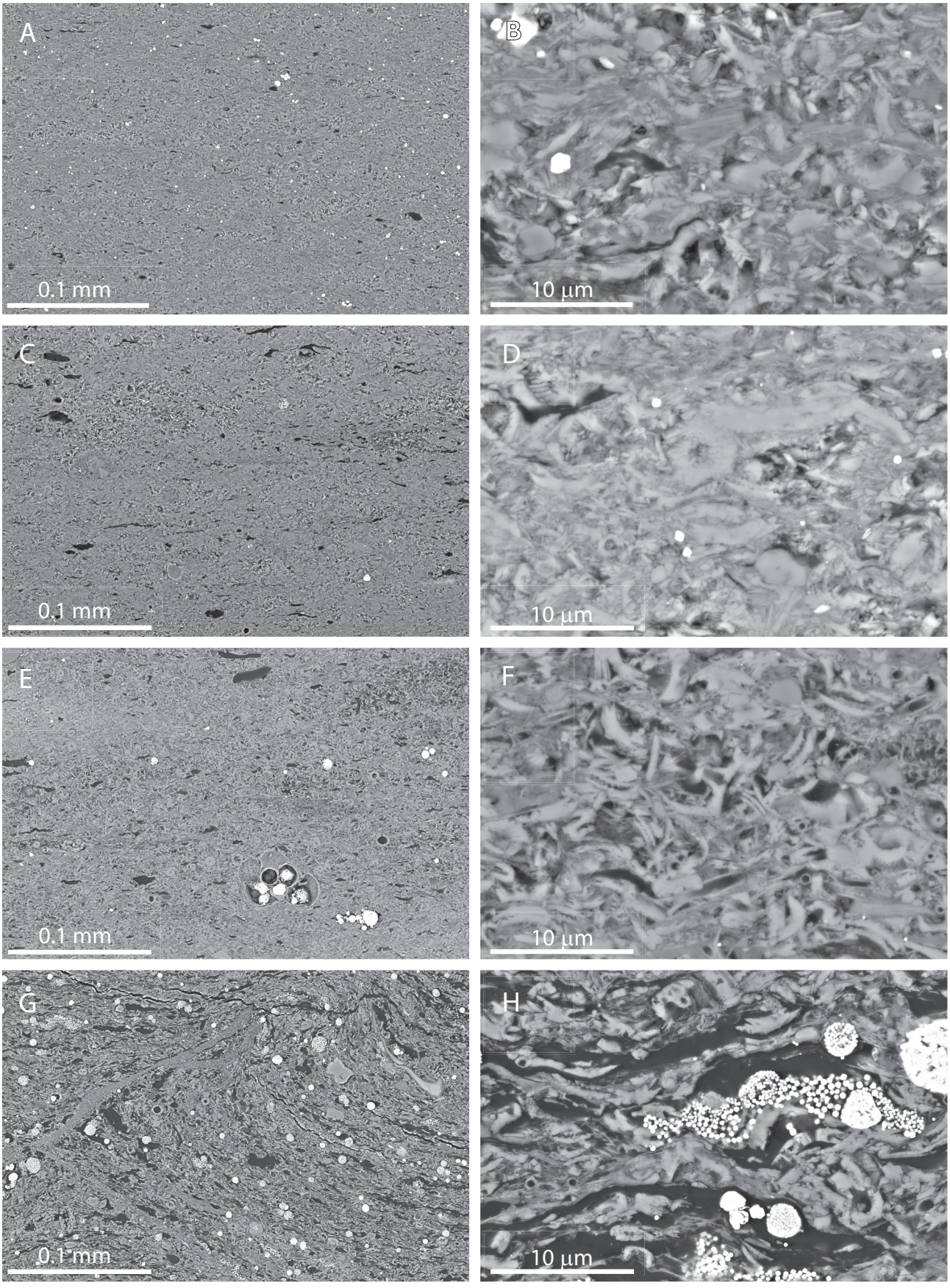


Fig. A2. Backscattered electron micrographs, illustrating texture (left) and pore geometry (right) of Facies 2b (biomottled slightly marly chalk; **A–T**), Facies 3b (biomottled marly chalk; **U–HH**) and Facies 4b (biomottled chalky marlstone; **II, JJ**). (**A**, **B**) Sample from 8390′, Lower Sola Formation. (**C**, **D**) Sample from 8433′1″, Middle Tuxen Formation. (**E**, **F**) Sample from 8459′10″, Middle Tuxen Formation. (**G**, **H**) Sample from 8472′, Middle Tuxen Formation. (**I**, **J**) Sample from 8492′11″, Lower Tuxen Formation. (**K**, **L**) Sample from 8505′, Lower Tuxen Formation. (**M**, **N**) Sample from 8511′1″, Lower Tuxen Formation. (**O**, **P**) Sample from 8512′9″, Lower Tuxen Formation (**Q**, **R**) Sample from 8550′5″, Lower Tuxen Formation. (**S**, **T**) Sample from 8560′, Lower Tuxen Formation. (**U**, **V**) Sample from 8424′11″, Middle Tuxen Formation. (**W**, **X**) Sample from 8450′11″, Middle Tuxen Formation. (**Y**, **Z**) Sample from 8451′11″, Middle Tuxen Formation. (**AA**, **BB**) Sample from 8480′3″, Middle Tuxen Formation. (**CC**, **DD**) Sample from 8485′, Middle Tuxen Formation. (**EE**, **FF**) Sample from 8559′1″, Lower Tuxen Formation. (**GG**, **HH**) Sample from 8566′1″, Lower Tuxen Formation. (**II**, **JJ**) Sample from 8604′2″, Valhall Formation. Arrow colours signify: pink: quartz silt, blue: calcite- and pyrite-cemented microfossils, orange: kaolinitic claystone clast.


A
0.1 mm
B
10 µm
C
0.1 mm
D
10 µm
E
0.1 mm
F
10 µm
G
0.1 mm
H
10 µm

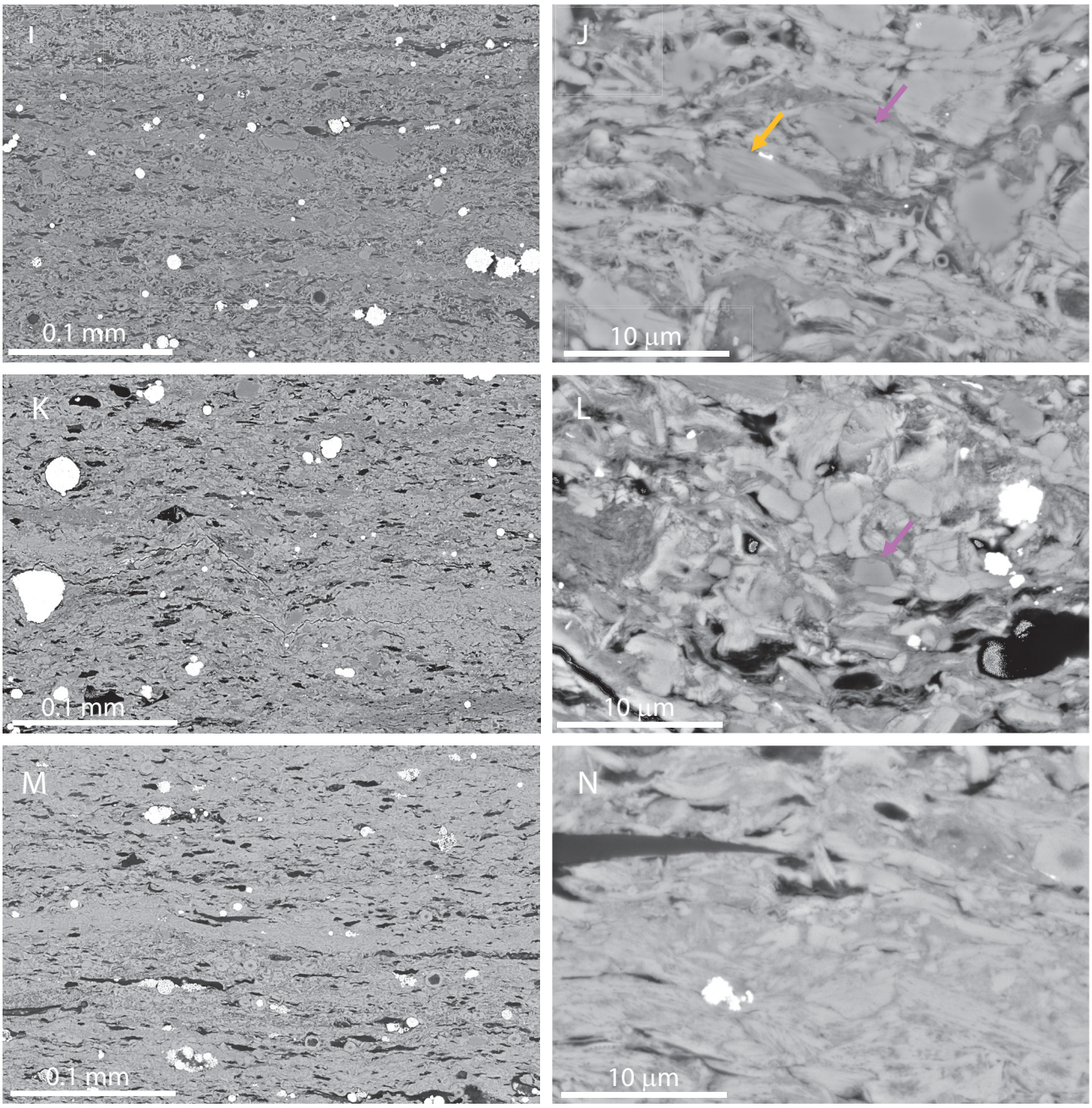
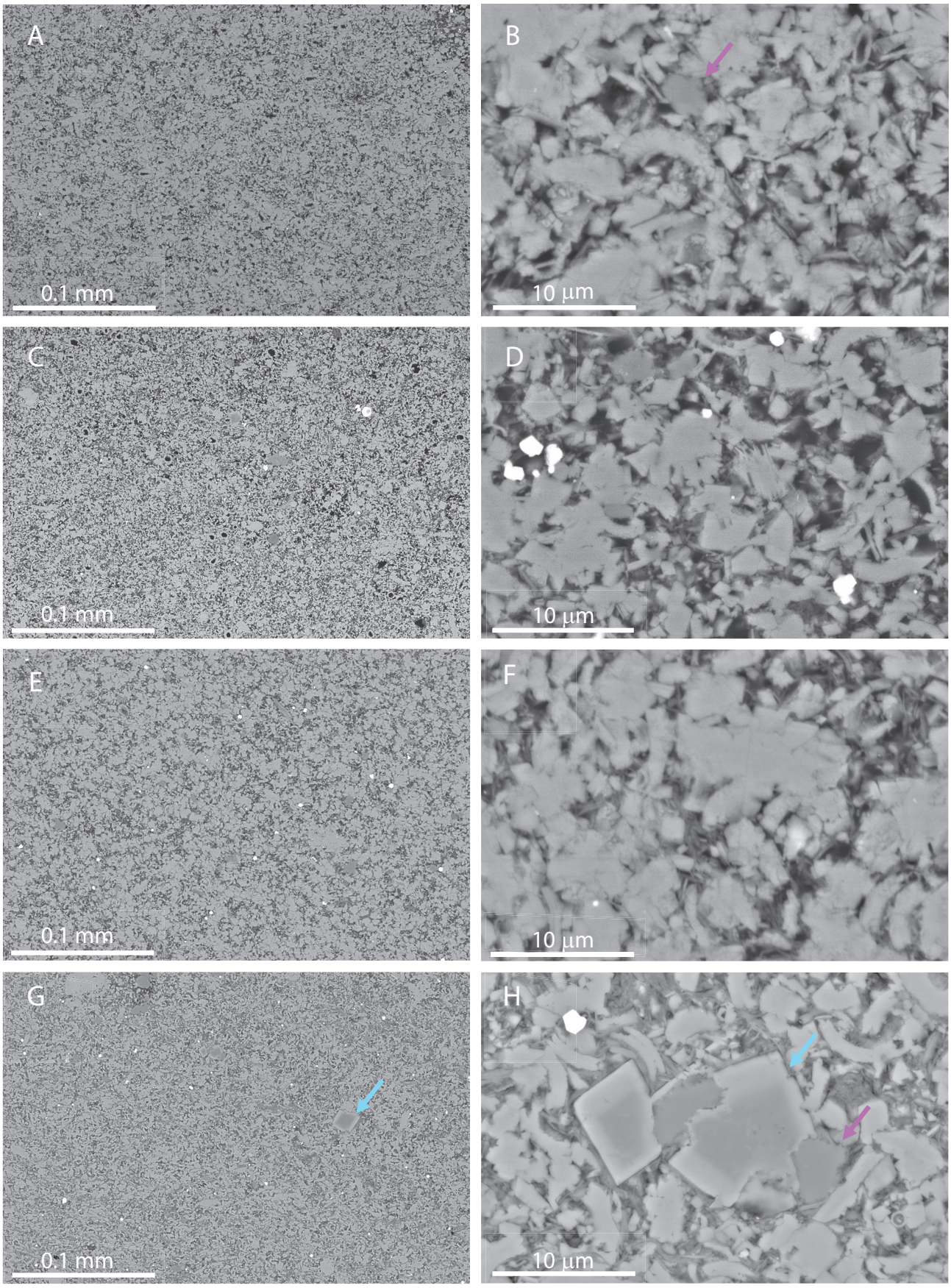


Fig. A3. Backscattered electron micrographs, illustrating texture (left) and pore geometry (right) of Facies 5c (parallel-laminated marlstone). (**A, B**) Sample from 8393'11'', Lower Sola Formation. (**C**, **D**) Sample from 8446'3'', Middle Tuxen Formation. (**E**, **F**) Sample from 8486', Munk Marl Bed. (**G**, **H**) Sample from 8487'1'', Munk Marl Bed. (**I**, **J**) Sample from 8488'4'', Munk Marl Bed. (**K**, **L**) Sample from 8490'3'', Munk Marl Bed. (**M**, **N**) Sample from 8491'1'', Munk Marl Bed. Arrow colours signify: pink: quartz silt, orange: kaolinitic claystone clast.

Fig. A4. Backscattered electron micrographs, illustrating texture (left) and pore geometry (right) of Facies 2y (shear-deformed slightly marly chalk). (**A, B**) Sample from 8515'2'', Lower Tuxen Formation. (**C**, **D**) Sample from 8557'11'', Lower Tuxen Formation. (**E**, **F**) Sample from 8581'1'', Lower Tuxen Formation. (**G**, **H**) Sample from 8582', Lower Tuxen Formation. Arrow colours signify: pink: quartz silt, light blue: calcite-rimmed dolomite crystal.


A
0.1 mm
B
10 µm
C
0.1 mm
D
10 µm
E
0.1 mm
F
10 µm
G
0.1 mm
H
10 µm

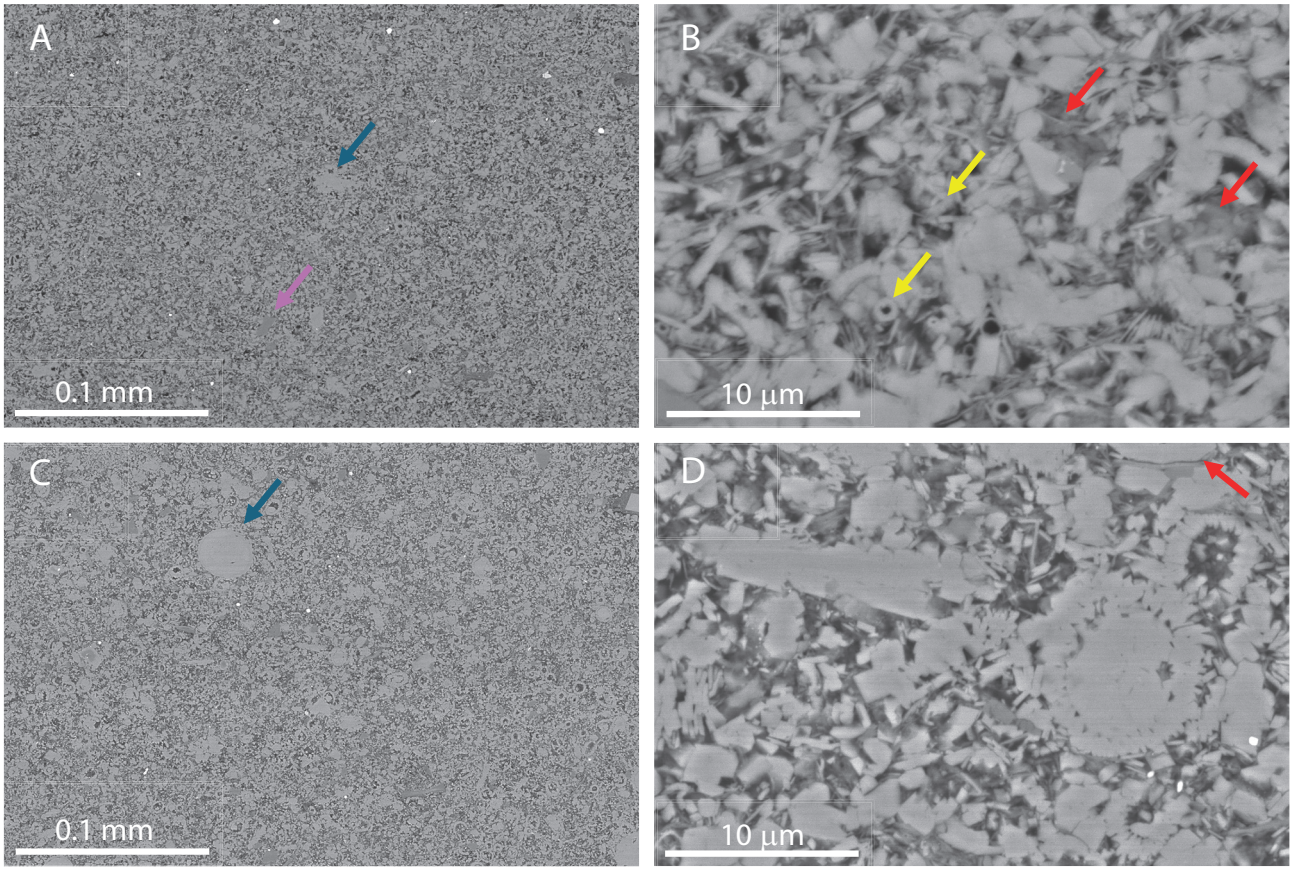


Fig. A5. Backscattered electron micrographs, illustrating texture (left) and pore geometry (right) of Facies 2z (silicified slightly marly chalk). (**A, B**) Sample from 8494'1", Lower Tuxen Formation. (**C**, **D**) Sample from 8541'11", Lower Tuxen Formation. Arrow colours signify: pink: quartz silt, blue: probably cemented calcitic microfossil or fossil clasts, red: possible silica cement.

Instructions to authors

See also www.2dgf.dk/publikationer/bulletin/vejledning.html

The Bulletin publishes articles normally not exceeding 30 printed pages, and short contributions not longer than 4 pages. Longer articles and monographs are also published, but in this case it is advisable to consult the chief editor before submitting long manuscripts. Short contributions may be comments on previously published articles, presentation of current scientific activities, short scientific notes, or book reviews.

Manuscripts with complete sets of illustrations, tables, captions, etc., should be submitted electronically to the chief editor (obe@geus.dk). The **main text** with references and figure captions should be in Word format, figures should be in either pdf, jpeg, or tiff format, and tables should be in Excel or Word format. Word tables should be ordinary text files with tab spacing between table columns; Word's 'table function' is discouraged. Compare published articles for table layout.

Manuscripts will be reviewed by two referees; suggestions of referees are welcome. The final decision on whether or not a manuscript will be accepted for publication rests with the chief editor, acting on the advice of the scientific editors. Articles will be published in the order in which they are accepted and produced for publication.

Manuscript

Language – Manuscripts should be in English. Authors who are not proficient in English should ask an English-speaking colleague for assistance before submission of the manuscript.

Title – Titles should be short and concise, with emphasis on words useful for indexing and information retrieval. An abbreviated title to be used as running title may also be submitted.

Abstract – An abstract in English must accompany all papers. It should be short, factual, and stress new information and conclusions rather than describing the contents of the manuscript. Conclude the abstract with a list of key words.

Main text – Use 1.5 or double spacing throughout and leave wide margins. Italics should be used only in generic and species names and in some Latin abbreviations (e.g. c, *et al.*, ibid., op. cit).

Spelling – Geological units named after localities in Greenland, formal lithostratigraphical units and intrusions named after localities in Greenland remain unchanged even if the eponymous locality names have since been changed in accordance with modern Greenlandic orthography.

References to figures, tables and papers – References to figures and tables in the text should have the form: Fig. 1, Figs 1–3, Table 3 or as (Smith 1969, fig. 3) when the reference is to a figure in a cited paper.

References to papers are given in the form Smith (1969) or (Smith 1969). Combined citations by different authors are separated by a semicolon; two or more papers by same author(s) are separated by commas. Citations are mentioned chronologically and then alphabetically. Use '*et al.*' for three or more authors, e.g. Smith *et al.* (1985).

Reference list

Use the following style:

Smith, A.A. 1989: Geology of the Bulbjerg Formation. Bulletin of the Geological Society of Denmark 38, 119–144. [Note that name of journal is given in full].

Smith, A.A., Jensen, B.B. & MacStuff, C.C. 1987: Sandstones of Denmark, 2nd edition, 533 pp. New York: Springer Verlag. [For more than 10 authors, use first author followed by *et al.*].

Smith, A.A., Jensen, B.B. & MacStuff, C.C. 1992: Characterization of Archean volcanic rocks. In: Hansen, D.D. *et al.* (eds): Geology of Greenland. Geological Survey of Denmark and Greenland Bulletin 40, 1397–1438. [More than three editors – therefore *et al.* form is used].

Sorting – Danish letters æ, ø and å (aa) are treated as ae, o and a (aa), respectively.

References are sorted by:

1) Alphabetically by the first author's surname. 2) Papers by one author: two or more papers are arranged chronologically. 3) Papers by two authors: alphabetically after second author's name. Two or more papers by the same two authors: chronologically. 4) Papers by three or more authors: chronologically. Papers from the same year are arranged alphabetically after second, third, etc. author's name. Authors themselves are responsible for the accuracy and completeness of their references. The reference list must include all, and only, the references cited in the paper (including figures, tables etc).

CrossRef

Please add hyperlinks to Crossref DOI when you create your list of references whenever possible.

Illustrations

May be prepared in either black and white or colour. There is no colour charge. Horizontal illustrations are much to be preferred. Size of smallest letters in illustrations should not be less than 5.5 pt. Remember scale.

All figures (including photographs) should be submitted in electronic form ready for direct reproduction, i.e. having the dimensions of the final figure with a standard resolution of 300 dpi for photographs. Preferred formats are pdf, tiff and jpg.

Size – Width: All widths up to full page width (170 mm) are accepted. Maximum height is 223 mm. Design figure contents to match the preferred figure size.

Captions – Captions to figures and plates must be delivered on separate pages, preferably at the end of the manuscript.

Supplementary data files

Supplementary files are accepted. Such files may provide e.g. analytical data tables, detailed data documentation, illustrations with special effects, or videos.

Proofs

Authors receive page proofs of the article after technical production. The cost of any alterations against the final manuscript will be charged to the author.

Content, vol. 71

Fabricius, I.L. & Lauridsen, B.W.: LOwer CRETAceous project, summary of results.....1

Lauridsen, B.W., Lode, S., Sheldon, E., Frykman, P., Anderskouv, K. & Ineson, J.: Lower Cretaceous (Hauterivian–Aptian) pelagic carbonates in the Danish Basin: new data from the Vinding-1 well, central Jylland, Denmark.....7

Lorentzen, M.C.L., Bredesen, K., Smit, F.W.H., Hansen, T.H., Nielsen, L. & Mosegaard, K.: Mapping Cretaceous faults using a convolutional neural network – A field example from the Danish North Sea.....31

Jelby, M.E., Ineson, J.R., Thibault, N., Bodin, S., Blok, C.N., Edvardsen, N., Clemmensen, T.S., Buls, T. & Anderskouv, K.: Facies and depositional processes of Lower Cretaceous carbonates, Danish Central Graben.....51

Ineson, J.R., Petersen, H.I., Andersen, C., Bjerager, M., Jakobsen, F.C., Kristensen, L., Mørk, F. & Sheldon, E.: Early Cretaceous stratigraphic and basinal evolution of the Danish Central Graben: a review.....75

Blok, C.N., Adatte, T., Ineson, J.R., Sheldon, E., Jelby, M.E., Smit, F.W.H., Lauridsen, B.W., Anderskouv, K. & Bodin, S.: Clay mineral assemblages as a tool in source-to-sink studies: an example from the Lower Cretaceous of the North Sea Basin.....99

Fabricius, I.L. & Meireles, L.T.P.: Assessment of pore collapse in North Sea Lower Cretaceous carbonates using downhole elastic strain.....115

Fabricius, I.L., Hjuler, M.L., Jelby, M.E. & Anderskouv, K.: Microscopic character of the Lower Cretaceous Tuxen and Sola formations in the Boje-2C well, Danish Central Graben.....127

Instructions to authors:
See inside the back cover and also www.2dgf.dk/publikationer/bulletin/vejledning.html